International Atomic Energy Agency

INDC(NDS)-251
Distr.: L

INDC

INTERNATIONAL NUCLEAR DATA COMMITTEE

NUCLEAR DATA FOR NEUTRON EMISSION IN THE FISSION PROCESS

Proceedings of a Consultants' Meeting organized by the International Atomic Energy Agency and held in Vienna, Austria, 22 - 24 October 1990

Compiled by

S. Ganesan
IAEA Nuclear Data Section

November 1991

IAEA NUCLEAR DATA SECTION, WAGRAMERSTRASSE 5, A-1400 VIENNA

INDC(NDS)-251
Distr.: L

NUCLEAR DATA FOR NEUTRON EMISSION IN THE FISSION PROCESS

Proceedings of a Consultants' Meeting organized by the International Atomic Energy Agency and held in Vienna, Austria, 22 - 24 October 1990

Compiled by

S. Ganesan
IAEA Nuclear Data Section

November 1991

Abstract

This document contains the proceedings of the IAEA Consultants' Meeting on Nuclear Data for Neutron Emission in the Fission Process, Vienna, 22 - 24 October 1990. Included are the conclusions and recommendations reached at the meeting and the papers presented by the meeting participants. These papers provide a review of the status of experimental and theoretical data on neutron emission in spontaneous and neutron induced fission with reference to the data needs for reactor applications oriented towards actinide burner studies. The specific topics covered are the following: experimental measurements and theoretical predictions and evaluations of fission neutron energy spectra, average prompt fission neutron multiplicity, correlation in neutron emission from complementary fragments, neutron emission during acceleration of fission fragments, statistical properties of neutron rich nuclei by study of emission spectra of neutrons from the excited fission fragments, integral qualification of nu-bar for the major fissile isotopes, nu-bar total of ^{239}Pu and ^{235}U, and related problems.

Reproduced by the IAEA in Austria
November 1991

91-05933

Foreword

Upon recommendation of the International Nuclear Data Committee (INDC), the International Atomic Energy Agency convened a Consultants' Meeting on Nuclear Data for Neutron Emission in the Fission Process. The meeting took place in Vienna, Austria, 22-24 October 1990.

The primary objectives of the meeting were:

(1) to review the needs and the experimental and theoretical status of data on neutron emission in fission;

(2) to discuss methods of calculations of neutron data for unknown cases for minor actinides etc. (of importance to waste incineration studies); and

(3) in the case of identified urgent needs, to formulate and establish specific tasks and goals for a new Co-ordinated Research Programme on "Physics of Fission Neutron Emission and its Nuclear Data Applications". This CRP will be oriented towards data needs of actinide burners.

The Agency wishes to express its sincere thanks to Mr. S.S. Kapoor and Mr. M.V. Blinov for their excellent chairmanship during the meeting. The Agency would like to thank all individuals and institutions who have contributed to the preparation of the present document. The Agency would also like to thank all members of the Consultants Meeting, who materially contributed to its successful completion.

CONTENTS

SESSION II. PROGRESS IN NEUTRON MULTIPLICITY CALCULATIONS AND MEASUREMENTS

SESSION III. STUDY OF SPECIFIC EFFECTS IN NEUTRON EMISSION IN FISSION AND THEORIES FOR NEUTRON EMISSION IN FISSION

Summary report, conclusions and recommendations

Preamble

The IAEA Consultants' Meeting on "Nuclear Data for Neutron Emission in the Fission Process", was held at the IAEA Headquarters, Vienna, during October 22-24, 1990. The Meeting addressed itself to the following two main objectives:

(1) to review the needs and the experimental and theoretical status of data on neutron emission in fission, and

(2) in the case of identified urgent needs, to formulate and establish specific tasks and goals for a new Co-ordinated Research Programme "Physics of Fission Neutron Emission and its Nuclear Data Applications". This CRP should be oriented towards actinide burner studies.

The meeting took into account the outcome of the previous Consultants' Meeting on this subject held in Mito City, Japan, 24-27 May, 1988.

I. Summary of Presentations

The discussions of the IAEA Consultants' Meeting on "Physics of Neutron Emission in Fission" held in Mito City in 1988 were taken into consideration and further new information was presented on the following aspects:

(i) The need of improved neutron multiplicity data $\bar{\nu}$ (A,E_n) (as a function of fragment mass number A and incident neutron energy E_n) for major actinides and missing data on $\bar{\nu}$ (A,E_n) for minor actinides of relevance to waste incineration.

(ii) The need of data on fission neutron spectra $N(E,E_n)$ for various nuclides, including minor actinides of relevance to waste incineration.

(iii) Application of new techniques for measuring $\bar{\nu}$ and N(E) as a function of neutron energy.

(iv) New data on $\bar{\nu}$ (E_n), neutron spectra N(E) for specified incident neutron energies for several nuclei. Several data gaps over the incident energy range were noted. In some cases, there is no data at all.

(v) New results obtained from multi-parameter studies of neutron emission in fission. These results give essential information on fission neutron emission and, in particular, on nuclear level densities of neutron-rich fragment nuclei. Such data often cannot be obtained by other means.

(vi) Further refinements of theoretical models for prediction of fission neutron observables showing the contiderable progress achieved since the late seventies.

(vii) Several questions are still to be resolved concerning the ability to extrapolate from known fission neutron data to that for unknown cases.

(viii) New, improved results for fission neutron data systematics based on the present status of fission neutron theory.

II. Present Status of the Field

It was noted that most fission neutron data in the major evaluated files are based on sparse experimental data and empirical relations which do not have a realiable physical foundation. A complete and physically consistent evaluation of fission neutron observables has been performed in only one known case (^{235}U in ENDF/B-VI). It is completely lacking for most major and all minor actinides. At present, most nuclear data files lag behind the theoretical advances that have been made in this field and discussed at this meeting. For example, the following are the statistics on the total fission neutron spectrum (MT=18) contained in ENDF/B-V for 40 nuclei:

Maxwellian spectrum (single temperature)	17
Maxwellian spectrum (array of temperatures)	18
Energy-dependent Watt spectrum	5
Total	40

Thus, in 35 of 40 cases the Maxwellian distribution is used. In 17 of the 35 cases, a single Maxwellian temperature represents the complete energy dependence. Moreover, in 16 of these 17 cases, the single Maxwellian temperature has the same value, namely, T_M=1.33 MeV. This situation is largely unchanged in ENDF/B-VI. Clearly, it is time to take advantage of the increased predictive power of new theoretical models under development.

Recognizing the status of $\bar{\nu}$ data presented at the Mito Meeting in 1988, it was noted that only limited experimental data have been measured since that time. An intercomparison of recent $\bar{\nu}$ data files available has not yet been performed. Such an intercomparison, in addition to theoretically based evaluations, would be an important first step in improving the status of libraries, in particular for minor actinides where measured data are extremely sparce or totally missing.

It was emphasized that the knowledge of the incident energy dependence of fission neutron spectra is of importance for several emerging applications in nuclear technology such as waste incineration reactors, high burn-up reactors, fusion blankets in hybrid reactors, etc. However, at present, measurements of fission neutron spectra at different incident energies are very sparse for many actinide nuclei. Given that precision measurements of such data are very difficult (e.g. for minor actinide nuclei), one would have to rely in most cases on theoretical predictions.

Following the recommendations of the Mito Consultants' Meeting in 1988, several groups presented new experimental data on fission neutron spectra at several incident energies as well as for spontaneous fission (^{248}Cm). They are discussed in the body of these proceedings.

Considerable progress has been achieved in the eighties in correlation experiments providing fundamental information on fragment de-excitation. In particular, energy and angular distributions and multiplicity distributions of fission neutrons as a function of fragment parameters (mass number, kinetic energy) were measured (Geel, St.Petersburg, BARC, Dresden) and are presented in both the Mito proceedings and in this volume.

It has become clear that the information deduced from such experiments is not only providing new insights into the fission process, but is also yielding input needed for improvements of existing theoretical models. Moreover, certain correlation measurements may be able to discriminate between the different theoretical models.

III. Needs

(A) Data needs for reactor applications including actinide burner studies

At present it is worth mentioning that the request lists for major and minor actinides respectively are different from the point of view of nature of the parameters requested and the related accuracies. The more stringent accuracies are for major actinides - but in a near future drastic changes can be expected on the needs for the minor actinides in relation to the actinide burning projects. Theoretical tools are available which are very useful to predict $\bar{\nu}$ and fission neutron spectra for unknown cases.

In the following we will consider separately the case of major and minor actinides focusing on needs for present reactor applications.

1. Major Actinides

For the cross section there are a few requests in the thermal and fast neutron energy ranges which will not be considered here. Multiple chance fission problems are considered as solved or potentially solved (with perhaps one exception related to ^{238}Pu production via ^{239}Pu(n,2n), where the (n,2n) cross section is required in the range 0-2 MeV above threshold). However, the statistical-model versions currently used yield different results on partial fission cross sections. Existing data should be verified.

Because of the relationship with the prompt multiplicity and its practical importance the energy dependence of the delayed neutron yield should be further investigated starting from the existing models (e.g. Lendl's model).

a) Prompt neutron multiplicities $\bar{\nu}_p(E_n)$

Problems still remain which are related to design and safety purposes (for inherently safe reactors):

^{239}Pu: Because of a lack of reliable experimental and/or model data in the very important 100 keV range, $\overline{\nu(E_n)}$ and $N(E,E_n)$ data in this range are strongly requested.

^{241}Pu: This nucleus becomes of importance because of strategies involving higher burnup rates and Pu recycling. The fluctuations in $\bar{\nu}(E_n)$ in the vicinity of the first resonance are not understood. In general the requested accuracy is not fully met up to 15 MeV.

^{240}Pu, ^{242}Pu: (inherently safe reactors)

The requested accuracy (1%) is not met.

^{235}U: The fluctuations above 1 eV which result in a lower averaged $\bar{\nu}(E_n)$ value (compared to thermal neutron induced fission) are of importance for epithermal advanced reactors. These should be fully explained.

^{233}U: (inherently safe reactors and fuel cycle problems)

The available experimental data are old and the requested accuracy (1%) is not met, especially in the resolved range.

^{232}Th (E_n > 1MeV) and ^{234}U (E_n > = 0.5 MeV)

For these nuclei involved in the thorium-uranium fuel cycle, the requested accuracy is not met.

b) Prompt neutron spectra $N(E,E_n)$

The importance of the low-energy neutrons (E < 300 keV) in most applications is stressed. This statement is especially relevant when one considers the relative weakness of the model for N(E) in this energy region (in the case of fragment parameter averaging as often applied) as well as the poor knowledge of the inelastic cross section (in the same energy region), which governs the neutron slowing down by heavy nuclei.

Generally, fission neutron spectra corresponding to thermal incident neutrons are used in reactor calculations because of the assumption of the small importance of the incident neutron energy dependenceat thermal energies. (However, this assumption should be verified or modified, if necessary). The gneral situation in this field of nuclear data application justifies the request of more precise data. Present files were based on rather old measurements. New experiments with the improved techniques presently available are strongly requested.

2. Minor Actinides

The present requests, which are derived from fuel cycle considerations, are for cross sections only, and it appears from validation on integral data that most of them are met, as the accuracy required is generally about ± 10%.

In the future, if actinide burning projects go ahead, then the needs will evolve towards strongly different requests, such as better accuracy on the cross sections and other types of data (e.g. $\bar{\nu}(E_n)$, $N(E,E_n)$ for the already identified isotopes (^{237}Np, various Am and Cm isotopes) and for new ones.

In the more stringent context of the burning of reactor actinides as fuel) delayed neutron yields will become more important.

3. Relative importances of $\bar{\nu}_p$ (E) versus $\chi(E,E_n)$ for reactor applications

Eric Fort (France) made a very interesting observation that recommendations for a CRP centered on the fission neutron spectra description would be a good choice because it is in that area that theory has real potentialities of high predictive power. But he stressed that the real needs for the present and near future are more for $\nu_p(E)$ than for $\chi(E,E_n)$. He reported that he has made some tests on one very simple system, JEZEBEL, and on a critical experiment MASURCA Z3 well representative of a FBR core. The calculations have been performed using a one dimensional transport method in the approximation P_3 S_{16} in a 40 points mesh for JEZEBEL and using a fast cell code and assuming the fundamental mode conditions for MASURCA Z3 experiment. The data processing has been performed using the NJOY code (version 89.62) in a 33 group scheme with a general 0.5 lethargy width. The chi vector has been obtained for a single energy of neutrons. Four different energies (namely: thermal, 0.5 MeV, 2 MeV, 14 MeV to which correspond 4 fission temperatures labelled below respectively as T_1, T_2, T_3, T_4) have been used in this calculation of the chi vector so as to explore the sensitivity of the results to the incident energy. Apart from an "old" temperature dependent spectrum to describe the energy distribution of fission neutrons, all the nuclear data were taken from JEF 2.1.

The results are as follows:

For JEZEBEL;

Tf (MeV)	T_1 = 1.39	T_2 = 1.398	T_3 = 1.421	T_4 = 1.58 (for ^{239}Pu)
K_{eff}	0.99638	0.99688	0.99832	1.00835
ΔK_{eff} %Thermal ("pcm = 10^{-5}")	0	50	194	1197

For MASURCA Z3, the difference in K_{eff} when using T_1 and T_3 (for each fissile/fertile nucleus) is ~ 100 pcm.

The conclusions reached by Fort based on the above exercise are:

The effect of incident energy on the fission spectrum is rather negligible for fission reactors, but is of importance for hybrid fusion fission reactors.

In other words, a CRP on fission neutron spectra appears more directed towards the needs of a long term future than towards the ones of the near future.

He recommended that it would be interesting, without any significant additional cost, to slightly enlarge the scope of the CRP by recommending at least ν_p measurements for some chosen actinides.

These ν_p measurements would feed, in an ulterior phase, the work of theorists inside/outside another CRP and would be, in any case, useful for the scientific community.

(B) Basic research (for development of fission neutron models with high predictive power)

Fission neutron theory for nuclear data applications relies on the following main parts

(i) fission theory (or corresponding phenomenological approaches) for describing fragment distributions (pre-neutron emission mass and charge yield distributions, fragment kinetic energy distributions, total excitation energy distribution and partition of excitation energy between complementary fragments.

(ii) the emission model for describing fragment de-excitation (e.g. Hauser-Feshbach theory, evaporation theory, statistical multi-step compound theory, etc.)

(iii) reaction theory to calculate multiple-chance fission probabilities for use in calculation of multiple-chance fission neutron spectra and multiplicities.

At present, part (i) contains the highest uncertainties. Substantial effort should be devoted to the energy partition problem, in particular to a theory that does not depend on the assumption of a minimum in the potential energy surface at the scission point.

The further development of the Hauser-Feshbach approach to the calculation of fission neutron observables requires simultaneous measurements of neutron and γ-ray distributions in emission energy and angle over fission fragment mass, (charge), and kinetic energy distribution in order to properly benchmark the Hauser-Feshbach approach. Suggested candidate experiments are

- ^{235}U+n (thermal), with total spin 3^- or 4^-,
- ^{239}Pu+n (thermal), with total spin 0^+ or 1^+,
- ^{252}Cf(sf), with total spin 0^+, and
- ^{248}Cm(sf), with total spin 0^+.

Dr. Kapoor raised an interesting question as to how the initial spins and parities of the compound nuclei would be important for the calculation of fission neutron properties which are primarily emitted from the fission fragments.

Dr. Madland mentioned that the H-F calculation of the de-excitation of fission fragments takes account of the neutron emission in competition with the gamma emission. In this way, a H-F calculation accounts for the dissipation of the total fission fragment excitation energy, which is what we wish to do. The gamma emission depends strongly on the angular momenta of the states and the neutron emission less strongly. The H-F calculation of the two processes in competition requires a specification of the fragment initital conditions. These include: excitation energy, spin, and parity. Since angular momentum is conserved, benchmark calculations/experiments where the total angular momentum of the compound fissioning nucleus is fixed at one value (spontaneous fission) or two values (thermal neutron fission) means that only two initial angular momentum distributions are involved (light and heavy fragment) instead of the usual three initial angular momentum distributions. The advantages of this choice are then obvious from the standpoint of understanding the dependencies within the calculation. What is at issue here is the best way to benchmark a H-F calculation of fission fragment de-excitation by neutron and gamma emission in competition.

Dr. Madland plans to do a test calculation in the near future.

The isospin dependence of global neutron optical model potentials and nuclear level densities should be improved over the current isospin treatments. This is required for more accurate descriptions of neutron emission occuring from (neutron-rich) fission fragments .

Fundamental investigations on fission neutron emission should be supported by the exchange of

- recent experimental data on P(ν: A, TKE) and N(E,Θ:A,TKE), and
- fission neutron codes (energy dependent version of the Los Alamos Madland-Nix code). Note that the TU Dresden code "FINESSE" is already available on request. A code "SCOFIN" is available at the Radium Institute, St. Petersburg.

This will enable analysis to be performed by more groups than are involved at present.

IV. Conclusions and Recommendations

(i) The present status in the field of fission neutron nuclear data exhibits some considerable deficiencies. In particular, the quality of data files in many cases corresponds to the status of fission physics which existed over twenty years ago. There is a remarkable contrast between the quality, accuracy, and complexity of current data files and the recent progress in high-quality measurements and theoretical understanding. Therefore, further activities in the evaluation of fission neutron data in a physically consistent manner are strongly recommended in order to meet all data requirements and in order to bring data files up-to-date as much as possible.

(ii) Work should be directed towards the development of fission neutron theory with high predictive power, which must be supported by high quality measurments at "typical" points enabling the sound verification of the theory. That is, it is not necessary to cover the whole energy range (0-20) MeV by experiments. Special emphasis is required in the resonance region, where fluctuations of fission neutron observables can be attributed to fission mode and fission channel effects, together with the influence of the (n,γf) process.

(iii) The ^{252}Cf fission neutron standards $\bar{\nu}$ and N(E) are well established, due to the much work in the eighties (considerably supported by the IAEA Nuclear Data Section). It is recommended to make practical use of these in all experiments, preferentially as a direct reference by simultaneous measurements under experimental conditions identical to those of the actinide nucleus being investigated.

(iv) A new Co-ordinated Research Programme on "Physics of Fission Neutron Emission and its Nuclear Data Applications" is strongly recommended. This CRP would be oriented towards actinide burner studies. It should involve the topics (A) measurements, (B) improvement of fission neutron theory, and (C) nuclear data activities. These topics are specified below.

(A) Measurements

- Precision measurements of $\bar{\nu}$, $P(\nu)$, and $N(E)$ at typical incident energy points, to satisfy the data needs highlighted in Section III.A (above) and for verification and adjustment of nuclear models. Besides spontaneous fission, the incident energies would be chosen from: thermal fission, threshold fission, and multiple-chance fission.

- Multiparameter investigations as mentioned in Section III.B comprising fundamental fission studies to support fission neutron theory development (e.g. that of fragment de-excitation mechanisms, level densities and optical potentials for neutron-rich fragments).

- Note: Due to the cost of high-quality actinide targets for this work, the Agency might give consideration to assisting financially in the purchase of such targets by user groups. This might be done through the auspices of IAEA research contracts. An alternative is to promote a system of target exchange between groups. In addition, technology and manpower transfer between well-equipped laboratories and less-equipped laboratories is recommended. Financial assistance for the purchase of the expensive data acquisition facilities which are needed for multiparameter experiments might also be considered.

(B) Improvement of Fission Neutron Theory

- Solution of the energy partition problem on the basis of sound theoretical treatments, together with the description of mass yield curves for any fission reaction.

- Application of the Hauser-Feshbach theory to fission neutron emission from the multitude of fragment configurations. Note that this type of calculation requires the adequate knowledge of the fragment occurrence probability as function of A, Z, TKE, excitation energy, and angular momentum (cf. Section III.B, above).

- Use of fragment temperature distribution models (Madland-Nix Theory, Dresden Theory FINESSE, etc.) for systematics of fission neutron data.

- Intercomparison of models/codes on the basis of standardized input data.

- Resonance fission studies relevant to fission neutron emission (cf. Section IV.(ii), above).

(C) Nuclear Data Activities

- Intercomparison of fission neutron data of different libraries and formulation of specific fission neutron data requests for major and minor actinides.

- Development of theoretically-based fission neutron data systematics.

- Derivation of new recommended data of fission neutron obervables $\bar{\nu}(E_n)$, $N(E,E_n)$, $P(\nu,E_n)$ etc. for E_b = 0-20 MeV for inclusion in present nuclear data libraries, i.e. data representation in ENDF/B-6 format.

- Sensitivity studies in order to compare the practical use of previous data representations: non energy dependent with the new engery-dependent formalisms.

A list of activities proposed by individual laboratories is given in the Appendix.

APPENDIX

SPECIFIC EXPERIMENTAL PROPOSALS FROM DIFFERENT LABORATORIES

These proposals were put forward by the representatives of the various laboratories present at the Consultants' Meeting. They represent work which could be anticipated to be done at the respective laboratories over the next few years.

(There is no significance attached to the order of presentation).

(A) Central Bureau for Nuclear Measurements, Geel, Belgium

(i) Measurements of $^{238}U(n,f)$ fission fragment parameters (e.g. mass yield, TKE, angular distribution) as a function of incident neutron energy for sub-threshold and near-threshold energies.

(ii) $^{252}Cf(sf)$ fission fragment parameters in correlation with prompt γ-ray emission.

(iii) $^{239}Pu(n,f)$ fission fragment parameters in the resonance region.

(B) Technische Hochschule Darmstadt, Germany

(i) Evaluation of experimental light fission fragmet yields of the odd-proton nucleus $^{243}Am^*$ (from $^{241}Am + 2n_{th}$), which were measured at the LOHENGRIN separator of ILL, Grenoble.

(ii) Measurement of $^{238}U(n,f)$ for $E_n \leqq 200$ MeV at the white neutron source at LAMPF, Los Alamos (collaboration with LANL and the University of Atlanta). Quantities measured are fission fragment energies and masses, and prompt neutron angular distribution and energies.

(iii) Experiment of $^{252}Cf(sf)$ at the Darmstadt-Heidelberg NaI crystal ball to be used as a neutron and γ-ray detector. It is planned to measure the correlation of fragments and long range α particle parameters with neutrons and γ-rays to improve knowlege on the binary and ternary fission process (collaboration with MPI Heidelberg and CENBG Bordeaux).

(C) Bhabha Atomic Research Centre (BARC), Bombay, India

Experiments for multiparamter-studies of fission neutrons being carried out at BARC, India, are aimed to provide information on the nuclear level densities of neutron rich fragment nuclei, and to resolve questions relating to the omission of pre-scission neutrons.

(D) Radium Institute, St. Petersburg, USSR

(i) Measurement of spontaneous fission neutron spectra for Cm isotopes.

(ii) Measurement of thermal and fast neutron induced fission neutron spectra for ^{235}U, ^{238}U, ^{232}Th, ^{237}Np, and others.

(iii) Measurement of the multiplicity distribution $P(\nu)$ for spontaneous and thermal neutron induced fission.

(iv) Theoretical calculations of the integral and differential spectra and of $\bar{\nu}$ for various nuclides and excitation energies.

(v) Study of the fission neutron emission mechanism for spontaneous and neutron induced fission.

(vi) Study of energy partition problem.

(E) Institute of Experimental Physics, Arsamas, USSR

(i) Measurement of $\bar{\nu}(E_n)$ and $E_\gamma(\bar{E}_n)$ in the incidence energy range 0.5-12 MeV for ^{241}Am, ^{243}Am, and ^{240}Pu.

(F) Institute of Physics and Power Engineering, Obninsk, USSR

(i) Measurements of neutron spectra of fission induced by 6, 8, and 14 MeV neutrons for ^{237}Np.

(G) Institute of Atomic Energy, Beijing, China

(i) Completion of the work "Prompt neutron spectrum of ^{238}U fission induced by 12 MeV neutrons" (perhaps at a further incidence energy point, 10 MeV). The fission mass yields can also be measured at the same incident energy point(s).

(ii) Improvement of $^{252}Cf(sf)$ neutron spectrum data in the low-energy part (measurement by using Li-glass detectors with much care taken over the efficiency calibration.

(iii) Investigation of γ-ray emission characteristics correlated with both fragment energy and fragment mass.

(iv) As a potential possibility, expansion of the incident neutron energy range for the above prompt neutron spectrum measurement by using a thick Be target (double TOF method).

(v) $\bar{\nu}$ measurements for minor actinides, provided that the actinide targets are available.

(H) Technische Universität Dresden, Germany

(i) Multiparameter investigation of total ($\bar{\nu}$, $\bar{E}\gamma$) and spectroscopic [$P(\nu)$, $N(E,\theta)$ for prompt neutrons and γ-rays] characteristics of fragment de-excitation in correlation with fragment parameters A, TKE, and Z (the latter one in the case of cold fission). This measurement, which will be based on a 4π-scintillator tank, a twin-ionization chamber with Frisch grids, neutron TOF-detector and γ-ray detector, will enable determination of the intricate fragment occurrence distribution as a function of A, Z, TKE, excitation energy, and angular momentum (co-operation with Hahn-Meitner-Institute, Berlin).

(ii) Systematics of fission neutron data for all major and most minor actinide nuclei, based on

- energy partition model (with phenomenological microscopic energies),
- temperature distribution model FINESSE,
- statistical multistep reaction theory with fission channel, in combination with the outcome of more fundamental studies. Data will be represented in ENDF/B-6 format.

(I) ANSTO, Lucas Heights, Australia

(i) Calculation and analysis of fission neutron spectra (FNS):

- Graphs of recommended FNS based on all current model versions (Madland-Nix model, cascade emission model, Hauser-Feshbach model, etc.) for the most important nuclei ^{252}Cf(sf), ^{235}U(n_{th},f), ^{239}Pu(n_{th},f), 2 MeV fission of ^{232}Th and ^{238}U, etc. (Scission neutrons to be excluded; the model intercomparison to be based on the same input data for each case, with the input data having previously been agreed upon by the various groups involved).

- Contributions to optimize input data sets (nuclear level density, optical model potential, fragment occurrence probabilities) on the basis of the model intercomparison.

(ii) Measurement of fission neutron spectra and neutron emission anisotropy:

- Proposal to measure the FNS for ^{239}Pu(n_{th},f) and ^{235}U(n_{th}f) (cf. Section III.B),

- Proposal to perform measurements directed to the determination of neutron anisotropy in the centre-of-mass system of fragments, since present informations are contradictory (anisotropy ratios in the range 0.01 - 0.1).

CRP Recommendations

1. Calculation of Fission Neutron Spectra

1.1. Graphs and tabulated values of recommended curves for the three models (Madland-Nix Model, Empirical Model and Hauser-Feshbach) should be produced for the important nuclei ^{252}Cf (SF), thermal fission of ^{235}U and ^{239}Pu, 2 MeV fission of ^{232}Th and ^{238}U for 0-20 MeV secondary neutron energy. Scission neutrons should be excluded.

It is important that each of the three curves for each nucleus must use the same input data , where these data are common to each model.

1.2. Also, the input data sets used should be agreed on and calculated between these groups providing the recommended curves and tabulated values and other interested parties.

Comments - Recommendations

1.1 and 1.2 will permit user laboratories to clearly see just how large any differences between the models are. They will also permit standardization of the input data sets.

- the types of data to be standardized are:

  . nuclear level density formulation and parameters
  . optical model potential
  . excitation energy of fission fragments
  . mass, charge, TKE yields of fission fragment
  . energy release for the particular fission split.

Both the averages and distributions of the input parameters should be standardized.

1.3. The question of a distribution of nuclear level density parameters should be examined in the Madland-Nix model.

1.4. Sensitivity studies should be carried out by actinide data groups and nuclear safeguards groups to compare the use of "older" representations of the fission neutron spectrum (FNS) with the use of new energy-dependent formalisms.

2. Measurements of Fission Neutron Spectra

2.1. Measurement of FNS for thermal fission of ^{239}Pu should be performed for the widest possible range of secondary neutron energy.

Comment

2.2. Further work on 2MeV neutron fission of ^{232}Th - in view of the limited amount of presently available data for this nucleus.

2.3. Measurements for determination of the size of the neutron anisotropy due to fragment spectra in view of competing estimates of its size (viz 0.1 versus 0.01 - 0.015).

2.4. The measurements of fission neutron spectra for spontaneous and neutron induced fission of Np, Pu, Am and Cm isotopes.

Comment

These data are needed for burnup problems but they are practically absent.

3. Multiparameter Data Needs

3.1. Multiparameter fission studies should be done on spontanous fission of ^{240}Pu, ^{242}Pu and ^{238}Pu, ^{241}Am, ^{243}Am, ^{244}Cm, ^{246}Cm and ^{248}Cm isotopes.

Measurement of the subthreshold fission, ^{231}Pa and ^{230}Th. These experiments give information on neutron sources for fission through the third minimum of the fission potential barrier.

3.2. Due to the cost of high quality nuclear targets for this work, the Agency should assist financially in the purchase of such targets by user groups. This might be done through the auspices of IAEA research contracts. Some financial assistance for purchase of the data acquisition facilities is needed. Similarly, some financial assistance is required for the costs of computing time on the large mainframes used in the theoretical analysis.

In addition, technology and manpower tranfer between well-equipped laboratories and less-equipped laboratories is recommended.

4. E. Fort (France) pointed out that there is a substantial background for an ambitious CRP. It will be useful to slightly enlarge the scope of the CRP by recommending at least ν_p measurements for some chosen actinides.

MECHANISMS OF FISSION NEUTRON EMISSION

H. Märten
Technische Universität Dresden, Institut für Kern- und Atomphysik
Mommsenstrasse 13, D-O-8027 Dresden, Germany

Abstract: The time evolution in fission is the starting point for discussing not only the main mechanism of fission neutron emission, the evaporation from fully accelerated fragments, but also possible secondary ones connected with dynamical features of nuclear fission. "Asymptotic" conditions as relevant for describing the particle release from highly excited, rapidly moving fragments are defined. Corresponding statistical model approaches to fission neutron emission, based on the adequate consideration of the intricate fragment occurrence probability, reproduce most of the experimental data. The remarkable influence of fission modes on neutron observables is analyzed in the framework of a macroscopic-microscopic scission point model consistent with energy conservation. Finally, chances and deficiencies for solving the mechanism puzzle are summarized.

1. INTRODUCTION

The release of neutrons in nuclear fission is strongly connected with the excitation of single-particle degrees of freedom in large-scale collective nuclear motions. Nuclear fission as a total rearrangement reaction of a quantummechanical many-body system is incompletely understood. Theoretical treatments as comprehensively reviewed by Moreau et al. /1/ reflect many capabilities for the qualitative and partially semi-quantitative description of most of the fission observables, but indicate also the present deficiencies. A brief characterization of the time evolution in fission related to particle emission is given in Section 2.

Experimental together with theoretical studies already reviewed elsewhere /2,3/ provided the basic understanding of neutron emission in fission. Accordingly, most of the fission neutrons are evaporated from fully accelerated fragments. However, the role of secondary mechanisms is still unclear. Several works in this field yielded contradictory results. Whereas complex statistical-model approaches (SMA) based on the evaporation theory (Weisskopf relation /4/) or the statistical theory of nuclear reactions (Hauser-Feshbach theory /5/), but accounting for the intricate fragment occurrence probability P depending on mass (A) and charge (Z) number, total kinetic energy (TKE), excitation energy E^*, and angular momentum J, is suitable to reproduce most of fission neutron observables (Section 3), approaches to secondary fission neutron emission are qualitative and yield only estimations of their characteristics (Section 4). The solution of this mechanism problem requires full-scale SMA calculations in comparison with complex experimental distributions to be obtained in multiparameter experiments involving fragment detection in combination with the spectroscopy of all fragment de-excitation products (neutrons and γ-rays mainly). Previous analysis procedures are discussed critically in Section 5.

In the case of sufficiently high incident energy multiple chance fission and, consequently, pre-fission neutron emission occurs. The competition between the particle and γ-ray emission channels as well as the fission channel was analyzed in the framework of a modified Hauser-Feshbach theory including pre-equilibrium emission /6,7/ and within the evaporation theory /8/. Recently the statistical multistep reaction theory has been extended to account for the fission channel in a simple approximation /9/. In particular, pre-fission neutron emission includes direct and pre-equilibrium contributions to be discussed in Section 6.

2. TIME EVOLUTION IN FISSION

2.1. From saddle to scission point

An actinide nucleus undergoing fission is characterized by the variables A_{FN}, Z_{FN}, E^*_{FN}, J_{FN}, and projection quantum number K_{FN} (FN - fissioning nucleus). These quantities define its fissility (Z^2_{FN}/A_{FN}), the fission probability (mainly via E^*_{FN}), the angular distribution of fission fragments (depending on J_{FN} and K_{FN}) and the occurrence probability $P(A,Z,TKE,E^*,J)$. Besides the influence of the transition states /10/ at both saddle points, the probability function P is mainly formed during the descent from the outside saddle point to the scission point. Whereas the potential energy at all deformation stages can be approximated by selfconsistent Hartree-Fock calculations /11/ or the macroscopic-microscopic method /12/, the time evolution of the fissioning nucleus and all its dynamic features, which is strongly related to nuclear inertia and dissipation, is still one of the most challenging topics in the field. Both time-dependent (microscopic) Hartree-Fock (TDHF) calculations /13/ and macroscopic approaches (based on surface-plus-window dissipation or stochastic forces diffusing the dynamical paths in phase space or any other) to fission dynamics /14,15/ have led to quite different pictures. According to various dynamical calculations /16-19/, which differ in regard to dissipation mechanism, the transition time between saddle and scission point is in the order of (2 - 6) 10^{-21} s. Extreme estimates /17/ ranges up to 1.3 10^{-20} s.

Phenomenologically, one can assume that the potential energy gain between saddle and scission point is the sum of a dissipative energy E_{dis} and the kinetic energy of collective degrees of freedom, whose translational part appears as pre-scission kinetic energy of the fragments E_{pre}. The first term give rise to a scission point temperature τ_{sc} influencing the microscopic terms of the potential energy. The definition of a scission point is crucial, since it is not defined by static conditions alone, but can be understood as random neck rupture /20/, since the rather small transition time for the descent from saddle to scission point hiddens the fissioning system to reach equilibrium at scission point. Scission itselfes corresponds to a rapid change of nuclear potential. Strong single particle excitations and, consequently, particle emission at scission seem to be possible (cf. Section 4.1).

For simplicity, it is, however, useful to formulate a phenomenological energy balance equation for the scission point (in the present version without the indication of the explicite dependence on mass and charge asymmetry, on deformation variables and τ_{sc})

$$Q + E^*_{FN} = \underbrace{E_{pre} + E_{coul}}_{\text{TKE}} + \underbrace{\overbrace{\sum_i E_{def}(i)}^{F} + \overbrace{E_{dis} + E^*_B}^{E^*_{sc}}}_{\sum_i E^*(i)} , \qquad (1)$$

where Q is the total energy release for the given fragmentation $(A_1/A_2;Z_1/Z_2)$. The total intrinsic excitation energy E^*_{sc} at scission is assumed as sum of E_{dis} and the excitation energy E_B^* at the second saddle. The variable F is the potential energy at scission, whose two parts, the Coulomb potential energy E_{coul} and the deformation energies $E_{def}(i)$ of the individual fragments (i), depend on the deformation (represented by a set of parameters). Eq. (1) together with the assumption of minimum F at scission may be used to deduce approximative scission point conditions defining the partition of the total available energy on both fragments /21/.

2.2. Post-scission dynamics

Besides the acceleration of the fragments in the Coulomb field starting with the initial condition E_{pre} at scission and resulting in TKE, the deformation energy dissipates into intrinsic excitation energy of the individual fragments. According to Eq. (1), $E^*(i)$ is additionally defined by a certain part of E^*_{sc}. This fraction may be calculated by thermodynamic assumptions /21/. The time evolution of these simultaneous processes, which occur within about 3 10^{-20} s after scission mainly /22/, is not well understood. At the beginning of the post-scission dissipation, which immediately follows the descent from saddle to scission point with the relevant dissipation, states far from equilibrium conditions are shortly occupied. Accordingly, non-equilibrium particle emission should be expected (cf. Section IV.2). In respect to neutron emission during fragment acceleration, the time evolution of the internal fragment dynamics is of high importance. That is, since the neutron emission time (corresponding to a certain fragment kinetic energy) defines emission kinetics and, therefore, the angular correlations between neutron and fragment.

2.3. "Asymptotic" conditions

Due to the dynamic processes discussed above, the probability function P depends on time. However, it is useful to define "asymptotic" conditions achieved after fragment acceleration (effectively finished at about 3 10^{-20}s after scission) as well as dissipation of E_{def} into intrinsic excitation energy distributed among the single particle degrees of freedom according to equilibrium. These conditions hold before any de-excitation process. Hence, we have

$$TKE = E_{pre} + E_{coul}, \tag{2}$$

$$E^*(i) = E_{def}(i) + f(i)\ E^*_{sc}, \tag{3}$$

where f(i) is the fraction of scission point excitation energy coming to fragment (i). In regard to the probability function $P(A,Z,TKE,E^*,J)$, it is emphasized that for a given nucleon number partition $(A_1/A_2;Z_1/Z_2)$ resulting in a defined Q value, a distribution in TKE and E^* appears, where the constraint

$$Q + E^*_{FN} = TKE + \sum_i E^*(i) \tag{4}$$

must be met. For fixed $(A_1/A_2;Z_1/Z_2)$ and TKE, the ratio $E^*(1)/E^*(2)$ is distributed around an average value due to phase space conditions /23,24/. Obviously, the "asymptotic" distribution $P(A,Z,TKE,E^*,J)$ is the starting point for a SMA to neutron evaporation from fully accelerated fragments.

3. NEUTRON EVAPORATION FROM FULLY ACCELERATED FRAGMENTS

3.1. Experimental informations

Fission neutron emission was already found and roughly explained in 1939, i.e. a short time after the discovery of nuclear fission (Ref. /25/ and references therein). Stimulated by urgent nuclear data needs, prompt fission neutron spectra were measured for various nuclei in the early years of nuclear technology. They were successfully described in the framework of rather simple evaporation models assuming emission from fully accelerated fragments /26-28/. First measurements of angular correlations between fission fragments and neutrons confirmed the above assumption of the main emission mechanism. Based on Bohr's and Wheeler's hypotheses, that "hydrodynamical" distortions at the scission point should cause a further component, i.e. the so-called scission neutrons, several groups performed more sophisticated experiments started in the sixties /29-33/ and continued until the present time /34-52/. Such measurements provided data on yields, energy and angular distributions of fission neutrons in correlation with fragment parameters (A,TKE). In spite of some different, sometimes contradictory conclusions, the most important result of all these works was the verification of neutron evaporation from fully accelerated fragments as the main emission mechanism. For secondary mechanisms and problems related to the analysis of experimental data, see Sections 4 - 5.

3.2. Statistical-model analysis

The adequate theoretical description of fission neutron emission should involve the complex fragment occurrence probability $P(A,Z,TKE,E^*,J)$ in order to account for the diversity of fragment configurations. Neglecting all secondary mechanisms, i.e. considering "asymptotic" conditions as discussed above, the standard statistical theory of de-excitation of highly excited nuclei can be applied to calculate fission neutron characteristics [multiplicity distributions $P(\nu)$ with the average neutron yield $\bar{\nu}$, double-differential distributions $N(E,\theta)$ in emission energy E and angle θ with reference to light-fragment direction, energy spectra $N(E)$, as well as their correlation to fragment parameters]. Such a SMA can be based on the scheme represented below. Here, the "asymptotic" fragment distribution $P(A,Z,TKE,E^*,J)$ is splitted into $P(E^*,J:A,Z,TKE)$ for fixed A, Z, and TKE and $P(A,Z,TKE)$. Note that cascade emission in steps (i) of different particles π and γ-rays is considered. The centre-of-mass (CMS) spectrum $\varphi_\pi(\varepsilon_\pi)$ is represented by the spectral emission width $\Gamma_\pi(\varepsilon_\pi:E^*,J)$ according to the Hauser-Feshbach theory /5/:

$$\varphi_\pi(\varepsilon_\pi) = \sum_i \int dE^* \sum_J P_i(E^*,J) \frac{\Gamma_\pi(\varepsilon_\pi,E^*,J)}{\sum_{\pi''} \Gamma_{\pi''}^{tot}(E^*,J) + \Gamma_\gamma^{tot}(E^*,J)}, \quad (5)$$

$$\Gamma_\pi(\varepsilon_\pi,E^*,J) = (2\pi\ \rho(E^*,J))^{-1} \sum_{J'} \rho^\pi(U_\pi,J') \sum_{l_\pi,j_\pi} T^\pi_{lj}(\varepsilon_\pi), \quad (6)$$

where ρ is the level density, and T_{lj} is the transmission coefficient for angular momentum l and channel spin j ($\vec{j} = \vec{l} + \vec{s}$) with s as the particle spin. Excitation energy U and spin J′ of the rest nucleus after particle emission is given by

$$U_\pi = E^* - B_\pi - \varepsilon_\pi, \text{ and } \vec{J} = \vec{J}' + \vec{l}_\pi + \vec{s}_\pi, \quad (7)$$

respectively (B_π - separation energy of particle π). Starting with the initial distribution $P_{i=0}(E^*,J)$, all $P_i(E^*,J)$ for $i\geq 1$ are deduced from the distribution of the preceding emission step using (7). Considering CMS anisotropy due to fragment spin J (calculated either via the Legendre polynoms $P_l^2(\cos\vartheta)$ /53/ for given l or by a semi-classical approach /54/), one obtains the double differential probability $\varphi_\pi(\varepsilon_\pi,\vartheta_\pi:A,Z,TKE)$ in CMS, which has to be transformed into the corresponding laboratory system (LS) distribution $N_\pi(E,\theta:A,Z,TKE)$ on the basis of the kinematic relations

$$\varepsilon = E + E_f - 2\ (E\ E_f)^{1/2}\cos\theta, \tag{8.1}$$

$$E = \varepsilon + E_f + 2\ (\varepsilon\ E_f)^{1/2}\cos\vartheta, \tag{8.2}$$

$$N(E,\theta) = (E/\varepsilon)^{1/2}\ \varphi(\varepsilon,\vartheta). \tag{9}$$

(E_f - fragment kinetic energy per nucleon).
Finally, the total LS emission probability is given by

$$N_\pi(E_\pi,\theta_\pi) = \sum_{A,Z} \int dTKE\ N_\pi(E,\theta:A,Z,TKE)\ P(A,Z,TKE). \tag{10}$$

Besides $P(A,Z,TKE,E^*,J)$, which is - in most cases - not known with sufficient accuracy and/or complexity, global descriptions of nuclear level densities and transmission coefficients for neutron-rich fission fragments are necessary preconditions for full-scale calculations following the scheme outlined above.

Level densities: Budtz-Jorgensen and Knitter /51/ analyzed average level density parameters a(A) for fission fragments on the basis of experimental multiparameter data. As shown in Fig. 1, these data can be well described on the basis of a semi-empirical approach including microscopic effects (shell energy, pairing energy) /55/. In this calculation, ρ was deduced as function of average rest-nucleus excitation energy obtained from cascade evaporation calculations /23/ and for average pairing energies.

Optical potential: Various global parameterizations /56-59/ of the neutron optical potential were tested /3/ within fission neutron observables calculations. Fig. 2 represents the course of the compound-nucleus formation (inverse) cross section obtained

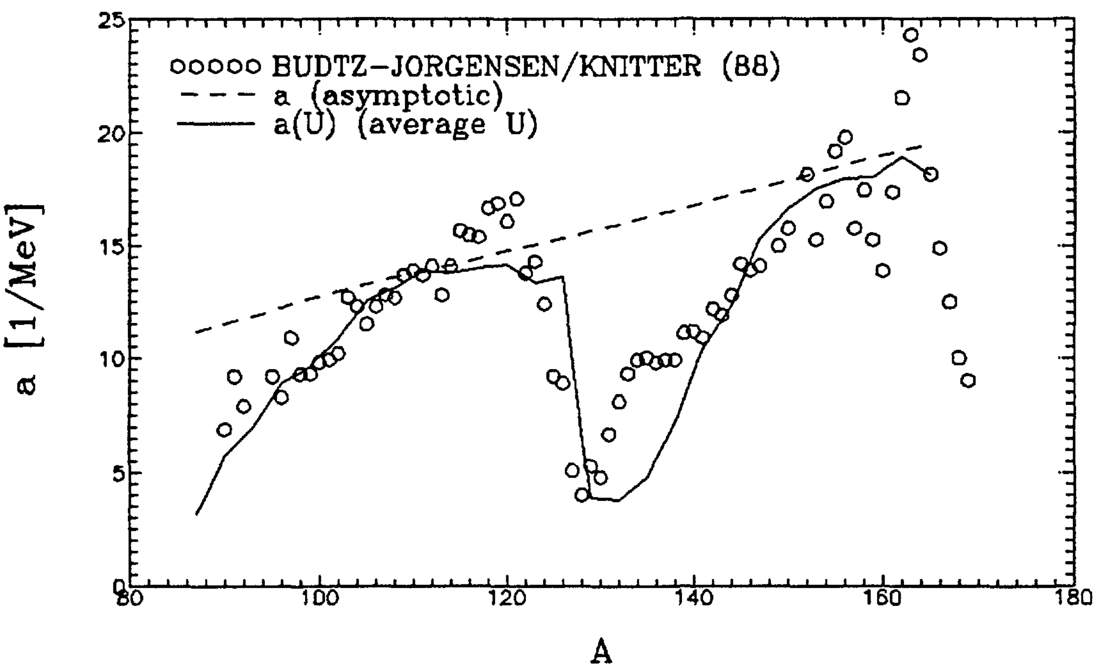

Fig. 1 Level density parameter (a) for neutron-rich fission fragments from ^{252}Cf(sf) (circles - /51/, solid line - calculation /55/ as function of average rest-nucleus energy /23/, dashed line - asymptotic value, i.e. for vanishing microscopic energies)

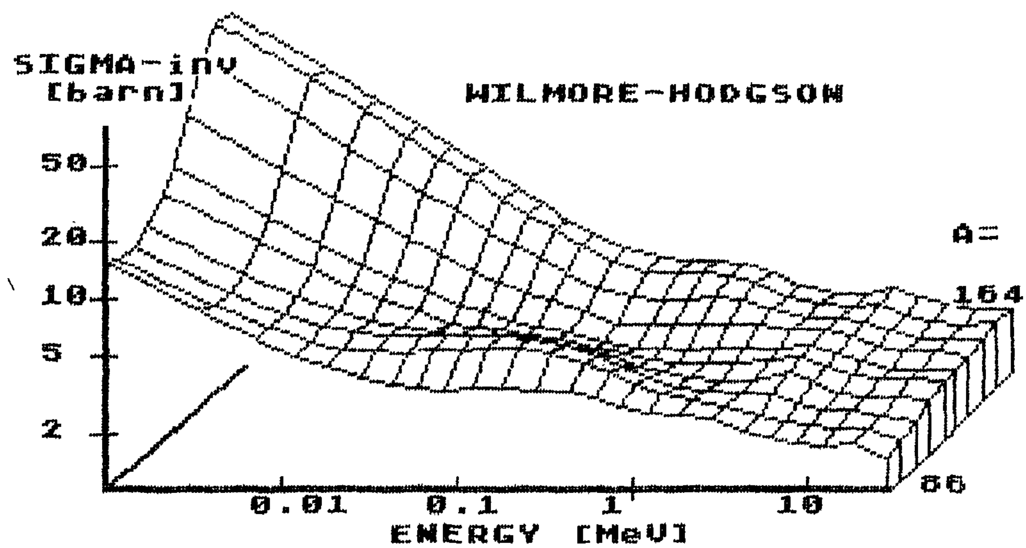

Fig. 2 Compound-nucleus formation cross section for neutron-rich fission fragments (global optical potential taken from Ref. /58/)

for fission fragments in the 87 - 165 mass number range. Note the remarkable mass number dependence at low energy, which is of importance in understanding differences in differential neutron characteristics between light and heavy fragments, e.g. at CMS energies $\varepsilon \rightarrow 0$, i.e. for $E \rightarrow E_f$ and $\theta \rightarrow 0$. Within the global optical potential parameterization, the consideration of the isospin dependence /57/ is very important for applications to neutron-rich fission fragments. However, further uncertainty factors (range of applicability concerning energy range, mass number range, reaction channels etc.) do not automatically favour such types of potential parameterization against others.

As already summarized in /3/, the idealized SMA outlined above has to be simplified to make it tractable. In particular, the fragment occurrence distribution is not known in its full complexity (even in the most promising case of ^{252}Cf(sf)). Hence, simplifications concern the fragment distribution $P(A,Z,TKE,E^{*},J)$ by reducing it to average values of the fragment variables as well as the evaporation formalism. The following types of fission neutron models are used:

Hauser-Feshbach models /60-62/ including the spin dependence of neutron emission in competition to γ-ray and charged particle release (Eqs. 5-7).

Cascade evaporation models /23,28,52/ based on the Weisskopf formula, i.e. neglection of spin effects on emission spectra.

Temperature distribution models /8,63/ assuming a distribution in rest-nucleus temperature instead of a fragment distribution in E^{*}.

Statistical Multistep Compound Theory /52/ based on master equation approach simulating dissipation after scission point and accounting for possible non-equilibrium effects (cf. Section 4.2).

Any other, more rough models not discussed here.

Besides the fundamental ansatz to describe the emission spectrum for given A, Z, E^{*} (and J), the account for $P(A,Z,TKE,E^{*},J)$ to more or less extent gives the possibility to distinguish between different models.

The Figs. 3-6 represent some examples of calculational results reproducing experimental data on energy spectra $N(E)$ and double-differential emission distributions $N(E,\theta)$ for ^{252}Cf(sf). The calculations were performed in the framework of either the Hauser-Feshbach model /62/ or the cascade evaporation (Weisskopf) model /23,52/ for a rather complex fragment distribution $P(A,TKE,E^{*})$ with $\bar{Z}(A)$ and $\bar{J}(A)$.

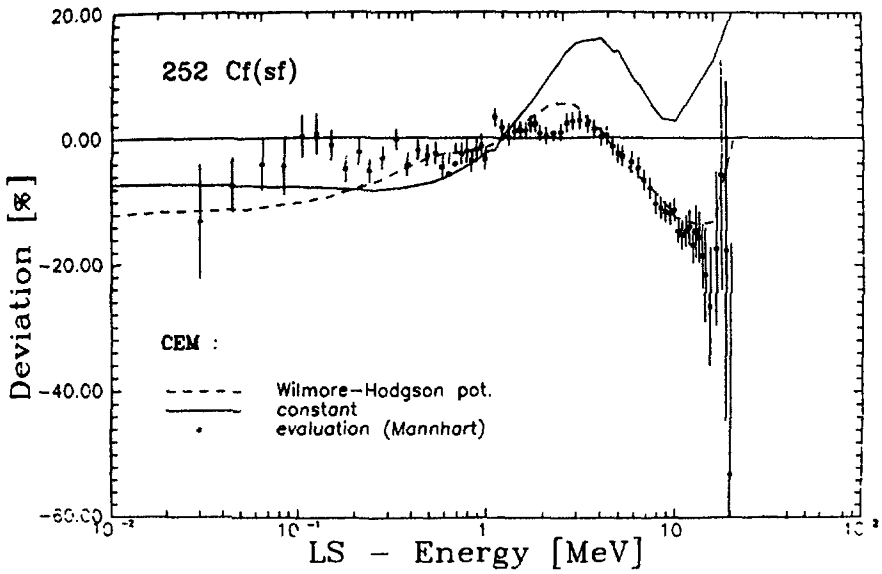

Fig. 3 The energy spectrum of neutrons from $^{252}Cf(sf)$ represented as percentage deviation D from a reference Maxwellian distribution with a "temperature" parameter T = 1.42 MeV (dots - evaluation /64/, lines - cascade evaporation calculation for global optical potential taken from /58/ as well as for constant inverse cross section of compound nucleus formation)

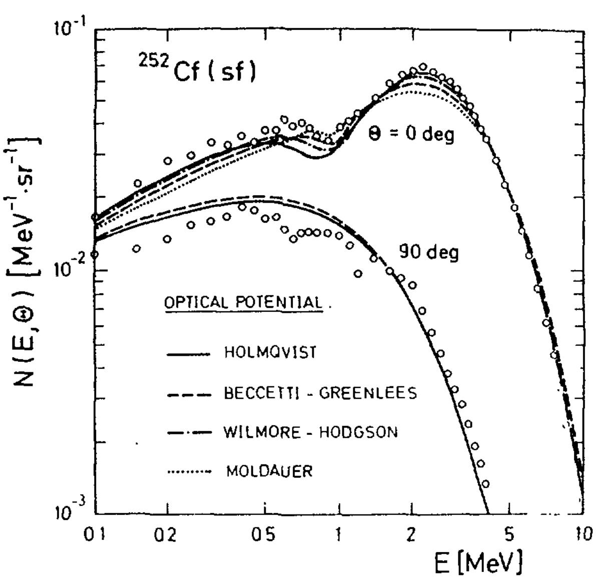

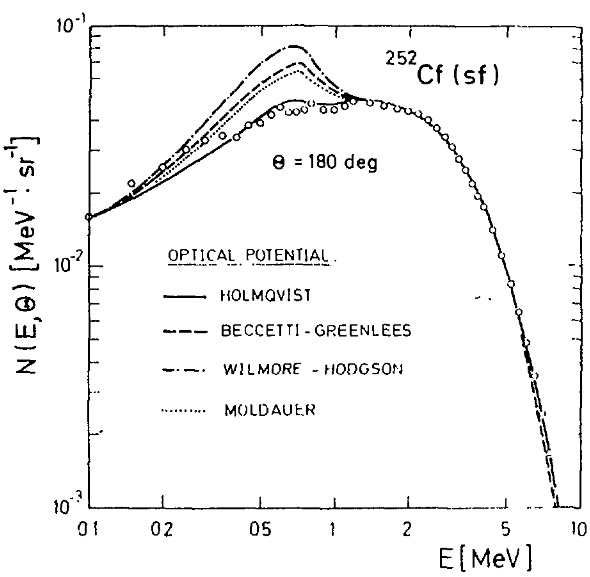

Fig. 4 Differential neutron spectra of $^{252}Cf(sf)$ neutrons at θ = 0 and 90 deg (left) and θ = 180 deg (right) (circles - experimental data /65/, lines - cascade evaporation calculation for several global optical potentials /56-59/ as indicated)

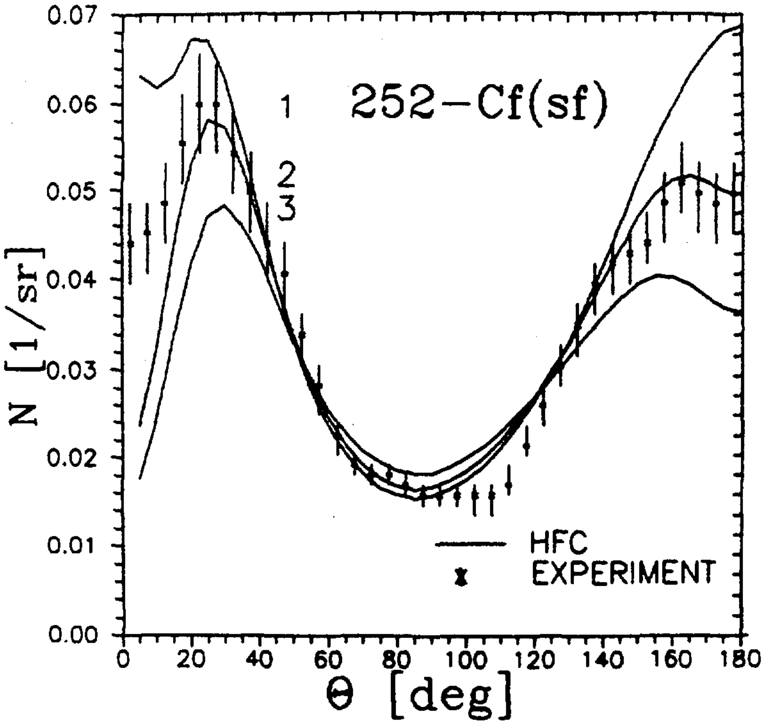

Fig. 5 Angular distribution of $^{252}Cf(sf)$ neutrons at E = 1 MeV (dots - experimental data /65/, lines - Hauser-Feshbach calculation for different choices of γ-ray emission width description /62/)

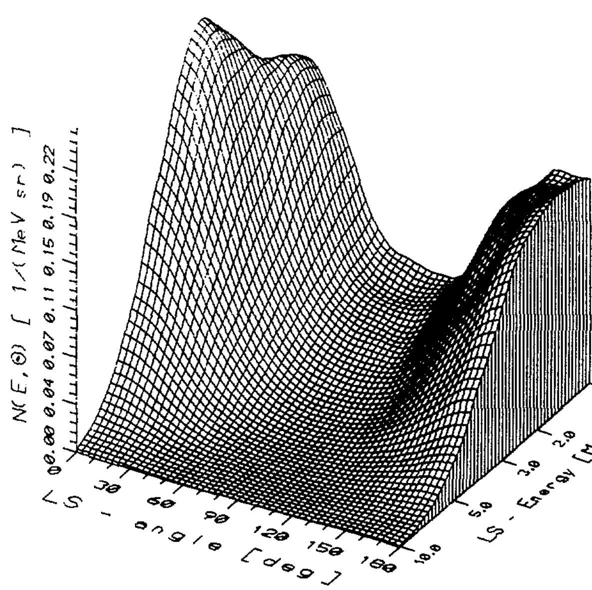

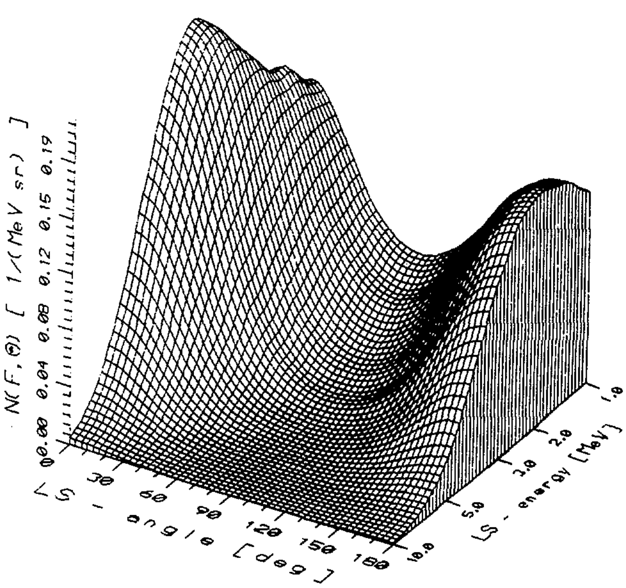

Fig. 6 Plot of the double differential distribution of $^{252}Cf(sf)$ neutron emission $N(E,\theta)$ (left - experimental data /65/, right - cascade evaporation calculation /52/)

The CMS neutron spectra are commonly fitted to the ansatz

$$\varphi(\varepsilon) = [\ T^{\lambda+1}\ \Gamma(\lambda+1)\ ]^{-1}\ \varepsilon^{\lambda}\ \exp(-\varepsilon/T) \tag{10}$$

including the "hardness" or "temperature" parameter T and the "shape" parameter λ.

As discussed elsewhere /66/, λ as relevant for low CMS energy defines the course of the LS $N(E,\theta)$ distribution for $E \to E_f$ and $\theta \to 0$ (i.e. $\varepsilon \to 0$, cf. (8) and (9)). The cascade evaporation model reproduces fairly well the data deduced from experiment /51/. Note that (due to the rough approximation of the spectral shape by (10)) the parameter λ deduced from the whole spectrum differs from the value λ obtained by fitting the low-energy spectrum part. Whereas the first one is determined by the level density description and $P(E^*)$, the second one depends on optical potential, the degree of cascade emission, and the strength of γ-ray emission at E^* above neutron separation energy. The Figs. 7-9 represent calculational data in comparison with experimental ones.

The agreement between experimental data and SMA calculations confirms the assumption that (at least most of) fission neutrons are evaporated from fully accelerated fragments. However, the

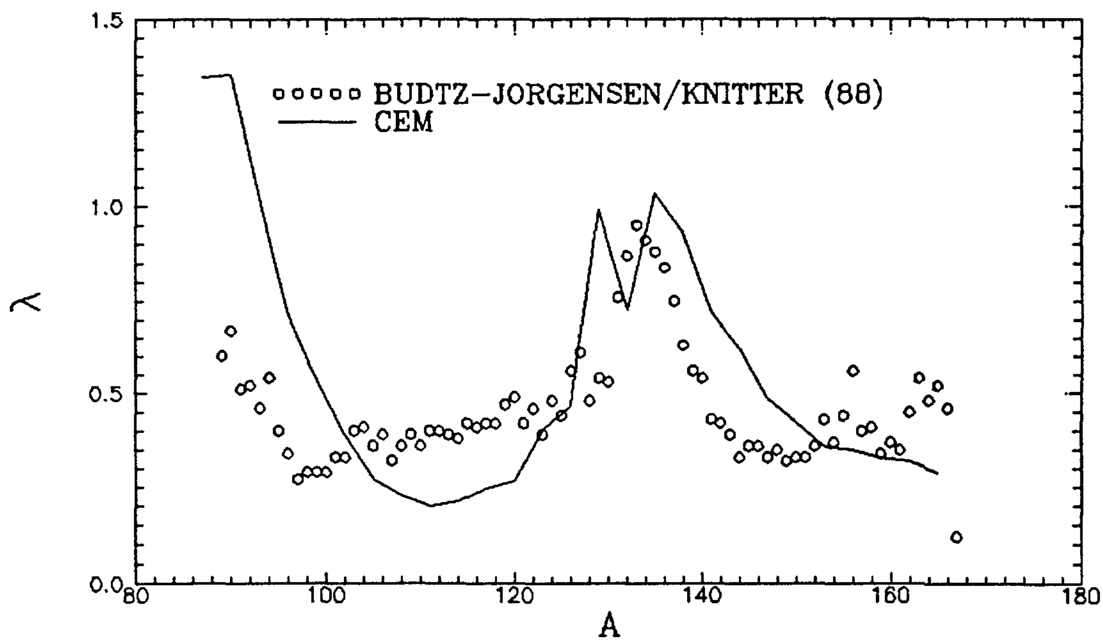

Fig. 7 CMS spectral "shape" parameter λ for $^{252}Cf(sf)$ neutron emission (dots - experimental data /51/, line - cascade evaporation calculation /66/)

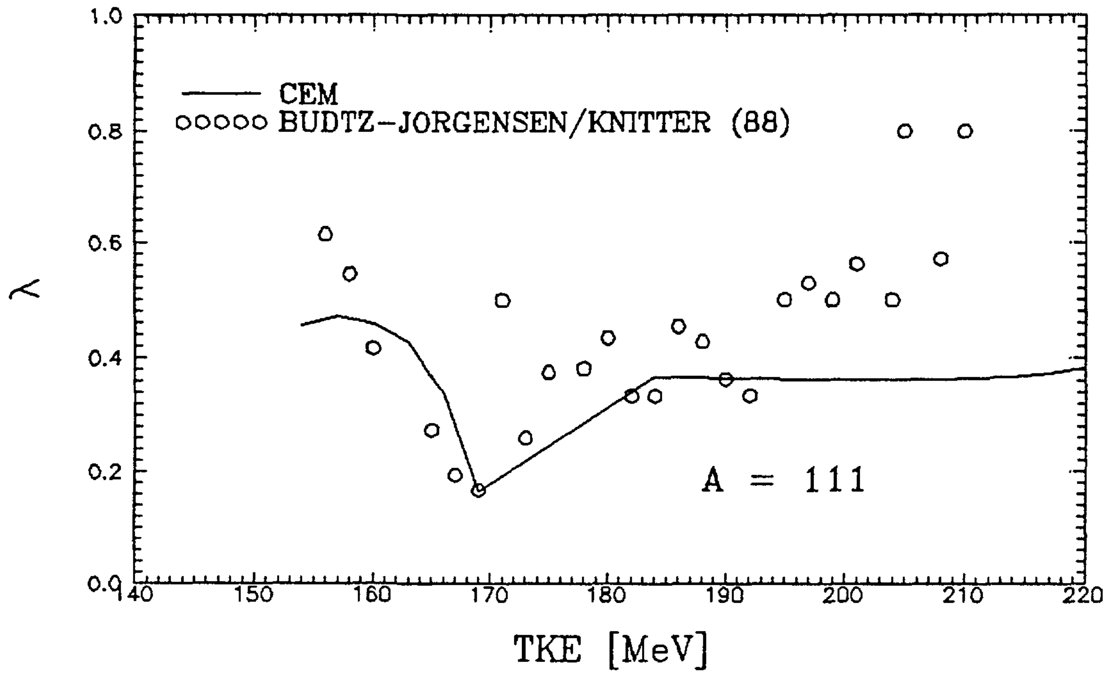

Fig. 8 The same as for Fig. 7, but for fixed A = 111 and in dependence on TKE

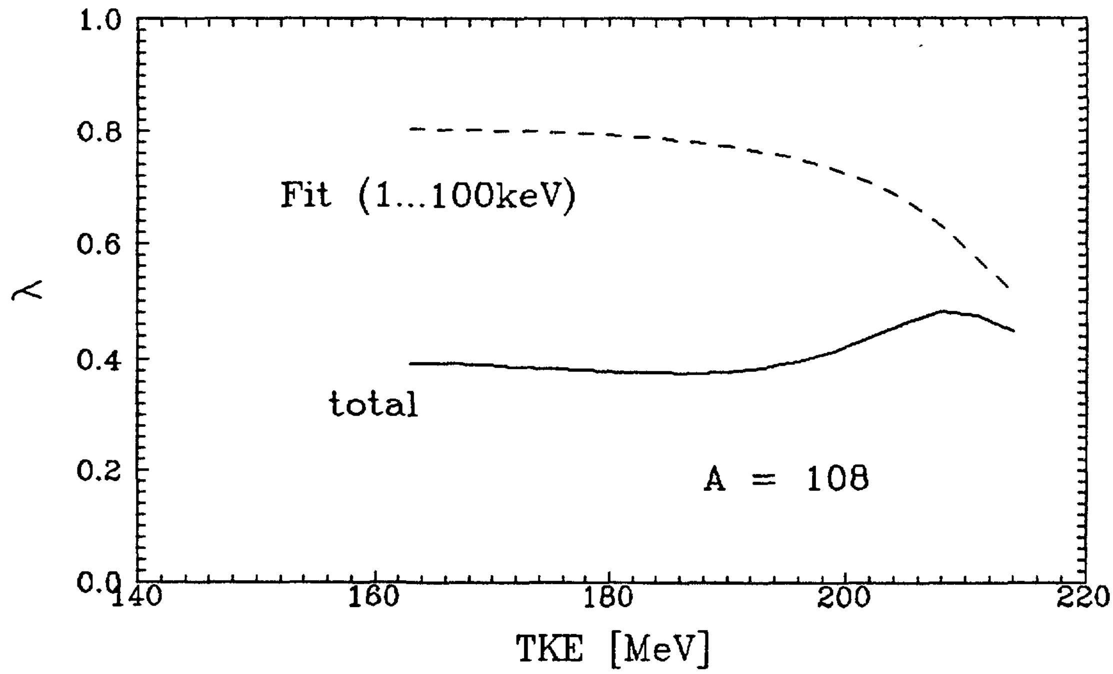

Fig. 9 Spectral "shape" parameter λ deduced from the total CMS 252-Cf(sf) neutron spectrum on the one side and fitted to the low-energy region (1 - 100 keV) on the other side (cascade evaporation calculation). Note that $\lambda > 0.5$ (as obtained for low emission energy) causes a dip in the $N(E,\theta)$ distribution at $E \to E_f$ and $\theta \to 0$ (cf. Fig. 6).

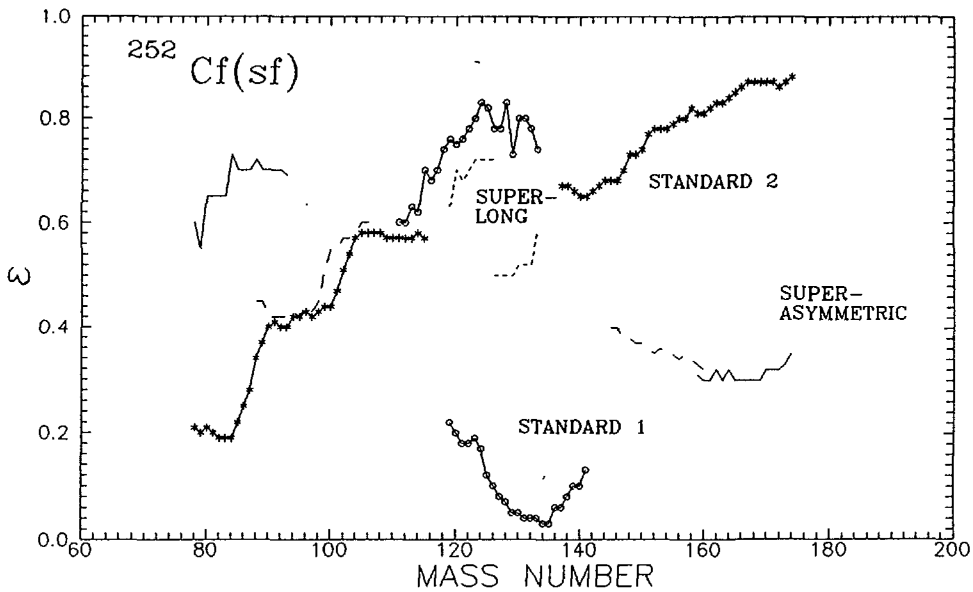

Fig 10 Position of the extrema in the scission point potential energy surface as function of individual fragment deformation ϵ. These extrema correspond to the so-called fission modes. The denotation corresponds to that one of Brosa /68/.

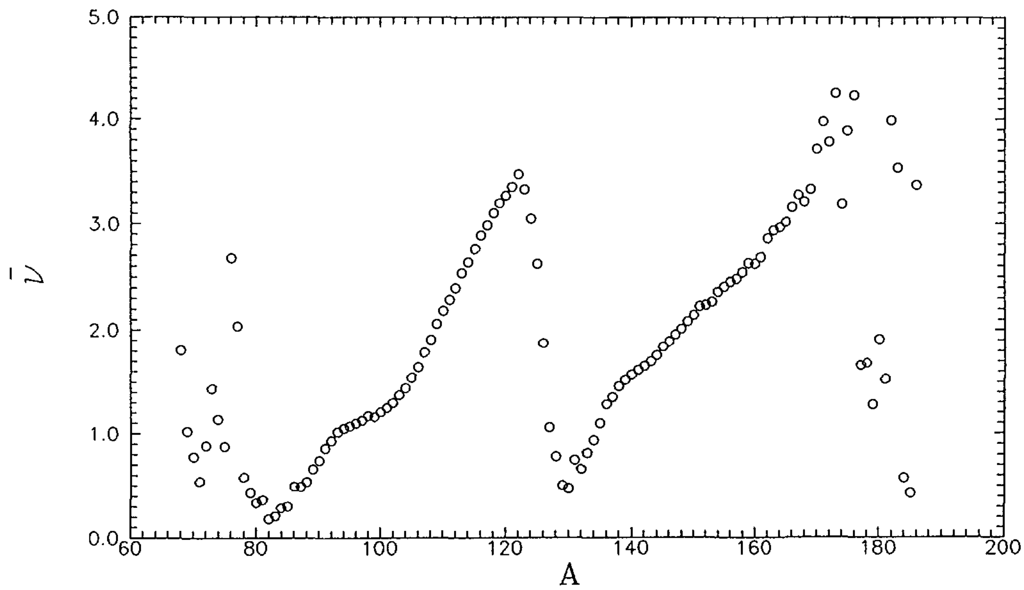

Fig. 11 Average neutron multiplicity versus fragment mass number for 252-Cf(sf) (dots - experimental data /51/). The abbreviations indicate the fission modes forming the triple saw-tooth (cf. Fig. 10).

calculational examples shown above were based on fragment occurrence distributions deduced from experimental data on fragment yields, neutron multiplicity distributions and fission γ-rays /23/. The prediction of P(...) on theoretical basis involves rather large uncertainties. Nevertheless, it can be used for qualitative studies as shown below.

3.3. Fission modes and their influence on neutron observables

The multimodal fission model by Brosa et al. /67/ predicts preferred fission channels (corresponding to paths, i.e. ridge lines, in potential energy surface covering the range from saddle to scission point). Their appearance is the reason for the saw-tooth like neutron multiplicity curve $\bar{\nu}(A)$ /68/. Already in the framework of a macroscopic-microscopic scission point model with account for energy balance (1) /21a/ fission modes may be deduced. They correspond to extrema in the potential energy surface in the deformation space close to scission point. Within the ε-parameterization /69/ of deformed fragments at scission, the positions of these extrema have been determined as function of individual fragment deformation ε at scission point. The result is represented in Fig. 10. Accordingly, average neutron multiplicity $\bar{\nu}(A)$ reflects the occurrence of the fission modes as function of mass asymmetry. In particular, the triple saw-tooth measured by Budtz-Jorgensen and Knitter /51/ can be explained (as already done by Brosa). Results are shown in Fig. 11.

Finally, we discuss the influence of fission modes on the distribution in E^* for A = 132, i.e. the nearly double-magic fragment. It arises in the standard 1 fission mode mainly. However, a competing fission channel for this mass split is standard 2. Fig. 12 represents the distribution $P(E^*)$ obtained in

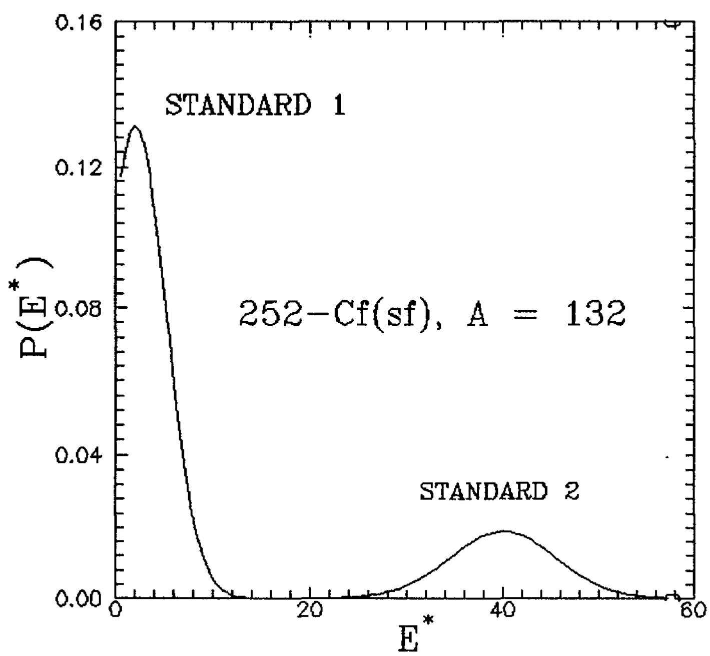

Fig. 12 Calculational distribution $P(E^*)$ for the fragment with A=132 from 252-Cf(sf)

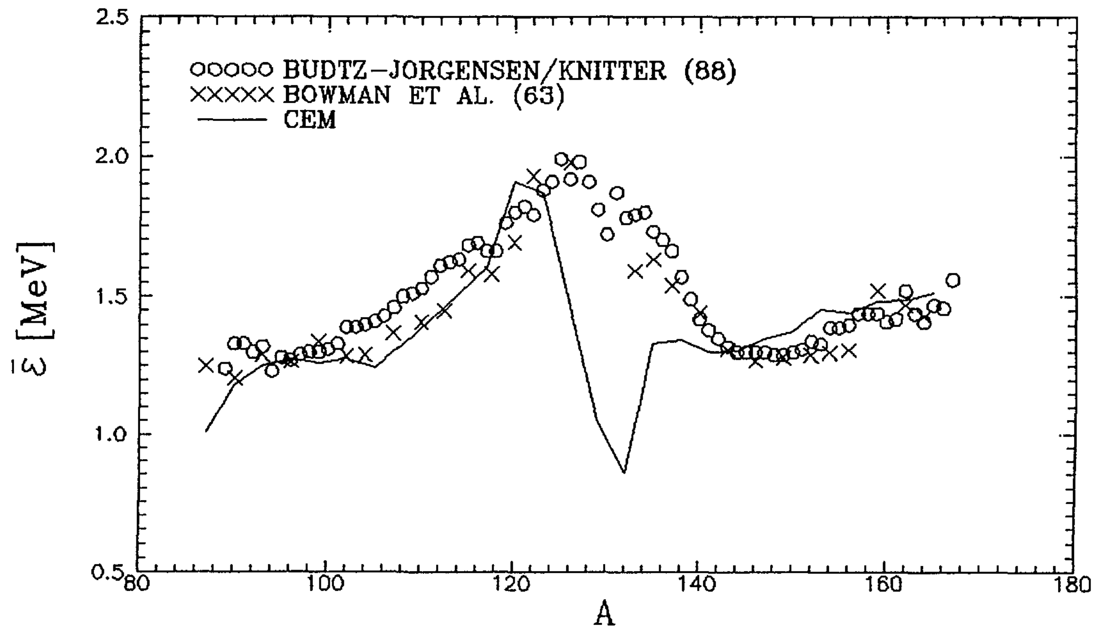

Fig. 13 Average CMS emission energy of neutrons from ^{252}Cf(sf) as function of fragment mass number (dots - /51/, crosses - /32/, line - cascade evaporation calculation)

the framework of the above scission point model. It shows a high-energy component due to standard 2. Its yield is strongly parameter dependent. It should be taken as an qualitative picture. However, this appearance gives a possible explanation of the old discrepancy between measured average CMS emission energies of neutrons from ^{252}Cf(sf) and evaporation calculations for A around 132 (Fig. 13).

4. "SECONDARY" MECHANISMS

The most challenging question in fission neutron mechanism studies concerns any deviations from the "normal" one, which are due to "non-asymptotic" conditions.

4.1. Scission neutrons

Started in the early sixties, several groups /32-36/ analyzed multiparameter data on fission neutron emission, e.g. angular inclusive or exclusive distributions, in order to derive informations about scission neutrons. The analysis procedures were commonly based on the assumption that

(i) scission neutrons are emitted isotropically in LS, and

(ii) simple evaporation ansatzes with parameters deduced from the experiment (!) describe the "normal" component due to statistical neutron emission from fully accelerated fragments.

In most cases, the enhancement of the θ=90 deg data (either yield or spectral distribution) with reference to the evaporation calculation was interpreted as due to scission neutrons. Their total yield was found in the range between 0 % /35/ and 25 % /37/. Further studies included the investigation of scission neutron yield as function of TKE. Here, an increase /43/, independence /37/ as well as decrease /42/ was found by different authors. Contradictory results were also published about the average emission energy of scission neutrons: 1.65 MeV /42/, 2.0 MeV /44/, 2.4 MeV /37/, and 2.6 MeV /32/ (for ^{252}Cf(sf)). More recent studies indicate that the scission neutron yield is very small (according to /70/, $\bar{\nu}_{sc}$ = (0.01 ± 0.003), i.e. about 0.27 %, with an average emission energy of 0.4 MeV for ^{252}Cf(sf)) or vanishing /50/ (estimation of a 5 % upper yield of secondary neutrons accounting for theoretical as well as experimental uncertainties). A brief evaluation of analysis procedures will be given in Section 5.

The theoretical understanding of particle emission close to scission point is still a challenging problem. After a more general discussion by Stavinsky /71/, Fuller /72/ was the first who studied the effect of single-particle excitation due to rapid changes of the nuclear potential during the descent from saddle to scission point. In /73/, calculations were performed for more realistic potentials. However, the strong dependence of the calculated particle yields on input parameters (e.g. time constants) do not allow for any definite conclusions about this mechanism. Rubchenya /74/ investigated single-particle excitations due to the snatching of a strongly deformed fragment just after scission. Consequently, scission neutrons are expected for scission configurations with high deformation of at least one fragment. Based on a similar picture, Mädler /75/ proposed the catapult mechanism and studied it within time-dependent Hartree-Fock calculations. The two-centre shell model connected with the assumption of an "activated" particle was the basis for the study by Milek et al. /76/. The angular distributions calculated in this work are clearly not isotropic, but exhibit an interference structure. These results are in contradiction with the previous assumption that scission neutrons are an isotropic component /32/.

4.2. Neutron emission during fragment acceleration

The scission neutron mechanisms proposed by Rubchenya, Mädler, and Milek et al. must be classified into a time scale just after scission, i.e. these are, strictly speaking, part of neutron emission during fragment acceleration. In general, this component firstly discussed by Eismont /77/ and studied by Pik-Pitchak /78/ within a simple evaporation approach ("abrupt" dissipation limit) has to be separated from the main evaporation mechanism because of different kinematic conditions and other excitation states in the dissipating fragments. Earlier works were based on the assumption that the asymptotic excitation energy is already available at scission point /78,79/ (i.e. "abrupt" dissipation) and that neutrons are evaporated from thermal equilibrium. This gives rise to an enhancement of neutron emission in equatorial direction ($\theta \cong$ 90 deg). Considering the post-scission dynamics studied by Samanta et al. /80/, different versions of characteristic dissipation time scales were assumed in the framework of a time-dependent cascade evaporation model in /81/. It was shown that the influence of the neutron emission during fragment acceleration on the total distribution $N(E,\theta)$ is strongly dependent on the characteristic dissipation time. Within the "moderate" limit /80/ ("slow" dissipation), neutron emission is reduced at θ close to 90 deg because of the "weak" CMS spectra in the time range up to about 5 10^{-20} s after scission. The opposite effect appears assuming "abrupt" dissipation (as already discussed). Neutron evaporation during fragment acceleration is illustrated in the Figs. 14-16.

The figures show clearly that the emission component of neutrons appearing during fragment acceleration is strongly dependent on dissipation mechanism, which is, however, not well understood. Hence, the effect studied gives rise to principal theoretical uncertainties of fission neutron calculations and, consequently, of mechanism studies.

A statistical description of neutron emission during fragment acceleration within multistep reaction theory was firstly proposed in /52/. According to Eq. (3), the fragments at scission point are

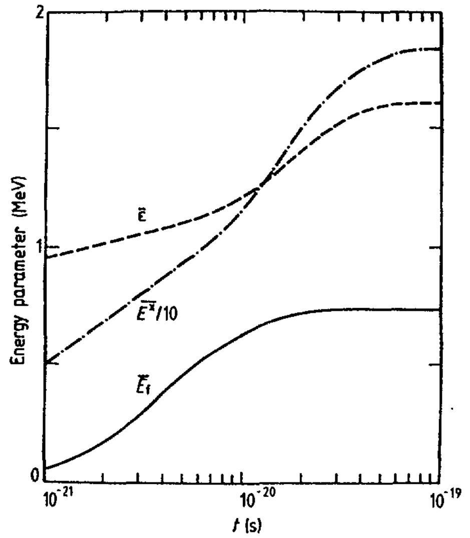

Fig. 14 Kinetic energy per nucleon and excitation energy of symmetric fragments from 252-Cf(sf) and average CMS energy of neutrons as function of time after scission /81/

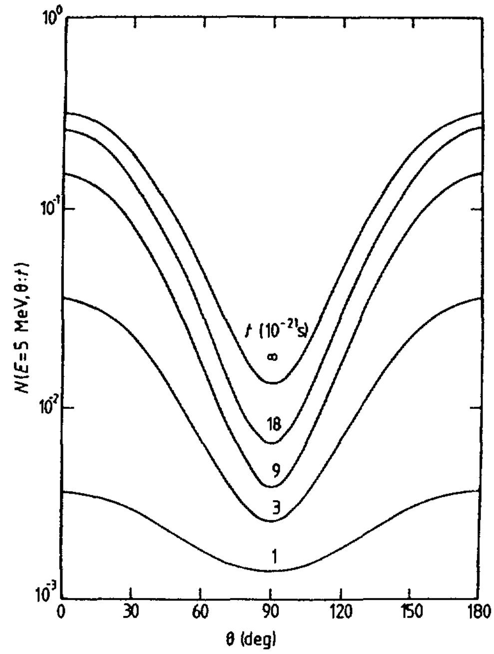

Fig. 15 Angular distribuzion of neutrons for fixed LS energy (E = 2 MeV) as function of t /81/

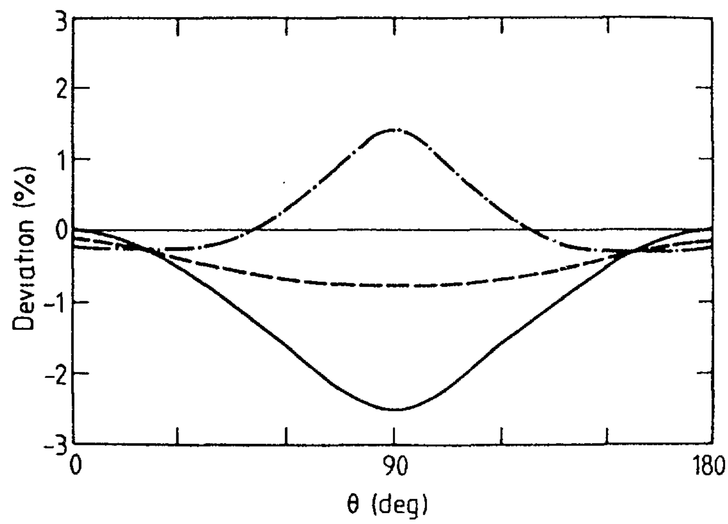

Fig. 16 Percentage deviation of the total angular distributions of E = 2 MeV neutrons from the "asymptotic" SMA calculation. Calculations were performed for "abrupt" (solid), "fast" (dashed), and "moderate" (dashed-dotted) dissipation /81/.

characterized by deformation energy $E_{def}(i)$ and a certain fraction f(i) of intrinsic excitation energy E^*_{sc} available at scission. In order to simulate an initial distribution $p_o(n)$ in exciton number n one may assume

$$p_o(n) = \alpha\, \delta_{nn_o} + (1-\alpha)\, \delta_{n\bar{n}} \tag{11}$$

with the initial exciton number (doorway state) n_o as the starting condition for dissipation of E_{def} into intrinsic excitation energy, and $\bar{n}$ as the average exciton number corresponding to the the fraction $f(i)E^*_{sc}$, which is assumed to be in thermal equilibrium. The fraction α is given by the ratio

$$\alpha = E_{def} / (E_{def} + f\, E^*_{sc}) = E_{def} / E^*. \tag{12}$$

It can be deduced in the framework of an energy partition model (scission point model) with account for energy conservation as proposed in /63,82/. The statistical multistep reaction theory /83,84/ can be applied to the present problem. The statistical multistep compound part (SMC)

$$\varphi^{SMC}(\varepsilon) \sim \sum_n \tau_n/h \left[\Gamma_n^{(o)\uparrow}(\varepsilon) + \Gamma_n^{(-)\uparrow}(\varepsilon) \right] \tag{13}$$

as evident here is described on the basis of the master equation (in time-integrated form)

$$- h\, p_o(n) = \Gamma_{n-2}^{(+)\downarrow}(\varepsilon)\, \tau_{n-2} + \Gamma_{n+2}^{(-)\downarrow}(\varepsilon)\, \tau_{n+2} - \Gamma_n\, \tau_n \tag{14}$$

leading to the average lifetime τ_n of the exciton state n. The damping width $\Gamma^{\downarrow}$ and the escape width $\Gamma^{\uparrow}$ enter the equations for exciton number changes $\Delta n = +2$, 0, and -2 corresponding to the superscripts (+), (0), and (-), respectively. The total width Γ_n is the sum of all damping and escape width. Within the closed-form SMC approach applied here, all matrix elements for bound-bound transitions I^2_{BB} cancel exactly in the sum of Eq. (13), since the matrix elements for bound-unbound transitions defining the escape widths are represented in terms of I^2_{BB}. Hence, the shape of the SMC spectrum is independent of I^2_{BB}, but is mainly determined by the single-particle state density. This SMC approach has successfully been verified (cf. applications to nuclear reactions up to energies of about 100 MeV /84/ together with the description of the statistical multistep direct part). The SMC approach to fission neutron emission was tested at first assuming the equilibrium limit (emission from fully accelerated fragments). An example is shown in Fig. 17.

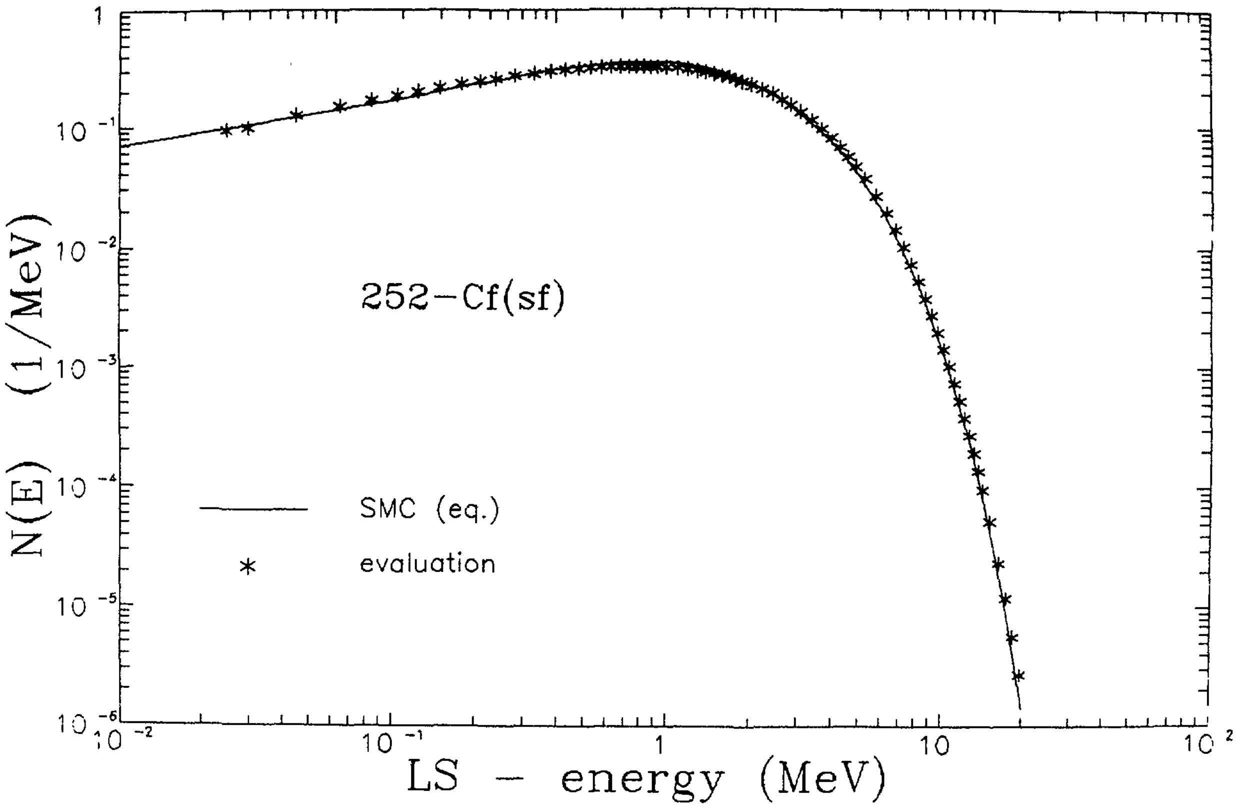

Fig. 17 SMC spectrum of $^{252}Cf(sf)$ neutrons (equilibrium limit) in comparison with Mannharts /64/ evaluation (taken from /52/)

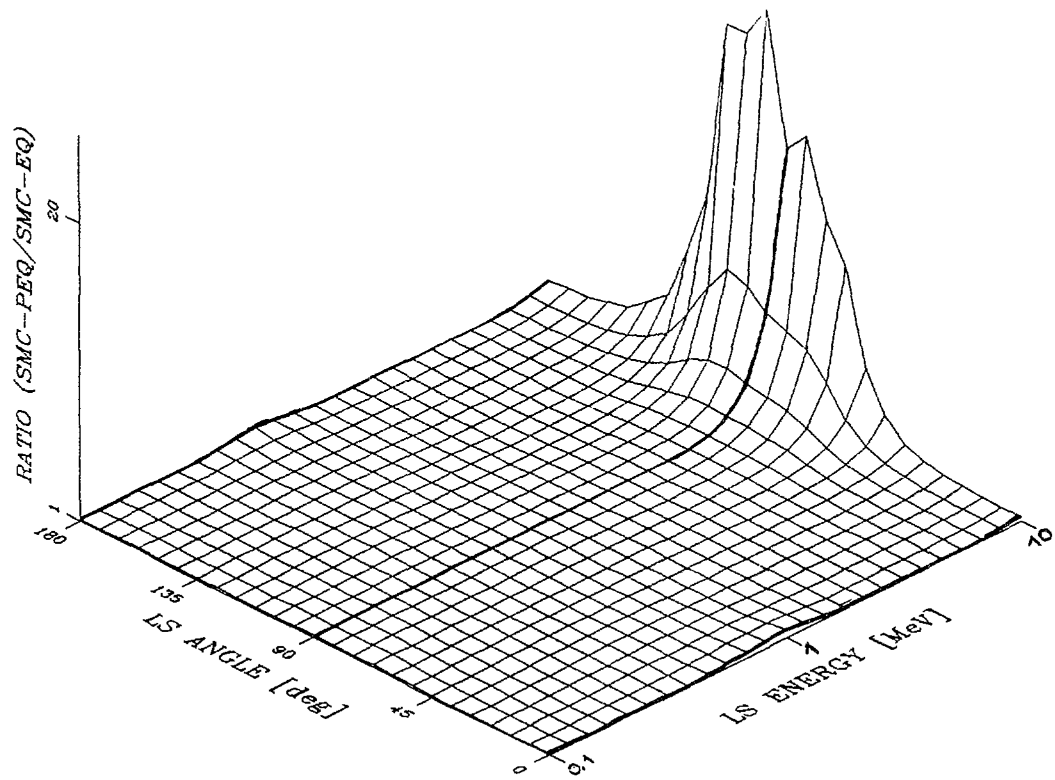

Fig. 18 Ratio of SMC to SMC(eq) calculation for $^{252}Cf(sf)$ in the LS variable field (E,Θ)

The SMC results including preequilibrium emission during fragment acceleration, which were obtained with account for CMS-LS transformation as function of time after scission, do not significantly differ from the equilibrium limit SMC(eq) but in equatorial direction and at high energies. This fact is illustrated in Fig. 18. The LS variable region at θ close to 90 deg and at high emission energy is characterized by a very low emission probability, where experimental data exhibit rather large uncertainties. Recent measurements /50,51,85/ indicate that a preequilibrium component is probably existing. However, a clear confirmation of this effect is still open.

4.3. Neutrons from ^{5}He-decay after ternary fission events

Neutron release in nuclear fission after the decay of ^{5}He nuclei was studied by Cheifetz et al. /86/. However, ternary fission events with ^{5}He production is very rare. About 11 % of α particles from ^{252}Cf(sf) fission are originally released as n-unstable ^{5}He nuclei which decay with a halflife of about 8 10^{-22} s /86/. Calculations were performed /2/ assuming isotropic decay in CMS, a time-dependent distribution of ^{5}He kinetic energy, and an angular distribution of ^{5}He nuclei with reference to fission axis as for ^{4}He. The result is shown in Fig. 19. As to be expected, the angular distribution is pronounced at equatorial direction. The course of the 1 MeV angular distribution is caused by kinematic effects.

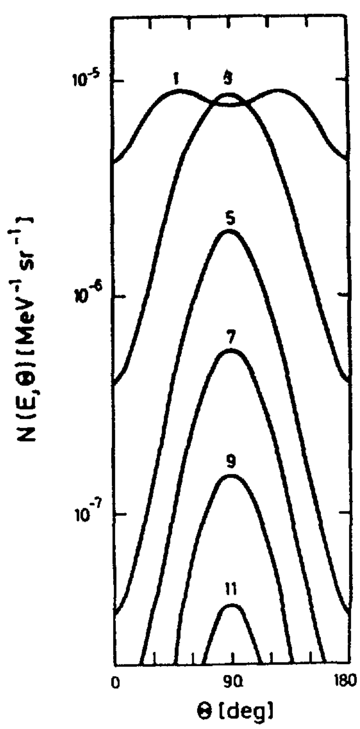

Fig. 19 Calculated angular distribution of neutrons from 5-He decay (parameter - LS energy [MeV])

Comparing these results with the total distribution of fission neutrons one can see that this component is less important.

5. THE MECHANISM PUZZLE - CHANCES AND DEFICIENCIES

In summary, it is emphasized that mechanisms of neutron emission in low-energy fission other than evaporation from fully accelerated fragments are really secondary. Deviations of differential (exclusive) experimental data from SMA predictions are commonly a consequence of non-adequate assumptions concerning the fragment distribution P (in particular, drastic variable averaging), sometimes neglection of fission mode influences as discussed above and rough CMS spectrum approximations. Only after clarifying these circumstances, one should draw definite conclusions about any secondary mechanisms. The derivation of CMS spectrum parameters from experimental data and the application of such (rough) spectrum ansatzes to describe differential LS emission probabilities as done in several previous works must be evaluated as at least crucial. Chances to get more informations about fission neutron mechanisms should be seen in combining further precise exclusive measurements of multiparameter fission neutron data with detailed theoretical descriptions on the basis of full-scale fragment distributions as discussed in this work.

6. MULTIPLE-CHANCE FISSION

At neutron incident energy above about 6 MeV, multiple chance fission reactions (n,xnf) appear in neutron induced reactions of actinide nuclei. The neutrons emitted before, but in coincidence with fission are called pre-fission neutrons. Their emission mechanisms are identical to those known from nuclear reaction studies. Besides equilibrium emission described by the use of statistical methods (Hauser-Feshbach, Weisskopf-Ewing, or any other), pre-equilibrium emission and direct processes appear. From the energetic point of view, the only one condition for a multiple chance fission is the constraint that the rest excitation energy after one (or more) neutron emissions is above the fission barrier B_f. The partial fission cross sections together with the pre-fission neutron spectra were described within the evaporation limit /8/ or by using Hauser-Feshbach theory extended by a pre-equilibrium description /6,7/ (code STAPRE). Recently, Polster /9/ proposed a method for including the fission channel in the statistical multistep reaction theory of Kalka /84/. Here, fission is a further competing channel within SMC. The exciton-number dependent fission escape widths were deduced on the basis of statistical arguments:

$$\Gamma^{\uparrow}_{nf}(E^{*}_{FN},E') = \rho_n(E^{*}_{FN}-B_f-E') \,/\, [\, 2\pi\, \rho_n(E^{*}_{FN})\,] \tag{15}$$

with E′ as the energy of the collective fission degree of freedom. Here, E^{*}_{FN} is the excitation energy of the actinide compound system decaying either by particle (neutron) emission, γ-ray emission or fission. Results are presented for neutron induced fission of ^{238}U in Fig. 20 and 21.

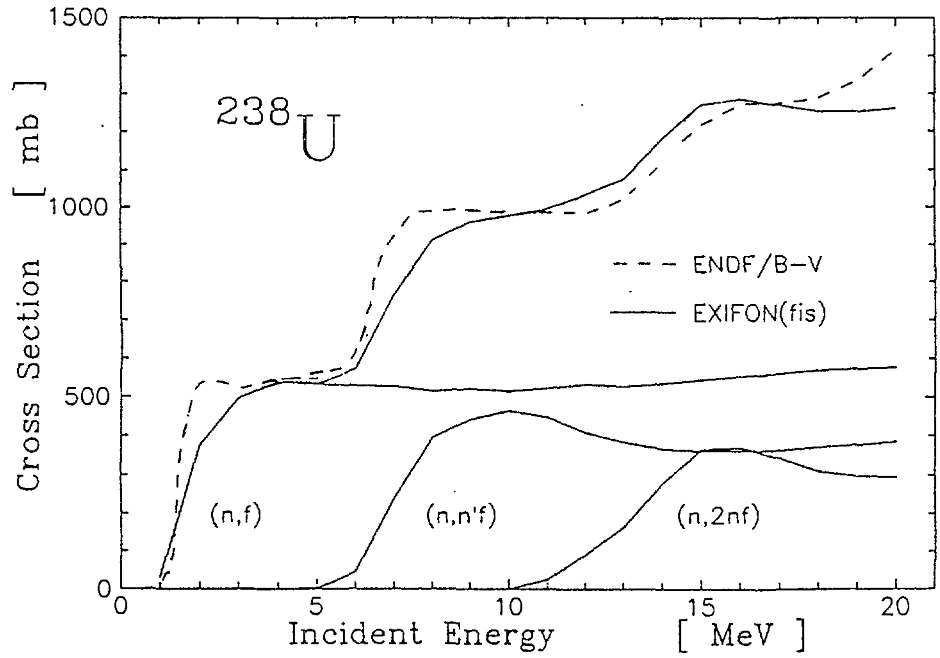

Fig. 20 Fission cross section for $^{238}U(n,xnf)$. Calculated results obtained within statistical multistep reaction theory extended by the fission channel are compared with ENDF/B-V data.

The fission neutron spectrum for ^{238}U + n (14.7 MeV) consists of three partial post-fission neutron spectra calculated by the use of FINESSE /63/ (on the basis of an macroscopic-microscopic energy partition model including mass asymmetry dependence) as well as the pre-fission neutron spectra from the (n,nf) and the (n,2nf) reaction obtained within EXIFON (statistical multistep reaction theory code /84/) extended by the fission channel. The calculated data are in good agreement with measured results.

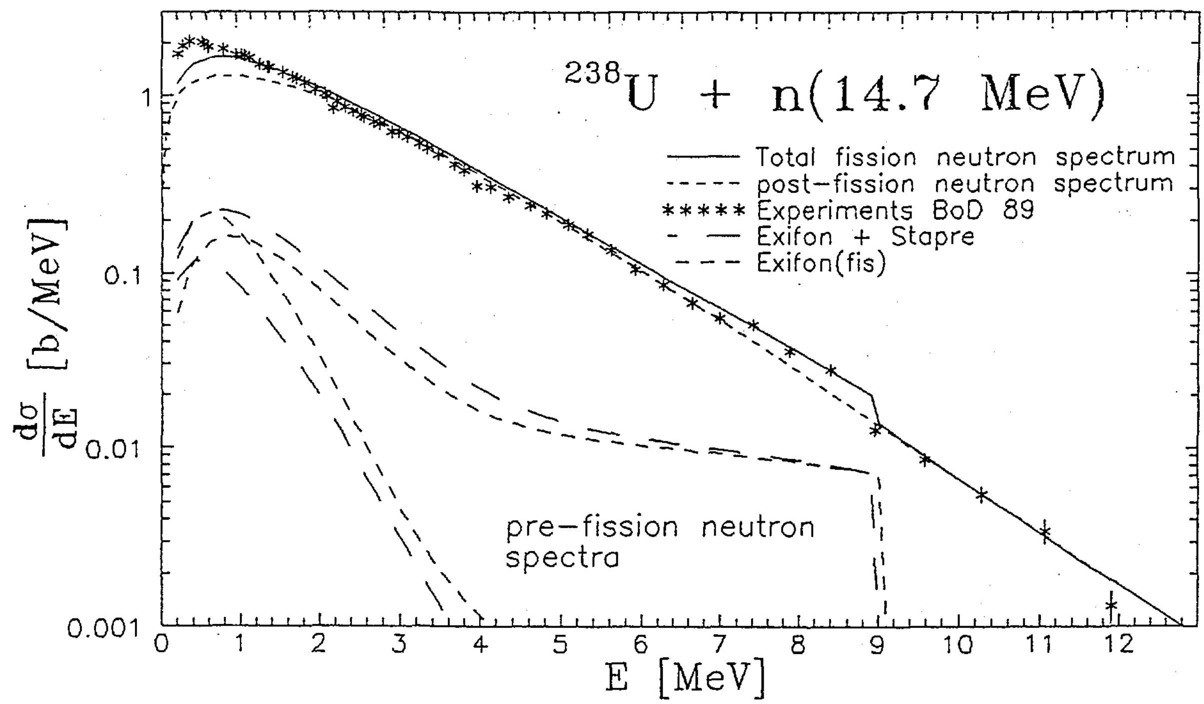

Fig. 21 ^{238}U fission neutron spectrum at 14.7 MeV incidence energy (* - /87/). EXIFON results are presented for two versions: (i) EXIFON including renormalization on the basis of STAPRE partial fission cross sections, (ii) EXIFON with fission channel.

7. SUMMARY

The present review on mechanisms of fission neutron emission started with a brief discussion of dynamical aspects in nuclear fission, since neutron release in fission is strongly connected with the time evolution of the fissioning/scissioning system. Whereas fission neutron observables are well reproduced on the basis of statistical model approaches assuming equilibrium emission from fully accelerated fragments, all possible mechanisms appearing in time scales close to scission point are less understood. At present, it is not possible to draw any definite conclusions about the features of secondary mechanisms, e.g. in quantitative manner. However, several theoretical works discussed in this paper give hints about main characteristics. The representation of the SMA outcomes were mainly based on results obtained at TU Dresden. Nevertheless, the present review gives a general evaluation of experimental and theoretical work in the field.

Clearly, post-fission neutron emission is mainly due to evaporation from fully accelerated fragments. The present status of our knowledge about secondary mechanisms is still crucial.

However, it is justified to consider only equilibrium from fully accelerated fragments in calculations for practical purposes (provided that the main characteristics like the complex fragment occurrence probability are adequately accounted for).

Finally, it is pointed out that any investigations of fission neutron emission mechanisms have to involve sufficient complexity and accuracy in experiment and theory in order to avoid nonreliable conclusions. Any results should be carefully evaluated considering experimental as well as theoretical uncertainties.

References

/ 1/ J. Moreau and K. Heyde, "Theoretical Models of Mass Distributions", Chapter 7 of the "Nuclear Fission Review", ed. C. Wagemans, in press

/ 2/ H. Märten et al., Proc. XVth Int. Conf. on Nuclear Physics - Nuclear Fission, 11 - 15 Nov 1985, ZfK-592 (1986), p. 1

/ 3/ H. Märten, Proc. of the Workshop on Applied Nuclear Theory and Nuclear Model Calculations for Nuclear Technology Applications, Trieste, 15 Feb - 19 Mar 1988, ed. M.K. Mehta and J.J. Schmidt, World Scientific (1989), p. 850

/ 4/ J.M. Blatt and V.F. Weisskopf, Theoretical Nuclear Physics (New York, 1952)

/ 5/ W. Hauser and W. Feshbach, Phys. Rev. 87 (1952) 366

/ 6/ M. Uhl and B. Strohmaier, Report IRK-76/01, IRK Vienna (1976); and Program Manual for STAPRE code, NEA Data Bank (1981)

/ 7/ A.V. Ignatyuk et al., Yad. Fiz. 47 (1988) 355

/ 8/ D.G. Madland and J.R. Nix, Nucl. Sci. Eng. 81 (1982) 213

/ 9/ D. Polster, Proc. XXth Int. Conf. on Nuclear Physics, 12 - 16 Nov 1990, Gaussig near Dresden, in press

/10/ S. Bjornholm and J.E. Lynn, Rev. Mod. Phys. 52 (1980) 725

/11/ J.F. Berger et al., Nucl. Phys. A428 (1984) 23c

/12/ V.M. Strutinsky, Nucl. Phys. A 502 (1989) 67c

/13/ J.W. Negele, Rev. Mod. Phys. 54 (1982) 913

/14/ G.D. Adeev and V.V. Pashkevich, Nucl. Phys. A 502 (1989) 405c

/15/ H.A. Weidenmüller, Nucl. Phys. A 502 (1989) 387c

/16/ K.T.R. Davis et al., Phys. Rev. C 13 (1976) 2385

/17/ J.W. Negele et al., Phys. Rev. C 17 (1978) 1098

/18/ N. Carjan et al., Nucl. Phys. A 452 (1986) 381

/19/ J.R. Nix and A.J. Sierk, Los Alamos National Laboratory Report, LA-UR-87 (1987) 133

/20/ U. Brosa et al., Z. Naturforschung 41A (1986) 1341

/21/ H. Märten, Proc. Int. Conf. on the Fiftieth Anniversary of Nuclear Fission, Leningrad, 16 - 20 Oct 1989, in press; and A. Ruben et al., Z. Phys. A 338 (1991) 67

/22/ B.C. Samanta et al., Phys. Lett. 108B (1982) 83

/23/ H. Märten and D. Seeliger, J. Phys. G10 (1984) 349

/24/ H. Nifenecker et al., Proc. IAEA Symp. on Physics and Chemistry of Fission, Rochester, 13 - 17 Aug 1973 (IAEA, Vienna, 1974) p. 117

/25/ N. Bohr and J.A. Wheeler, Phys. Rev. 56 (1939) 426

/26/ N. Feather, U.S. Atomic Energy Commission, Document BR 335 A (1942), unpublished, cf. Ref. /24/

/27/ B.E. Watt, Phys. Rev. 87 (1952) 1037
/28/ J. Terrell, Phys. Rev. 113 (1959) 527
/29/ R.R. Wilson, Phys. Rev. 72 (1947) 189
/30/ J.S. Fraser, Phys. Rev. 88 (1952) 536
/31/ V.N. Nefedov, J.E.T.F. 38 (1960) 1657
/32/ H.R. Bowman et al., Phys. Rev. 126 (1962) 2120, and Phys. Rev. 129 (1963) 2133
/33/ S.S. Kapoor et al., Phys. Rev. 131 (1963) 283
/34/ K. Skarsvag and K. Bergheim, Nucl. Phys. 45 (1963) 72
/35/ C.P. Sargent et al.,Phys. Rev. B137 (1965) 89
/36/ J.C.D. Milton and J.S. Fraser, Proc. IAEA Symp. on Physics and Chemistry of Fission, Salzburg, 22 - 26 Mar 1965 (IAEA, Vienna, 1965), Vol. II, p. 39
/37/ M.V. Blinov et al., Yad. Fiz. 12 (1970) 41, and Yad. Fiz. 16 (1972) 1155
/38/ C.J. Bishop et al., Nucl. Phys. A 198 (1972) 161
/39/ Z. Fraenkel et al., Phys. Rev. C 12 (1975) 1809
/40/ S. Nair et al., J. Phys. G 3 (1977) 949
/41/ S. Nair et al., J. Phys. G 3 (1977) 965
/42/ V.M. Piksaikin et al., Yad. Fiz. 25 (1977) 723
/43/ Yu.S. Samyatnin et al., Yad. Fiz. 29 (1979) 595
/44/ P. Riehs, Acta Phys. Austr. 53 (1981) 271
/45/ Yu.A. Vasilyev et al., IAEA-Report INDC(CCR)-177/L (1982) 49
/46/ E.A. Seregina et al., Yad. Fiz. 42 (1985) 1337, and Yad. Fiz. 43 (1986) 1092
/47/ C. Budtz-Jorgensen and H.H. Knitter, Radiation Effects 93 (1986) 341
/48/ H. Märten et al., Radiation Effects 93 (1986) 41
/49/ O.I. Batenkov et al., Proc. IAEA Cons. Meeting on Physics of Neutron Emission in Fission, Mito, 24 - 27 May 1988, INDC(NDS)-220/L (IAEA, Vienna, 1989) 207
/50/ H. Märten et al., Proc. Int. Conf. on Nuclear Data for Science and Technology, Mito, 30 May - 3 Jun 1988, ed. S. Igarasi (JAERI, Saikon Publ. Co., Ltd., 1988), p. 683
/51/ C. Budtz-Jorgensen and H.H. Knitter, Nucl. Phys. A 490 (1988) 307
/52/ K. Arnold et al., Nucl. Phys. A 502 (1989) 325c
/53/ A. Gavron, Phys. Rev. C 13 (1976) 2561
/54/ T. Ericson and V.V. Strutinsky, Nucl. Phys. 8 (1958) L 84 (Errata: Nucl Phys. 9 (1959) 689
/55/ K.-H. Schmidt et al., Z. Phys. A 308 (1982) 215
/56/ B. Holmqvist, Arkiv Fysik 38 (1968) 403
/57/ F.D. Becchetti and G.W. Greenlees, Phys. Rev. 182 (1969) 1190
/58/ D. Wilmore and P.E. Hodgson, Nucl. Phys. 55 (1964) 673
/59/ P.A. Moldauer, Nucl. Phys. 47 (1963) 65
/60/ J.C. Browne and F.S. Dietrich, Phys. Rev. C 10 (1974) 2545
/61/ B.F. Gerasimenko and V.A. Rubchenya, Atomnaya Energia 59 (1985) 335
/62/ D. Seeliger et al., loc. cit. /21a/, and INDC(GDR)-056/L (1989)
/63/ H. Märten et al., Proc. Int. Conf. on 50 YEARS WITH NUCLEAR FISSION, Gaithersburg, 25 - 28 April 1989, ed. by J.W. Behrens and A.D. Carlson, ANS (1989), Vol. II, p. 743
/64/ W. Mannhart, Handbook of Nuclear Activation Data, Technical Report Ser. 273 (IAEA, Vienna, 1987) 163
/65/ H. Märten et al., Nucl. Instr. Meth. A 264 (1988) 375
/66/ H. Märten, Proc. Int. Conf. on Physics and Chemistry of Fission, Gaussig near Dresden, 21 - 25 Nov 1988, ed. by H. Märten and D. Seeliger, ZfK-732, p. 155

/67/ U. Brosa et al., Z. Naturforschung 41a (1986) 1341
/68/ U. Brosa, Phys. Rev. C 38 (1988) 1944
/69/ R.W. Hasse and W.D. Myers, Geometrical Relationships of Macroscopic Nuclear Physics, Springer-Verlag (1988) 44
/70/ U. Brosa and H.H. Knitter, loc. cit. /66/, p. 145
/71/ V.S. Stavinsky, J.E.T.P. 36 (1959) 629
/72/ R.W. Fuller, Phys. Rev. 126 (1962) 684
/73/ Y. Boneh and Z. Fraenkel, Phys. Rev. C 10 (1974) 893
/74/ V.A. Rubchenya, preprint RI-28 (Radium Institute Leningrad, 1974)
/75/ P. Mädler, Z. Phys. A 321 (1985) 343
/76/ B. Milek et al., Phys. Rev. C 37 (1988) 1077
/77/ V.P. Eismont, Atomnaya Energia 19 (1965) 113
/78/ G.A. Pik-Pitchak, Yad. Fiz. 10 (1969) 321
/79/ D.J. Hinde et al., Phys. Rev. Lett. 52 (1984) 986
/80/ B.C. Samanta et al., Phys. Lett. 108 B (1982) 83
/81/ H. Märten and D. Seeliger, J. Phys. G 14 (1988) 211
/82/ A. Ruben et al., Z. Phys. A 338 (1991) 67
/83/ H. Kalka et al., Z. Phys. A 329 (1988) 331
/84/ H. Kalka, submitted to Z. Phys. (1991)
/85/ D. Seeliger et al., Yad. Fiz. 47 (1988) 635
/86/ E. Cheifetz et al., Phys. Rev. Lett. 29 (1972) 805
/87/ G.S. Boikov et al., loc. cit. /21/

PROMPT NEUTRON SPECTRUM MEASUREMENT OF THE URANIUM-238 FISSION INDUCED BY 12 MeV NEUTRONS

Li Anli, Bai Xixiang, Wang Yufeng, Wang Xiaozong,

Meng Jiangchen and Huang Shengnian

(China Institute of Atomic Energy, P.O.Box 275-46,Beijing)

Abstract

Using double TOF method, a measurement of prompt neutron spectrum for 12 MeV neutron induced fission of ^{238}U has been made at the CIAE Tandem Van de Graaff accelerator. Preliminary results are presented.

INTRODUCTION

The prompt fission neutron spectrum has long been investigated since the discovery of the fission phenomenon. A comprehensive review and thorough discussion of the status from both experimental and theoretical sides were given at the IAEA CM on "Physics of Neutron Emission in Fission" held in May, 1988.[1] So far the experimental data for the fast neutron induced fission, especially for the incident neutron energy higher than 8 MeV, are very scarce. Difficulties arose mainly due to the small cross section (compared with thermal neutron induced fission) and the interference by the break up neutrons in the D(d,n) source. Only existed works are of the 14 MeV energy point where the T(d,n) source can be used. To fill the gap, we have made an attempt recently to measure the prompt neutron spectrum for the fission of U-238 induced by 12 MeV neutrons, by using double TOF method. It is also interesting from the theoretical side since at this energy the second chance fission is mixed with the first chance fission. The method is very similar to the one used in BRC laboratory by Bertin et. al.[2] The measurement has not been completed yet due to some problems, e.g., insufficient beam time and so on. In the present paper only a description of the experiment and some preliminary results are presented.

EXPERIMENT

The experiment was carried out at the CIAE tandem Van de Graaff accelerator of the type HI-13. The arrangement is shown in Fig.1.

NEUTRON SOURCE. To obtain 12 MeV neutrons we used D(d,n)He-3 reaction. A pulsed beam of deuterons were obtained from the accelerator with the pulse width less than 1 ns and repetition rate 4 MHz. The energy of the deuterons was E_d = 9.4 MeV. The average current was about 1 μA. The neutron producing target is a cell 2.5 cm long filled with 4.3 atm. pure deuterium gas. The window of the cell was made of Havar foil of 5.27 mg/cm^2 thick. At zero degree direction neutron beam of 12 MeV was obtained. A timing signal can be picked off from a small device located near the gas target.

FISSION CHAMBER. In order to distinguish the primary 12 MeV neutrons from the break up neutrons with lower energies and to select out fission neutrons from other secondary neutrons, fast signals of fission fragments have to be used. For this purpose a multisectional fission chamber was constructed. The chamber of cylindrical shape was made of ordinary steel. The thickness of the wall was 1 mm. Altogether one hundred stainless steel plates with natural uranium deposits on

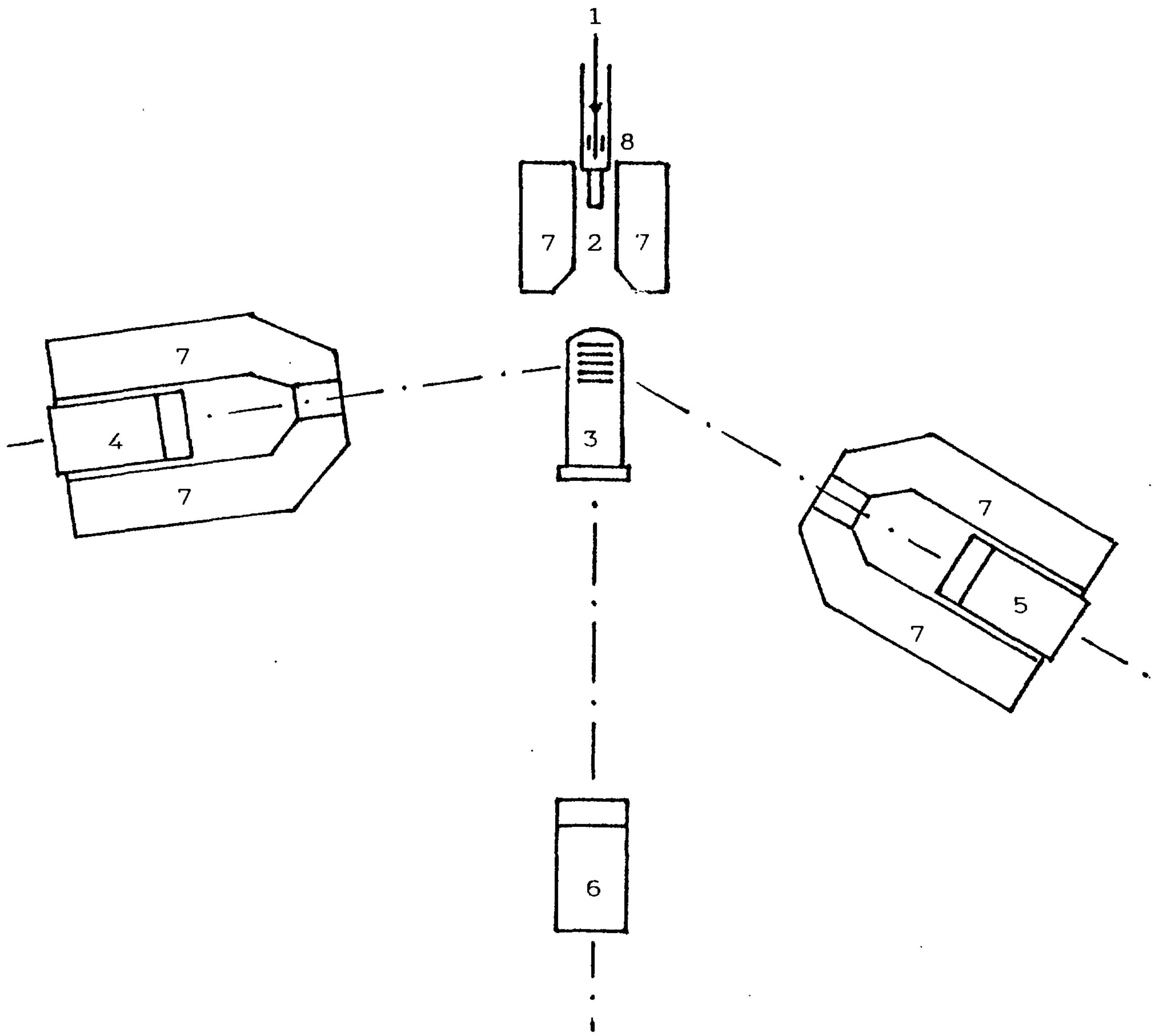

Fig.1. Experimental set up.

1. Deuteron beam
2. Deuterium gas target
3. Fission chamber
4. Right neutron detector
5. Left neutron detector
6. Zero degree monitor
7. Shieldings
8. Pick off

both surfaces were contained in the chamber. The diameter of the deposits was 8 cm. The total amount of the uranium reaches 5 g. These 100 plates were divided into 8 sections, each of them has its own electronics and can give separate outputs. This has to be done for two reasons: The first one is to decrease the capacities among the plates and hence the rise time of the fission signals. The second reason is in such a way one can reduce the uncertainty of the flight path between the neutron detectors and the location where fissions occur. The distance between the centres of the gas cell and the chamber was 64 cm. The fission fragment signals of each section and the pick off signals were used as the start and stop of the TAC respectively. A primary neutron TOF spectrum was measured for each section and a gate was set for 12 MeV monoenergetic peak in the spectrum. The signals in this gate were put in coincidence with those of neutron detectors to select

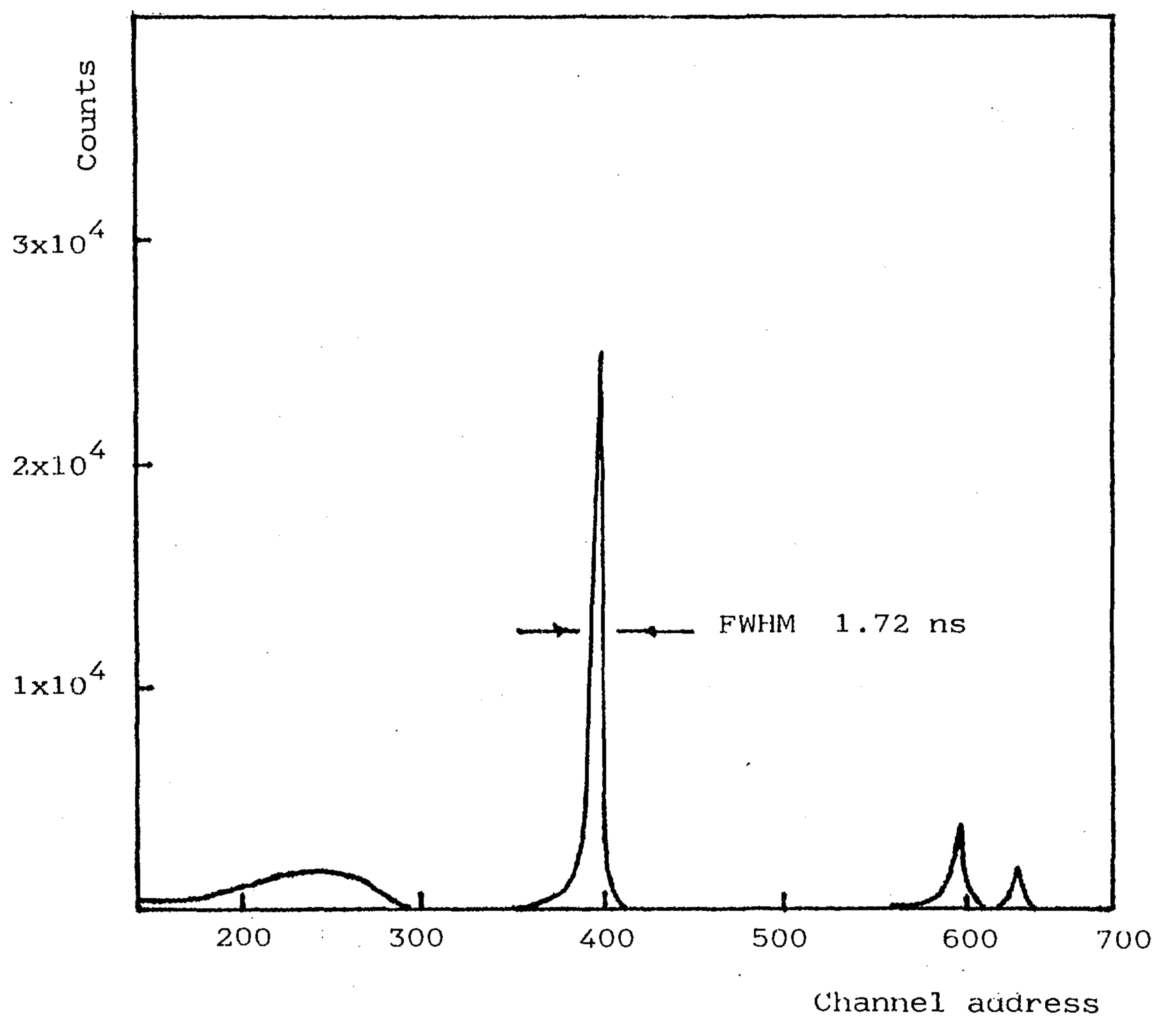

Fig.2 Primary neutron TOF spectrum measured by zero degree monitor detector.

the fission events induced by 12 MeV neutrons from those induced by break up neutrons.

NEUTRON DETECTORS. Two identical heavy shielded neutron detectors were used. The detectors were Chinese made liquid scintillators 25 cm in diameter and 5 cm thick. The relatively large area of the scintillator has the advantage of increasing the counting rate but not losing the accuracy. The neutron detectors were placed on opposite sides of the fission chamber, one was the left detector located at 60 degree direction with respect to the beam axis,the other was the right detector at 80 degree. The flight path was 2.5 m for both detectors. Two biases were used for each detector, one was an electronic bias set at 1/3 Cs (i.e., about 0.5 MeV proton energy), so that the available minimum energy of the fission neutron spectrum was below 1 MeV; the other was a higher bias set at 1 Cs by computer to upgrade the effect-to-background ratio in high energy region of the fission neutron spectrum; and a neutron γ ray discriminator was added to eliminate the γ ray background.

The efficiency of these detectors were calculated using the standard code of NEFF4[3]. Experimentally it will be determined through the n-p scattering method. In addition, the efficiency will also be checked by measuring the standard fission neutron spectrum of Cf-252 spontaneous fission.

MONITOR. A smaller liquid scintillation neutron detector of the size $\Phi 10\times5$ cm was placed at zero degree direction and 3.1 m away from the gas target and was used as a monitor of the TOF spectrum of the primary neutrons. A typical measured TOF spectrum of the primary neutrons was shown in Fig.2. From the figure one can see that the 12 MeV monoenergetic peak is separated quite well from the break up group. A gate including this monoenergetic peak only was set and the integral counts in this gate were recorded as a normalization standard of the primary neutrons for each experimental run instead of beam current integral during the data acquisition.

ELECTRONICS. The block diagram of the electronics is shown in Fig.3. Altogether eight ADCs were adopted,two of them were used to record primary neutron TOF spectra for the fission chamber and the monitor detector respectively; the others were used to record fission neutron TOF spectra, pulse height spectra and neutron gamma ray discrimination spectra for two neutron detectors respectively. In addition, a 12 bit input register was used: bits 2 to 9 were connected with 8 timing outputs from 8 sections of fission plates respectively to determine which section the fission event belongs to;bit 11 was used to determine whether right or left neutron detector the event comes from; and bit 12 is for judging random coincidence between the outputs of the fission chamber and the neutron detectors.

In the XSYS data acquisition and analysis system based on VAX-11/780 computer used in present measurement the maximum number of spectra specified is 64 and the maximum size of each event analysis file is 4096 bytes. These parameter limits made only a part of the spectra can be shown on screen of a Tektronix terminal. The data were stored event by event into buffer tapes during the experiment. The buffer tape sto-

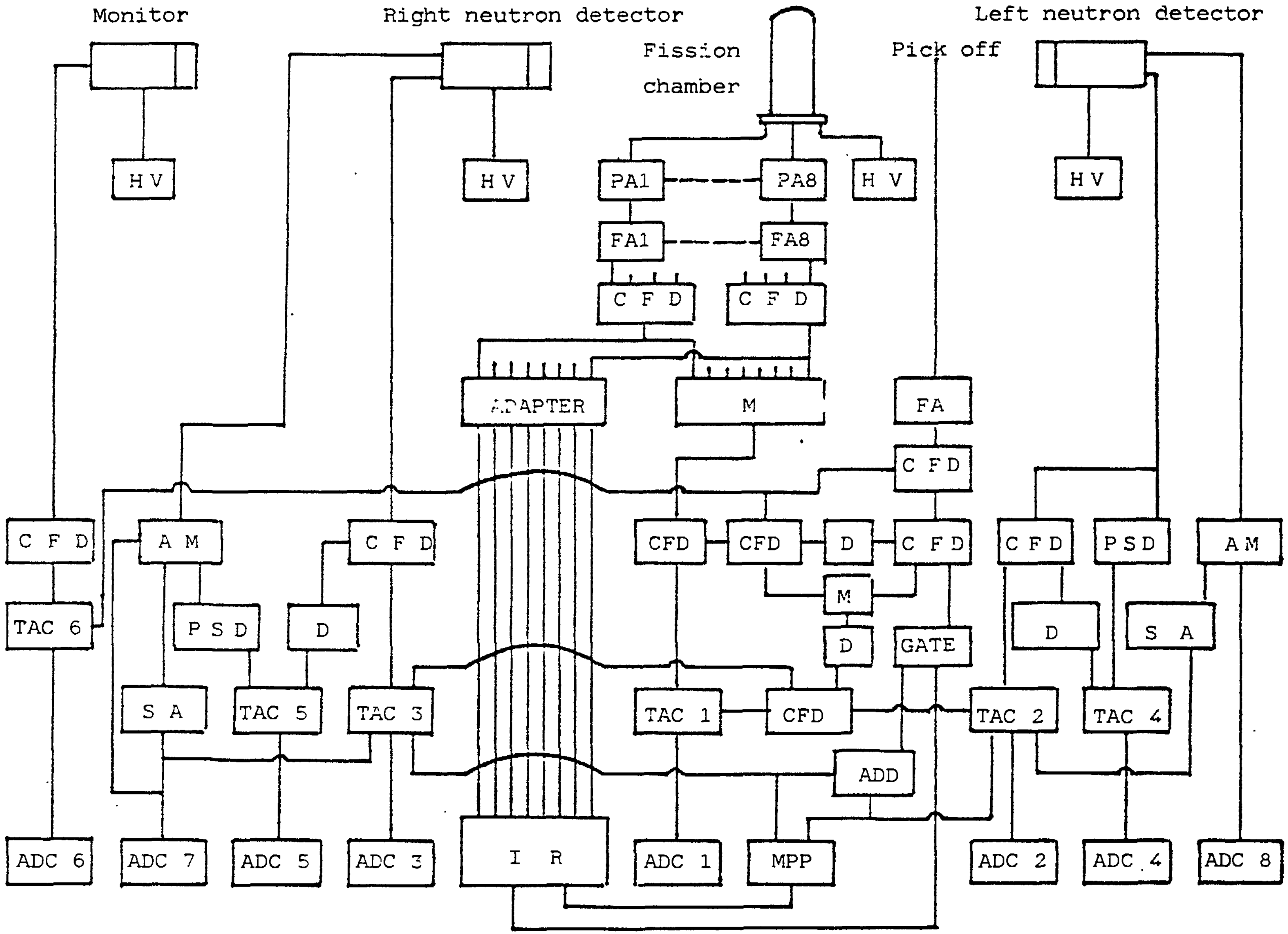

Fig.3 Block diagram of electronics

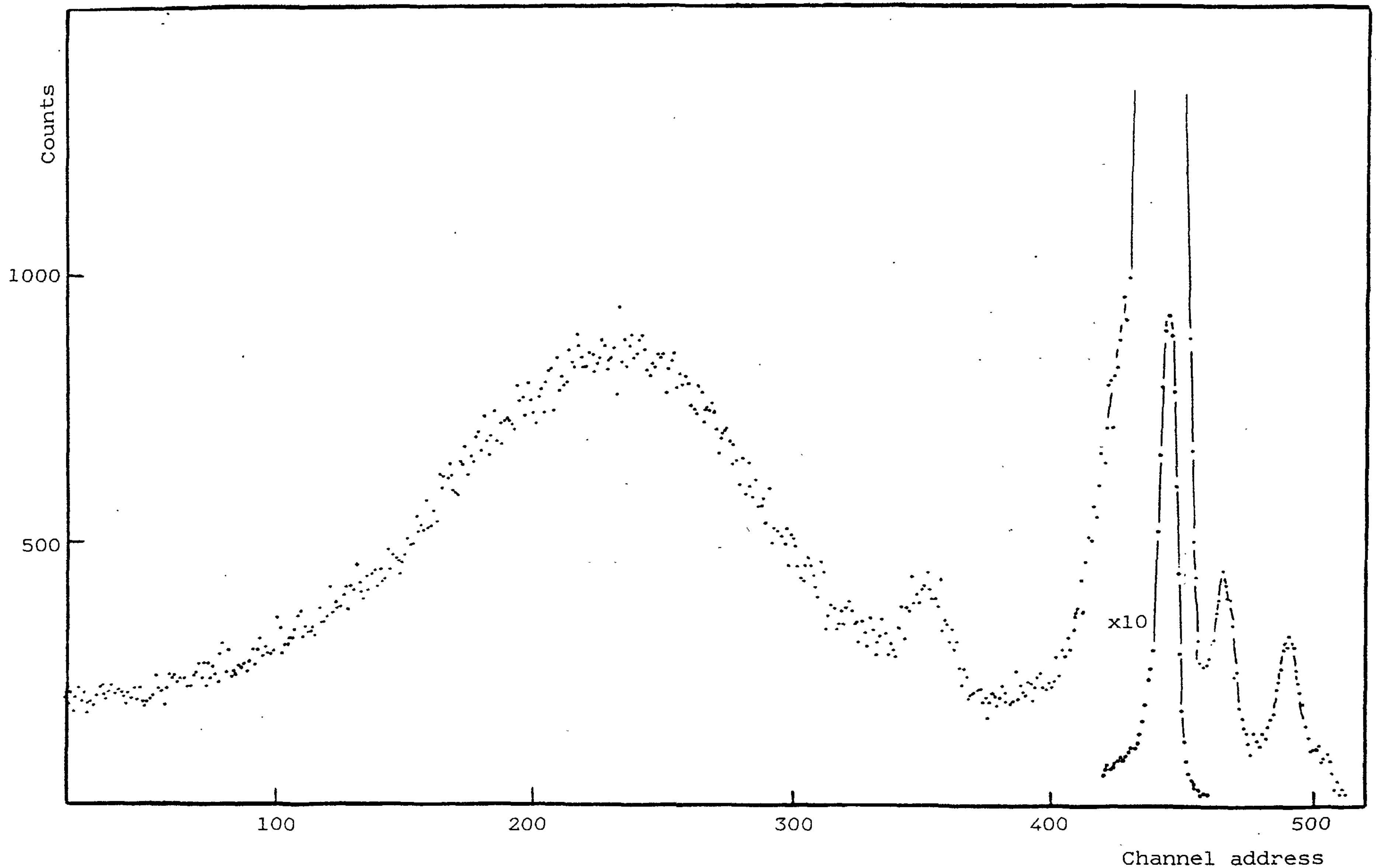

Fig.4 TOF spectrum for right neutron detector (low bias)

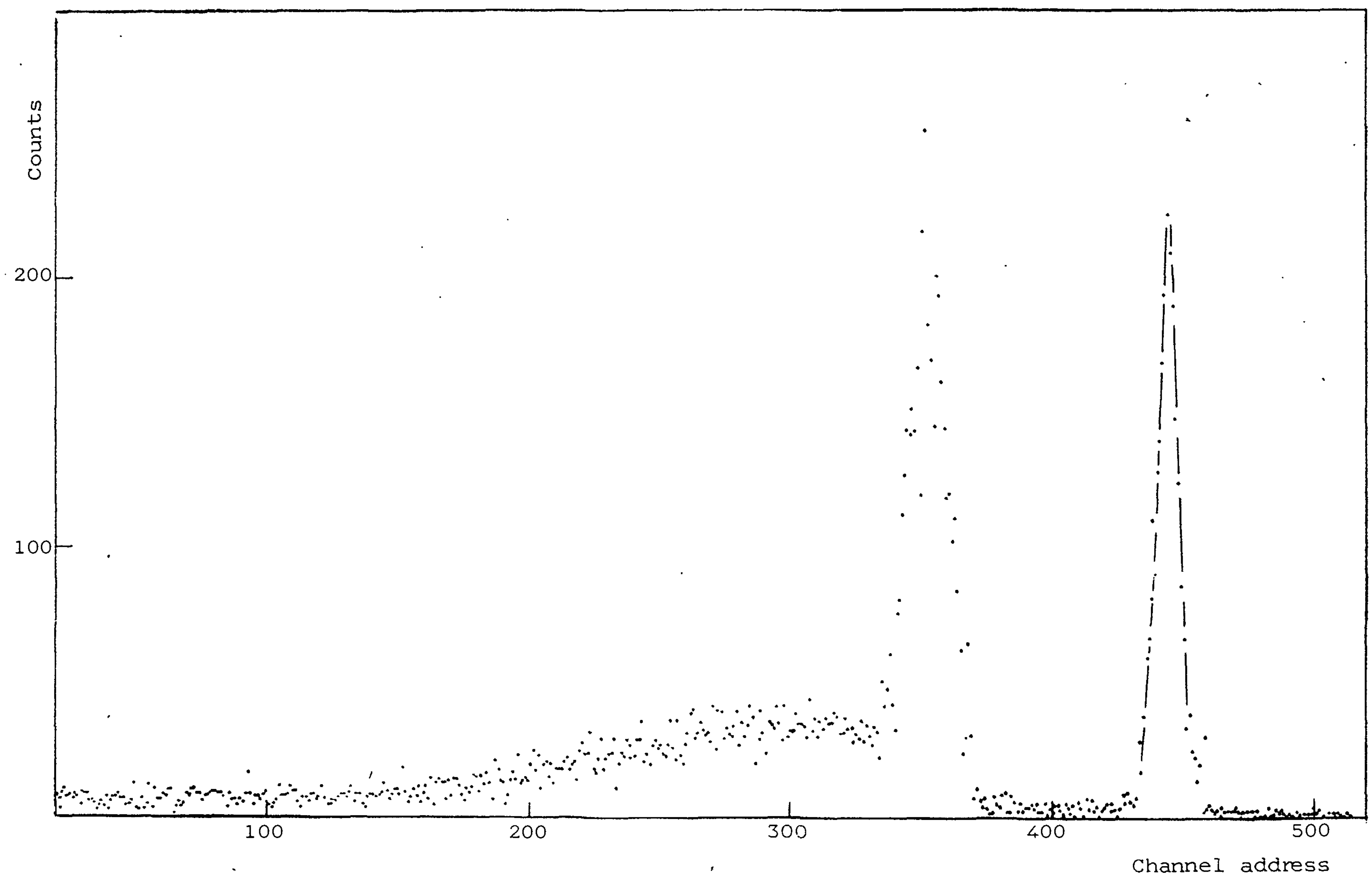

Fig.5   Random coincidence spectrum for right detector (low bias)

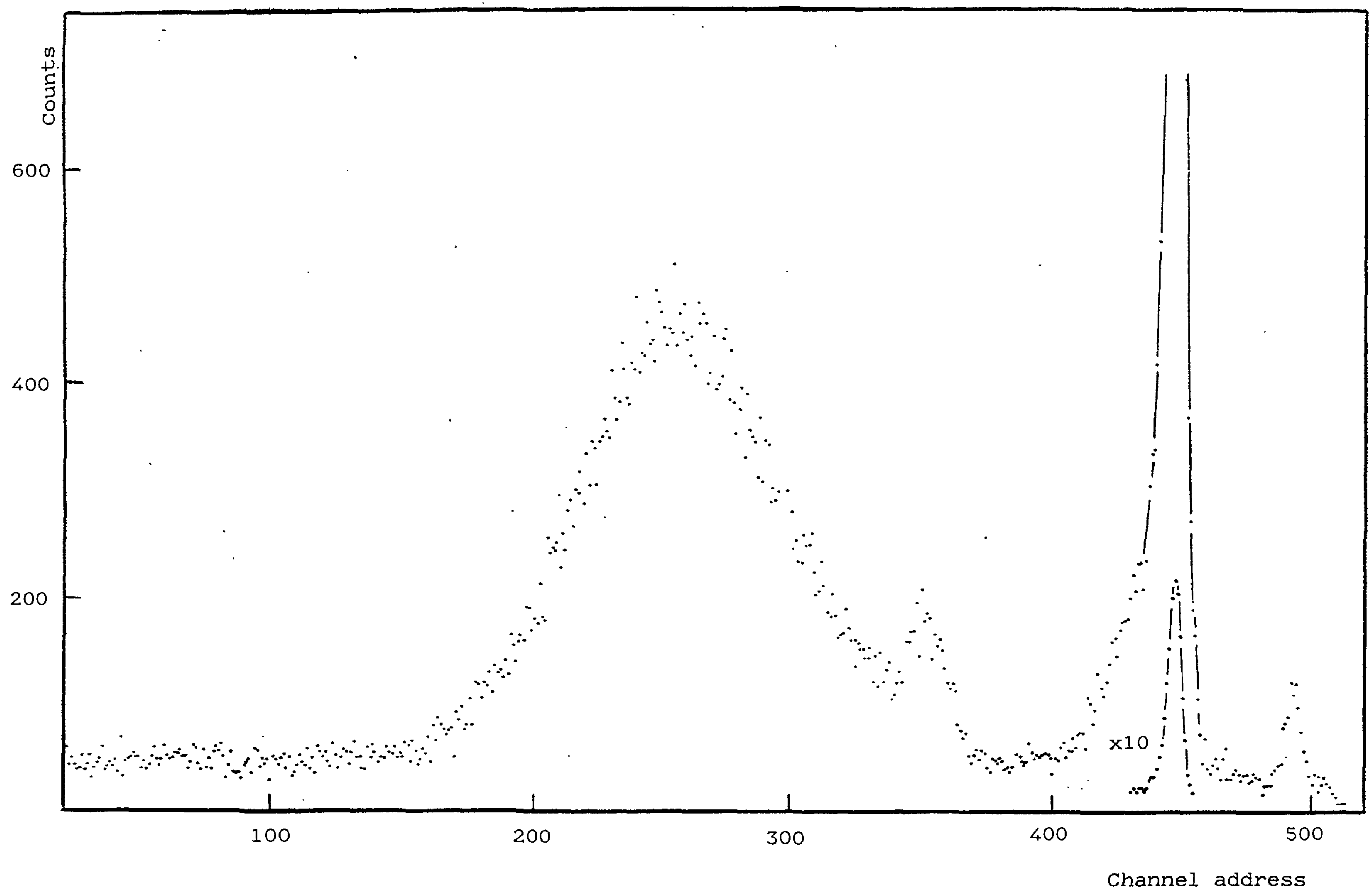

Fig.6 TOF spectrum for right neutron detector (high bias)

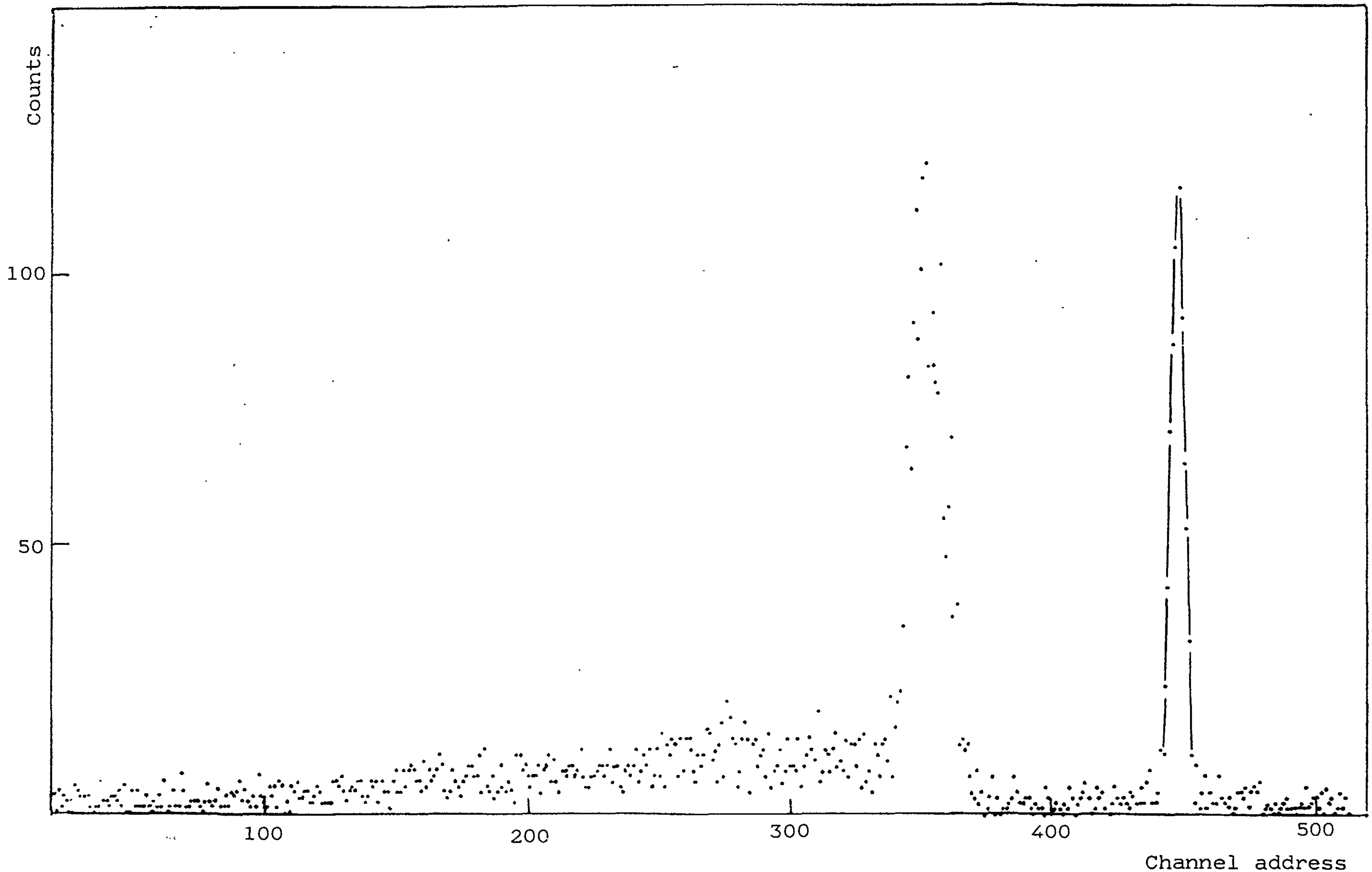

Fig.7 Random coincidence spectrum for right detector (high bias)

rage allows us to reproduce the experiment offline latter and then the data analysis and corrections will be carried out.

PRELIMINARY RESULTS

Fig.4 shows the TOF spectrum obtained by using the right neutron detector with low bias after subtraction of the background, i.e., (A-B), where A is the spectrum for events selected by a window including 12 MeV primary neutron monoenergetic peak only, B is the spectrum for a window with same width but set at the right side of the monoenergetic peak. Fig. 5 is the result of (C-D), where C and D are the same as A and B respectively, but for the random coincidence. The real spectrum should be (A-B)-(C-D). Two small peaks on the right side of the prompt γ-ray peak in Fig.4 are attributed to the γ rays emitted from two diaphragms hit by the pulsed deuteron beam. The data acquisition time was 90 hours. Figs. 6 and 7 are those for high bias also from right detector. The FWHM of the γ-ray peak was about 4.1 ns for the low bias case, and was 3.1 ns for the high bias.

It seems that some modifications are neccesary in the next data acquisition, for example, the flight path of the primary neutrons should be increased to get better separation of the monoenergetic peak from break up neutrons.

REFERENCES

[1] Physics of Neutron Emission in Fission, Proceedings of a CM organized by the IAEA and held in Mito City,Japan,24--27 May 1988, ed. H.D.Lemmel, June 1989, NDC(NDS)-220.

[2] Bertin et al., NEANDC-INDC Rapport EA-R-4913,1978.

[3] Dieze G. and Klein H., PTB-ND-22.

FISSION NEUTRON SPECTRUM OF ^{232}Th
FOR 2 MeV NEUTRONS: COMPARISON OF
EXPERIMENTAL DATA WITH A
MADLAND-NIX MODEL CALCULATION

R. L. WALSH

Australian Nuclear Science and Technology Organisation
Lucas Heights Research Laboratories
Private Mailbag 1, Menai, NSW 2234, Australia
Fax No: 61-2-543-9265

G. CHIRCU

University of New South Wales
PO Box 1, Kensington, NSW 2033, Australia
Fax No: 61-2-663-2188

Abstract

We compare the recent experimental data reported by Baba et. al., for fission neutron spectrum of ^{232}Th with that of calculations using the theoretical model of Madland-Nix.

1. INTRODUCTION

In this paper we have compared some recent experimental data for the fission neutron spectrum (FNS) of ^{232}Th (Baba et al., [1]), with the now well-established Madland-Nix model [2]. The general-purpose MNM version of this model has been used, because of its ready applicability to a wide range of nuclei. In addition, the MNM used here is extended [3] to incorporate the spin of the fission fragment.

The MNM is an evaporation model. Details of its formalism may be found in [2].

2. RESULTS

2.1 ^{252}Cf(sf)

It is useful to first compare the FNS data of [1] for ^{252}Cf(sf) with the evaluation of Mannhart [4] and an MNM calculation [3]. This is because the ^{252}Cf(sf) FNS system is widely used as a standard. Figure 1

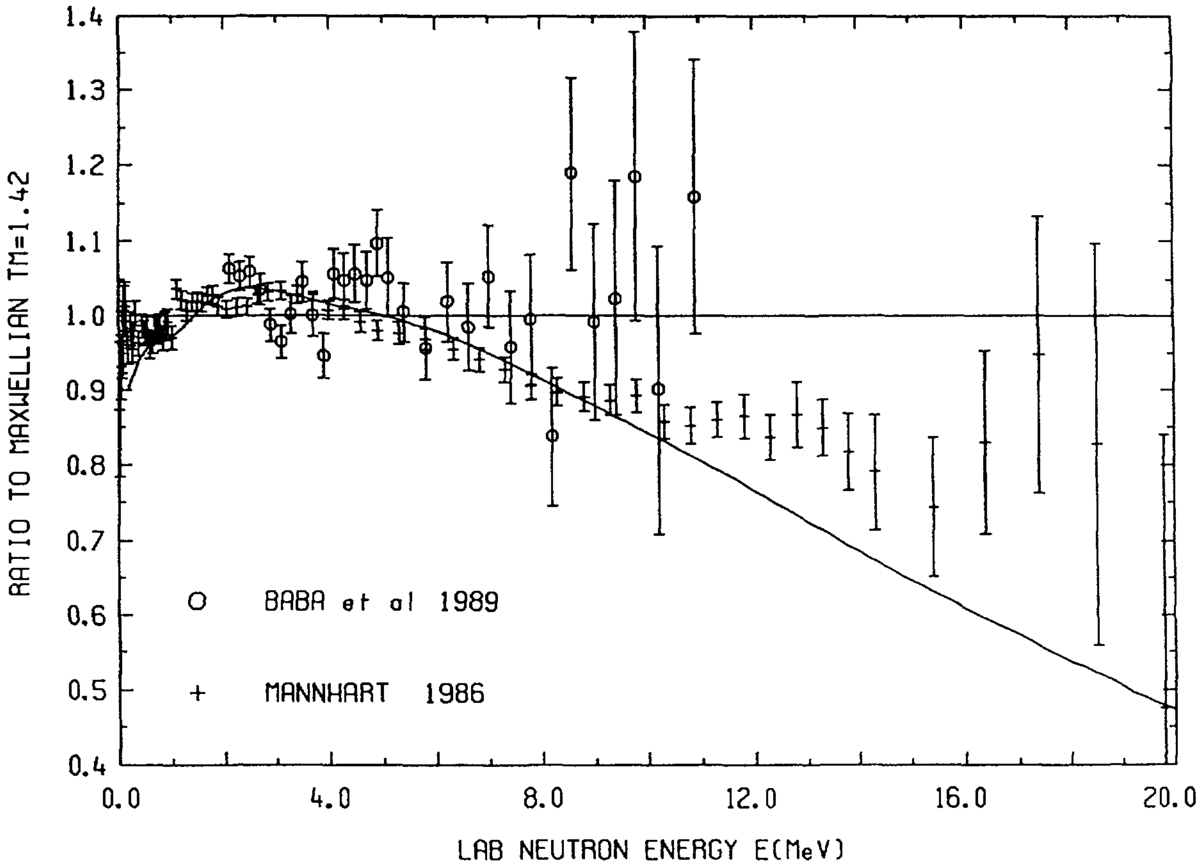

<u>Figure 1</u> Comparison of FNS data for ^{252}Cf(sf) of Baba et al. [1] with an MNM calculation (continuous line) [3] and with the evaluation of Mannhart [4]. The nuclear level density parameter used in the MNM calculation is a = A/(9.3 MeV), obtained by chi-square minimisation. The presentation is relative to a Maxwellian spectrum with temperature parameter TM = 1.42.

shows this comparison. The continuous curve is the MNM calculation with level density parameter optimised to a = A/(9.3 MeV). The Baba et al. data are normalised to the present calculation, and thus to the Mannhart evaluation. Above 6 MeV, it is seen that the data of [1] appear to follow the trend of the Maxwellian (TM = 1.42), rather than follow the well-known divergence below it that is seen in the Mannhart evaluation [4] and the MNM calculation [3].

Below 6 MeV, all three sets agree reasonably well.

2.2 <u>^{232}Th + n (2 MeV)</u>

Figure 2 compares our calculation with the ^{232}Th data of [1]. (The continuous line includes fragment spin, the dashed line neglects it). The

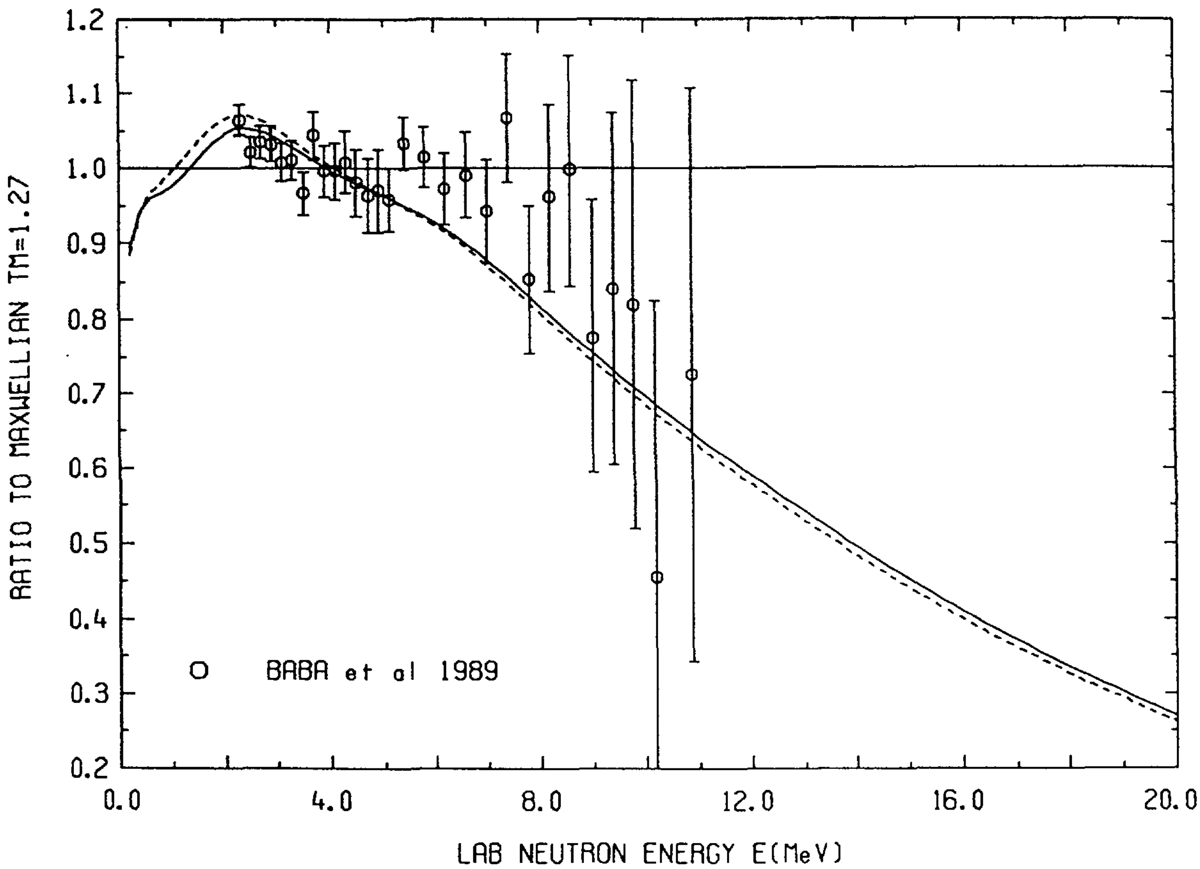

<u>Figure 2</u> Comparison of FNS data for ^{232}Th + n (2 MeV) of Baba et al. [1] with present MNM calculation. Level density parameter used in the calculation is a = A/(11 MeV). Continuous line includes fragment spin; the dashed line neglects it.

presentation is relative to a Maxwellian spectrum with TM = 1.27, which is the TM value used in ENDF/B-IV [5]. Again, the data of [1] are normalised to the continuous line calculation. The level density parameter in our calculation here is a = A/(11 MeV), the value recommended in [2] for wide applicability.

It appears that the ^{232}Th data of [1] tend to follow the present MNM calculation more closely than for the ^{252}Cf(sf) case, in particular in the region above 6 MeV.

2.3 Optimisation of Level Density Parameter

We have sought to find the optimum value for the level density parameter by minimising the chi-square value, using the data of [1] and the present MNM calculation. The chi-square variation is shown in Figure 3. Chi-square is a minimum for a = A/(11.4 MeV), at a value of 0.90 per

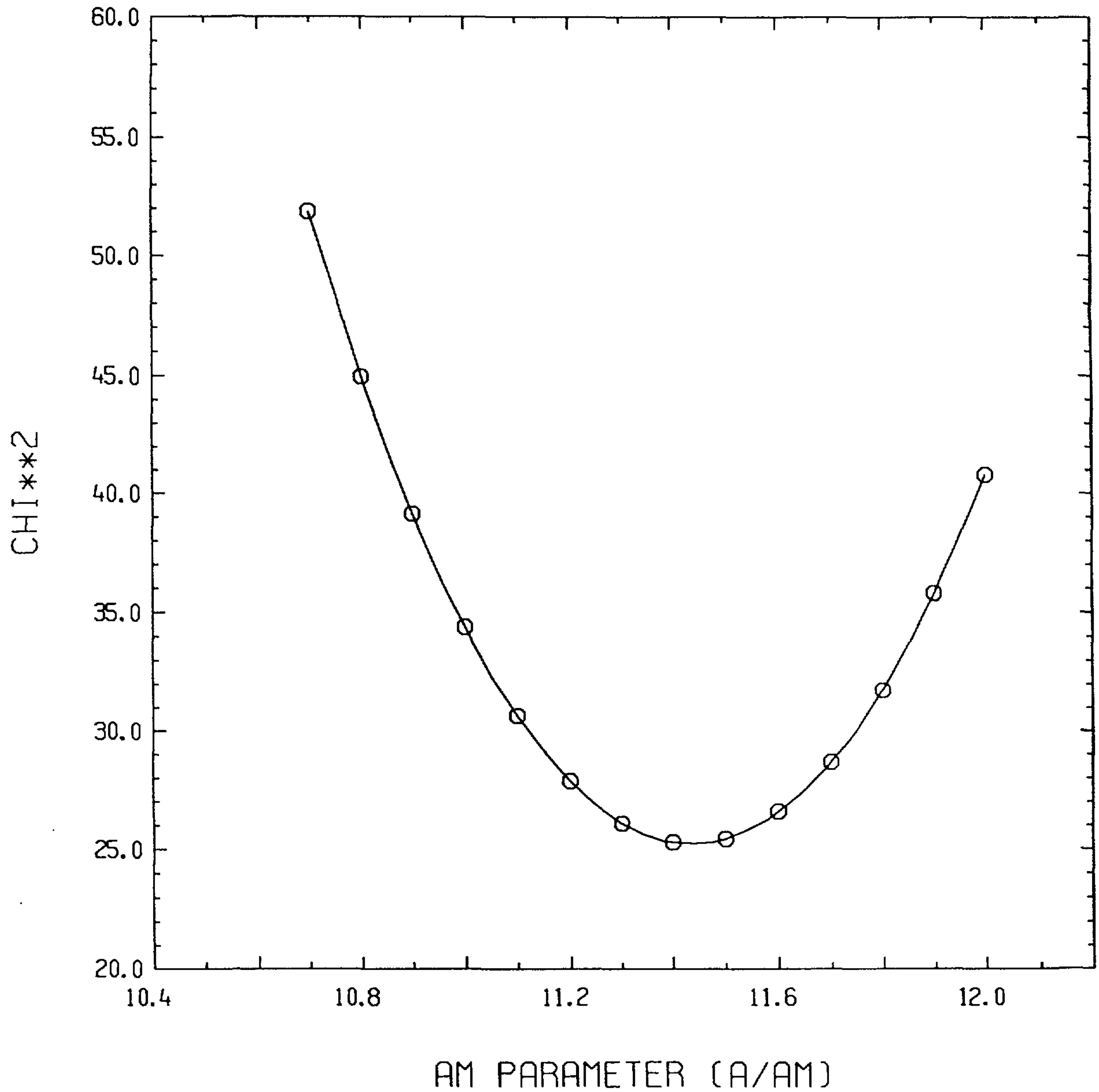

Figure 3 Variation of chi-square determined from ^{232}Th + n (2 MeV) data of [1] and the present calculation, as a function of the level density parameter. Chi-square is seen to be a minimum at a = A/(11.4 MeV).

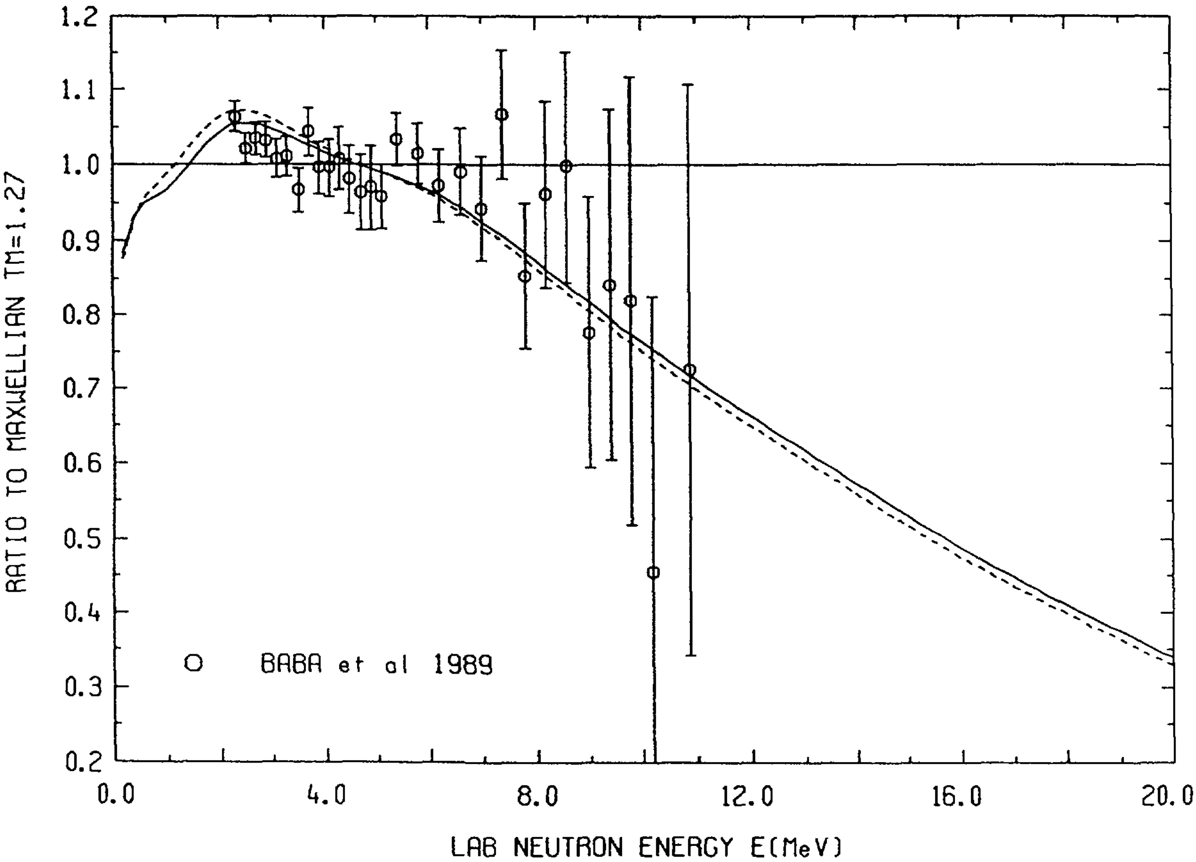

<u>Figure 4</u> As for Figure 2, but employing the optimised value a = A/(11.4 MeV) in the present calculation.

degree of freedom. If this optimised value of a is used in our calculation, the result shown in Figure 4 is obtained.

<u>REFERENCES</u>

1. Baba, M. et al. (1989). Report JAERI-M 89-143. Also see Proc. IAEA Consultants' Meeting, 'Physics of Neutron Emission in Fission', Mito, Japan, 24-27 May 1988 for preliminary data.
2. Madland, D.G. and Nix, J.R., Nucl. Sci. Eng., <u>81</u> (1982) 213.
3. Walsh, R.L., Nucl. Sci. Eng., <u>102</u> (1989) 119.
4. Mannhart, W., Proc. IAEA Group Meeting Neutron Sources, Leningrad, USSR, 9-13 June 1986, p.158, IAEA (1987).
5. Garber, D., 'ENDF/B-IV', Report BNL-17541, 2nd edition, Brookhaven National Laboratory (October 1975).

Representation of Fission Neutron Spectrum
by Non-equitemperature Madland-Nix Model

Takaaki Ohsawa

Atomic Energy Research Institute, Kinki University
3-4-1 Kowakae, Higashi-osaka, 577 Japan

Abstract

The original formulae in the Madland-Nix formalism were slightly modified to take into account the difference in the temperature of the two fragments. The non-equitemperature model was applied to analyze the data of the fission spectra for neutron induced fission of ^{235}U and ^{239}Pu and spontaneous fission of ^{252}Cf.

I. Introduction

Exact analysis of nuclear characteristics of fast reactors requires exact knowledge of the fission neutron spectrum. According to a recent sensitivity analysis[1], the fission neutron spectrum of ^{239}Pu is one of the important factors that affect the calculated effective multiplication factor and control rod worths of a fast reactor. Study on extended burnup of LWR-fuels and of nuclear incineration systems add further importance to the fission neutron spectrum data for many actinides at higher as well as at lower incident energies.

The Madland-Nix (MN) model[2] for fission neutron spectrum calculation was successfully applied for analysis and evaluation of important fissionable nuclides. The evaluation of fission neutron spectra for major actinides in the Japanese Evaluated Nuclear Data Library, Version 3 (JENDL-3) was also based on the model together with the parameters recommended by Madland and Nix.

However it has been recognized that the MN model underestimates the spectrum in the regions below ~0.5MeV and above ~7MeV. Several attempts have been made to improve the model.[3-5]

Walsh[3] examined the possibility of improving the calculated spectrum by taking into account the anisotropy of neutron emission in the center-of-mass system. He demonstrated that better agreement with experimental data could be obtained by assuming the anisotropy coefficient b (in the form $1+b\cos^2\theta$) to be 0.1. However, this value seems to be too large in view of the recent experimental data by Budtz-Jørgensen *et al.*[6](b=0.015), and by Batenkov *et al.*[7](b=0.04) both for $^{252}Cf(sf)$.

Madland *et al.*[4] presented a preliminary results of their efforts to improve and refine the model by replacing the average values of the fragment mass, charge, and kinetic energy with the distributions themselves on a point-by-point basis. This refined model yielded the spectrum in slightly better agreement with measured data but did not yet reproduce the experimental spectrum.

Another approach by Märten *et al.*[5] is to consider the mass dependence of the average excitation energy, the average kinetic energy of the fission fragment per nucleon, and the inverse cross section of compound-nucleus formation. This generalization resulted in better agreement with experimental data, at least at very low and very high emission energies. A disadvantage of this method is that the mass-dependent quantities required as input are not always available for every fissionable nuclide.

One of the important assumptions of the Madland-Nix model is the triangular distribution of the nuclear temperature. This assumption is equivalent to assuming that the excitation energy distribution is uniform, which is appropriate at high excitaion energies but become less adequate at low excitation energies. So there may be some room for improvement in this respect.

Generally speaking, it is natural that using many empirical data as input leads to better results. From the point of view of an evaluator, who is confronted with evaluations of nuclear data for many nuclides, it is desirable to have a model with a set of parameters systematics that provides acceptable results with less amount of input data within a short calculation time and that is applicable to estimate the spectra even for nuclides for which no or scarce experimental data are available. Also for the purpose of sensitivity analysis of integral experiments, it is useful to have a model with small amount of input parameters.

As an attempt in this direction, we tried to take into consideration the difference in the nuclear temperatures of the two fragments *not* at the scission point *but* at the time of prompt neutron emission, since it is physically reasonable to assume that the nuclear temperatures characterizing the neutron emission from the two fragments are different for different fragment masses due to different initial deformation energies and also due to different level density parameters.

II. The Non-equitemperature Assumption

In the original MN model, it is assumed that the same temperature distribution $P(T)$ applies to both the light and heavy fragments. This would be the case, if the nuclear system were in ***statistical equilibrium*** at the scission point, with the excitation energy and level density parameter of each fragment proportional to its mass number. Actually it is questionable if statistical equilibrium should be established at the scission point, since the fission process is not only a statistical but also a dynamical process. Even if equilibrium is established in partitioning of the internal excitation energy at the scission point, the total excitation energy available for neutron emission is composed of internal excitation energy $a_i T_{0i}^2$ and the deformation energy D_i at the scission point, the latter being eventually converted into the internal excitation energy. Thus, the average initial total excitation energy of the fragment i is expressed as

$$\langle E^*_i \rangle = a_i T_{0i}^2 + D_i \quad (i = \mathrm{L\ or\ H}) \tag{1a}$$
$$= a_i T_{mi}^2 \tag{1b}$$

where T_{mi} is the maximum temperature for fragment i, L and H standing for light and heavy fragments, respectively. The deformation energy D_i at the scission point is strongly affected by the nuclear structure of the fragments so that the temperatures T_{mi} for the two fragments are generally not equal. This fact has been evidenced by the multi-parameter measurement of fission fragments and fission neutrons performed at Geel[6] (Fig.1). In the case of ^{252}Cf(sf), the ratio of nuclear temperatures averaged over light and heavy fragments $\langle T_L \rangle / \langle T_H \rangle$ is 1.13.

In this respect, it is interesting to note that Wilkins *et al.*[3] have found that the fragment deformation $\beta(A)$ at the scission point show a saw-tooth behavior very similar to the neutron multiplicity $\nu(A)$ (Fig.2). This suggests that the deformation energy is greater than the excitation energy at the scission point, *i.e.* $D_i > a_i T_{0i}^2$. This fact accounts for the non-uniform (also saw-tooth-like) distribution of the nuclear temperature versus mass number A, as was observed in the Geel data.

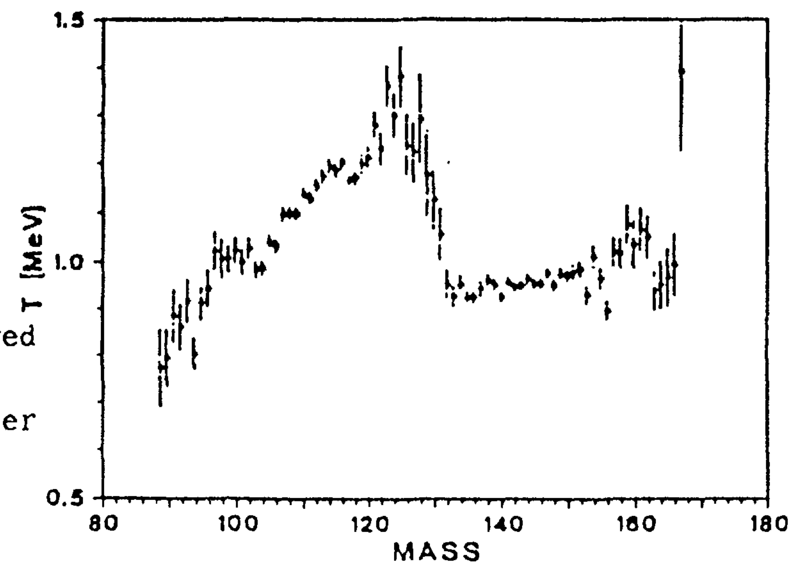

Fig.1
The neutron temperature derived from neutron spectra plotted versus the fragment mass number (Budtz-Jørgensen *et al.*[6]).

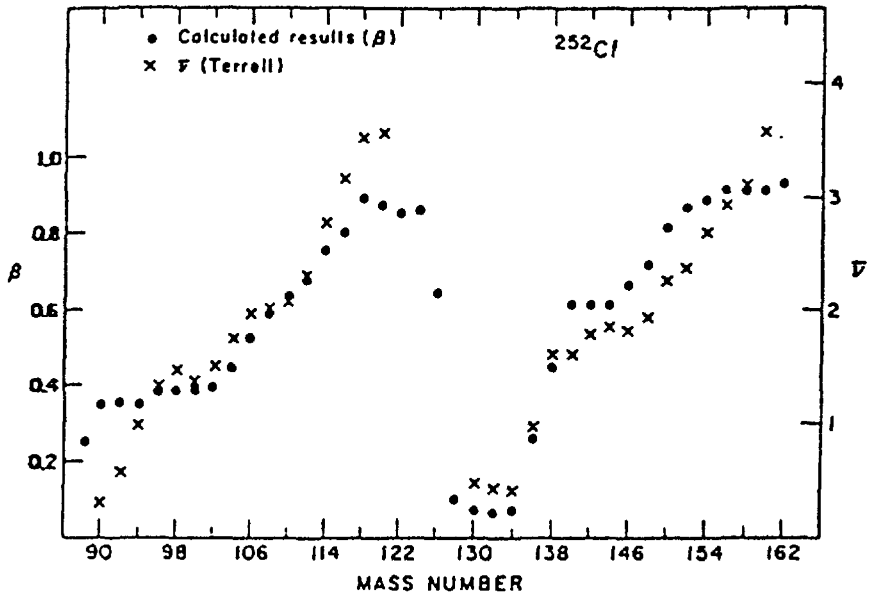

Fig.2 The fragment deformation $\beta(A)$ calculated for ^{252}Cf(sf) compared with the neutron multiplicity $\nu(A)$ (Wilkins *et al.*[9]).

III. Calculation with the Non-equitemperature Model

The present calculation is essentially based on the formalism of Madland and Nix[2]. The constant compound-formation cross-section model was used for the sake of simplicity. The maximum (sharp cutoff) nuclear temperature T_m is approximately related to the average total excitation energy $\langle E^* \rangle$ by

$$\langle E^* \rangle = \langle E_r \rangle + B_n + E_n - \langle E_k \rangle = aT_m{}^2 \qquad (2)$$

where $\langle E_r \rangle$ is the total energy release, B_n the neutron separation energy, E_n the incident neutron energy, $\langle E_k \rangle$ the total kinetic energy, and a the level density parameter given by $a = A/C$ (C = 8~11). The total energy release $\langle E_r \rangle$ of fission was calculated according to the seven-fragment approximation[2] using the mass formula of Tachibana, Uno, Yamada and Yamada (TUYY)[9], which was claimed to yield the appropriate mass even for nuclei far from the beta-stability line. The total kinetic energy of the fragments was taken from the work of Unik *et al.*[10]

The original formulas in the Madland-Nix formalism were somewhat modified so as to take into account the difference in temperature of the two fragments. Since the nuclear system is not in statistical equilibrium and the excitation energy is not proportional to the fragment mass number, we can write as follows:

$$\langle E^*{}_L \rangle = (A_L/C)T_{mL}{}^2 , \qquad (3a)$$

$$\langle E^*_H \rangle = (A_H/C)T_{mH}^2, \tag{3b}$$

$$\langle E^* \rangle = \langle E^*_L \rangle + \langle E^*_H \rangle = (A/C)T_m^2. \tag{3c}$$

$$A = A_L + A_H \tag{3d}$$

(If the system were in statistical equilibrium, then the equality $T_{mL} = T_{mH} = T_m$ would hold.) Then we have

$$A_L T_{mL}^2 + A_H T_{mH}^2 = A T_m^2. \tag{4}$$

Defining the ratio of the temperatures for the light and heavy fragments as $R_T = T_{mL}/T_{mH}$, we obtain

$$T_{mL} = [A R_T^2/(A_L R_T^2 + A_H)]^{1/2} T_m, \tag{5a}$$

$$T_{mH} = [A/(A_L R_T^2 + A_H)]^{1/2} T_m. \tag{5b}$$

IV. Results and Discussion

1. Effects of Changes in Input Data

Prior to performing the calculations with the non-equitemperature model, the sensitivity to changes in input parameters was analyzed on the basis of the original MN model. Different values of $\langle E_r \rangle$, $\langle E_k \rangle$, and a were used and the resultant spectra were compared. As can be seen from Figs.3a - 3c, it was found that in all these cases the calculated spectra shifted to one side, *i.e.*, when the high energy component was increased, the low energy component was decreased, and *vice versa*. It was not possible to increase *both* the high and low energy components *at the same time*, as required to improve agreement with experimental data.

2. Spectra Calculated with the Non-equitemperature MN Model

The non-equitemperature model was applied to analyze the data of the fission neutron spectra for ^{235}U(n,f), ^{239}Pu(n,f) and ^{252}Cf(sf). The quantities used as input data are summarized in Table 1.

Figure 4 compares the spectra for ^{235}U(n,f) for E_n = 0.53MeV calculated with different ratios R_T of the two temperatures. It can be observed that *(a)* if the temperature ratio was taken greater than unity, then both the low- and high-energy components were increased, and as a

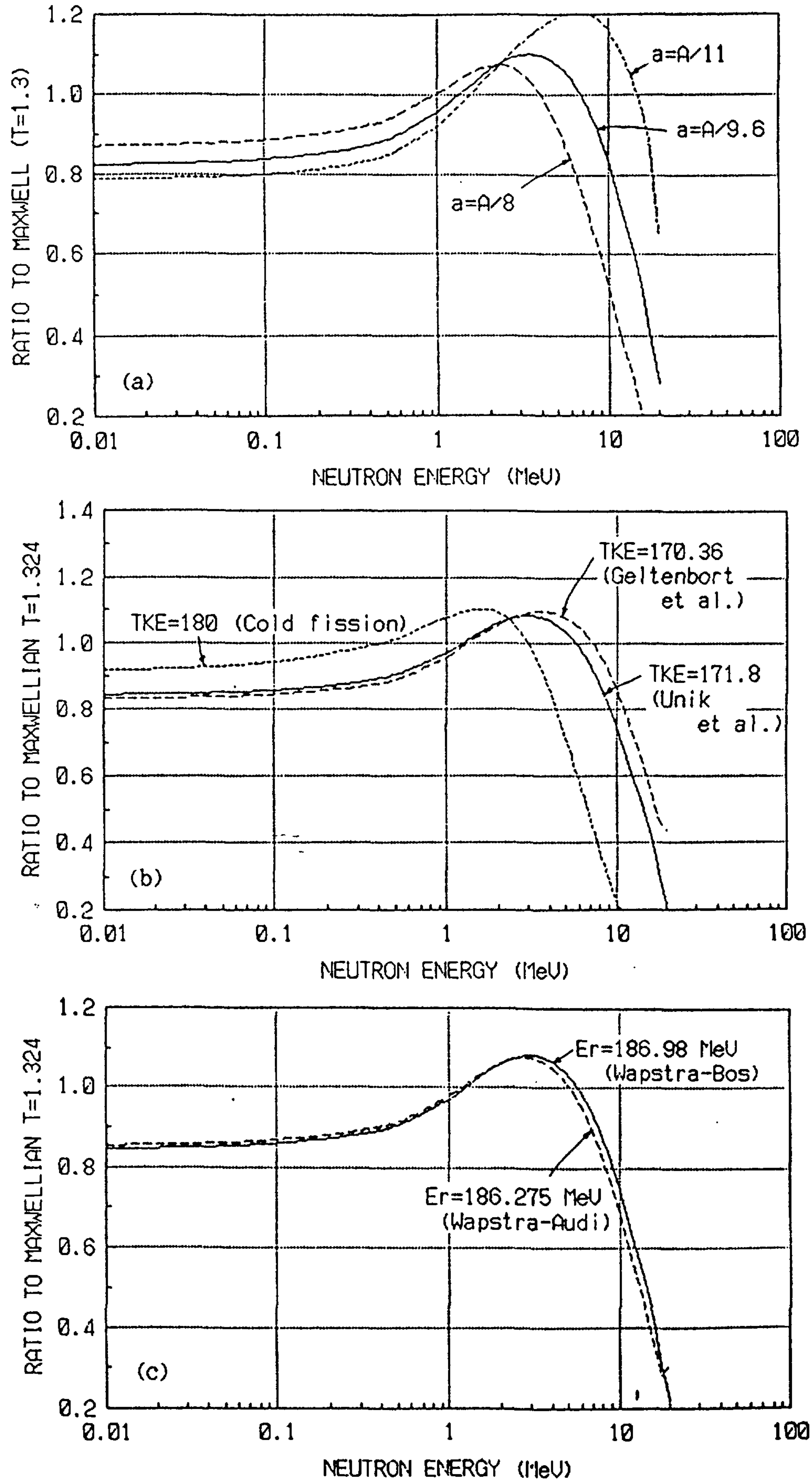

Fig.3 Dependence on input parameters; (a) Level density parameter, (b) Fragment total kinetic energy, (c) Total energy release.

Table 1. Input parameters used in the present calculation. The value marked with * is that calculated with the Möller-Nix mass formula, as used by Madland *et al.*[17]. This value was chosen just for comparison purpose. The TUYY mass formula yielded 215.998 MeV.

Quantity	U-235		Pu-239		Cf-252	
$\langle E_r \rangle$	185.896	MeV	198.088	MeV	218.886	MeV*
$\langle E_k \rangle$	171.8	MeV	177.1	MeV	185.9	MeV
a	$A/9.6$	MeV^{-1}	$A/8.5$	MeV^{-1}	$A/8.0$	MeV^{-1}
A_H	140		140		144	
A_L	96		100		108	

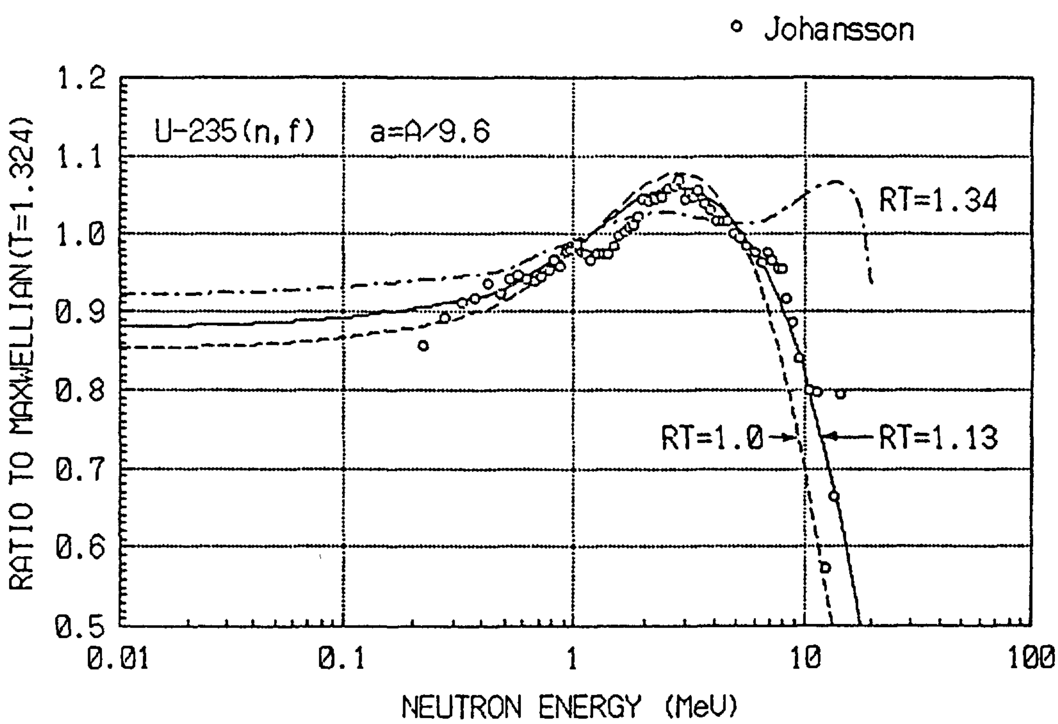

Fig.4 Fission neutron specra for $^{235}U(n,f)$ for E_n = 0.53 MeV. The ratios to Maxwellian spectrum with T_M = 1.324 (the value adopted in JENDL-2) are plotted.

result, *(b)* the spectrum fits better with the experimental data. The value R_T=1.13 was taken from the Geel data[6]. This value was obtained for $^{252}Cf(sf)$ and not for $^{235}U(n,f)$, but since we do not have corresponding data for $^{235}U(n,f)$, we tentatively used this value. This value was found to give a spectrum in better agreement with the experimental data of Johansson[11]. The value R_T=1.34 was that suggested by Kapoor[12].

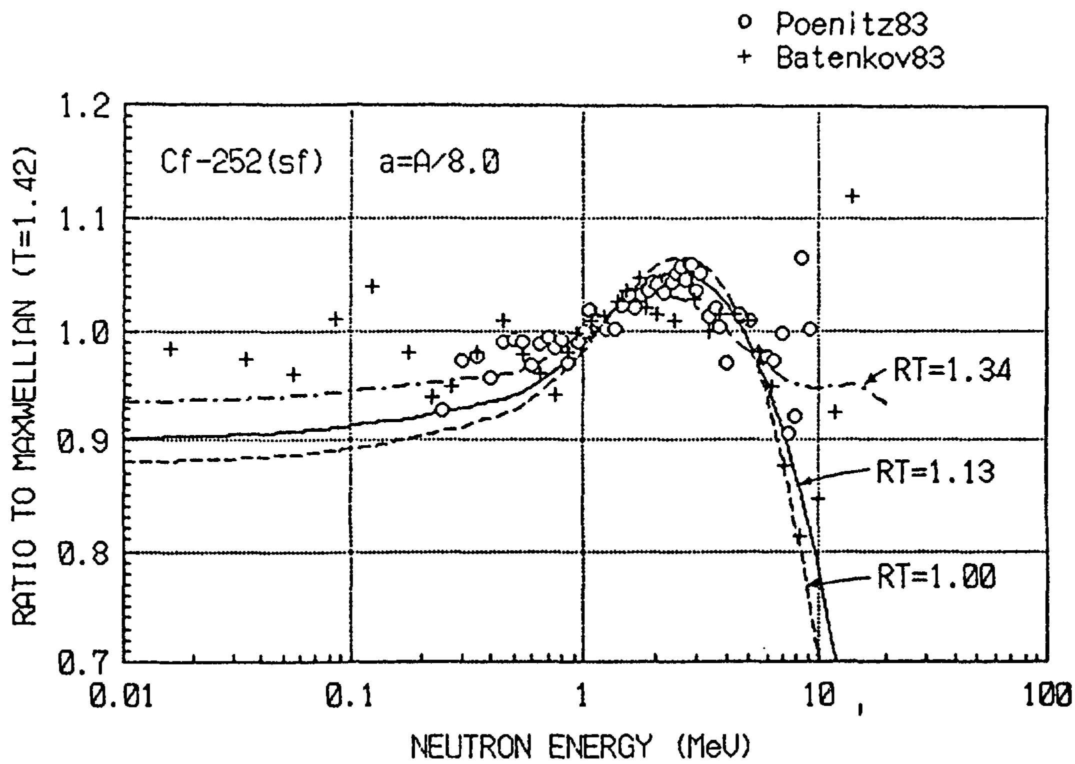

Fig.5 Fission neutron spectra for ^{252}Cf(sf).

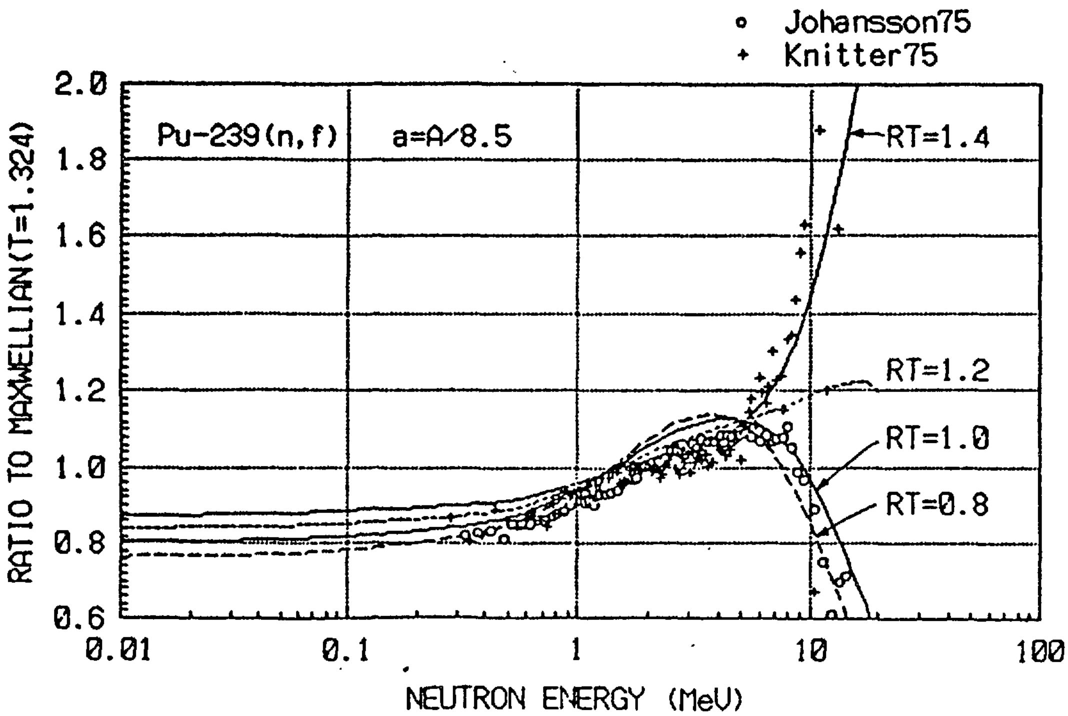

Fig.6 Fission neutron spectra for ^{239}Pu(n,f) for E_n = 0.53 MeV.

This value seems to be too large. Figure 5 shows the results for ^{252}Cf(sf). The experimental data were taken from the works of Poenitz and Tamura[13] and Batenkov *et al.*[14] Also in this case, better agreement was obtained by assuming non-equality of nuclear temperatures, although there still remain some discrepancies in the high and low energy ends of the spectrum.

The case for ^{239}Pu(n,f) is rather uncertain, because the two sets of experimental data, plotted in Fig.6, show different behavior in the region above 5 MeV. The data of Johansson *et al.*[15] are represented well with R_T=1.0, while those of Knitter[16] are represented with R_T=1.4.

V. Concluding Remarks

The main conclusions to be drawn from the present preliminary analysis are as follows:

a) Taking into account the non-equality of nuclear temperatures for the two fragments had greater effects than other factors in improving the calculated spectral shapes, increasing *both* the low- and high-energy neutron components.

b) For ^{235}U(n,f) and ^{252}Cf(sf), reasonable choice of the temperature ratio R_T lead to better agreement between the calculated and experimental spectra. For ^{239}Pu(n,f), conclusion must be postponed until the discrepancies between experimental data are resolved.

c) The non-equitemperature model should further be tested on other nuclides and at higher incident energies. It would be interesting to know how the temparature ratio changes when the excitation energy of the fissioning system is increased.

References

1) T.Takeda, H.Matsumoto and Y.Kikuchi, J. Nucl. Sci. Technol. 27, 581 (1990)
2) D.G.Madland and R.J.Nix, Nucl. Sci. Eng. 81, 213 (1982)
3) R.L.Walsh, Nucl. Sci. Eng. 102, 119 (1989)
4) D.G.Madland, R.J.LaBauve and J.R.Nix, *Physics of Neutron Emission in Fission*, Proc. of a Consultants' Meeting, Mito, 1988, INDC(NDS)-220, p.259 (1989)
5) H.Märten and D.Seeliger, Nucl. Sci. Eng. 93, 370 (1986)
6) C.Budtz-Jørgensen and H.H.Knitter, *Physics of Neutron Emission in Fission*, Proc. of a Consultants' Meeting, Mito, 1988, INDC(NDS)-220, p.181 (1989)
7) O.I.Batenkov, A.B.Blinov, M.V.Blinov, S.N.Smirnov, *ibid.* p.207 (1989)
8) B.D.Wilkins *et al.*, Phys. Rev. C14, 1832 (1976)

9) T.Tachibana, M.Uno, M.Yamada and S.Yamada, Private communication (1986)
10) J.P.Unik, J.E.Gindler, L.E.Glendenin, K.F.Flynn, A.Gorski, and R.K. Sjoblom, *Physics and Chemistry of Fission*, Int. Symposium, Rochester, Vol.II, p.15 (1973)
11) P.I.Johansen and B.Holmqvist, Nucl. Sci. Eng. 62, 695 (1977)
12) S.S.Kapoor, R.Ramanna and P.N.Rama Rao, Phys. Rev. 131, 283 (1963)
13) W.P.Poenitz and T.Tamura, Proc. Int. Conf. on Nuclear Data for Science and Technology, p.473 (1983)
14) O.I.Batenkov, M.V.Blinov, G.S.Boykov, V.A.Vitenko, V.A.Rubchenya, Proc. IAEA Consultants' Meeting on the ^{235}U Fission Cross-Sections and the ^{252}Cf Fission Neutron Spectrum, Vienna 1983, p.161 (1983)
15) P.I.Johansson, B.Holmqvist, T.Wielding and L.Jeki, Proc. Conf. on Nuclear Cross Sections and Technology, Washington, Paper GB-8 (1975)
16) H.H.Knitter, Atomkernenergie 26, 76 (1975)
17) D.G.Madland, R.J.LaBauve and J.R.Nix, *Nuclear Standard Reference Data*, Proc. of IAEA/AG Meeting, Geel, 1984, IAEA-TECDOC-335 p.267 (1985)

Determination of Nuclear Level Densities of Neutron Rich Fragment Nuclei from Measurement of Prompt Neutron Emission Spectra

M.S.Samant, R.P.Anand, R.K.Choudhury, S.S.Kapoor, K.Kumar, D.M.Nadkarni and A.Saxena

Nuclear Physics Division
B.A.R.C., Bombay 400 085

ABSTRACT

The energy distributions of the prompt fission neutrons in the rest frame of the fragments in $^{235}U(n_{th},f)$ were determined from the measurement of the spectra of prompt neutrons emitted along the direction of motion of fragments. The fragment energies were measured by a pair of surface barrier detectors in one set of measurements and gridded ionisation chamber in other set of measurements. The energy of neutrons were measured by the time of flight method using a NE213 scintillation detector. The data were analysed event by event to deduce neutron energies in the rest frame of the emitting fragment and thereby determine the neutron energy spectra and the neutron multiplicities as a function of fragment mass. The neutron emission spectra were also calculated with a statistical model code with shell and excitation energy dependent level density formulation to deduce the level densities of the neutron rich fragment nuclei through comparison of the calculated results with the experimental values.

INTRODUCTION

The energy distributions of the prompt fission neutrons in the rest frame of the fragments contain information on the statistical properties of the excited fission fragments, and their analysis can provide valuable information about the level densities of the neutron rich fragment nuclei. Detailed measurements of the multiplicity and energy spectra of neutrons as a function of mass, charge and kinetic energy of fragments are therefore important for carrying out direct comparisons with the predictions of statistical cascade calculations. Extensive measurements have been carried out in the past[1-10] on neutron emission characteristics in low energy fission of various fissioning nuclei. In a recent work[11], Budtz-Jorgensen et al have reported measurements of neutron emission spectra and temperatures of fragments of specified masses in the spontaneous fission of ^{252}Cf. Since neutron emission from fragments is a statistical cascade emission process and successive neutrons are emitted from the nuclei having different temperatures, the temperature determined from a Maxwellian distribution fit to the centre of mass spectrum gives an effective temperature (T_{eff}) of the excited fragment. The results of ref.11 have been discussed in terms of the T_{eff}, which in turn was related to the level density parameter.

The level density parameter of the fragments is better determined by directly comparing the measured T_{eff} with that obtained from the statistical cascade calculations which explicitly take into account multiple neutron emission. In this work we report our measurements on fission neutrons from which fragment temperatures and neutron multiplicities are deduced from the centre-of-mass spectra of the prompt neutrons emitted from the fragments in thermal neutron induced fission of ^{235}U. The results are analysed with the statistical evaporation code ALICE-II using shell dependent level densities of the excited fission fragments. The experimental details for the measurement of the neutron emission spectra and the methods of the statistical model calculations are described in the following sections.

EXPERIMENTAL SETUP

The experiment was performed using the thermal neutron beam from the CIRUS reactor at the Bhabha Atomic Research Centre in Bombay. Fig.1 shows the time of flight setup used to measure the neutron energy spectrum along the direction of emission of the fragments. The energies of the two fission fragments were recorded in coincidence to enable the determination of fragment masses for each event. In the first experiment, the fission fragments were detected with surface barrier detectors, placed on either side of a ^{235}U source. A 100 μg/cm^2 ^{235}U target electrodeposited on 160 $\mu g/cm^2$ Ni backing served as the fission source. The surface barrier detectors were located at 2.5 cm and 3.5 cm on either side of the target, which assured that both the fragments were detected in coincidence without any bias due to loss of collinearity of the two fragments from the extended source and neutron emission effects. A 5cm x 5cm NE213 scintillation detector which served as the neutron detector was placed collinear to the two fragment detectors at a distance of 66.8 cm from the ^{235}U target.The neutron detector was well shielded with 7 cm of lead surrounded by 50 cm of borated paraffin in a cylindrical geometry in order to reduce the background. The pulse shape discrimination property of the NE213 detector was applied to seperate neutron and gamma events using the crossover technique. The energy signals from the two fission detectors, the time of flight of the neutrons, the pulse shape signal and the pulse height of the neutron detector were recorded in list mode for offline analysis.

In the second type of experiments, a back-to-back gridded ionisation chamber was used to measure the energies and angles of the fission fragments. The grid pulse heights were used to determine the fragment angle with respect to the electric field direction of the ionisation chamber. The NE213 neutron detector was placed along the field direction in line with the ^{235}U source. The fission source was deposited onto a gold coated thin VYNS backing which was mounted on the cathode plate. The induced signal at the cathode was used to derive the start signal for the neutron time of flight measurements. The analysis procedure for energy and angle determination of fission fragments has been described in an earlier work[12]. Analysis of neutron spectra were carried out by electronically collimating the fragments to a cone of opening angle of $\pm 18^\circ$ with respect to the electric field direction.

DATA ANALYSIS AND RESULTS

About 2×10^5 and 1.5×10^4 coincidence events were recorded in the two experiments respectively. The fragment energy calibration in both the experiments and the angle calibration in the second

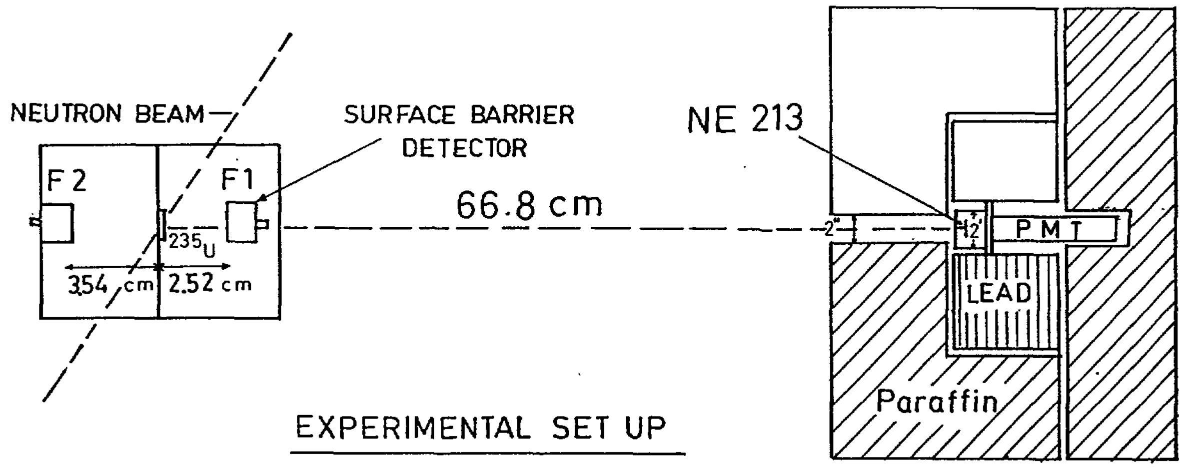

Fig. 1. Schematic diagram of the TOF setup for the experiment with surface barrier fission fragment detectors.

experiment with the gridded ionisation chamber, were done using the unbiased singles events which were taken from the online data recorded in coincidence with the random background in the time of flight spectrum. The energies of the two fission fragments were determined after correcting for the energy loss in the target and backing, for pulse height defect of the silicon surface barrier detectors[13] and for neutron emission using data of Maslin et al[14]. The preneutron fragment masses and kinetic energies were obtained in an iterative way using the mass and momentum conservation relations. The preneutron emission average total kinetic energy of the fragments thus obtained was found to be 171.8±1.5 MeV, in good agreement with recent literature data[15]. The peak to valley ratio in the fragment mass distribution was found to be about 100:1 and 300:1 in the two experiments, giving a mass resolution of 2-3 mass units.

Fig.2(a) shows a typical neutron time of flight spectrum in the first experiment obtained from event-by-event analysis after making corrections for the spread in the time of arrival of the fission fragments in the semiconductor detector. The time resolution of the setup as determined from the FWHM of the prompt gamma peak was about 2 ns. The pulse shape discrimination spectrum is shown in Fig.2(b). The gamma ray events were drastically cut down by gating the time of flight spectrum with a 2-dimensional gate of the pulse shape discrimination and the pulse height signals of the neutron detector. This was

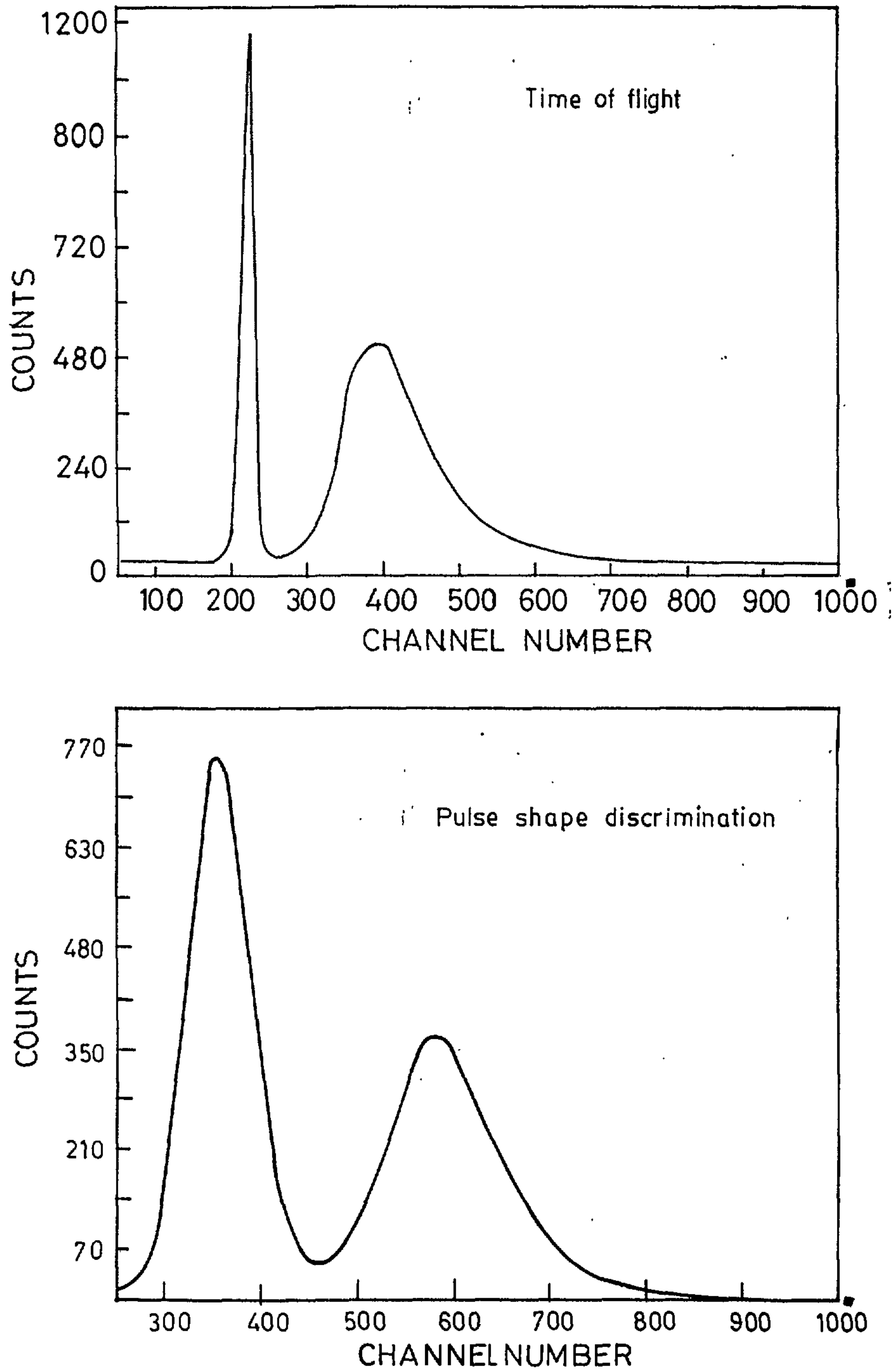

Fig. 2. (a). Neutron time of flight spectrum in Expriment-I
(b). Pulse Shape Discrimination spectrum in Experiment-I.

very effective in significantly reducing the contamination of the background and the fission gamma events in the high energy part of the neutron time of flight spectrum.

The detection efficiency of the neutron detector as a function of neutron energy was experimentally determined in a separate experiment by measuring the neutron energy spectrum in

^{252}Cf fission, intergated over all angles. This was done by mounting a ^{252}Cf source inside a mini-ionisation chamber to detect the fragments in 2π geometry and measuring the time of flight neutron spectrum without disturbing the geometry of the experimental setup. The measured ^{252}Cf neutron spectrum was compared with the theoretical form of the energy spectrum given by Madland and Nix[16] to deduce the efficiency of the neutron detector. The average efficiency of the neutron detector was found to be fairly constant over a broad energy range from 1 to 7 MeV, lying between 0.3 to 0.4 except near the threshold, which was found to be about 120 keV electron equivalent.

The multiparameter data of fragment kinetic energies and neutron time of flight (TOF) (and also of fragment-neutron angle in the second type of experiments) were analysed event-by-event. The neutron TOF gave the laboratory energy of the neutron which was then transformed to the centre of mass energy η after making the kinematic transformation involving the energy per nucleon of the emitting fragment. The neutrons were assumed to be emitted from the fragment moving towards the neutron detector. Due to strong focussing of the neutrons due to fragment motion, the contribution from the complementary fragment is expected to be less than a few percent in most cases and moreover the neutrons from these events will appear in the very low energy region. Hence this assumption is fairly well justified for all fragment masses. Following the above procedure the centre-of-mass spectra were generated as a function of various mass groups of four mass units each. The correction to these spectra from the random background neutron events were estimated from the average background per channel on the left of the gamma peak and on the extreme right of the neutron tail below the neutron detector threshold in the time of flight spectrum. The neutron multiplicities in the first experiment were derived from the experimentally measured neutron yeilds per fission, after correcting for the kinematic focussing effects. In the second experiment due to 4π geometry the neutron multiplicities were obtained directly from the ratio of the coincidence to the singles data. The experimental results on the average neutron multiplicity obtained with the two experiments were found to

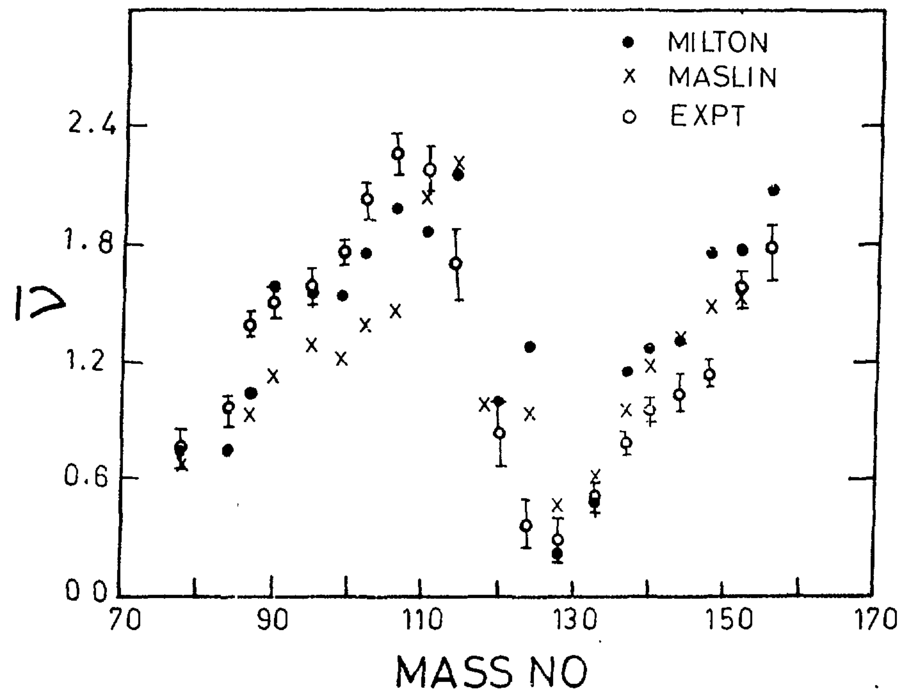

Fig. 3. Average Neutron multiplicity as a function of fragment mass. (o o o - present work, • • • - Milton et al [17], x x x - Maslin et al [14])

agree very well. Fig.3 shows the results of the neutron multiplicity $\bar{\nu}(m)$ as a function of fragment mass corresponding to the average values for the two experiments. The results of some of the earlier work[14,17] have also been shown in the figure. It is seen that the present $\bar{\nu}(m)$ values agree fairly well with the earlier avaliable data. However near A=100-110 amu the various data sets show a large scatter which may be connected with the mass resolution effects and proper correction of fragment recoil effects.

The neutron C.M. energy spectra were analysed in the following manner. According to standard nuclear evaporation theory the centre of mass neutron energy spectrum corresponding to a fixed residual nuclear temperature T is approximately given by Weisskopf theory[18] as

$$N(\eta) = \text{Const.} * \eta * \exp(-\eta/T) \qquad (1)$$

The evaporation spectrum for neutrons emitted in a cascade process is slightly modified and it was shown by Lecouteur and

Lang[19], that the spectrum can be represented as

$$N(\eta) = Const.*(\eta^{\lambda}/T_{eff}^{\lambda+1})* \exp(-\eta/T_{eff})....(2)$$

where T_{eff}= (11/12) T and λ = 5/11 for multiple neutron emission and λ = 1 for single neutron emission. It was also shown in Ref.19 that the energy spectrum gets further modified if evaporation takes place from a nucleus having a spread in the initial excitation energy.

We have carried out a parametric study of the neutron spectra calculated from an evaporation code for various nuclei over a range of initial excitation energies taking into account the cascade emission effects. The calculated spectra were fitted to the expression,

$$N(\eta) = Const.* \eta^{\lambda} * \exp(-\eta / T_{eff})..........(3)$$

and it was shown that the value of λ varies from about 1 at low excitation energies to about 0.5 for higher excitation energies where multiple neutron emission takes place.

Fig.4 shows the plots of the present experimental results in the form of ln $(N(\eta)/\sqrt{\eta})$ versus η for various fragment mass groups. The T_{eff} parameter was determined by fitting the observed centre of mass energy spectra with Eq.(3). The value of λ used for the fits was taken to be equal to 1 for cases where $\bar{\nu} \leq 1$ and 0.5 for those with $\bar{\nu}$ >1. Fig.5 shows the values of T_{eff} as obtained from these fits. The figure contains the results of both the experiments for the sake of mutual comparision of the experimental results. The two sets of data are found to be in good agreement with each other. It is seen from the figure that the T_{eff} parameter does not have a sawtooth dependence as a function of fragment mass,as is the case for the neutron multiplicities.

The present results on $\bar{\nu}(m)$ and $T_{eff}(m)$ were used to calculate the average excitation energy of fragments of specified mass m as follows:

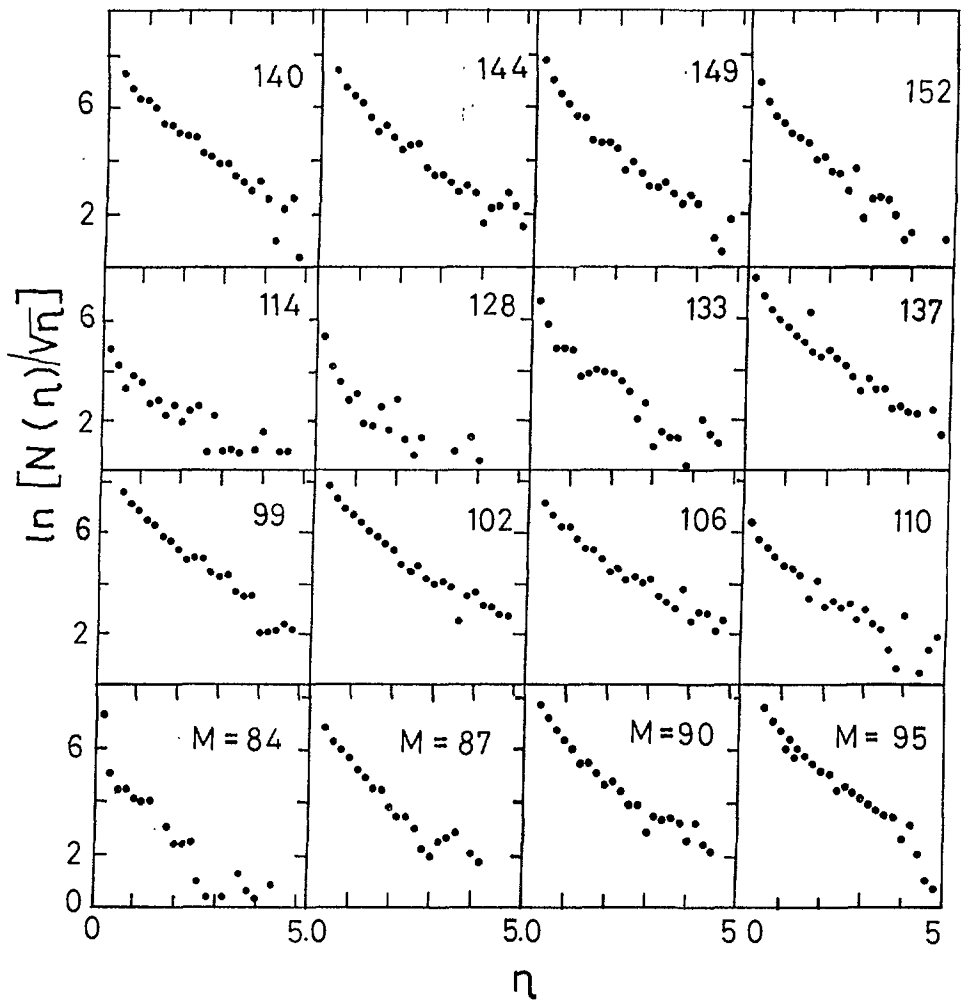

Fig. 4. Plots of neutron centre-of-mass spectra for various fragment mass groups.

$$\overline{E}_x(m) = \overline{\nu}(m)*[\overline{B}_n(m) + 3/2\ T(m)] + \overline{E}_\gamma(m)$$

where $\overline{B}_n(m)$ is the neutron binding energy for the particular mass group averaged over various fragment atomic numbers, and $\overline{E}_\gamma(m)$ is the average energy released by the gamma emission. The $\overline{B}_n(m)$ values were calculated taking into account the fragment charge distributions, and using the values of the neutron binding energies from the mass tables[21]. The $\overline{E}_\gamma(m)$ values were taken from the data of Pleasonton et al[22]. The total excitation energies of the fragments obtained by adding the excitation energies of the complementary fragments were found to be in agreement with the estimates of excitation energies obtained from total kinetic energy measurements[23] within about 2 MeV. The

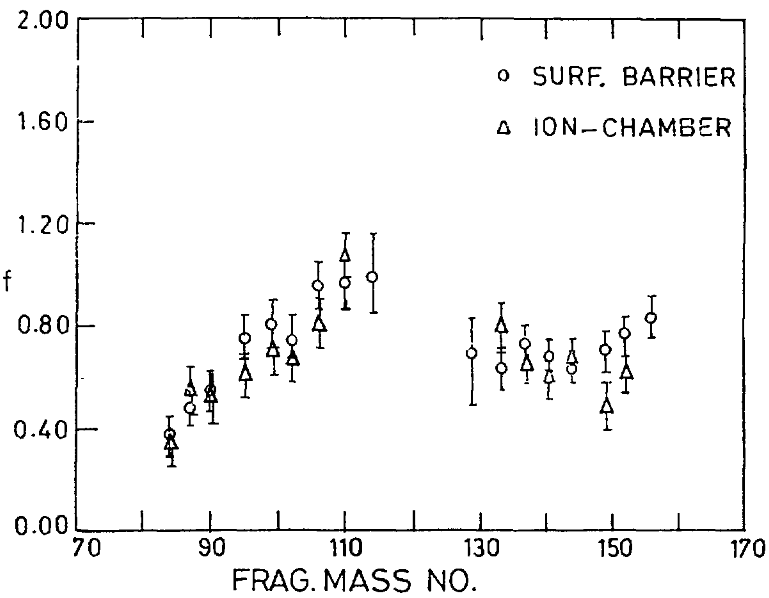

Fig. 5. Variation of T_{eff} with fragment mass.
(o o o – Experiment-I, △ △ △ – Experiment-II)

excitation energies calculated as above for individual fragment masses were then used as inputs to calculate the neutron emission spectra from an evaporation model code wherein the level density formulations could be changed as desired. The present calculations were done using the ALICE code[24] after incorporating a shell dependent level density formula[25] to take into account the excitation energy dependence of shell effects and the level density parameter 'a' corresponding to the liquid drop model, was kept as a free parameter. The ground state shell correction energies which go as inputs for the level density calculations were taken from the experimental shell correction energies given in Ref.26. These values were also suitably averaged to take into account the fragment charge distributions and spread in the masses for each mass group. Evaporation cascade calculations were carried out with a distribution in the excitation energy of each fragment for which the average was taken as mentioned above and the variance (σ^2_{Ex}) was estimated from the observed spread in the total fragment kinetic energy distributions[23]. It was assumed that the excitation energy spread of each fragment is in proportion to its average excitation energy. The calculations were carried out for level density parameter a = A/7 and A/10 and also with and without the shell correction in the level density expression to estimate the

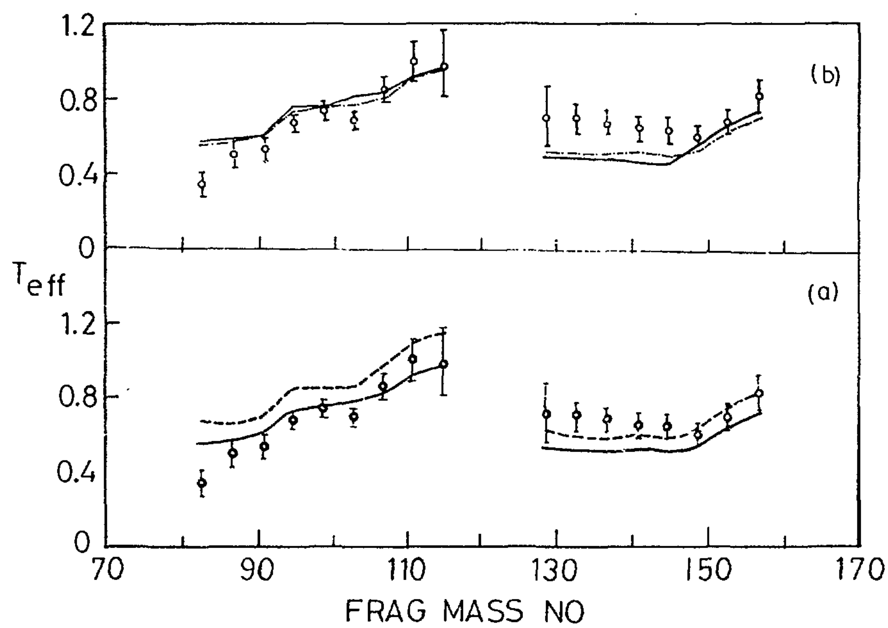

Fig. 6(a). Comparision of experimental and calculated values of T_{eff} as a function of fragment mass. Calculations include shell corrections in the level density formula (o o o – experimental values, ________ – calculation with a = A/7, _ _ _ _ – calculation with a = A/10)

6(b). Comparision of experimental and calculated values of T_{eff} with (_._._._) and without (________) inclusion of shell correction in the level density formula for a = A/7.

relative importance of the various parameters in the determination of neutron energy spectra. The calculated neutron spectra were also fitted to Eq.(3) in the same way as the experimental spectra, to define T_{eff} values for the calculated neutron spectra. Fig.6(a) and 6(b) give a comparision of the experimental T_{eff} values as a function of fragment mass with those calculated from the evaporation code. The experimental values of T_{eff} correspond to the average of the two experiments. It is seen from Fig.6 that the calculated T_{eff} values are sensitive to the level density parameter 'a', but are only marginally affected by the inclusion of shell corrections in the level density formula. The calculated results are therefore not affected by any uncertainties in the shell correction energies. It was also found that in the mass region A = 128–134 amu where the average excitation energies are small there is a marked effect of the inclusion of spread in the excitation energy of the fragments on the calculated T_{eff} values. As seen from the figure, in general, a better fit is obtained for all fragments with the level density parameter a = A/7, except in the mass region of A=128-140 amu, where a = A/10 gives a closer agreement to the experimental data. The reason for two different values of the 'a' parameter needed to fit the data in different fragment mass regions, is not clear at present. Further detailed measurements of neutron spectra from mass and kinetic energy selected fragments will be useful to make more definitive calculations for comparison with the data.

SUMMARY

Neutron emission spectra from fission fragments in thremal neutron induced fission of ^{235}U were determined from the measured spectra at 0° with respect to the direction of motion of the fission fragments. These centre of mass neutron spectra were then used to determine the temperatures of excited neutron rich fragments. Statistical model evaporation cascade calculations using shell dependent level density expressions show that after incorporating proper spread in the excitation energy of the fission fragments, the nuclear temperatures can be explained for all fragment masses with the level density parameter a = A/7 except in the mass region of A = 128-140 amu where a = A/10 gives a closer agreement to the experimental data. The reason for two different values of the 'a' parameter needed to fit the data in different fragment mass regions, is not clear at present.

REFERENCES

(1) H.R. Bowman et al, Phys. Rev. 126 (1962) 2120
(2) S.S. Kapoor et al, Phys. Rev. 131 (1963) 283
(3) V.F. Aplain et al, Nucl. Phys. 71 (1965) 553
(4) K. Skarsvag et al, Nucl. Phys. A163 (1970) 82
(5) A. Gavron and G. Fraenkel, Phys. Rev. C9 (1974) 632
(6) J.W. Boldeman et al, Aust. J. Phys. 24 (1971) 821
(7) C. Signarbieux et al, J. Phys., 33 (1972) 8
(8) D.C. Hoffman et al, Phys. Rev. C21 (1980) 637

(9) E.A. Sergina et al, Yad. Fiz. 42 (1985) 1337
(10) R.L. Walsh, Nucl.Phys. A469 (1987) 333
(11) C.Budtz-Jorgensen and H.H.Knitter, Nucl.Phys. A490 (1988)307
(12) R.K.Choudhury et al, Nucl.Inst. & Method. 164 (1979) 323
(13) H.W.Schmitt et al, Phys. Rev. B137 (1965) 837
(14) E.E.Maslin et al, AWRE Report No. O-43/67, June 1967
(15) C.Budtz-Jorgensen et al, Nucl.Inst. & Method. A258 (1987)209
(16) D.G.Madland and J.R.Nix,in Proc.Conf. on Nucl. data for Sci. & Tech. Antwerp, Belgium, Sept. 6-10 (1982) p 473
(17) J.C.D.Milton and J.S.Fraser,Proc. Symp. on Phys.and Chem. of fission,Salzburg, Vol.II (1965) p 39
(18) V.F.Weisskopf, Phys. Rev. 52 (1937) 295
(19) K.J.LeCouteur and D.W.Lang, Nucl. Phys. 13 (1959) 32
(20) K.Kumar et al, Proc. N.P.Symp.(DAE),India, Vol.33B (1990)155
(21) Atomic Mass Adjustment Tables, Nuclear Data Section, IAEA , (1983)
(22) F.Pleasonton et al, Phys. Rev. C6 (1972) 1023
(23) M.N.Rao , Ph.D. Thesis, Utkal University, India (1990)
(24) M.Blann , LLNL Report No. UCID-20169 (1984) unpublished
(25) S.K.Kataria et al, Phys. Rev. C18 (1978) 549
(26) P.A.Seeger and W.M.Howard, Nucl. Phys. A238 (1975) 491

Studies of Prompt Neutron Spectra and Angular Distributions from Fragments of Specified Mass and Kinetic Energy in $^{235}U(n_{th},f)$

M.S.Samant, R.P.Anand, R.K.Choudhury,
S.S.Kapoor and D.M.Nadkarni

Nuclear Physics Division
B.A.R.C., Bombay 400 085

ABSTRACT

Measurements of prompt neutron spectra and angular distributions from mass and kinetic energy selected fission fragments have been carried out in the thermal neutron fission of ^{235}U. Neutron energy was determined by the time of flight technique and the energy and angle of the fission fragments were measured using a back-to-back gridded ionisation chamber. In the preliminary analysis the angular distributions for a typical mass pair of M_L=96 amu and M_H=140 amu for different kinetic energy windows were compared with Monte Carlo calculations for neutron emission from fully accelerated fragments. The calculations were done using the measured centre of mass neutron spectra and neutron multiplicities for emission taking place from both fragments. Detailed analysis is still in progress for determination of the neutron spectra and angular distributions for various fragment mass pairs, which will be used to estimate the component of prescission neutrons in the fission process.

INTRODUCTION

Prompt neutron emission in thermal neutron induced fission of ^{235}U and spontaneous fission of ^{252}Cf has been studied in great detail[1-15] to understand the mechanism of emission of the prompt neutrons. While it is well established that fission neutrons are emitted primarily during deexcitation of the fully accelerated fragments, the question regarding a small fraction which may be emitted either during the act of scission, or during saddle to scission dynamics, or during the fragment acceleration phase is still not satisfactorily answered experimentally. The present models, to calculate laboratory fission neutron spectra by combining the theoretical neutron emission spectra of fragments from cascade calculations with the kinematic effects of fragment motion, have neglected consideration of prescission neutrons. On the other hand, more accurate information on this component will not only lead to further refinement in the models to calculate fission neutron spectra, but will also provide a better insight on the fission process. Recent studies on prompt neutron emission in heavy ion induced fission reactions show that in many systems the number of prescission neutrons emitted is much higher than that expected from statistical models, thereby leading to the conclusion of prolonged saddle to scission transition times in the fission process (for a review see ref.16). This calls for a reexamination of the characterstics of neutron emission in the low energy fission process. The yield of prescission neutrons as deduced in earlier studies[1-13] for $^{235}U(n_{th},f)$ and spontaneous fission of ^{252}Cf range from 5% to 25%. The variation of the prescission neutron yield with total kinetic energy of the fragments obtained by different authors[6,11,12] also exhibit strong contradictions. However the recently measured anisotropy data[14-15] for the case of $^{252}Cf(sf)$ are in good agreement with the evaporation calculations from the fully accelerated fragments, leading to the conclusion that the yield of prescission component is either zero or less than 5%.

The question of whether or not the prescission neutron component is present, is answered by comparison of the experimental neutron-fragment angular correlations with those calculated from kinematical considerations assuming neutron emission from fully accelerated fragments. The calculated neutron angular distribtion is, however, very sensitive to the emission spectrum of neutrons in the rest frame of fragments. In the earlier analyses, the emission spectra have been obtained from evaporation type calculations and any uncertainty in the calculation of the emission spectra would affect the conclusions on the prescission neutron emission. In the present work, the aim is to carry out a self consistent analysis by using the experimentally measured neutron spectra in the rest frame of fragments for calculation of the neutron-fragment angular correlations to be able to reach model independent conclusions regarding prescission neutron emission for the case of thermal neutron induced fission of ^{235}U.

EXPERIMENTAL SETUP AND ANALYSIS

A back-to-back gridded ionisation chamber[17] was used to measure the energy and angle of both the fission fragments as shown in Fig.1. The chamber consisted of a central cathode and two parallel plate ionisation chambers with frisch grids in a back-to-back geometry. The distance between the anode and the grid was 0.7 cm and between the cathode and grid was 3.0 cm. A

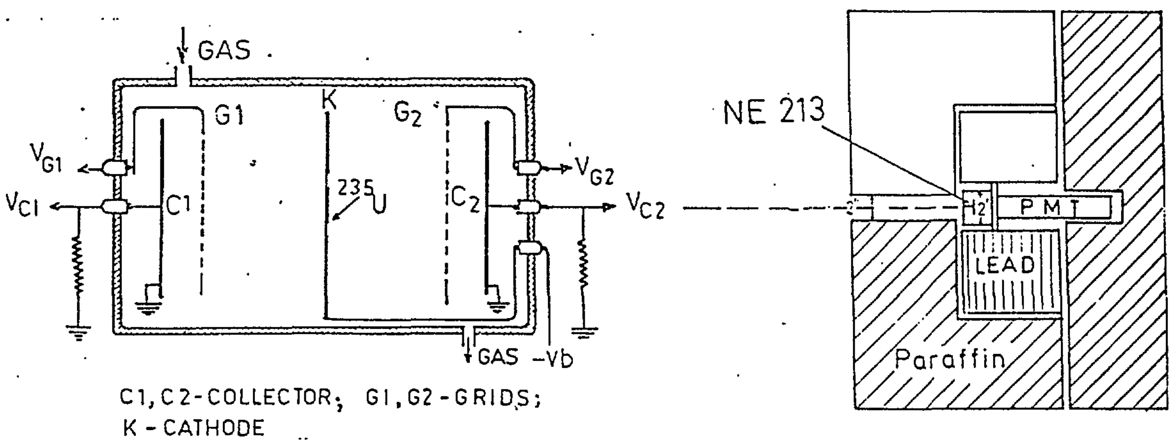

Fig. 1. Schematic diagram of the experimental setup.

^{235}U source of 60 μg/cm² thickness on a thin VYNS backing was made electrically conducting by covering it with 20 μg/cm² of gold, and was directly mounted in the centre of the cathode. The complete assembly was then housed in a brass chamber ,which was filled with P-10 gas at 1.1 atm pressure. The gas was then continuously purified by passing it over heated calcium filings. A 5cm x 5cm NE213 liquid scintillation detector was used to detect neutrons. The detector was placed at a distance of 70 cm from the Uranium target along the direction of the electric field of the ion-chamber. The neutron detector was adequately shielded with 7 cm of lead and 50 cm of borated paraffin on all sides, for suppressing the background neutrons and gammas. The neutron energy was measured with the time of flight technique, with the start signal taken from the common cathode of the ion-chamber and the stop signal taken from the neutron detector. The pulse heights of the two collectors (V_{c1},V_{c2}), grids (V_{G1},V_{G2}), neutron time of flight, pulse shape discrimination and pulse height signals of the neutron detector were recorded event by event on a magnetic tape.

A total of 3.6×10^6 coincident events were collected out of which about 10^6 events correspond to prompt neutron coincidences. The time resolution as seen from the prompt gamma peak of the neutron time of flight spectrum was about 2.5 ns. Singles binary events were also recorded for the calibration of the grid distribution for determination of the angle of the fission fragments. The threshold of the neutron detector was set at 60 keV electron equivalent energy by using an ^{241}Am source. This threshold is equivalent to a neutron energy of about 200 keV. The pulse shape discrimination signal was used to differentiate the neutrons from gamma rays, which greatly improved the high energy part of the neutron energy spectrum. The neutron events were selected offline by using a two dimensional gate on the neutron time of flight and pulse shape of the neutron detector pulses. The efficiency of the neutron detector as a function of neutron energy was determined by comparing the measured ^{235}U-neutron spectrum in 4π geometry with the known theoretical spectrum shape[18]. The efficiency values also agreed well with the results of Monte Carlo calculations for the efficiency of the neutron detector. These efficiency values were used to correct the neutron spectra as a function of energy.

The singles binary data from the ion-chamber were analysed to obtain the calibration of the grid pulses for event by event angle determination. The method of analysis for angle determination using the grid and collector pulse heights has been described elsewhere[19]. The angular resolution was determined from the difference between the angles of the complementary fission fragments measured on the two sides of the ionisation chamber and was seen to be in the range of 3° to 5° FWHM as shown in Fig.2. The event by event angle determination enabled collimation of the fragments to any angle in a cone along the

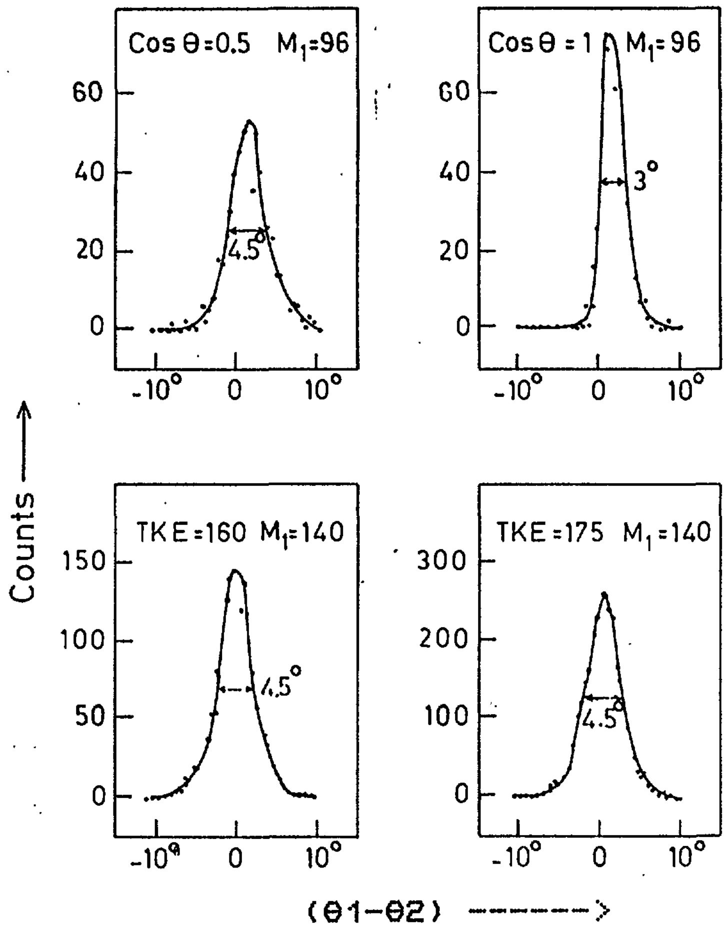

Fig. 2. Distributions in the difference of the fragment angles obtained on either side of the chamber for certain fragment mass, kinetic energy and angle bins.

field direction. A peak to valley of 300:1 in the mass distribution was obtained for fragments emitted upto $\theta = 85°$ with respect to the field direction. The events between $\theta = 85°$ to $90°$ were highly degraded in energy due to target thickness effects and were neglected for further analysis. Preliminary results obtained on the energy spectra and angular distributions of neutrons for a typical mass pair of $M_L=96$ amu and $M_H=140$ amu are reported in the following section.

RESULTS

The centre of mass neutron energy spectra were determined event by event from the measured energy spectrum of neutrons after collimating the events to an angle of ±18° with respect to the field direction for various fragment masses. These spectra

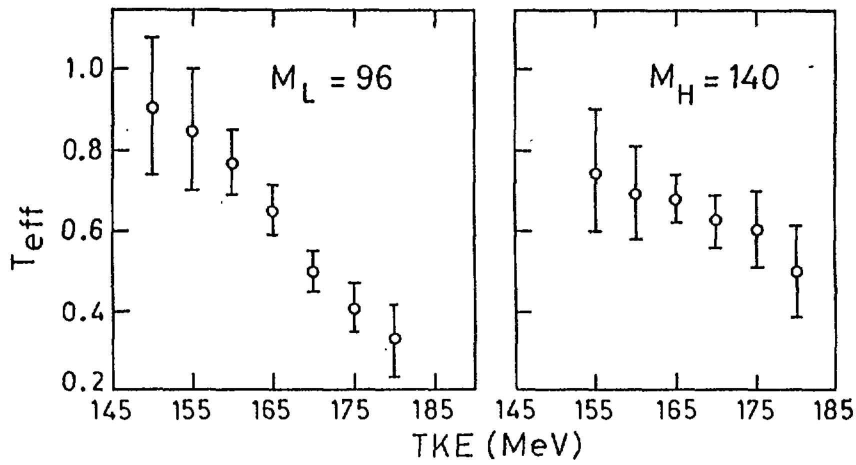

Fig. 3. Variation of T_{eff} with total kinetic energy of the fragments for the mass pair of M_L= 96 and M_H=140 amu

were then fitted to the standard evaporation spectrum

$$N(\eta) = \text{Const.}* \eta^{\lambda} * \exp(-\eta/T_{eff})$$

where η is C.M. energy of the neutron and T_{eff} is the effective temperature of the fragments and T_{eff}=(11/12)T. Here λ was taken to be equal to 1 for cases where $\bar{\nu} \leq 1$ and 0.5 for the cases when $\bar{\nu} > 1$, where is the neutron multiplicity. The results on the variation of T_{eff} with fragment mass have been presented elsewhere in the present proceedings. Here we report more detailed results for a typical mass pair of M_L=96 and M_H=140 amu. Fig.3 shows the results on the variation of T_{eff} as a function of total kinetic energy (TKE) of the fragments for this mass pair. It is seen that T_{eff} decreases strongly with increasing fragment kinetic energy.

The angle between the neutron detector and the fragment direction was determined from the event-by-event analysis of the data. Neutron angular distributions for various mass and kinetic energy bins were obtained by normalising the coincidence data with the unbiased singles angular distributions. Fig.4 shows the angular distributions of neutrons obtained for this mass pair (96/140) for various total kinetic energy bins. This figure also shows the results of calculated angular distributions for these cases using a Monte Carlo procedure. The calculations were done by assuming the neutrons to be emitted isotropically in the

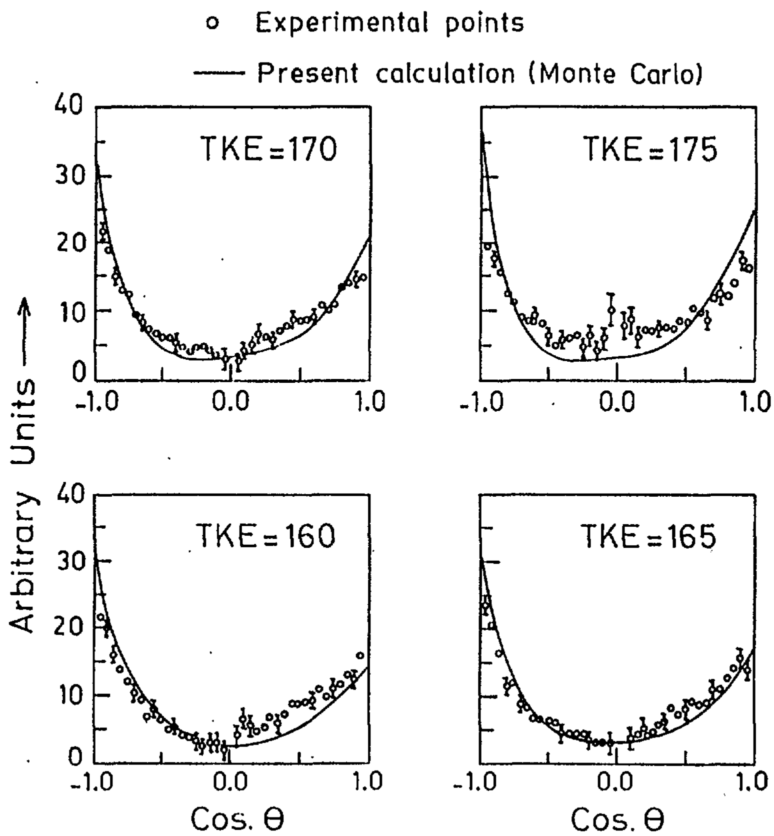

Fig. 4. Angular Distributions for the mass pair of M_L= 96 amu and M_H= 140 amu for various TKE bins. (o o o – experimental data, ________ – Monte Carlo calculations)

fragment centre of mass frame, from fully accelerated fission fragments. The centre of mass neutron energy spectra for various TKE windows were taken from the present measurements as shown in Fig.3. The contributions from the two fragments were added in proportion to the neutron multiplicites for the light and heavy fragments(ν_L and ν_H) for the various TKE windows. The calculated distributions are seen to reproduce the observed behaviour to a large extent in all the cases. However the calculated distributions are seen to be somewhat more anisotropic than the experimental values and the deviations increase with increasing TKE values. Since neutron multiplicities decrease significantly at large TKE values, the random background may assume a larger proportion as compared to the true coincidence events. The present data on angular distributions have not been corrected for the random contributions. Another factor responsible for giving low measured anisotropies could be the finite angular resolution of the experiment. Both the above effects must be included in the analysis of the data before a proper comparision of the results can be carried out with the theoretical calculations. Further analysis to include the various corrections to the data to determine the neutron angular distributions for different fragment mass and kinetic energies is in progress.

SUMMARY

The present paper deals with an experiment aimed to measure neutron energy spectra and angular distributions in thermal neutron fission of ^{235}U.The measurements were done using a back-to-back gridded ionisation chamber for determination of fragment energies and angles along with a NE213 detector for determination of neutron energy. Preliminary results for the mass pair of 96/140 have been reported in the text and more detailed analysis is in progress.

References

(1) H.R.Bowman, S.G.Thomson, J.C.D.Milton, W.J.Swiatecki, Phys.Rev. 126 (1962) 2120

(2) S.S.Kapoor, R.Ramanna, P.N.Ramarao, Phys.Rev. 131 (1963) 283

(3) K.Skarsvag and K. Bergheim, Nucl.Phys. 45 (1963) 72

(4) C.P.Sargent, W.Bertozzi, P.T.Thomas, J.L.Matthews, Phys. Rev. B137 (1965) 89

(5) J.C.D.Milton, J.S.Fraser, Physics and Chemistry of Fission, Proc.IAEA Symp, Sälzburg,1965, Vol.2 (1965) 39

(6) M.V.Blinov, N.M.Kasarinov, I.G.Krisyuk, Yad. Fiz. 12 (1970) 41 and Yad. Fiz. 16 (1972) 1155

(7) C.J.Bishop, I.Halpern, R.W.Shaw, R.Vandenbosch, Nucl.Phys. A198 (1972) 161

(8) Z.Fraenkel, I.Mayk, J.P.Unik, A.J.Gorski, W.D.Loveland, Phys. Rev. C12 (1975) 1809

(9) S.Nair,D.B.Gayther, J. Phys. G3 (1977) 949

(10) S.Nair,D.B.Gayther,B.H.Patrick,E.M.Bowey, J. Phys. G3 (1977) 965

(11) V.M.Piksaikin,P.P.Dyatchenko,L.S.Kuzaeva, Yad. Fiz. 25 (1977) 723

(12) J.S.Samyatnin, D.K.Ryasanov, B.G.Basova, A.D.Rabinovich, V.A.Koristilev, Yad. Fiz. 29 (1979) 595

(13) P.Riehs, Acta. Phys. Austr. 53 (1981) 271

(14) H.Marten,D.Seeliger, Proc.Int.Conf.on Nucl.Data for basic and applied science, Santa Fe, USA, May,13-17,1985

(15) C.Butz-Jorgensen,H.H.Knitter, Nucl. Phys. A490 (1988)307

(16) S.S.Kapoor, Proc. INDC Meeting on Physics of Neutron Emission in Fission, Mito City, Japan, IAEA, June, 1989, INDC-(NDS)-220, p 221

(17) R.K.Choudhury et al, Nucl. Inst. & Meth. 164 (1979) 323

(18) J.Neill, Report GA-9753 (1969)

(19) M.S.Samant, R.P.Anand, R.K.Choudhury, D.M.Nadkarni and S.S.Kapoor, To be published

THE FISSION NEUTRON SPECTRUM OF ^{237}Np.

A.M.Trufanov, G.N.Lovchikova, B.V.Zhuravlev, S.E.Sukhikh, A.V.Polyakov, V.A.Vinogradov.

Institute for Physics and Power Engineering, Obninsk, USSR.

A.Ruben, U.During.

Technische Universität, Dresden, Germany.

Abstract

Prompt neutron spectra from the fission of Np-237 induced by 6.0 MeV neutrons have been studied. Measurements were carried out by the use of the time-of-flight method at the EGP-10M tandem accelerator. A gaseous tritium target was applied as neutron source.

Prompt fission neutron spectra have been measured at the angle 90 deg. with respect to incident neutron direction. The measured spectra have been fitted to Maxwellian distribution.

In this paper we present the results of fission neutron energy spectra measurements of ^{237}Np at incident neutron energy 6.0 MeV. It is necessary to note, that there is a little of fast neutron induced fission data in the MeV-region of incident neutrons due to big experimental difficulties. There are some difficulties in comparison experimental date with theoretical calculations from lack of fission neutron spectra induced by fast neutrons.

The prompt fission neutrons spectra measurements were carried out at the fast neutron Time-of-Flight spectrometer with a tandem accelerator EGP-10M as a basic [1] . Gas tritium target have been used as a neutron source. The neutron yield of a neutron-production target was 10^8 n/sr·μC under the 0^o angle, the energy resolution was 50 - 70 keV.

The multi-plate fission chamber [2] wich consists of 40 hemispherical plates (electrodes) with 500 mg ^{237}Np on them has been located at 17 cm distance from the gas tritium target center. The multi-plate fission chamber electrodes were divided on sections with 200 - 300 pf electricity capacity in each section for

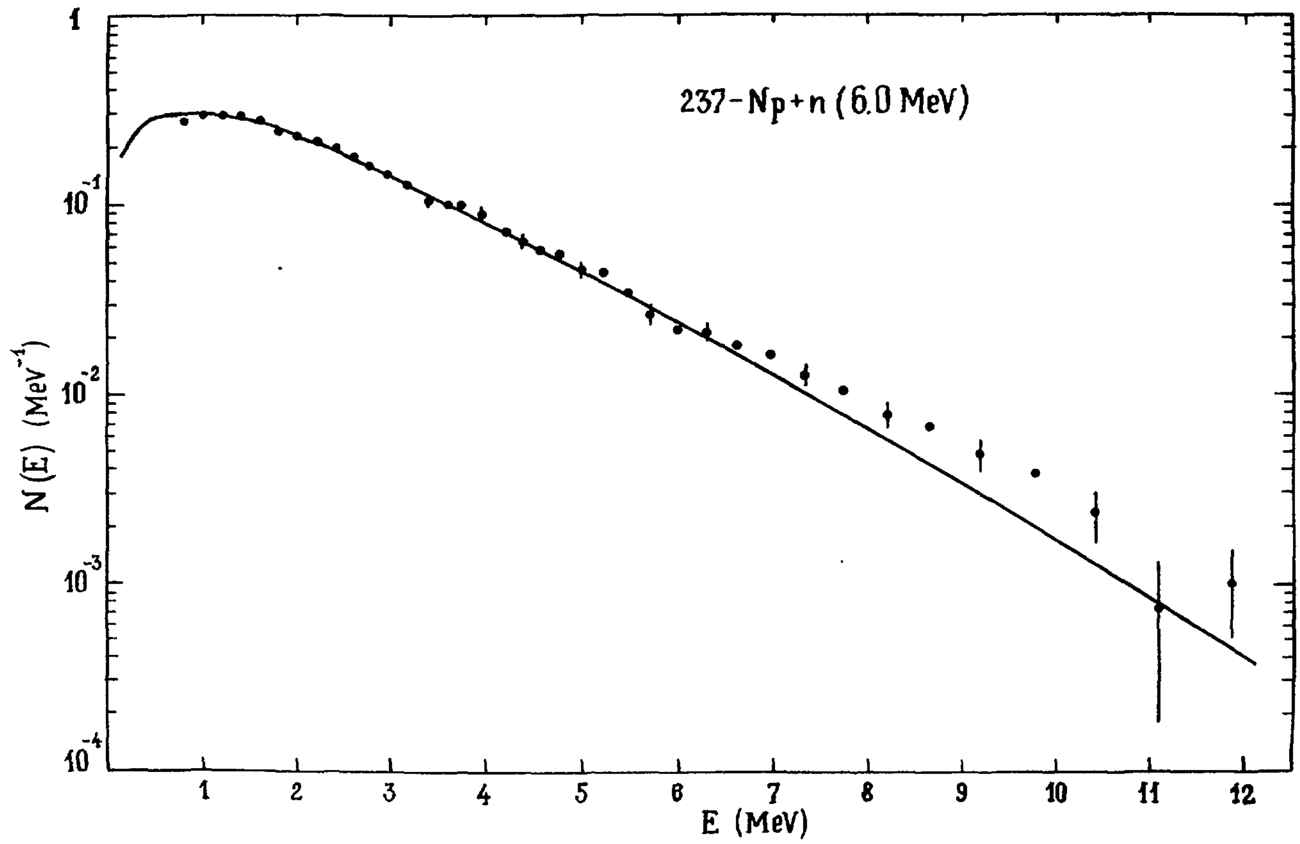

the simplification of puls fast component extraction used us a time mark from the chamber.

The fission neutrons were registred by scintillation detector placed at the 130 cm distance from the center of the chamder. Detector was consisted of a cylindrical stylben scintillator with 6.3 cm in diameter and 3.9 cm thickness viewed by a FEU-30 photomultiplier. The registration efficiency of the detector was about 30 % with a threshold about 0.4 MeV, time resolution of the spectrometer was 5 ns. The neutrons and γ-rays induced impulses form division electronic scheem was used for the suppressing of the γ-rays registration. The neutron detector efficiency was obtained by measuring of ^{252}Cf (sf) neutron spectrum as a standart[3]. The ^{237}Np prompt neutron spectrum and ^{252}Cf (sf) neutron spectrum were measured under the same conditions.

The prompt fission neutron spectra measurement were carried out for angle 90^{o} with respect to proton beam direction.

The following points have been taken into consideration specially under processing:

1. The stability of the neutron detector efficiency wich determinates the accuracy of neutron spectra form.

2. Constancy of energy resolution of spectrometer due to it's time resolution.

3. The influence of constant background component.

Measured fission neutron spectra of ^{237}Np is shown in Fig.1 without energy resolution correction. The appoximation of the measured fission neutron spectra by Maxwellian distribution results in parameter T = 1.486 MeV and therefore the middle energy of spectra is 2.23 MeV. The data are compared with calculations carried out in the FINESSE model framework for fissioning actinide nuclei(solid line) [4] .

REFERENCES

1. V.G.Demenkov et al., Report FEI-2013, Obninsk, USSR, 1989
2. S.E.Sukhikh et al., Report FEI-1927, Obninsk, USSR, 1988.
3. W.Mannhart, LOG. Cit. 161, 194.
4. D.Seeliger et al., INDC(GDR)-057, IAEA, Vienna, 1990

SPONTANEOUS FISSION NEUTRON SPECTRUM MEASUREMENT OF CURIUM-248.

O.I.Batenkov, A.B.Blinov, M.V.Blinov, A.S.Krivokhatski, B.M.Alexandrov.
V.G.Khlopin Radium Institute, Leningrad, USSR.

Abstract

The energy distribution of neutrons in the spontaneous fission of ^{248}Cm was measured relative to that in the spontaneous fission of ^{252}Cf. The experimental results are discussed in the light of comparison with Maxwell distribution.

The knowledge of the spontaneous fission neutron spectra is of interest both for studying the process of heavy nuclei fission, and for practical tasks in connection with the accumulation of heavy elements in nuclear reactors.

The available information is very limited and in literature there are only data for spontaneously fissile nuclides ^{240}Pu, ^{242}Pu, ^{244}Cm, ^{246}Cm, ^{248}Cm, ^{252}Cf /1-4/. For all the nuclides, except ^{252}Cf -the international standard of neutron spectrum, the spectrum shapes were measured with a low accuracy and in a comparatively narrow range of neutron energies. For ^{248}Cm there is practically information only about the middle energy of the spectrum /4/.

At the same time ^{248}Cm is of special interest because, on the one hand, its half-life ($\tau \sim 4x10^5$ years) is essentially greater than that of ^{252}Cf ($\tau \sim 2.7$ years), and on the other hand, the intensity of ^{248}Cm spontaneous fission is high enough ($\sim 10^4$ fiss/mgs) which enables to use it in various scientific and practical purposes. It was suggested for application as a source of standard spectum /5/ for long-time measurements requiring a practically unchanged intensity of fissions in a sample.

METHOD AND APPARATUS.

A multidimensional time-of-flight neutron srectrometer was used for measurement of the ^{248}Cm spontaneous fission neutron spectrum. The ^{248}Cm neutron spectrum was measured relative to ^{252}Cf .

For this purpose a special source of fissions was manufactured, representing a thin platinum disc (0.1 mm thick), on one side of which was Cf and on the other, Cm layer. The californium and curium used for preparation of the source were of high purity. The isotope composition of the curium source was as follows: ^{244}Cm - 0.04%, ^{245}Cm - 0.2%, ^{246}Cm - 4.5%, ^{248}Cm - 95.2%. The shape of spontaneous fission in the curium layer from ^{252}Cf impurities did not exceed 5%, the alpha activity of the layuer due to the ^{244}Cm impurity increased by eight times. The layers were made by the vacuum thermal evaporation method (the layers diameter being 7 mm). The intensity of fissions in the curium layer was $2x10^4$ fiss/min, and in the californium layer - 10^5 fiss/min. Both sources of fissions were covered with thin films (40 μg/cm² thick). The electrons knocked out from the films at fragments passing, were registrated by means of detectors based on microchannel plates (MCP), due to which the registration and the time reference was done for all the events of fission of Cf and Cm.

To check the detection of fragments within the angle 2π a comparison of the amplitude distribution of pulses from MCP was done in coincidence with neutrons and without coincidences (fig.1).

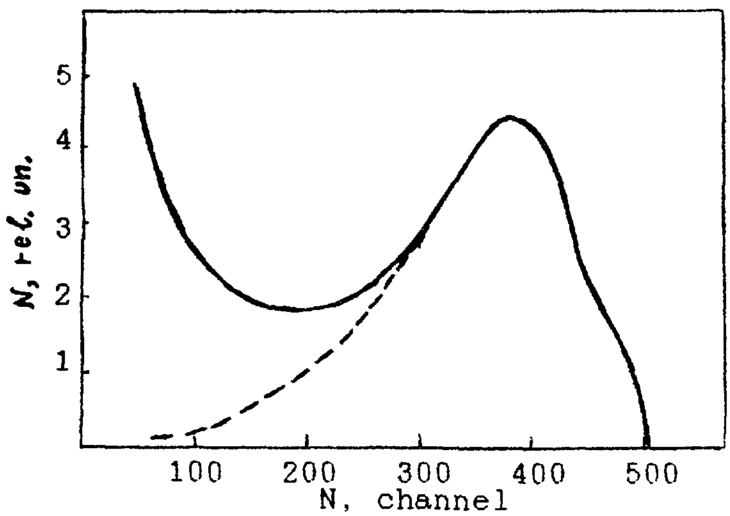

Figure 1. The amplitude distribution of pulse from MCP
--- coincidence with neutron pulses
— without coincidence

It was obtained on the basis of analysis of these data and measurements with the use of semiconductor detectors, that not less than 98% of all fragments were registrated. A stilbene crystal 50x30 mm with a photoelectron multiplier FEU-30 was used as the neutron detector. To decrease the number of background neutrons and to improve the time resolution, a two-threshold system of neutron registration was used. The values of the upper and low thresholds were a function of the neutron energy (fig.2).

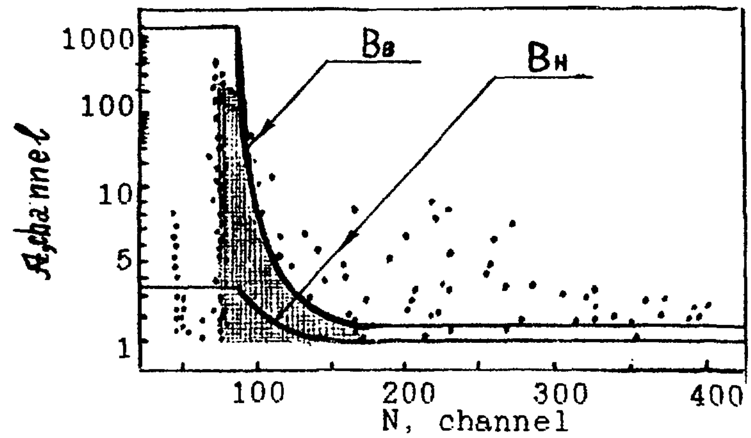

Figure 2. The time (N) - amplitude (A) dependence for neutron channel
Bв - upper threshold of neutron registration
Bн - low threshold

The time resolution for energies over 1 MeV was 0.6 ns, and for small energies, 1 ns. The separation of neutrons and gamma-quanta was done by means of the use of the pulse shape. The suppression factor for neutron energies about 0.5 MeV was 10^4, below 0.5 MeV - 10^2. All this enabled to carry out measurements in the neutron energy range 0.1 - 10 MeV.

Cf and Cm neutron spectra were measured simultaneously, using the same neutron and fragment electronic channels. This reduced to minimum the effects of instability of the electronics and the detectors. In order to increase the precision two neutron detectors were used simultaneously, placed diametrically opposite relative to the layer. The measurements were done on three time-of-flight bases : 15, 30, 60 cm.

In fig. 3 there are presented the results of measurements of the ^{248} Cm spontaneous fission neutron spectrum in reference to the ^{252} Cf neutron spectrum.

Check measurements were also done, with turning by 180° and with placing the neutron detector by the normal to the layer and at an angle 70°. All the data well agreed (2-8 %) within the measurement error limits.

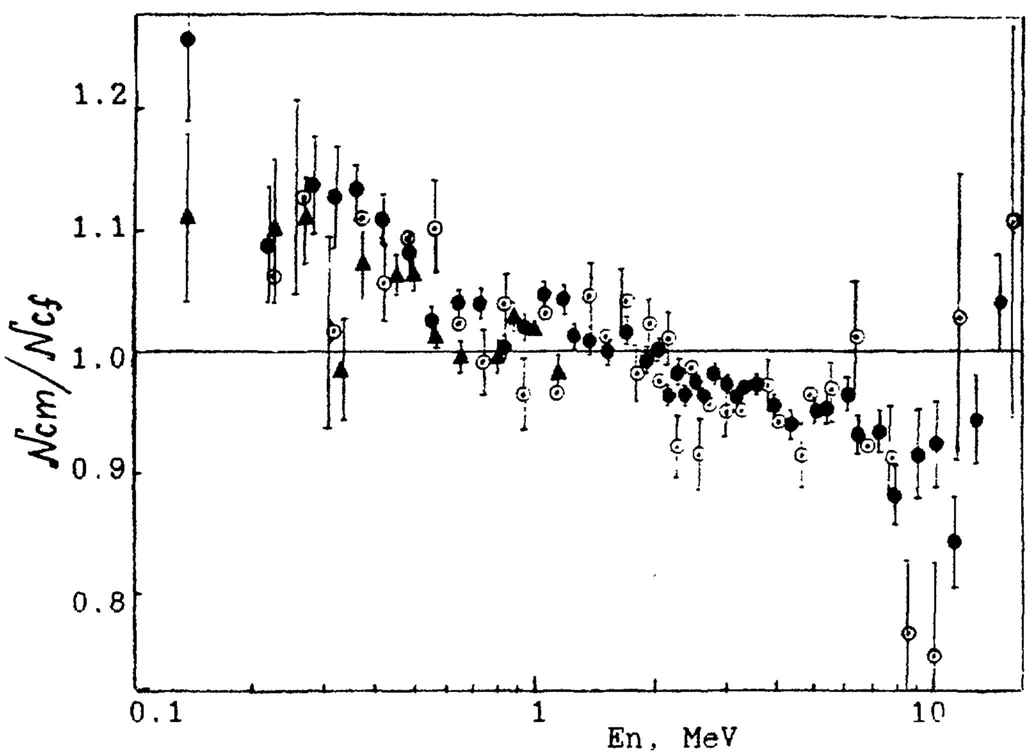

Figure 3. The ratio of the energy distribution of Cm spontaneous fission neutrons to the neutron energy distribution for Cf.
The measurements at various time - of flight bases: (▲) - 15cm., (●) - 30cm., (O) - 60cm.

RESULTS AND DISCUSSION

The ^{248}Cm spontaneous fission neutron spectrum is shown in fig.4 as a relation to the Maxwell distribution with T=1.38 MeV. Such a representation has been recently used for description of fission neutron spectra, because it allows to present results graphically most precisely. The value T=1.38 MeV was chosen proceeding from the best fitting of the energy range 0.75 - 6 MeV.

The errors in fig.4 include statistical and systematical errors, as well as errors in determination of the standard spectrum shape /3/. As the measurements for Cm and Cf were carried out under strictly equal conditions of registration of fragments and neutrons, the systematical errors were reduced to minimum and slightly influenced the final results.

Proceeding from average energy of neutron spectrum $\bar{E}$=2.069 + 0.008 MeV, the average Maxwell temperature of the spectrum (T eff.= 2/3 $\bar{E}$) was determined. It turned out to be T=1.379 + 0.005 MeV. Using the Terrell systematics /10/ based on approxi-

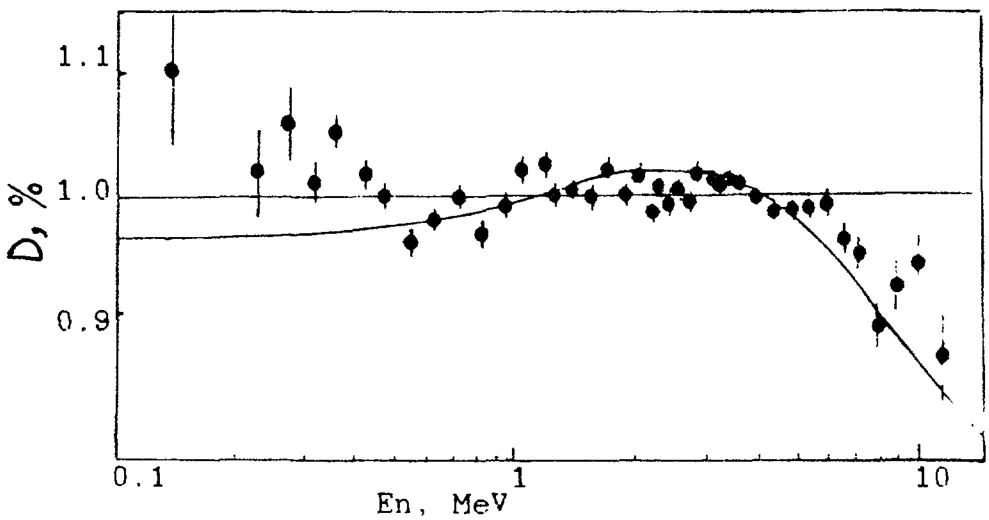

Figure 4. The deviation of the integral neutron spectra for Cf and Cm from Maxwell distributions.
(●) - the data of this paper for ^{248}Cm (T=1.38 MeV)
(—) - the data [3] for 252Cf (T=1.42 MeV).

mate statistical calculations gives T= 1.383 MeV, which quite corresponds to the data of experiment.

Studying the ^{252}Cf spontaneous fission neutron energy spectrum /3/ showed that there is a difference between the measured spectrum and various statistical calculations in the low-energy part of spectrum (En < 0.5 MeV) /6 - 7/. In work /8/, on the basis of analysis of differential measurements data, it was treated as a manifestation of a new mechanism of neutron emission. This effect seems to be connected with the emission close to the instant of the nucleus scission. However, the discrepancy of the experimental and the calculation data did not yet give confidence in such an interpretation of results. Measurements done this work for the first time point out to the reality of the given effect. As one can see from fig.4, in the neutron energy range below 0.5 MeV quite a strong excess of the spectrum intensity over the Maxwell distribution with T=1.38 MeV is observed for ^{248}Cm. Theoretical calculations of the ^{248}Cm spontaneous fission neutron spectrum are absent. The course of the statistical calculated spectrum for ^{252}Cf / 6-7 / in the low energy range goes markedly lower that the corresponding Maxwell distribution. Calculations done for the thermal neutron fission of ^{239}Pu /9/ (in these cases the neutron multiplicities ($\bar{\nu}$) for ^{248}Cm and ^{239}Pu are close) also show a lower intensity of the spectrum in comparison with the corresponding Maxwell distribution in the neutron energy range less that 0.5 MeV. Therefore, the observed excess of neutrons in the low energy range for ^{248}Cm may be treated as a manifestation of the neutron emission mechanism connected with emission of neutrons at the earlier stages of spontaneous fission process. As the contribution of additional mechanism, connected with emission of low energies neutrons ($E_n < 0.5$ MeV), considerably greater for ^{248}Cm than for ^{252}Cf, then it seems interesting to measure neutron spectra in this energy region at fission of different nuclides.

Thus, measurements of the ^{248}Cm spontaneous fission neutron spectrum has been done with high precision in this work. The results of the measurements show a possibility of its use as a standard neutron spectrum.

REFERENCES

1. Alexandrov B.M. et. al., Atomnaya Energia, 1974, v.36, p.282.
2. Belov L.M. et.al., Yad. Fiz., 1969, v.9, p.421.
3. Mannhart W., Proc. IAEA Group Meeting on Neutron Sources, Leningrad, USSR, June 1986, p.158.
4. Zhuravlev K.D. et. al., Nejtr. Fiz., Kiev, 1974, v.4, p.57.
5. Alexandrov B.M., et. al., Abstraacts, International Conference " Actinides-89", Tashkent, USSR, Sept. 24-29, 1989, p. 43
6. Madland D., Labauve R., Preprint LA-UR-84-129, 1984.
7. Gerasimenko B.F., Rubchenya, Nejtr. Fiz., Kiev, 1984, v.1, p.349
8. Batenkov O.I. et. al., Atomnaya Energia, 1988, v.64, N.6, p.429.
9. Marten H., Seeliger D., Nucl. Sci. Eng. 1986, v.93, p.370.
10. Terrell J., Phys. Rev., 1959, v. 113, p.527.

FISSION NEUTRON MULTIPLICITY CALCULATIONS

H. Märten, A. Ruben, and D. Seeliger
Technische Universität Dresden, Institut für Kern- und Atomphysik
Mommsenstrasse 13, D-O-8027 Dresden, Germany

Abstract: *A model for calculating neutron multiplicities in nuclear fission is presented. It is based on the solution of the energy partition problem as function of mass asymmetry within an phenomenological approach including temperature-dependent microscopic energies. Nuclear structure effects on fragment de-excitation, which influence neutron multiplicities, are discussed. Temperature effects on microscopic energy play an important role in induced fission reactions. Calculated results are presented for various fission reactions induced by neutrons. Data cover the incident energy range* 0-20 *MeV, i.e. multiple chance fission is considered.*

1. INTRODUCTION

Fission neutron multiplicity data for major as well as minor actinides are of essential importance in various nuclear technology applications. Together with the availability of experimental results, consistent theoretical approaches are necessary preconditions for further evaluations. The consideration of the energy balance equation

$$\bar{Q} + E^*_{cn} = \overline{TKE} + \bar{E}^*_{tot}, \tag{1}$$

where Q - total energy release in the fission process,
E^*_{cn} - excitation energy of the fissioning nucleus,
TKE - total kinetic energy of the fragments,
$\bar{E}^*_{tot}$ - total excitation energy of the fragments,

must be required obviously. The average number of fission neutrons is strongly correlated with $\bar{E}^*_{tot}$. However, the reliable calculation of this quantity can only be performed considering the complexity of the fission process in an adequate manner and accounting for fragment de-excitation due to neutron and γ-ray emission mainly. The present work relies on a simple scission point model /1/ for solving the energy partition problem in fission, i.e. the partition of E^*_{tot} on both complementary fragments, as function of mass asymmetry. In addition to previous descriptions, systematic trends of various energy terms with relevance to scission point conditions as well as nuclear structure effects in fragment de-excitation are discussed in more detail.

2. ENERGY PARTITION MODEL (SCISSION POINT MODEL)

2.1. Energy balance equation

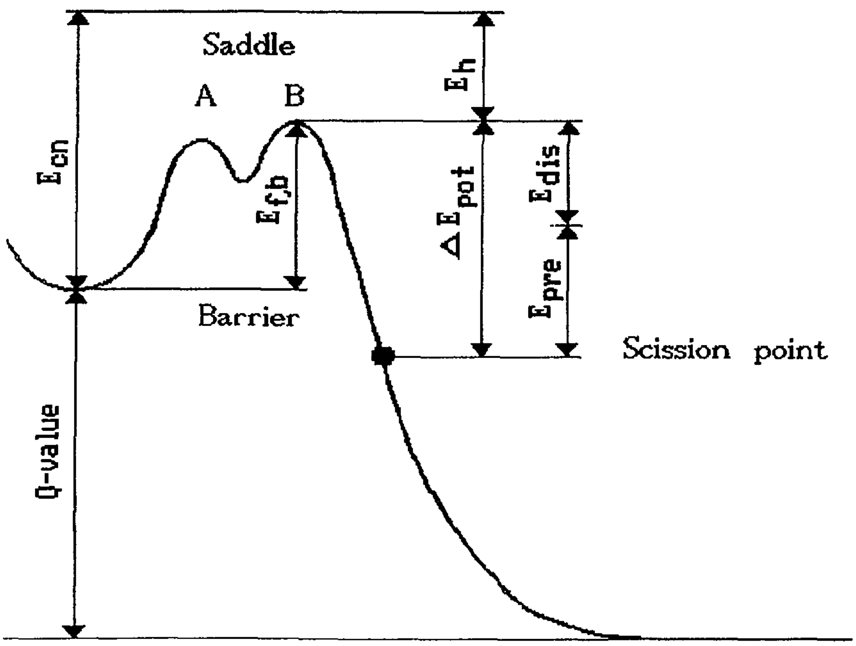

Fig. 1 Scheme of induced nuclear fission illustrating various energy terms explained in the text

The basic idea of the scission point model /1/ used is a detailed energy balance for any induced or spontaneous fission reaction. Fig. 1 represents a general scheme of fission illustrating the energy terms which are important during the fission process starting with a compound-nucleus with excitation energy E_{cn}, passing the double-humped fission barrier with the heights $E_{f,A}$ and $E_{f,B}$, and arriving at the scission point. The scission point energy terms are defined with reference to saddle B. Here, the intrinsic excitation energy is assumed to be

$$E_h = E_{cn} - E_{f,B} - \Delta_p \qquad (2)$$

with the constraint $E_h \geq 0$, i.e. E_h vanishes in the case of spontaneous and sub-barrier fission. Δ_p is the pairing gap above barrier B including a temperature dependence according to Kristiak /2/.

The potential energy release between second saddle and scission is assumed to be the sum of pre-scission kinetic energy E_{pre} and dissipative energy E_{dis}. The sum $E_{dis}+E_h$ corresponds to the total intrinsic energy at scission point (E_{int}) and is distributed on the complementary fragments according to statistical assumptions. The energy balance equation in more detailed form reads

$$\bar{Q}\left[\frac{A_1}{A_2}\right] + E_{cn} = \underbrace{E_{pre} + \mathrlap{\overbrace{\phantom{E_{coul}\left[\frac{A_1}{A_2}\right] + E_{def}^{(1)} + E_{def}^{(2)}}}^{F\left[\frac{A_1}{A_2}\right]}} E_{coul}\left[\frac{A_1}{A_2}\right]}_{\overline{TKE}\left[\frac{A_1}{A_2}\right]} + \underbrace{E_{def}^{(1)} + E_{def}^{(2)} + \overbrace{E_{dis} + E_h}^{E_{int}^{(1)}+E_{int}^{(2)}}}_{\bar{E}^*\left[\frac{A_1}{A_2}\right]} \qquad (3)$$

where

E_{coul} - Coulomb potential energy at scission,

$E_{def}^{(i)}$ - deformation energy of fragment (i) at scission,

E_{dis} - dissipative energy,

$E_{int}^{(i)}$ - intrinsic excitation of fragment (i) at scission,

E_h - intrinsic excitation energy ("heat") at second saddle,

F - potential energy at scission for given mass asymmetry,

E_{pre} - pre-scission kinetic energy.

The deformation-dependent part of scission point potential F is minimized in order to deduce the most probable energy partition at scission.

For neutron multiplicity calculations, the "asymptotic" excitation energy of a single fragment (after dissipation of deformation energy into intrinsic energy, but before de-excitation) is of special interest. It is obtained by

$$\bar{E}^*(A_i) = E_{def}^{(i)} + E_{dis}^{(i)} \qquad i=1,2 . \qquad (4)$$

Further, the total kinetic energy of fission fragments for given mass number ratio is given by

$$\overline{TKE}(A_1/A_2) = E_{coul}(A_1/A_2) + E_{pre}. \tag{5}$$

2.2. Liquid drop model and microscopic energies

Within the present scission point model TSM (two-spheroid model /1/), the scission configuration is assumed to consist of two spheroidally shaped fragments, whose dips are separated by a distance $d \sim 1$ fm (consequence of nuclear interaction of both fragments with diffuse surface). E_{coul} is assumed to be the coulomb repulsion energy of two charges effectively located at the centers of the fragments. The deformation energy is taken to be quadratic in radius change with reference to a spherical nucleus with radius $R^{(i)}$ considering the fragment deformability α. As shown by Terrell /3/, the deformability α is related to the stiffness parameter (quadruple deformation).

Minimizing the potential energy F at scission in regard to variation of fragment deformation, the most probable scission configuration is determined. However, nuclear stiffness influences the amount of deformation energy for given deformation essentially. Using an empirical relation between stiffness and shell correction energy $\delta W(A)$ /4/, the TSM has been used to deduce effective $\delta W(A)$ for typical deformed fragments at scission. Hence, the remarkable deficiencies of the simple TSM are compensated by deducing the microscopic energy from well-known fission data. However, the diminution of shell correction energy due to intrinsic temperature τ at scission has to be considered.The temperature τ can be calculated on the basis of the Fermi-gas model approach,

$$E_{int}^{(i)}(A) = a^{(i)}(A)\, \tau^2 \tag{6}$$

($a^{(i)}(A)$ - level density parameter according to Ignatyuk et al. /5/). The intrinsic energy at scission E_{int} includes both dissipative energy E_{dis} and heat energy above the second fission barrier E_h. The partition on the fragments is defined by the condition of equal intrinsic temperatures τ of complementary fragments at scission ($\tau^{(1)}=\tau^{(2)}$).

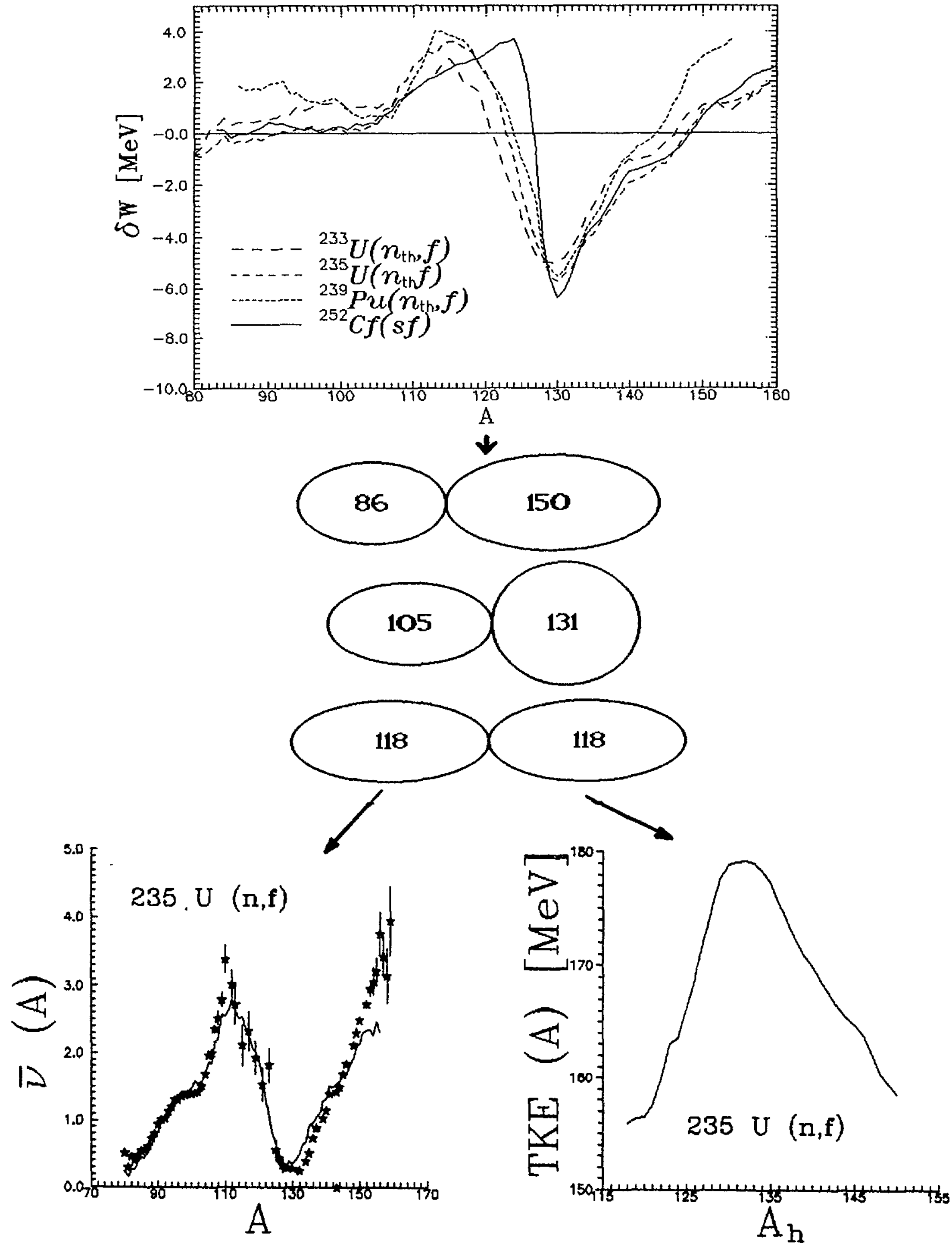

Fig. 2 Calculated semi-empirical shell correction energies (τ=0) for different fission reactions. The influence of shell structure on the fragment characteristics is illustrated for three fragment pairs with different deformations. Thus, the connection between high deformation and high neutron emission /6/ (left) as well as between vanishing deformation and maximum TKE /7/ (right) is illustrated.

For applications of the formalism outlined above to any fission reaction, sets of semi-empirical, model-dependent shell-correction energies were deduced for the well-investigated fission reactions $^{252}Cf(sf)$ and $^{235}U(n_{th},f)$. Both sets are nearly identical /1/ and correspond to microscopic calculations qualitatively. The actual $\delta W(A)$ function are determined by interpolation of the parameter set (reduced to zero temperature) and by considering the intrinsic excitation. Fig. 2 shows the calculated phenomenological shell correction energies reduced to zero excitation at scission ($\tau=0$) for different fission reactions. It has been found that the dependence $\delta W(A)$ /1/ is quite similar for fissioning systems (Th-Cf) in the most probable mass regions. On the other hand, a direct correspondence between fragment characteristics and deformation is obvious.

2.3. Dissipative energy

A relatively crucial problem in nuclear fission studies is the degree of intrinsic excitation during the descent from second saddle point to scission point.One method to deduce E_{dis} by analyzing the proton pairing effect δ_p was presented by Gönnenwein /8/. Dissipative energies, which increase with fissility Z^2/A from about 3 MeV in the case of Th up to 11 MeV for Cf, were estimated.

First applications of the TSM have shown that the calculated energy partitions are rather sensitive to the dissipative energy. It has been found that an approximative parameterization of Gönnenwein's E_{dis} data for any TSM application is not reliable. Therefore, dissipative energies have been adjusted for many fissioning systems in the Th-Cf region as described in /1/, i.e. that the TSM set of equations is solved by including experimental TKE und $\bar{\nu}$ data. Note that in contrast to /1/ the proton pairing for ^{252}Cf is assumed to be about 5%. This yields a higher dissipative energy for heavy fissioning nuclei as deduced in /1/. These new values as well as the data deduced by Gönnenwein are plotted in Fig. 3 for different fission reactions.

2.4. Pre-scission kinetic energy

E_{pre} can be understood as the translational part of collective degrees of freedom with relevance to the descent from saddle point to scission point. For TSM calculations, E_{pre} as

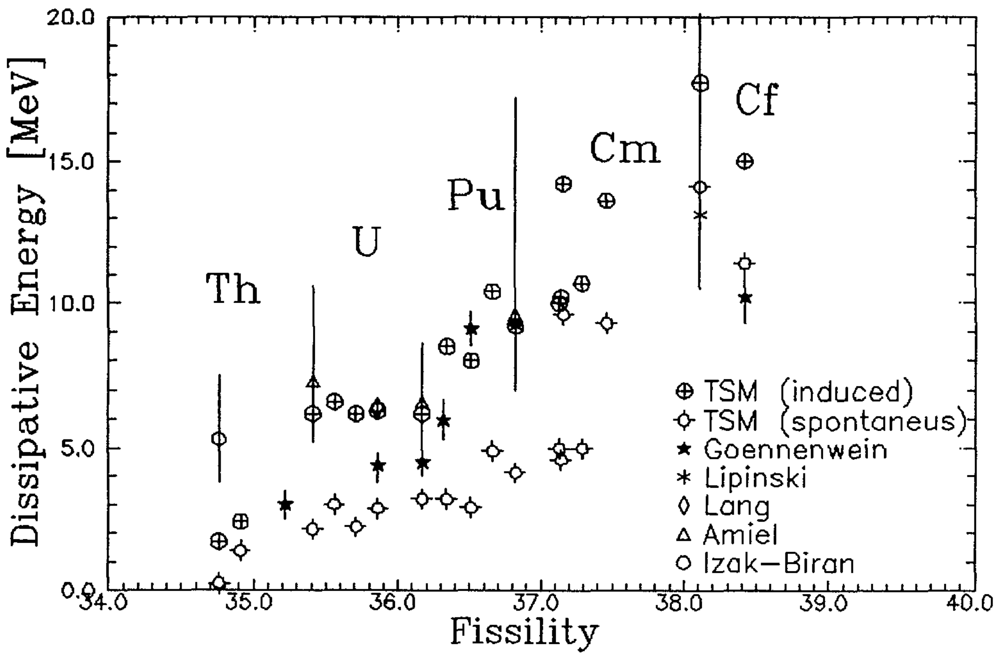

Fig. 3 TSM fitted dissipative energies as function of fissility Z^2/A for different fission reactions in comparison with the data deduced from proton odd-even effects /9-12/ by Gonnenwein /8/ (guide line for induced fission)

function of mass and charge of the fissioning nucleus was approximated on the basis of /8/ by

$$E_{pre} = \left[2.24 \frac{Z_{FN}^2}{A_{FN}} - 69.5 \right] \text{MeV}, \qquad (7)$$

2.5. Spontaneous versus threshold fission

Obviously, the starting conditions for spontaneous and threshold fission are quite different. In the latter case, ΔE_{pot} is effectively enhanced (with reference to spontaneous fission) by the value of the fission barrier. To deduce the consequence to differences in E_{dis} and E_{pre}, we assume that the fragmentation process is separable into two phases /1/:

(i) *Charge separation connected with rather strong friction:* The main part of potential energy gain is concentrated on E_{dis}.

(ii) *Neck formation and rupture in conjunction with a pre-acceleration of the nascent fragments:* The potential energy release in this phase yields higher E_{pre} mainly.

It is likely that differences between threshold and spontaneous (tunneling) fission concern the first phase predominantly. Consequently, for sufficiently high ΔE_{pot}, especially the dissipative energy should differ for spontaneous and threshold fission. E_{pre} can be assumed to be equal in both cases. As shown in Fig. 4 (right), $\overline{TKE}$ differences are very small for $Z^2/A \geq 36$, . On the other hand, there are increasing differences in the average neutron multiplicity $\Delta\bar{\nu}$ as a measure of dissipative energy (Fig. 4, left).

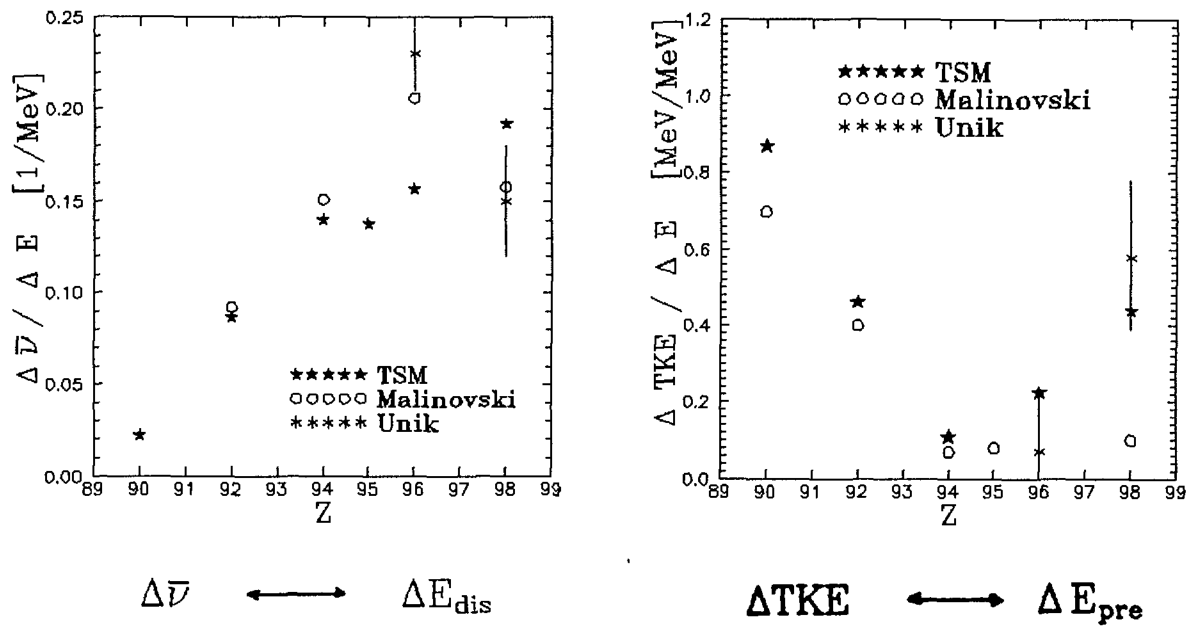

Fig. 4 Changes of $\bar{\nu}$ and TKE from spontaneous to threshold fission according to Malinovski /13/ and Unik /14/ and fitted results obtained in the framework of TSM

However, for rather light fissioning nuclei ($Z^2/A \leq 36$), phase (2) is shifted close to barrier penetration in the case of spontaneous fission. E_{pre} and, consequently, $\overline{TKE}$ becomes lower compared to threshold fission. In this case smaller differences in E_{dis} yield in a decrease of $\Delta\bar{\nu}$. As depicted in Fig. 4 this interpretation is confirmed by the experimental-data trends.

3. FRAGMENT DE-EXCITATION

To deduce fission fragments neutron multiplicities an energy balance of fragment de-excitation was proposed /1/ including the evaporation of neutrons (multiplicity $\bar{\nu}$, average energy $\bar{\varepsilon}$ in the center-of-mass system CMS) and γ-ray emission (average total energy $\bar{E}_\gamma$),

$$\bar{E}^*(A_i) = \bar{\nu}(A_i)\,(\bar{B}_n(A_i) + \bar{\varepsilon}(A_i)) + \bar{E}_\gamma(A_i). \tag{8}$$

The average neutron separation energy for primary fragments $\bar{B}_{n,o}(A)$, i.e. before neutron emission, is calculated on the basis of mass tables /15/ using an approximative charge distribution according to Wahl /16/. To consider the increase of $\bar{B}_n(A)$ with $\bar{\nu}$ due to the shift of the fission fragments towards the line of β-stability, these data are corrected according to

$$\bar{B}_n(A) = \bar{B}_{n,o}(A) + C\,\bar{\nu}(A) \tag{9}$$

with the correction factor C ($\approx$ 0.2 for U, $\approx$ 0.1 for Cf). Fig. 5 shows the increase of the neutron separation energy with neutron emission as function of fragment mass for three fission reactions. The different lines correspond to those values of the emission of the first, second and third neutron.

According to the results of Frehaut /17/, the average total gamma energy is assumed to be linear in neutron multiplicity. Thus, $\bar{E}_\gamma(A_i)$ is given in the Th-Cf region by the following approximation

$$\bar{E}_\gamma(A) = [\ G_1(A)\,\bar{\nu}(A) + 2.2\ ]\ \mathrm{MeV} \quad , \tag{10}$$

where G_1 is a parameter depending on A /17/.

4. NEUTRON MULTIPLICITY VERSUS FRAGMENT MASS NUMBER AND TOTAL KINETIC ENERGY

The dependence of neutron multiplicity versus fragment mass number and total kinetic energy has been studied in several experiments /18-20/ in the case of ^{252}Cf(sf). It has been found a nearly linear decrease of $\bar{\nu}$(TKE,A) with TKE for fixed A in a wide TKE and A range which can be understood in first order on the basis of energy conservation (eq. (1)). However, shell-effects depending on deformation and temperature at scission influence the slope $\partial\bar{\nu}/\partial$TKE for individual fragments.

Applying the TSM /21/ to solve this energy partition problem for fixed TKE (constraint) it was possible to reproduce the linear dependence. As shown in Fig. 6, the calculated slopes $\partial\bar{\nu}/\partial$TKE as function of fragment mass number are in a good agreement with

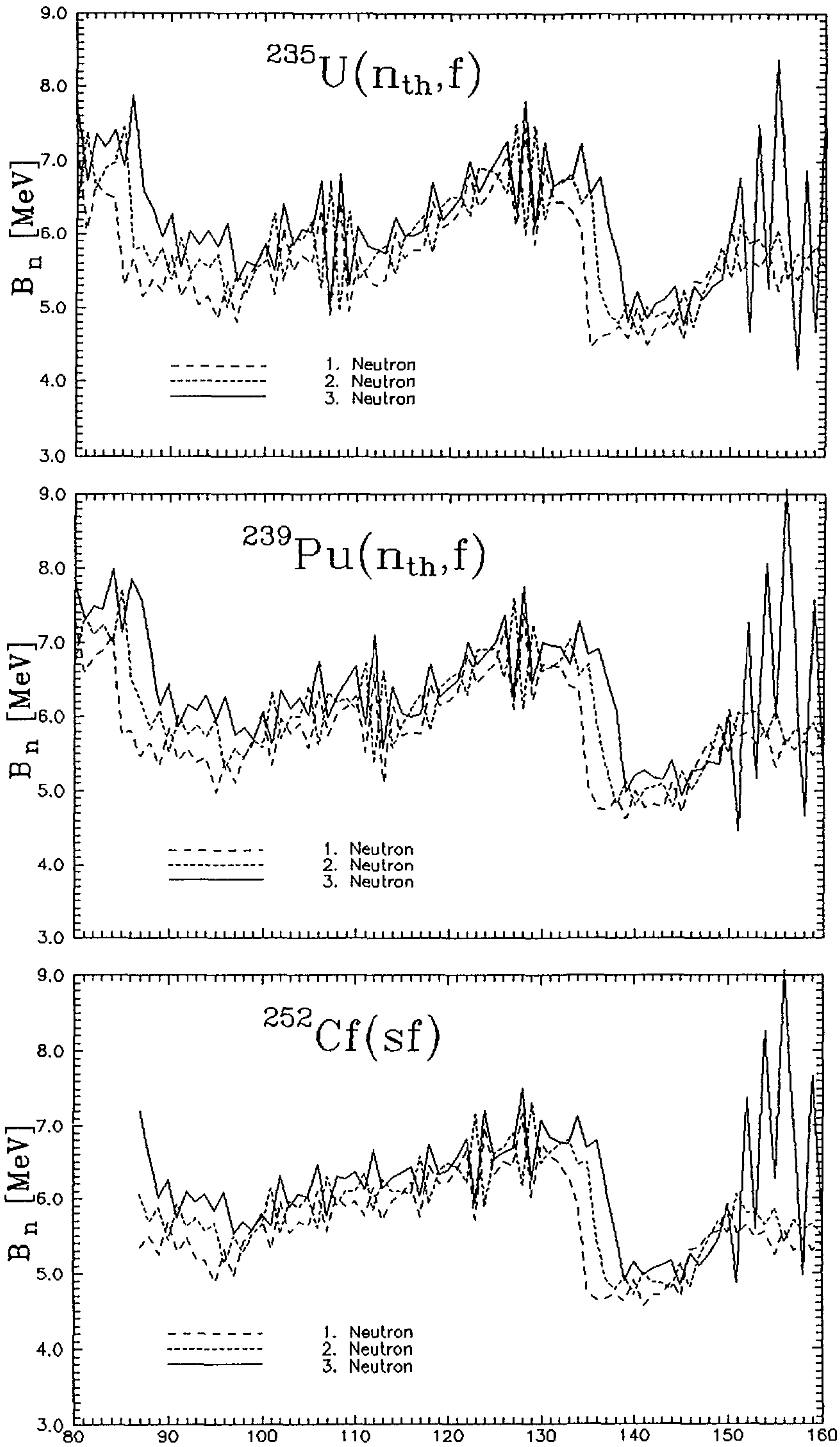

Fig. 5 Calculated neutron separation energy for fission fragments as function of mass number for the neutron induced fission of ^{235}U and ^{239}Pu and for the spontaneous fission of ^{252}Cf. The solid, short dashed, and long dashed lines correspond to the emission of the first, the second, and the third neutron, respectively.

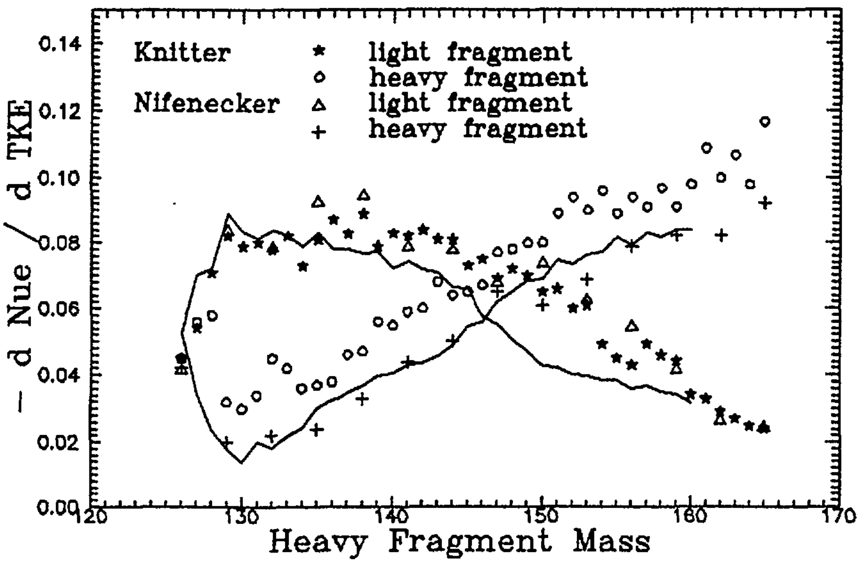

Fig. 6 Calculated slope $[\partial\bar{\nu}/\partial\mathrm{TKE}](A)$ for ^{252}Cf(sf) in comparison with experimental data /18,20/

experimental results. Thus, the conclusion can be drawn that the variation of $\bar{\nu}$ as function of TKE for the fragments of a given mass split can be understood as an effect of the fragment stiffness at scission influenced by the shell structure. The linearity in this behavior points to a nearly constant stiffness of the individual fragments.

5. MULTIPLE-CHANCE FISSION

In the case of higher incidence energies the emission of one ore more neutrons prior to fission becomes energetically possible. To account for this multiple chance fission, in general (n,jnf), the neutron multiplicities $\bar{\nu}_j(E_i)$ have been separately calculated for each chance j considering the diminution of compound nucleus excitation. The weight of each chance is identical with partial fission cross section $\sigma_{f,j}(E_i)$ to be calculated within reaction theory including the fission channel. Consequently, the total neutron multiplicity (pre-fission neutrons together with post-fission neutrons) is given by

$$\bar{\nu}_{tot}(E_i) = \frac{1}{\sigma_{f,tot}} \sum_{j=0}^{j_{max}} (\bar{\nu}_j(E_i) + j) \, \sigma_{f,j}(E_i) \qquad (11)$$

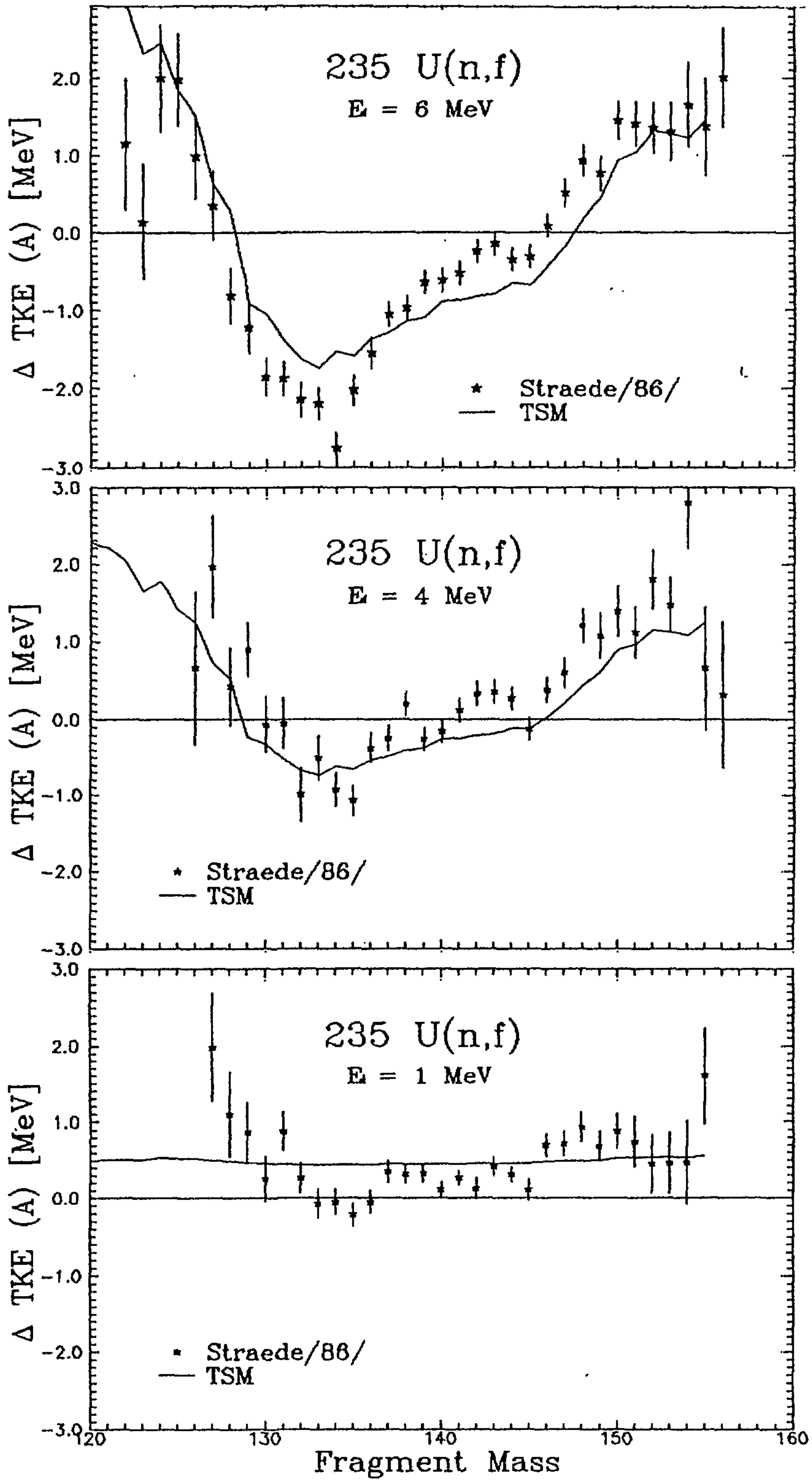

Fig. 7 Total kinetic energy of complementary fission fragments from ^{235}U(n,f) for 3 different incidence energies shown as difference to the value for thermal neutron induced fission (line - TSM, points - Straede /7/)

6. NEUTRON MULTIPLICITY IN INDUCED FISSION

A remarkable test of the accuracy of description of energy partition and neutron emission within the TSM was the study of several trends in TKE depending on fragment mass split and excitation energy of the fission nucleus. Therefore, these results /1/ are included before discussing the calculated neutron multiplicities. In general, an increasing incidence energy gives rise to a diminution of shell effects due to the higher excitation at scission. As presented in Fig. 7 for the neutron induced fission of ^{235}U, this is connected with a decrease of TKE in the TKE-maximum region (heavy fragments with A $\approx$ 130) and with an increase in the symmetric and strong asymmetric mass split region. However, there are deviations from this general behavior which differ for various fission reactions in the case of small incidence energies. In the framework of the TSM these changes in TKE can be explained by alterations in the heat energy above the second fission barrier due to pair breaking /1/. For E^*_{cn} within the pairing gap above the second saddle point, an increasing incidence energy give rise to higher TKE of the fission fragments. This circumstance is, however, effected by the second barrier height with reference to the first one. Whereas $E_{f,A}$ is lower than $E_{f,B}$ in the sub-U region (cf. example in Fig.8), the opposite behaviour was observed for actinides heavier than U. In the first case, pairing effects at saddle B are essential. A consequence is the characteristic dependence of TKE on incidence energy for Th, U, and Pu as shown in Fig. 9.

For this investigation as well as for the calculation of average neutron multiplicities, the knowledge of the fragment mass distribution Y(A) is required. It is approximated by a 5-Gaussian approach representing two asymmetric and one symmetric fission mode. The set of Gaussian parameters (including account for multiple-chance fission) was obtained by a complex fit as function of mass number of compound nucleus and incidence energy in the Th - Cf region. In Fig. 10, this approximation is shown for the thermal neutron induced fission of ^{235}U according to Straede /7/.

Finally, calculated average neutron multiplicities are shown for several fission reaction up to 20 MeV incidence energy. As described in paragraph 5, one has to account for multiple-chance

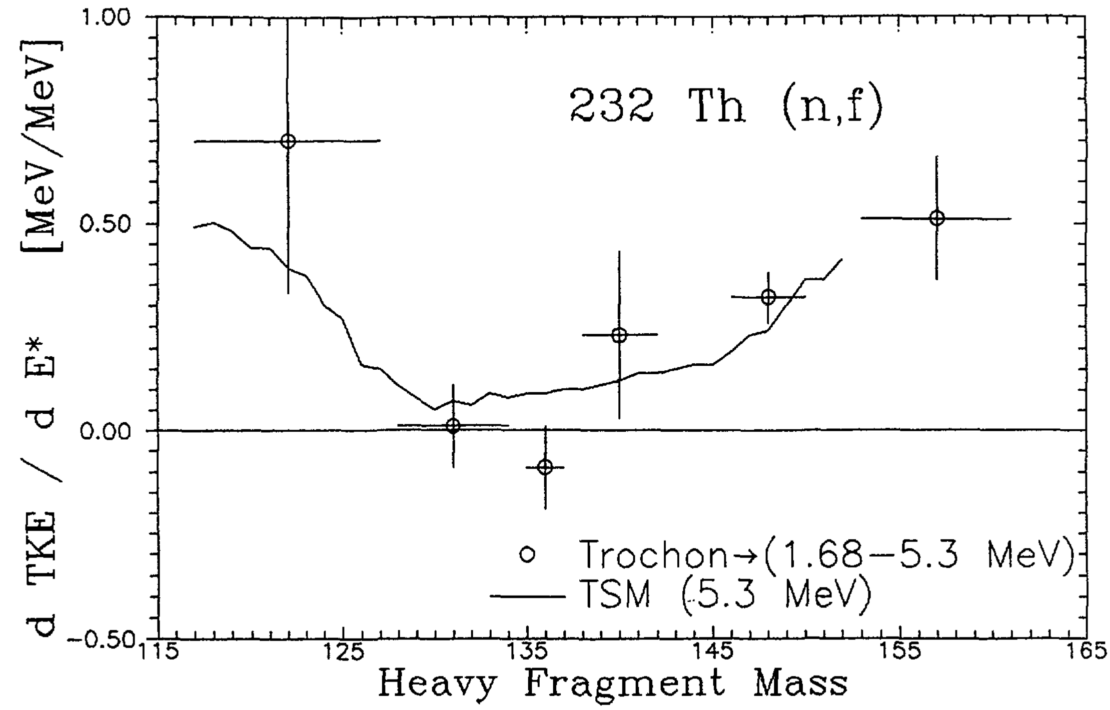

Fig. 8 Total kinetic energy as difference to the value of threshold fission plotted as function of the heavy fragment mass (solid line - TSM, points - Trochon /22/)

fission in this case. In the Figs. 11 - 13, average neutron multiplicities (including pre-fission neutrons!) as function of incidence energy are presented. The experimental data /26-28/ are well reproduced by TSM calculations.

Fig.11 shows $\bar{\nu}(E_i)$ for the neutron induced fission of ^{232}Th. In contrast to other fission nuclei (Fig. 12 and 13), there is a remarkable step-like behavior in $\bar{\nu}(E_i)$ above the threshold of the second chance ($\cong$ 6 MeV). Considering the higher neutron multiplicity of this chance $\bar{\nu}_2$ (enhanced by the post-fission neutron) this is due to the relative high values of the partial fission cross section for the second chance.

7. SUMMARY

It was shown that the calculation of fission neutron multiplicities requires a model for solving the energy partition problem in nuclear fission. The TSM as an energy-conservation consistent scission point model with semi-empirical, temperature-dependent shell correction energies for deformed fragments at scission is successful in describing the main fission

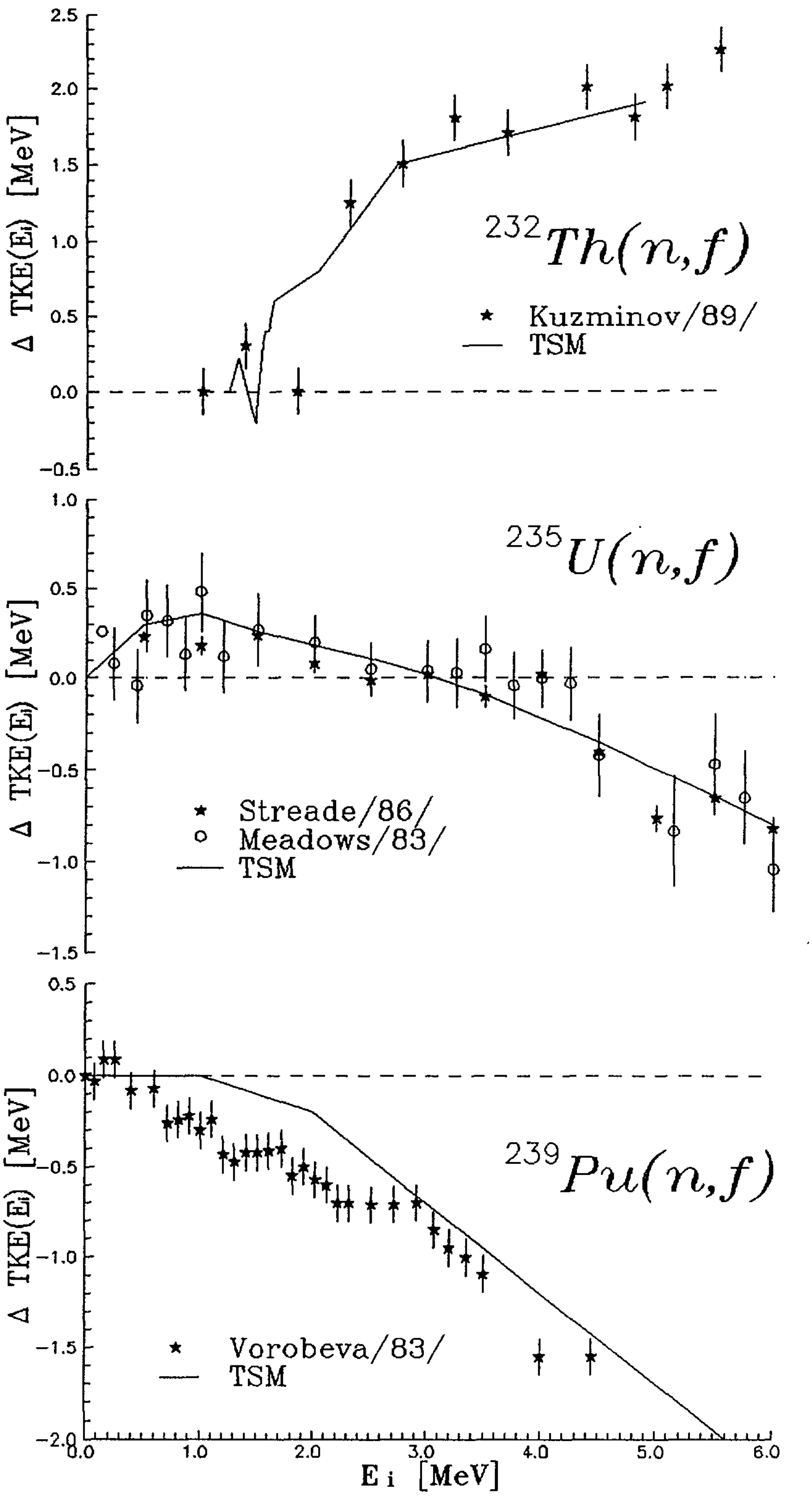

Fig. 9 Calculated average $\overline{TKE}$ as difference to the value of minimum (thermal or threshold) incidence energy for different incidence energies and various fissioning nuclei in comparison with experimental data /7/, /23-25/.

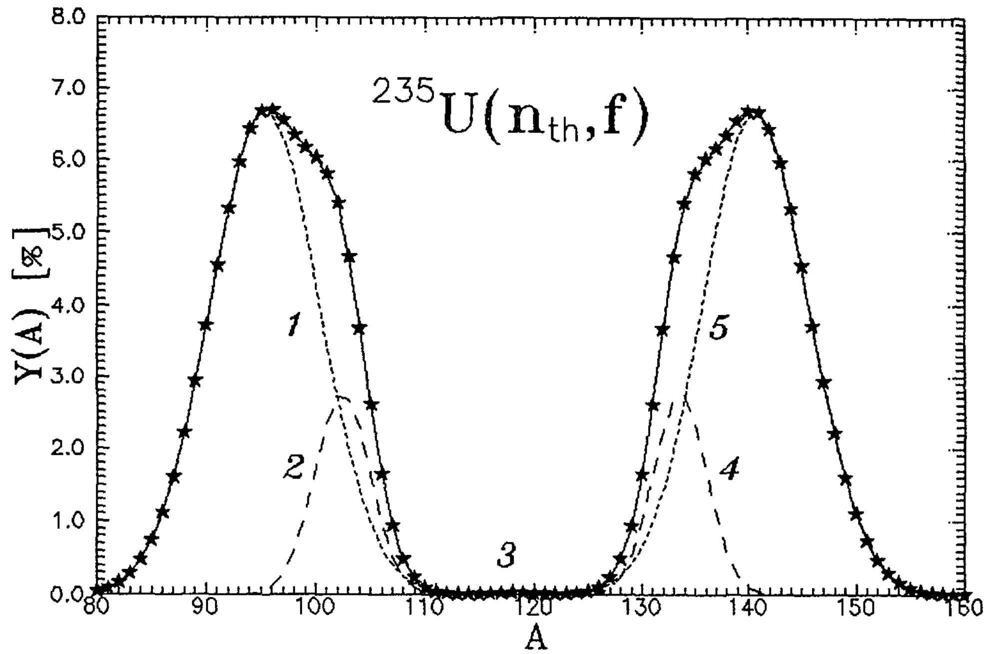

Fig. 10 5-Gaussian approximation of fragment mass yield distribution for $^{235}U(n_{th},f)$ according to Straede [7]

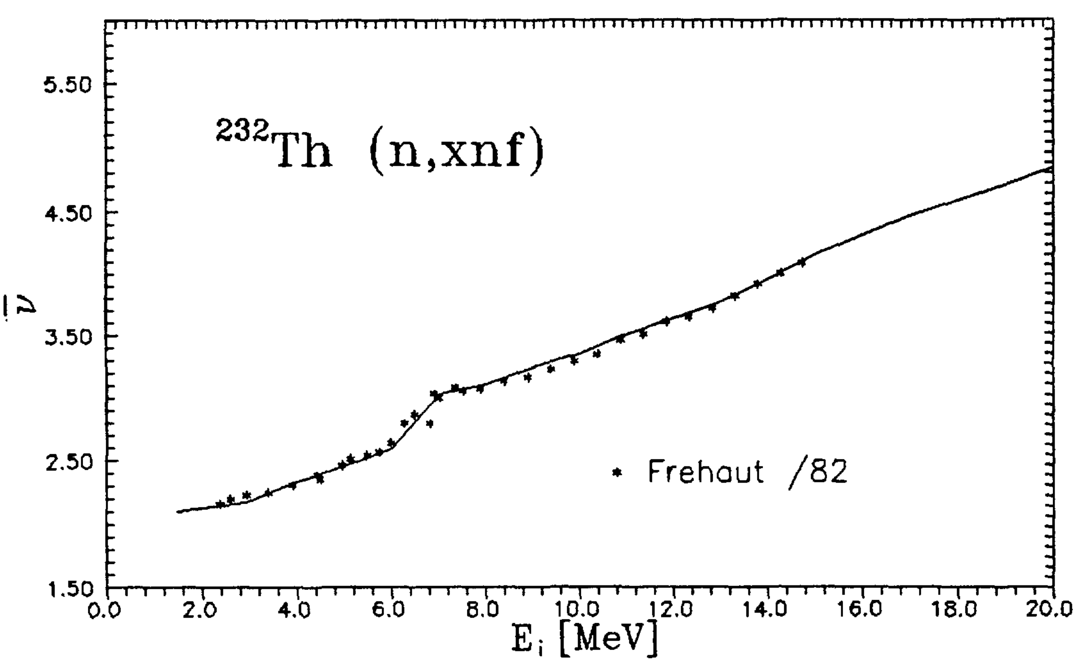

Fig. 11 Average neutron multiplicity as function of incidence energy for the neutron induced fission of ^{232}Th (experimental data were taken from Ref. /26/)

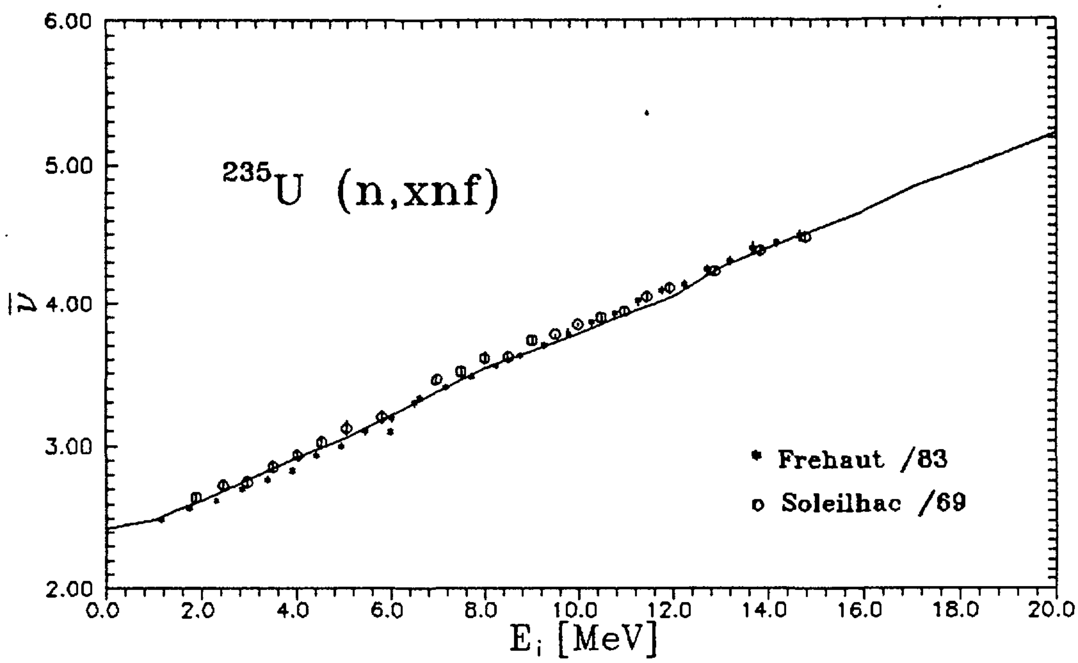

Fig. 12 Average neutron multiplicity as function of incidence energy for ^{235}U(n,f) (experimental data were taken from Ref. /26-27/)

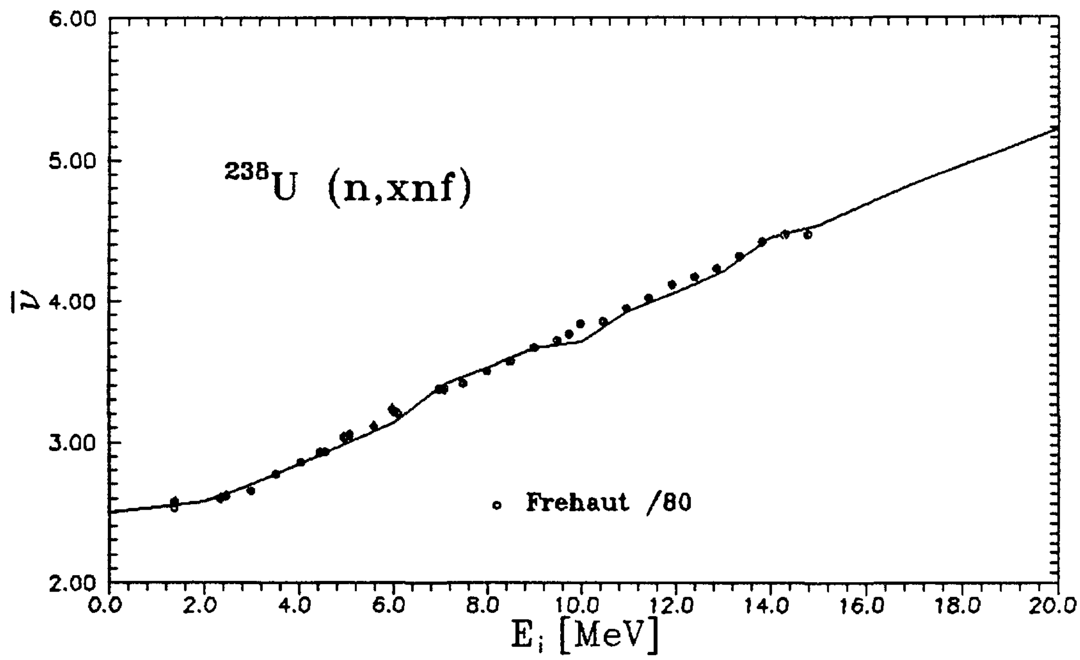

Fig. 13 Average neutron multiplicity as function of incidence energy for ^{238}U(n,f) (experimental data were taken from Ref. /28/)

fragment characteristics. As a test of the accuracy of the TSM calculations several trends in TKE data for induced fission were discussed. The average fragment excitation energies were used to obtain neutron multiplicities by the help of an energy balance of fragment de-excitation, which includes neutron evaporation and γ-ray emission. As shown by several examples, the dependence of $\bar{\nu}$ on incidence energy is well reproduced by the TSM. The TSM provides the basis for several applications as the calculation of fragment data as well as neutron emission probabilities. It is an essential basis for a fission neutron data systematics.

References

/ 1/ A.Ruben, H. Märten, and D. Seeliger, Z. Phys. **A 338**, 67 (1991)

/ 2/ J. Kristiak and J. Kliman, Proc. 5th Int. Symp. on Neutron Induced Reactions, Smolenice, 1988, Physics and Applications, Vol. **15**, ed. S. Gmuca, R. Antalik, and J. Kristiak, p. 305 (1988)

/ 3/ J. Terrell, Proc. IAEA Symp. on Phys. and Chem. of Fission, Salzburg, 1965 (Vienna, 1965) Vol. II, p. 3

/ 4/ M. Kildir and N.K. Aras, Phys. Rev. **C25**, 365 (1982)

/ 5/ A. V. Ignatjuk et al., Yad. Fiz. **42**, 569 (1985)

/ 6/ W. F. Apalin et al., Nucl. Phys. **71**, 553 (1965)

/ 7/ C. Ä. Straede et al., Nucl. Phys. **A462**, 85 (1987)

/ 8/ F. Gönnenwein et al., Proc. XVIIth Int. Symp. on Nucl. Phys., Gaussig (GDR), 1987, ZfK-**646**, 129 (1988)

/ 9/ R. J. Lipinski and B. W. Wehring, Phys.Lett. **66B**, 326 (1977)

/10/ W. Lang, PhD Thesis, "Nuklidausbeuten bei der Reaktion 235-U(n,f) als Funktion der kinetischen Energie der Spaltprodukte - Ein experimenteller Zugang zur Dynamik des Spaltprozesses", TH Darmstadt (1979)

/11/ S. Amiel et al., Phys. Rev. **C15**, 2119 (1977)

/12/ T. Izak-Biran and S. Amiel, Phys. Rev. **96**, 1059 (1954)

/13/ W. W. Malinovski, Yad. Const. **2**, 25 (1987)

/14/ J. P. Unik et al, Proc. IAEA Symp. on Phys. and Chem. of Fission, Rochester 1973, IAEA Vienna 1974, Vol II, p.19

/15/ Y. Ando et al., Report **JAERI-M83-025** (1983)

/16/ A. C. Wahl, Atomic Data and Nuclear Data Tables **39**, 1 (1988)

/17/ J. Frehaut, Proc. of Cons. Meeting on Physics of Neutron Emission in Fission, Mito, 1988 (IAEA Wien, 1989) INDC(NDS)-**220**, 99

/18/ H. Nifenecker et al., Proc. IAEA Symp. on the Physics and Chemistry of Fission, Rochester, 1973 (IAEA, Vienna, 1974), Vol. II, p.117

/19/ R. Schmidt-Fabian, PhD Thesis, "Messung der spontanen Spaltung von 252-Cf am Darmstadt-Heidelberger Kristallkugel-Spektrometer", Ruprecht-Karls-Universität Heidelberg (1988)

/20/ C. Budtz-Jorgenson and H.-H. Knitter, Nucl. Phys. **A490**, 307 (1988)

/21/ A. Ruben, and H. Märten, Z. Phys **A 337**, 237 (1990)

/22/ J. Trochon et al., Nucl. Phys. **A318**, 63 (1979)

/23/ A. A. Goveerdovski, B. D. Kuzminov, V. F. Mitranov, and A. I. Sergachev, Proc. of Cons. Meeting on Physics of neutron emission in fission, Mito 1988, IAEA, INDC(NDS)-220, p.59
/24/ V. G. Vorob'eva, B. D. Kuz'minov, and V. N. Manokhin, Report IAEA, INDC(CCP)-128/G+Sp
/25/ J. W. Meadows, Phys. Rev. **177**, 1817 (1969)
/26/ J. Frehaut et al., Proc. of Intern. Conf. on Nucl. Data for Science and Technology, 6-10 Sept. 1982, Antwerp D. Reidel Publishing Company, p. 78 (1983)
/27/ M. Soleilhac et al., Nucl. Energy **23**, 257 (1969)
/28/ J. Frehaut et al., "Recent results on ν-prompt measurements between 1.5 and 15 MeV", Paris (1980)

THE ENERGY DEPENDENCE MEASUREMENTS OF AVERAGE NUMBER OF PROMPT NEUTRONS FROM NEUTRON-INDUCED FISSION OF U-235, NP-237 AND PU-240 FROM 0.5 TO 12 MEV

Ju. A. Khokhlov, I. A. Ivanin, Ju. I. Vinogradov, V. I. In'kov, L. D. Danilin, V. I. Panin, V. N. Polynov

All-Union Scientific Research Institute of Experimental Physics

607200, Arzamas, Gorky region, USSR

The results of energy dependence measurements of average number of prompt neutrons from neutron-induced fission of U-235, Np-237 and Pu-240 from 0.5 to 12 MeV, are presented. A neutron source was generated by the uranium target of the linear electron accelerator of All-Union Scientific Research Institute of Experimental Physics, and energies of the neutrons incident on the fissile samples were determined by time-of-flight technique. The fission neutrons were detected by big liquid scintillator detector loaded with gadolinium, events of fission - by parallel plate avalanche detector for fission fragments.

INTRODUCTION

Organisation of present work was determined by task of measurements of average number of prompt neutrons $\overline{\nu}p$, emitted from heavy nuclei fission with high α-activity by neutrons with energy from 0.5 to 10 MeV. For this isotopes such data are either absent, or extremely small. On the first stage of this investigation $\overline{\nu}p(En)$ were measured for U-235, Np237 and Pu240. Existing experimental data for Np237 display systematic discrepancy [1-3], exeeding declared unsertanity of measurements, data for Pu-240 were obtained in two works [4,5], in one of them there was a big error [5].

1. EXPERIMENTAL METHOD

1.1. General technique of measerements

Geometry of experiment is presented in fig.1. The neutron source was uranium water cooling target of electron linac [7]. Measurements were carried out with next parameters of accelerator electron beam:

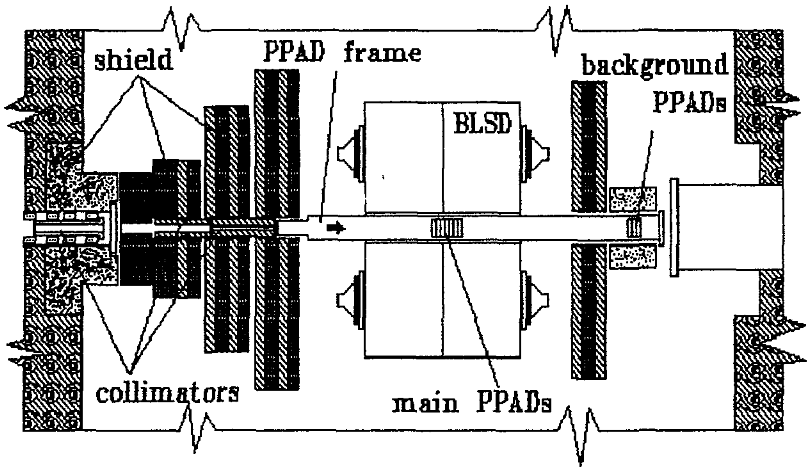

Fig 1. Geometry of experiment

- average electron energy - 50 MeV;
- average electron current - 220 μA;
- pulsed frequency - 2400 Hz;
- pulse width - 12 ns.

Neutron beam through a collimator system contained in evacuated tube fell on combination of parallel plate avalanche detectors (PPAD) with the samples of fissile isotopes placed in the center of big liquid scintillator detector (BLSD), of 400 litres volume, loaded with gadolinium. BLSD was installed behind shielding collimator 1.5 meters long, being a cylindrical system with alternating layers of iron shot with boron carbide and paraffin with boron carbide, which shielded detector against gamma-ray and neutrons emitted from linac target. Moreover, collimator formed neutron beam 20 mm in diameter.

Events of fission were registered by avalanch detector for fission fragments, neutrons - by BLSD via detection of capture gamma-rays on gadolinium.

Energy of induced fission neutrons was determined by standart time-of-flight technique. Moment of neutron take-off was fixed by registration of gamma-flash from target by fast scintillator detector, moment of fission - by pulse from PPAD. In this experiment flight-path was 28.5 m.

For continuous measurement of neutron background, correlated with neutron flow, behind the BLSD two PPAD's with U-235 and Cf-252 were installed. Act of fission in these PPAD's allowed detection of pulses from BLSD. Aditional shield placed between the neutron detector and "background PPAD" absorbed neutrons, which were emitted during fission in the latter.

Measurements relative to $\bar{\nu}_p$=3.756 for spontaneous fission of Cf-252 were carried out.

1.2. Neutron detector

Detector of neutrons was a cylindrical 800x800 mm tank, filled with liquid scintillator containing gadolinium. Scintillation from neutron capture gamma-rays on gadolinium were detected by twelve PMs, placed by six on each side of the tank.

BLSD detection efficiency of neutron was 0.659 at 2.5-MeV gamma-rays bias.

1.3. Parralel plate avalanch detector of fission fragments

Choice of PPAD for detection of fission acts was stipulated by a few reasons: high time resolution (less than 1 ns), small sensitivity to gamma-flash from linac

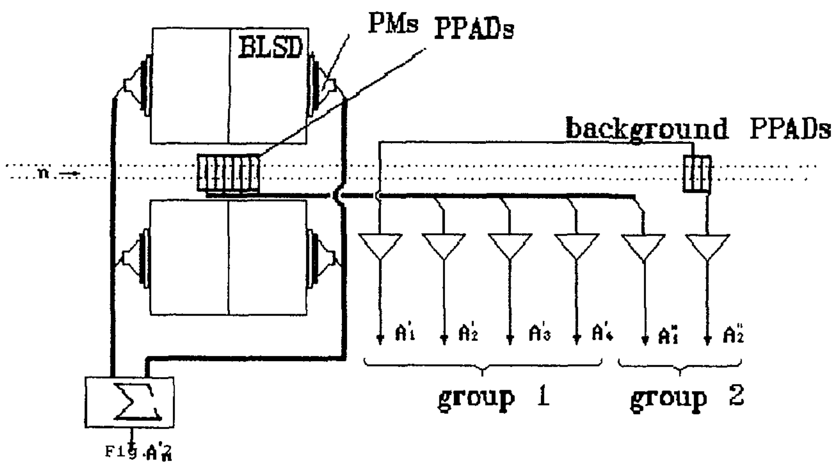

Fig.A'2 General scheme of detectors.

target, an ability to resolve pulses at fission fragments for high (near 10^8 α-decay in second) samples α-activity, and what had extreme importance, for such experiments - small pressure of working gas (1-5 Torr), because it determined a background of neutrons dispersed by materials in central channel of BLSD.

To lower background of scattering neutrons on PPAD materials special steps were undertaken. Vacuum frame of PPAD was a stainless steel tube four meters long, going from centre of collimator to other side of shield to exclude background of scattered neutrons on the detector windows. Fissile deposits were layered on silver 50-mm-diam and 2-mg/sm -thick foils (diameter of deposits was 20 mm), working gas (pentan) pressure in this experiment was 2

Torr. Every PPAD was constructed into independent block, which electrodes were connected with high frequency inputs, placed on the PPAD frame. In BLSD centre four avalanch detectors with deposites of U-235, Cf-252, Np-237 and Pu-240 were installed. In the "background PPAD" detectors with U-235 and Cf-252 were placed.

The general scheme of detectors in measuring pavilion is presented in fig. 2. Signals from fission fragments from PPAD after fast preamplifiers, were united into two groups. The first group included the signals for multiparameter analysis in 10.24 μs time-window (time-of-flight information). There were signals from PPADs with samples of U-235, Np-237, Pu-240 (in centre of BLSD) and from "background PPAD" with U-235 layers.

The second group included signals from "main PPAD" and "background PPAD" with Cf-252 layers for analysis in 200 μs time-window, delayed for 130 μs from the moment of neutron pulse. Existance of this group of signals makes possible determination of neutron detection efficiency of BLSD with correction for corresponding background.

During the experiment the acts of fission which were registered in any PPAD in 40 μs time-window were excluded from measurement.

Pulses from 12 PMs after amplification were summarised. The 30 μs time-gate for neutron counting was opened with 0.8 μs delay relative to act of fission to exclude fission prompt gamma-rays and recoil protons from detection.

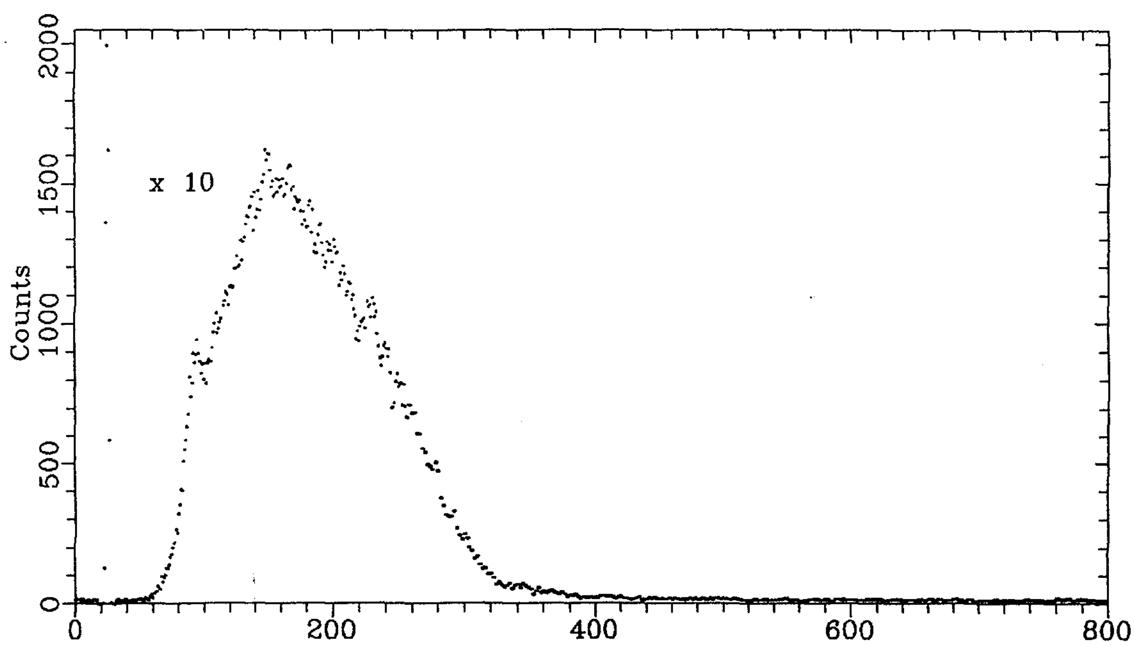

Fig. 3 Time-of-flight spectrum of Np^{237} fission

Table 1

Structure of registered data

Parameters	Name of spectrum Spectrum	Dimension	Type of data
	Time-of-flight interval, group 1		
t, p, n	TP - spectrum time-multiplicity	(1024x16)x4	Integer*2
t, n	T - time-of-flight spectrum, integrated over multiplicity	(1024)x4	Integer*2
p, n	P - spectrum of multiplicity integrated over time-of-flight	(16)x4	Real*4
q, n	Qf - pulse height distribution from PPAD	(512)x4	Integer*2
q, n	Qf - pulse height distribution from BLSD	(512)x4	Integer*2
	Calibration interval group 2		
q, n	Qf - pulse height distribution from PPAD	(512)x2	Integer*2
q, n	Qf - pulse height distribution from BLSD	(512)x2	Integer*2
p, n	P - spectrum of multiplicity	(16)x2	Real*4

Signals from BLSD after discrimination were sent to 100 MHz counter.

Time of flight of induced fission neutrons was determined by 10 ns time-to-digital converter. Structure of data which were registered during the experiment is presented in table 1.

Pulse height distributions from PPADs were registered for control of detection efficiency of fission fragments, the ones from BLSD - for additional control of BLSD efficiency. The time-of-flight spectrum of fission for Np-237 is presented in fig. 3.

2. MEASUREMENT RESULTS PROCESSING

2.1. Calculation and corrections

For each energy of induced fission neutrons $\bar{\nu}p(En)$ was determined using the relation

$$p(En) = \frac{\sum_{i=0}^{15} Pi(En)\, i}{\sum_{i=0}^{15} Pi(Cf\text{-}252)\, i} \bar{\nu}^{etalon} \quad , (1)$$

where

Pi(En) - observed probability of the detection of fission act with emission of i detected neutrons

En - neutron energy

Pi(Cf-252) - observed probability of the detection of fission act of Cf-252 with i detected neutrons

$\bar{\nu}^{etalon}$ - standart value of p for Cf-252(sf) is 3.756.

Energy of fissioning neutron was calculated from a well-known for relativistic neutron relation with photofission peak in time-of-flight spectrum.

2.1.1. "FALSE FISSION" CORRECTION. From every surface of two-dimensional spectrum TP(n,t) false acts were substracted, which formed such constant unchanging in time substrate (see fig. 3). Values of average numbers of "false fission" on one channel of time-of-flight spectrum with detection of i neutrons Ni(false) were determined in time interval, where the possibility of neutron induced fission has been obviously excluded.

Values of this correction to final results were +0.3% for U-235, +0.5% for Np-237, +1.1% for Pu-240.

Unscertainty after introducing this correction was included into statistical error of measurements.

2.1.2. DEAD TIME CORRECTION was calculated as a probability that two pulses from BLSD will not be resolved by electronics. One value of one was calculated from

$$Ni = \frac{Ni' - C_{i+1}^{2} Ni_{+1} R}{1 - C_{i}^{2} R} \qquad (2)$$

where

C_{i+1}^{2}, C_{i}^{2} - binomial coefficient two from i,i+1

Ni - initial multiplicity distribution

Ni' - multiplicity distribution after correction

R - parameter of dead-time correction

Parameter R calculated from

$$R = \frac{\tau_c + \tau_s}{\tau_c} 2\tau_d\, f\,(t)dt \qquad (3)$$

where

$f(t)$ - density of probability of neutron capture

τ_d - dead time of neutron counting.

Probability density of neutron capture was approximated by function

$$f(t) = e^{-t/\tau_c} (1 - e^{-t/\tau_s}) \qquad (4)$$

where

τ_c - time constant of capture

τ_s - time constant of slowing down.

Value of R in this experiment was 0.008.

Values of dead-time correction were changed in limits from -0.18% to +0.27% for U-235, from -0.11% to +0.3% for Np-237, from 0.03% to 0.42% for Pu-240 for energy of induced fission neutron 0.7 MeV and 10 MeV, respectively.

2.1.3 ACCOUNTING OF BACKGROUND. Ci(En) was calculated from total distribution of "effect and background" acts with detection of i neutrons for each energy from relation

$$C_n = N_i \cdot B_{n-i} \qquad (5)$$

where

C_i - probability of i neutrons recording without background

N_i - probability of i neutrons recording

B_{n-i} - probability of n-i background neutrons recording.

Bi distribution was found from two-dimensional time-of-flight spectrum TP(n,t) due to the "background PPAD" after dead-time correction. Average value of background was 0.42 pulses in 30 μs gate of neutron counting. The energy dependence of background in interval from 0.5 to 15 MeV was very low (0.0007 ± 0.0005)

This measuring method made possible detection of neutrons, emitted by fission of nuclei in "background PPAD". In one auxiliary experiment the gate of neutron counting was opened by chance and by acts of fission on "background PPAD". Observed effect totals value of this phenomena into p of -0.05%.

2.1.4. DELAY γ-RAYS OF FISSION CORRECTION wasn't made because bias for signals from BLSD was 2.5 MeV and its value would be less than 0.06%.

2.1.5. A DIFFERENCIES IN NEUTRON SPECTRUM CORRECTION wasn't made too. The dependence of efficiency of BLSD was calculated by Monte Carlo method from temperature of Maxwellian spectrum of neutrons from 1.30 to 1.45 MeV and variation of efficiency didn't exeed 0.1%.

2.1.6. CORRECTION OF MISCOUNT OF FISSION FRAGMENTS AND THICKNESS OF LAYERS. Investigation of dependence of observed p of Cf-252 from bias level from PPAD gave the next results: decrease of counting rate of avalanch detector by 30% didn't lead into to measuring value of p for Cf-252. This result was explained by 50%-pulse-height resolution of this type of counters. These detectors used for fission fragments reduced the selective detection of fragments. In present work deposits with thickness not more then 0.7 mg/sm were used. According to results presented in ref. 8, value of correction was no more then 0.04%.

2.1.7 CORRECTION OF DISPLACEMENT OF FISSILE SAMPLES was not made, because the total length of assembly of PPAD in this experiment was 51 mm and corresponding correction was less than 0.03%.

2.1.8 CORRECTION FOR ANISOTROPY OF FRAGMENTS. From Monte Carlo calculations, the efficiency of BLSD was changed to 0.2% with changing of anisotropy from 1.0 to 1.4.

2.2 Measurements error.

Error of measurements consisted of the statistical and systematic errors.

Systematic error included unintroduced correction: anisopropy of fission fragments 0.2%, dependence of efficiency of BLSD from difference in spectrum of neutrons from fission - 0.1%, delay γ-rays of fission - 0.06%, miscount of fission fragments and thickness of samples - 0.04%, displacement of layers relative to centre of BLSD - 0.03%

3. Results of measurement

Results of measurenent are presented on fig.4 - 7 and in table 2.

Figures 4 and 5 show experimental data for U-235 from 0 to 2.0 and from 2.0 to 12.0 MeV. Results of measurements have a good agreement with data of Gwin et al. [9] and Manero-Konshin evaluation [6].

Table 2

Measurements results of energy dependence of $\bar{\nu}p(En)$ for U-235, Np-237 and Pu-240

		U - 235			Np - 237			Pu - 240		
E1	E2	$\bar{E}$	$\bar{\nu}$	$\Delta\bar{\nu}$	$\bar{E}$	$\bar{\nu}$	$\Delta\bar{\nu}$	$\bar{E}$	$\bar{\nu}$	$\Delta\nu$
0.45	0.55	0.50	2.500	0.022	0.51	2.677	0.037	0.51	2.873	0.046
0.55	0.65	0.60	2.489	0.021	0.61	2.740	0.023	0.60	2.900	0.032
0.65	0.75	0.70	2.488	0.022	0.70	2.722	0.023	0.70	2.942	0.027
0.75	0.85	0.80	2.527	0.025	0.80	2.723	0.023	0.80	2.892	0.017
0.85	0.95	0.90	2.533	0.028	0.90	2.778	0.022	0.91	2.926	0.024
0.95	1.05	1.00	2.542	0.031	1.00	2.803	0.027	1.00	2.941	0.030
1.05	1.15	1.11	2.552	0.029	1.10	2.800	0.019	1.10	2.947	0.026
1.15	1.25	1.21	2.589	0.027	1.21	2.787	0.023	1.21	2.961	0.028
1.25	1.35	1.31	2.569	0.027	1.31	2.787	0.022	1.31	2.969	0.035
1.35	1.45	1.41	2.529	0.017	1.41	2.811	0.027	1.41	3.011	0.027
1.45	1.55	1.51	2.587	0.021	1.51	2.828	0.027	1.51	2.988	0.022
1.55	1.65	1.61	2.602	0.029	1.61	2.828	0.024	1.61	3.014	0.031
1.65	1.75	1.71	2.628	0.043	1.71	2.854	0.027	1.71	3.075	0.025
1.75	1.85	1.81	2.660	0.030	1.81	2.835	0.022	1.81	3.078	0.041
1.85	2.00	1.94	2.656	0.029	1.94	2.895	0.018	1.94	3.088	0.021
2.00	2.25	2.13	2.697	0.032	2.14	2.929	0.025	2.14	3.100	0.019
2.25	2.50	2.39	2.723	0.024	2.39	2.948	0.023	2.39	3.123	0.022
2.50	2.75	2.64	2.771	0.034	2.64	2.974	0.027	2.65	3.187	0.030
2.75	3.00	2.89	2.791	0.039	2.89	3.026	0.022	2.89	3.214	0.034
3.00	3.25	3.15	2.789	0.039	3.14	3.047	0.021	3.15	3.276	0.028
3.25	3.50	3.40	2.904	0.056	3.40	3.127	0.035	3.40	3.270	0.032
3.50	3.75	3.66	2.918	0.031	3.66	3.165	0.034	3.65	3.340	0.041
3.75	4.00	3.92	2.927	0.042	3.91	3.157	0.050	3.91	3.315	0.044
4.00	4.25	4.16	2.959	0.057	4.15	3.180	0.039	4.15	3.363	0.043
4.25	4.50	4.42	2.953	0.044	4.41	3.340	0.031	4.41	3.418	0.031
4.50	4.75	4.68	3.043	0.062	4.67	3.272	0.039	4.66	3.559	0.043
4.75	5.00	4.94	3.154	0.036	4.92	3.353	0.050	4.92	3.494	0.042
5.00	5.25	5.19	3.135	0.063	5.17	3.338	0.046	5.17	3.560	0.061
5.25	5.50	5.43	3.113	0.055	5.42	3.365	0.048	5.42	3.729	0.069
5.50	5.75	5.68	3.253	0.062	5.67	3.470	0.050	5.68	3.688	0.049
5.75	6.00	5.95	3.397	0.089	5.93	3.538	0.049	5.93	3.595	0.067
6.00	6.50	6.33	3.377	0.054	6.31	3.576	0.049	6.32	3.645	0.041
6.50	7.00	6.82	3.349	0.048	6.81	3.593	0.046	6.82	3.809	0.048
7.00	7.50	7.34	3.575	0.066	7.33	3.759	0.037	7.34	3.871	0.042
7.50	8.00	7.83	3.534	0.095	7.84	3.843	0.070	7.84	3.959	0.038
8.00	8.50	8.32	3.708	0.070	8.34	3.839	0.060	8.35	4.040	0.045
8.50	9.00	8.82	3.816	0.062	8.89	3.903	0.079	8.87	4.183	0.081
9.00	9.50	9.35	3.916	0.116	9.36	4.034	0.095	9.36	4.081	0.087
9.50	10.00	9.88	3.862	0.114	9.87	3.991	0.079	9.88	4.284	0.097
10.00	11.00	10.61	3.973	0.086	10.64	4.241	0.068	10.63	4.557	0.105
11.00	12.00	11.67	4.241	0.117	11.67	4.333	0.101	11.68	4.540	0.125

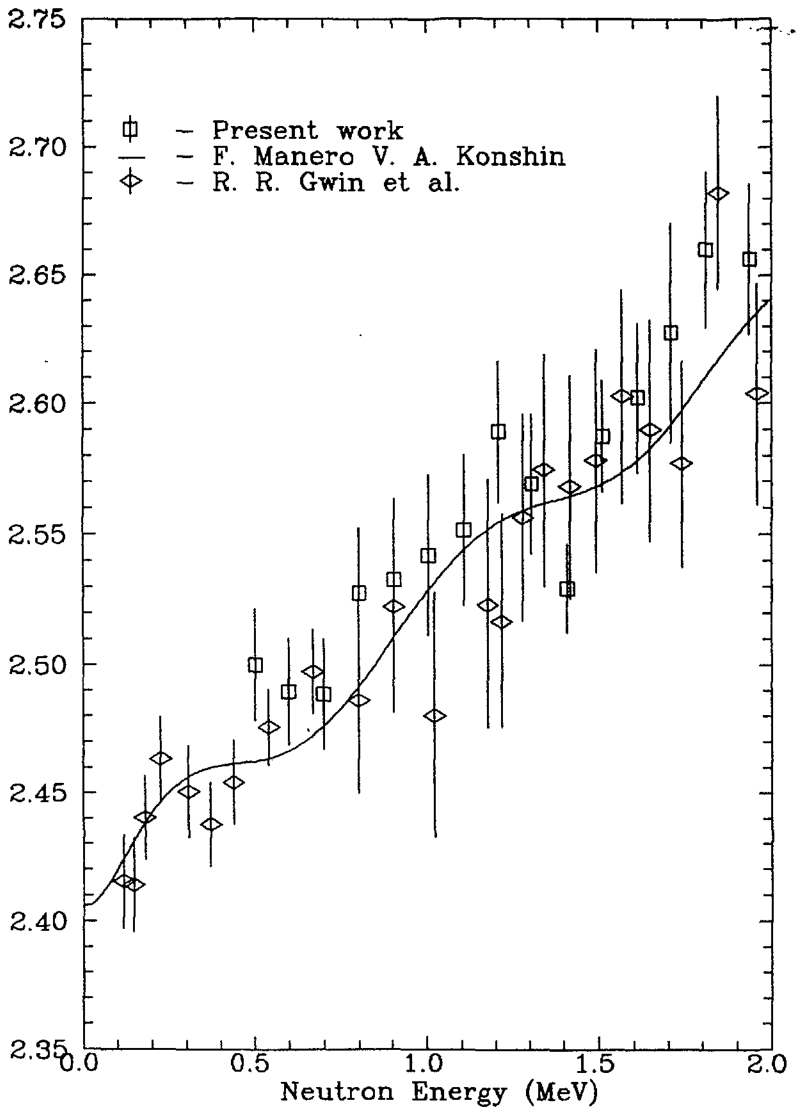

Fig. 4 The energy dependence of average number of prompt neutrons of U ^{235}(n,f)

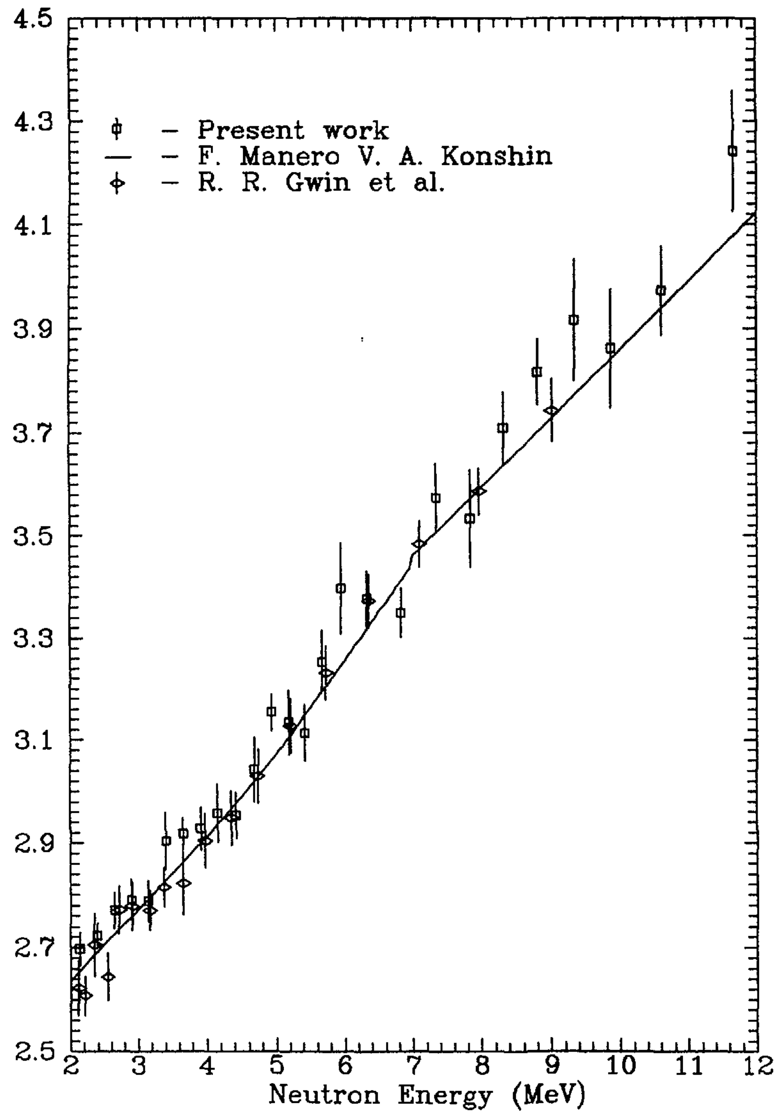

Fig. 5 The energy dependence of average number of prompt neutrons of U ^{235}(n,f)

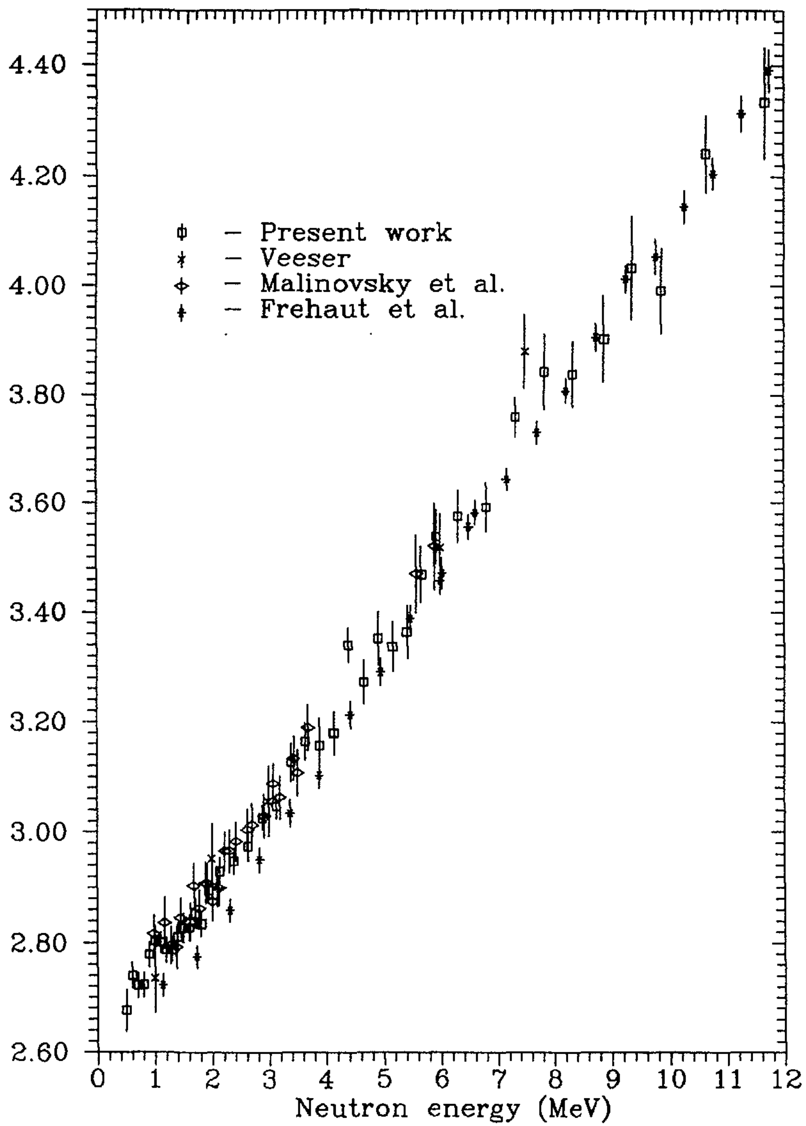

Fig 6 The energy dependence of average number of prompt neutrons of Np ^{237}(n,f)

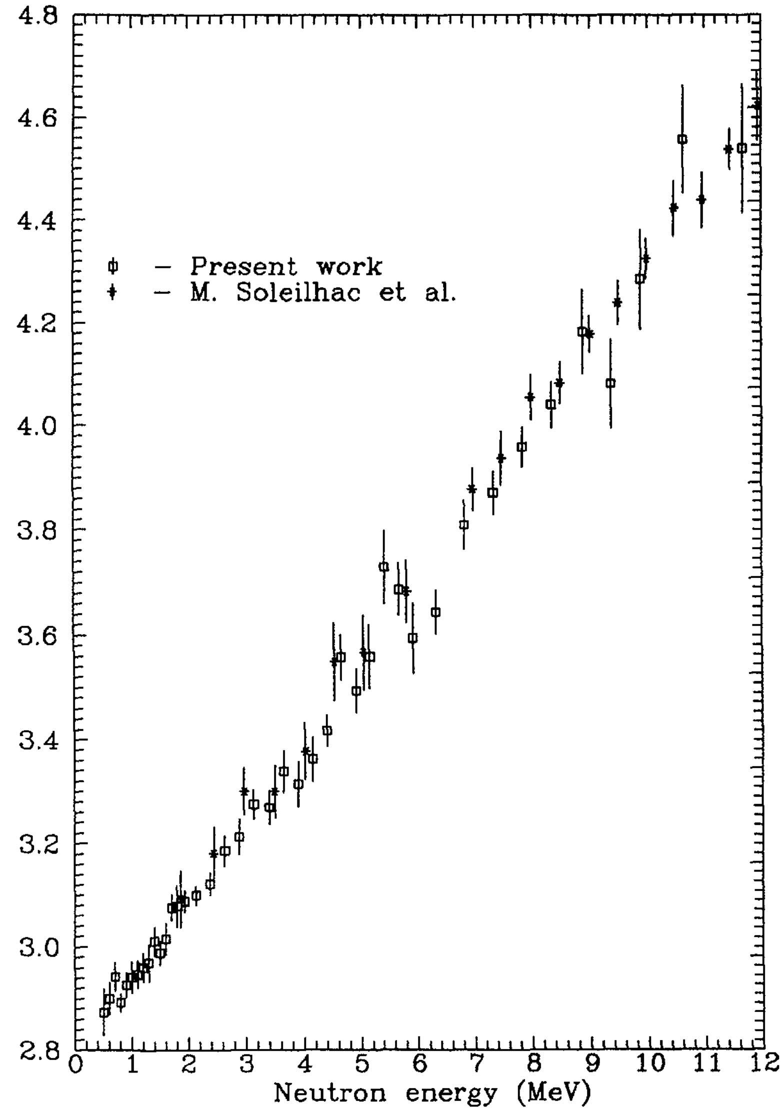

Fig. 7 The energy dependence of average number of prompt neutrons of Pu ^{240}(n,f)

Experimental data for Np-237 are presented in figure 6. Our data in 1.0-4.0-MeV-interval are 2% higher than the data of Frenaut et al. [2] and overlap with them after 5.0 MeV. In interval of energy from 0.5 to 6.0 MeV, present results have a good agreement with data of other works (see ref. [1-3]).

The data for Pu-240 well overlap with results of measurements of French group [4] in all energy interval.

REFERENCES

1. L. R. Veeser. Prompt neutrons from neutron-indused fission of Np-237// Phis. Rev. C - 1978. - v. 17., - p.385-387.
2. J. Freaut, A. Bertin, R. Bois Mesure de $\bar{\nu}$p et E , pour la fission de Th-232, U-235 et Np237 induite par des neutrons d'energie comprise entre 1 et 15 MeV.// In: Proc. of the Intern. conf. on Nuclear Data for science and tecnology., (Antwerp, Belgium, September, 1982). - 1983 - p.78-81.
3. В. Г. Воробьева, Б. Д. Кузьминов, В. В. Малиновский и др. Измерение среднего числа мгновенных нейтронов при делении ядер Np-237 нейтронами.// Вопросы атомной науки и техники. Сер. Ядерные константы, - 1980, - вып.3(38), с. 45-58.
4. J. Frehaut, M. Soleilhac, Mosinski G. Measure du nombre money p de neutrons promtsemis au cour de la fission induit dans Pu-240 et U-235 par des neutrons d'energie comprise entre 1,5 et 15 MEV.// В кн: Нейтронная физика. ч.3 (Материалы 2-й Всесоюз. конф. по нейтронной физике, Киев, 1973). Обнинск: ФЭИ, - 1974, - с.153-164.
5. М. В. Савин, Ю. А. Хохлов, Ю. С. Замятнин, И. Н. Парамонова Среднее число мгновенных нейтронов при делении U-235, Pu-239, Pu-240 быстрыми нейтронами. // In: Proc. of the 2nd Intern. Conf. on Nucl. Data for Reactors., (Helsinki, June, 1970). Vienna: IAEA, - 1970, - v.2, - p.157.
6. F. Manero, V. A. Kon'shin. Status of the energy-dependent $\bar{\nu}$-values for the heavy izotopes (Z>90) from thermal to 15 MeV and of ν-values for spontaneous fission. // Atomic Energy Rev. - 1972. - vol.10, p.637-756.
7. Г. П. Антропов, Н. А. Архангелов и др. Мощный линейный ускоритель для нейтронной спектроскопии.// Вопросы атомной науки и техники. Сер. Техника физического эксперимента. - - 1985, - вып.2(22), - с.3-5.
8. J. W. Boldeman, J. Frehaut The foil thickness correction in ν measurements and the (ν - n) dicrepancy. // Nucl. Sci. Eng. - 1980, - v.76, p.49-52.

9. R. Gwin, R. R. Spenser, R. W. Ingle. Measurement of the energy dependence of prompt neutron emission from U233, U235 and Pu239 for En=0,0005 to 10MeV relative to spontaneous fission of Cf252. // Nucl. Sci. Eng., - 1986, - v 94. - p.365-379.

INTEGRAL QUALIFICATION OF NU-BAR FOR THE MAJOR FISSILE ISOTOPES

Henry TELLIER
Service d'Etudes de Réacteurs et de Mathématiques Appliquées
Centre d'Etudes Nucléaires de SACLAY, France

Abstract

Using the well known tendency research method we validate the nuclear data for the thermal neutron reactor needs and deduce from it the best estimated values of ^{235}U and ^{239}Pu neutron data, including nu-bar. The estimated values of nu-bar total for ^{235}U and ^{239}Pu which give the best agreement with thermal reactor integral experiments are compared with JEF 2.0 and other evaluations.

I) INTRODUCTION

For safety and economic reasons, the reactor physicist and the reactor designer need to make neutron calculations of multiplying media with a very good accuracy. These computations are generally performed by solving the BOLTZMAN equation, with the help of very sophisticated codes. The nuclear data which are necessary for these codes are deduced, through the evaluated neutron data files, from direct nuclear measurements and theoritical models. Very often it is difficult to measure with a very good accuracy the variations, with the energy of the incoming neutron, of some nuclear properties. Consequently some of the best estimated values of the files have an uncertainty which is too large for the reactor physics needs. To improve the knowledge of these neutron parameters the reactor physicists use another type of measurement : the integral experiments. In the integral experiments, we use critical facilities and measure synthetic parameters which are representative of the neutron properties of the cell for the actual neutron spectrum. For example, we can measure critical sizes or bucklings. If the integral experiments are chosen with a very simple geometry and an asymptotic neutron spectrum, uniform lattices or homogeneous media for instance, we can perform their calculations without numerical approximation. Therefore, if we observe a difference between the computed value of a particular neutron parameter and the experimental value, this difference can be attributed to the input neutron data uncertainties. If we have at our disposal a set of integral experiments with differents neutron data sensitivies we can obtain informations or tendencies about the basic data. This proceeding is the well known tendency research method. We have used this method to validate the nuclear data for the thermal neutron reactor needs and we deduced from it the best estimated values of uranium 235 and plutonium 239 neutron data, including nu-bar, for the low energy neutrons.

II) PRINCIPLES OF THE TENDENCY RESEARCH METHOD

For each integral experiment (criticality factor, reaction rate ...) we know the experimental result Y_i and the measurement uncertainty E_i. In any case we can compute the same quantity which is a function of the neutron parameters x_k. The result of this calculation is F_i (..., x_k, ...). If we change the value of the neutron parameter k, which becomes $x_k + \Delta x_k$, the result of the computation is now F_i (..., $x_k + \Delta x_k$, ...).

The principle of the tendency research method is to choose the modification Δx_k of the neutron parameters in such a way that the quantity

$$Q = \sum_i \frac{1}{E_i^2} \left[Y_i - F_i (\ldots, x_k + \Delta x_k, \ldots) \right]^2$$

for all the set of integral experiments becomes minimum. Nowadays the magnitude of the main neutron cross sections are more or less well known. So, the modification Δx_k are expected to be small and we can make a first ordre expansion of the computed value

$$F_i (\ldots, x_k + \Delta x_k, \ldots) = F_i (\ldots, x_k, \ldots) + \sum_k \Delta x_k \frac{\partial F_i}{\partial x_k}$$

We can also replace the partial derivatives by the sensibility coefficients

$$S_{ik} = \frac{\Delta F_i}{\Delta x_k}$$

These sensibility coefficients (variation of the integral quantity F_i for a one per cent change of the parameter x_k) can be computed by the perturbation theory or a variationnal method.

With these assumptions we must now minimize the quantity

$$Q = \sum_i \frac{1}{E_i^2} \left[Y_i - F_i (\ldots, x_k, \ldots) - \sum_k S_{ik} \Delta x_k \right]^2$$

or if Y_i represents the difference between the experimental result and the computed value for the integral experiment i

$$Q = \sum_i \frac{1}{E_i^2} \left[\Delta Y_i - \sum_k S_{ik} \Delta x_k \right]^2$$

The minimization is done with the least square method. That is why, if we want to determine the modifications Δx_k with a good accuracy, it is necessary to use a set of integral experiments for which the sensitivity coefficients are as different as possible. To obtain different sensitivity coefficients we use multiplying media with different neutron spectrum from the well thermalized heavy water or graphite moderated lattices to the hard spectrum of the tight pitch light water reactor.

III) CHOICE AND INTERPRETATION OF INTEGRAL EXPERIMENTS

We have seen that two essential conditions must be satisfied if we want to obtain physical informations about the basic neutron data : simple geometry with asymptotic spectrum to avoid numerical approximations during the computation and different sensitivity coefficients to be able to disconnect the various neutron parameters. As a matter of fact an integral experiment gives a global result with depends on several neutron cross sections or nuclear data. To satisfy the first condition we have chosen a set of critical size measurements of uniform lattices and homogeneous media. In these cases the calculation of the reactor can be performed with a simple cell computation in fondamental mode and the neutron leakage can be simulated by the buckling. Thus, it is possible to use a very detailed mesh for the spatial and energy descriptions. Several types of moderator and moderating ratios allow to obtain various sensitivity coefficients. Different fuel compositions with only uranium or plutonium allow to separate the effect of each fissile isotope. For this study we used seventy buckling measurements, part of them are international benchmarks (such as TR or the OAK RIDGE spheres) or published experiments, french experiments constitute the remainder. The multiplying media which contain only uranium are :

- heavy water and natural uranium lattices
- graphite and naturel uranium lattices
- light water and low enriched uranium lattices with various moderations radios including tight pitch lattices
- homogeneous sphere with high enriched uranium.

The other experiments which contain only plutonium or a mixture of uranium and plutonium are :

- homogeneous light water and plutonium 239 media
- heavy water and mixed metallic fuel lattices
- light water and mixed oxide fuel lattices also including tight pitch experiments.

The effective multiplying coefficients of these experiments were computed with the APOLLO code which solves the BOLTZMAN integral equation by the collision probability method and in the multigroup approximation. Ninety nine groups were used to represent the energy range with forty seven groups in the thermal range below 2.7 eV. With this number of thermal groups, the reactor computations are sensitive to the shape of the cross section at low energy.

V) RESULT ANALYSIS

It is necessary to use a great number of groups to make very accurate calculations but, obviously, it is not possible with integral experiments to obtain informations for each group and each cross section. Nevertheless it is possible to choose a

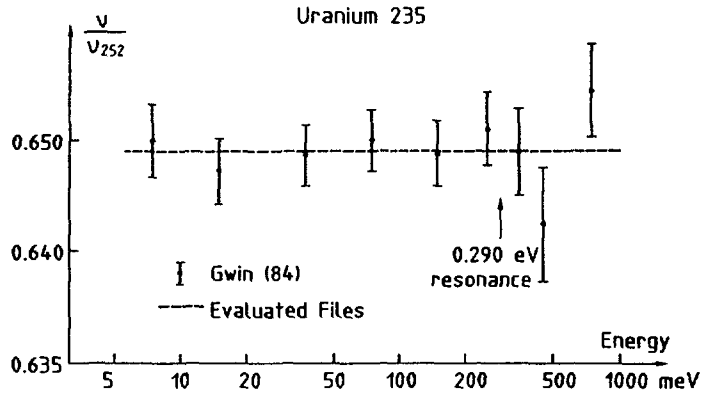

Figure 1

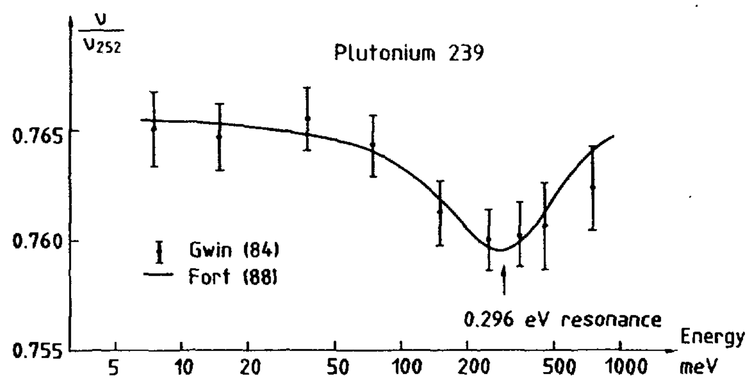

Figure 2

smaller number of synthetic neutron parameters which represent the general trend of the cross sections versus energy and split the energy range in three parts : the thermal, the resonance and the fast energy ranges. As we are interessed in the cross sections for the thermal neutron reactors, for which the low energy range is predominant, we can chose in the thermal energy range, where the cross sections vary smoothly the magnitude of the nuclear data for a given energy, 0.025 eV for instance. This implicates to have a good knowledge of the shape of the various neutron date in the vicinity of the thermal range. The synthetic parameter which are sensitive for thermal neutron reactor physics are the level of the neutron cross section in the thermal and fast range, the effective integrals in the resonance region and the migration area of the moderators. It is for these quantities that the tendency research method provided informations.

As starting point we used evaluated files which take into account the last microscopic measurements or theorical calculations. As for as nu-bar is concerned the recent experimental results in the thermal range are mainly those of OAK RIDGE for both uranium 235 and plutonium 239 [1]. For uranium 235 it is assumed that nu-bar has a flat shape in the thermal range as it can be seen on figure 1. Nothing appears around the 0.29 eV resonance. All the evaluated files adopt a constant value below 1 eV. For plutonium 239, nu-bar cannot be

Uranium fuel critical Experiments

$< k^{c}_{eff} - 1 > = (-10 \pm 428) . 10^{-5}$

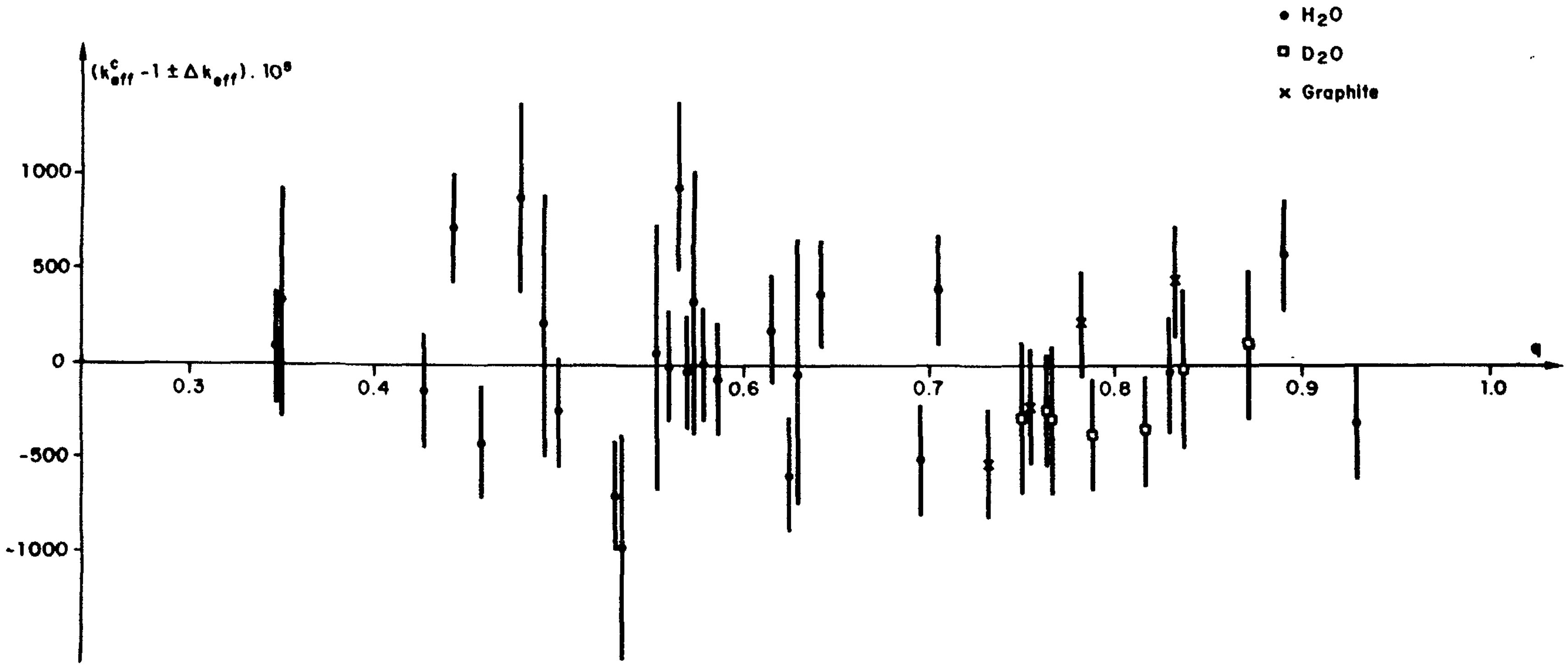

Figure 3

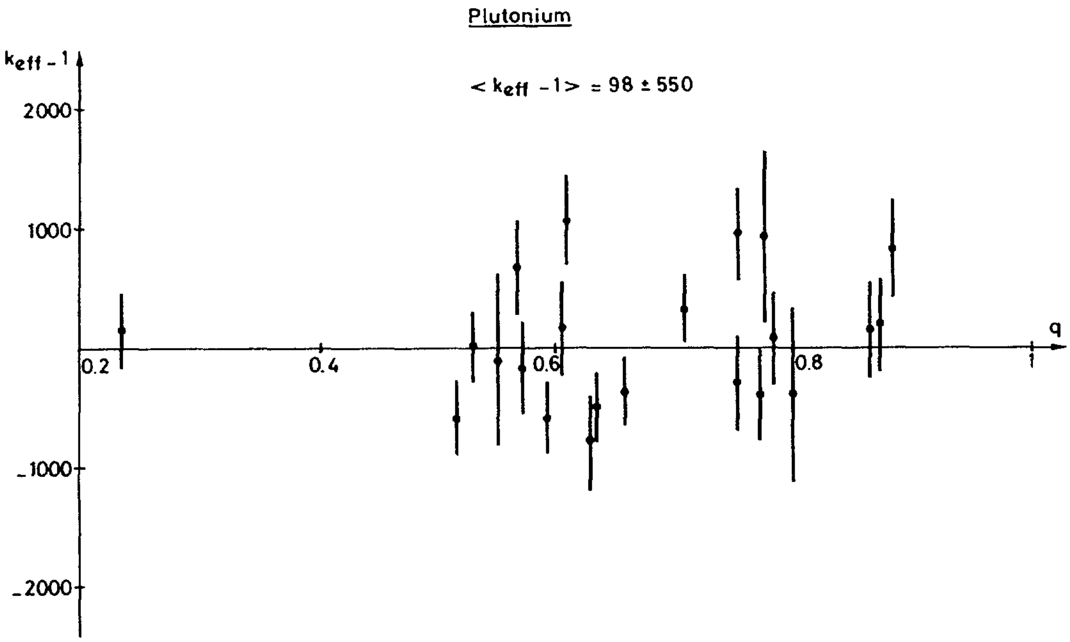

Figure 4

consider as constant as it is shown on figure 2 which represents the recent experimental results [1] and a theorical calculation which account for the (n, γ f) process and the spin effect [2]. It exist a strong dip in the 0.296 eV resonance which was not considered in the old evaluations. Even ENDF/B5 used a constant value, but JEF2.0 takes this dip into account. Consequently all our reactor calculations were carried out with JEF2.0 evaluated file.

The application of the tendency research method to the difference between the computed values of the effective multiplication coefficient of the multiplying media and the experimental ones which are equal to unity suggests some minor modifications of the initial neutron data. If we adopt these modifications the computation of all the set of integral experiments is satisfactory. This can be seen or figure 3. On this figure we show the difference between the computed keff and unity for the uranium 235 multiplying media ; the error bars are those of the experimental results. The abscissa q is

Table I
Nu-bar of major fissile isotopes

	U 235	Pu 239
ENDF/B5	2.4367	2.8914
JEF2.0	2.432	2.8772
Divadeenam (84)	2.425 ± 0.003	2.877 ± 0.006
Malinovsky (85)	2.424 ± 0.006	-
Axton (86)	2.426 ± 0.005	2.879 ± 0.006
This work	2.434 ± 0.004	2.875 ± 0.007

the slowing down density. It is the number of neutron which arrive below 2.7 eV for one emitted fission neutron. The high values of q correspond to the well thermalized lattices (heavy water or graphite moderated) and the low values to the tight pitch lattices. For the whole set of experiments the effective multiplying factor is on average well calculated. Figure 4 shows the similar results obtained with the experiments which contain plutonium.

The estimated values of nu-bar total for uranium 235 and plutonium 239 which give the best agreement with the integral experiments are given in table I. They are compared with the initial values of JEF2.0 and also other evaluations. According to the results of the tendency research it seems that the initial values of nu-bar which were recommended in the JEF2.0 file give satisfaction to the thermal neutron physisists. In the low energy range, no modification of the initial data is necessary, neither for uranium 235 nor for plutonium 239. The agreement with the recommendation of Divadeenam and of Axton is also good, althought these evaluations used only differential measurements.

To validate or to improve the knowledge of the basic data, the integral experiments are an efficient tool. They are complementary to the microscopic experiment. The later are necessary to determine accurately the shape of the neutron parameter versus energy, the former are useful to obtain the magnitude.

REFERENCES

[1] R. GWIN et al : Nuclear Science and Engineering, 87, 381 (1984)

[2] E. FORT et al : Nuclear Science and Engineering, 99, 375 (1988)

[3] M. DIVADEENAM and J.R. STHEN : Annals of Nuclear Energy, 8, 375 (1984)

[4] V.V. MALINOVSKY et al : Nuclear Data for Basic and Applied Science, Santa-Fé, II, 1475 (1985)

[5] E.J. AXTON : Geel Report GE/PH/01/86 (1986).

ON NU TOTAL OF ^{239}PU AND ^{235}U AND RELATED PROBLEMS

OR

ON THE INTEREST AND DIFFICULTY IN PRESERVING THE BASIC PHYSICS IN PREPARING NUCLEAR DATA FOR APPLICATION

E. Fort
DER/SPRC/LEPH - Batiment 230
Centre d'Etudes Nucleaires
de Cadarache
B.P. No. 1
F-13108 Saint-Paul-Lez-Durance
France

(Note by Compiler: A summary of this presentation which was made available by the author is reproduced below).

Summary

The evaluation work is dominated by the permanent search for the consistency required to preserve the basic Physics information - but the lack of information introduce practical limitations to this ambition.

The neutron emission by ^{239}Pu and ^{235}U have been taken as examples by way of illustration.

^{239}Pu.

In the resolved range a formalism has been proposed to produce a continous energy dependent curve $\nu_p(E)$ for the prompt fission neutron emission. This formalism takes into account the experimental evidence of the $(n,\gamma f)$ and spin competition - Fluctuations (dips) appear in the $\nu_p(E)$ curve and these have proved to be consistent with microscopic and also k_{eff} integral data. Extrapolation of this formalism to the unresolved range, deficient in experimental data, is straightforward only in so far as the "S" waves are concerned. - It happens that the consistency with GWIN's experimental data is perfect in the 4 kev region, but the explanation of the bump observed in the 20 - 50 kev region might depend, among others, on clear informations about the spin effect for higher spin values.

Thanks to a recent work by LENDL who computed the most probable charge of a given FP in a FP isobar distribution, the total delayed neutron yield is expressed as a function of energy in a way that preserves the consistency with the prompt neutron emission.

Concerning the total gammy energy released in prompt fission $<E_{\gamma t}>$, FREHAUT has shown for some nuclei (^{237}Np, ^{235}U....) a linear relationship with $\nu_p(E)$. Using systematics, established at thermal energy, it is possible to derive such a relationship for all fissible nuclei.

The prompt and delayed neutron yields and the total energy released in fission can be calculated with the same basic parameters as the fission cross sections.

This is true for ^{239}Pu for energies less than 4 kev. From this energy up to the second chance fission threshold the consistency of $\nu_p(E)$, $\nu_D(E)$ and $<E_{\gamma t}(E)>$ is preserved without any relation with $\sigma_f(E)$.

Above the second chance fission threshold the consistency is destroyed simply because the respective contributions of the first, second, third chance fissions to the total fission cross section are not known and are relevant to accurate theoretical calculations. A good knowledge of the first chance fission cross section would help in solving the standing problem of the competitive (n,2n) cross section.

^{235}U.

The situation for this nucleus is different. The fluctuations - observed in $\nu_p(E)$ are independent of spin and $(n,\gamma f)$ effect, since they result from fluctuations in the total kinetic energy of the fission fragments as measured by HAMBSCH and co-workers in GEEL. But it is difficult to translate this into an analytic formalism and the evaluation of $\nu_p(E)$, $\nu_d(E)$ and $<E_{\gamma t}(E)>$ is preserved in a large energy range since the relative proportions of the first and second chance fissions have been measured by FREHAUT up to the third chance fission threshold.

The conclusions concern essentially ^{239}Pu because of the particular status of the information related to this nucleus.

ν_p experimental data are needed in the range 1 kev - 100 kev

1. to fill the gap between 100 ev and 3 kev;
2. to confirm the important "bump" in the interval 20 kev - 50 kev of importance for FBR's critical mass prediction.

Informations on the 1^{st} chance fission cross section above 5.655 MeV would help in understanding the behaviour of the (n,2n) cross section in the 2 MeV range above the threshold and would ensure consistency with $\nu_D(E)$ calculations.

Concerning the $\nu_D(E)$ calculations the promising model by LENDL should be a little bit more worked at least to suppress the discontinuity in Zp(A).

In the field of gamma emission in prompt fission there are clear needs for new measurements:

1. In the thermal range to confirm the old data, possibly with improved detectors;

2. In the fission spectrum region to confirm present systematics indications.

SYSTEMATICS OF FISSION NEUTRON DATA

I. Düring, H. Märten, A. Ruben, and D. Seeliger
Technische Universität Dresden, Institut für Kern- und Atomphysik
Mommsenstrasse 13, D-O-8027 Dresden, Germany

Abstract: The present status of fission neutron data files does not correspond neither to the progress achieved in the field of experimental techniques and the theoretical understanding nor to various data requests. Sparse (and sometimes contradictory) experimental fission neutron data are not an adequate basis for evaluations at neutron incidence energies up to 20 MeV and beyond. The present (preliminary) systematics of fission neutron data has been based on

- a phenomenological scission point model with temperature-dependent microscopic energies for the description of energy partition in fission as function of mass asymmetry,
- a complex temperature distribution model (code FINESSE) for predicting multiplicities, energy and angular distributions of fission neutrons, and
- reaction theory including fission channel to account for multiple-chance fission and pre-fission neutron emission.

This theory complex was tested (and partially adjusted) in comparison with well-known fission data for various reactions. It is considered as a reliable basis for predicting fission data in unknown cases and for physically consistent evaluations. Calculational results of pure post-fission neutron spectra as well as total spectra including pre-fission neutron contributions for neutron incidence energies up to 20 MeV are presented and compared with recent experimental data. Based on the calculations for spontaneous and induced fission, a new relation between average emission energy $\bar{E}$ and average number of neutrons $\bar{\nu}$ has been derived. It includes the dependence on the fissility parameter Z^2/A. Group constants of neutron spectra for thermal neutron induced fission of ^{233}U, ^{235}U, and ^{239}Pu are presented.

1. INTRODUCTION

Fission neutron spectra N(E) and average numbers of fission neutrons $\bar{\nu}$ are essential data for nuclear technology. They were measured, calculated, compiled, and evaluated in many works. However, the present status can be summarized as follows:

(i) *Experimental data* are available for thermal-neutron induced fission of the major and some of the minor actinides, for fast-neutron induced fission at some incidence energy (E_i) points (MeV region, around 14 MeV), and for several spontaneous fission reactions (cf. CINDA). Most of the data were measured a long time ago on the basis of simple experimental techniques. The data are often contradictory.

(ii) *Theoretical approaches* to fission neutron emission have not yet been applied in a systematic manner for calculations of fission neutron data and for their check in regard of physical consistency.

(iii) *Data evaluations* were directly based on the few experimental data in combination with empirical relations.

(iv) *Nuclear data libraries* do not correspond to the present status of experiment and theory. They do not include fission neutron data in a reliable complexity, e.g. average parameters ($\bar{E}$ and $\bar{\nu}$) are not considered in their dependence on E_i in most cases. Spectral shapes assumed are either Watt or Maxwellian distributions, whose parameters are taken as identical and E_i-independent for most of the actinides.

Remarkable effort has been devoted to the precise determination of the ^{252}Cf(sf) standard in the last years /1-3/. The requirements to be met in fission data measurements and analysis were specified in detail. Remarkable progress was achieved in the theoretical understanding of fission and fission neutron emission /4/. The ^{252}Cf example shows the present possibilities in experiment and theory. Since a general improvement of the experimental fission neutron data basis is not realistic, further activities to improve the precision and the complexity of fission neutron data files should be based on adequate (i.e. physically consistent) theoretical approaches and a few precision experiments in order to check (or to adjust) the theory at typical points. The Madland-Nix Model (MNM)/5/ was the first, which was applied to systematic fission neutron data calculations in the case of ^{235}U (ENDF/B-VI) /6/. The present work relies on recent theoretical approaches developed at TU Dresden involving fission theory, complex fission neutron (evaporation) theory, and reaction theory with fission channel (applications to multiple chance fission).

2. THEORETICAL BASIS FOR DATA SYSTEMATICS

The yield and spectral distribution of fission neutrons are strongly dependent on fragment mass number. Accordingly, fission neutron data calculations should be performed in an adequately complex manner in order to provide physical consistency. Necessary preconditions are:

(i) the application of the statistical theory of neutron emission from highly excited, rapidly moving fragments (evaporation theory) to the fragment diversity represented by a complex occurrence probability in mass number A, excitation energy E^*, and kinetic energy E_k (or total kinetic energy TKE), i.e. $P(A,E^*,TKE)$,

(ii) the knowledge of the fragment distribution $P(A,E^*,TKE)$, i.e. application of fission theory to deduce necessary informations,

(iii) the application of reaction theory with fission channel to multiple chance fission reactions in order to calculate the partial fission cross sections $\sigma_{f,j}(E_i)$ (i.e. the weight of the chances j) as well as the spectral distribution of pre-fission neutrons.

After calculating the yield $\bar{\nu}(A)$ and the LS distribution $N(E,\theta:A)$ (with norm 1.) for given mass number (θ - angle of neutron emission with reference to fission axis), the total neutron yield and spectrum are given by

$$\bar{\nu} = \sum Y(A)\ \bar{\nu}(A), \tag{1}$$

$$N(E) = \sum Y(A) \int d\Omega\ [\bar{\nu}(A)/\bar{\nu}]\ N(E,\theta:A). \tag{2}$$

In the case of multiple chance fission of the type (n,jnf), j=0,1,2,... , Eqs. (1) and (2) are separately solved for each fission chance j, i.e. we obtain $\bar{\nu}_j$ and $N_j(E)$, with the weight

$$w_j = f(E_i) = \sigma_{f,j}/\sigma_f, \tag{3}$$

where the total fission cross section is

$$\sigma_f = \sum_j \sigma_{f,j}. \tag{4}$$

The total value $\bar{\nu}$ includes post-fission neutrons (number $\bar{\nu}_j$) as well as pre-fission neutrons (number j):

$$\bar{\nu} = \sum_j w_j \; (\bar{\nu}_j + j). \tag{5}$$

The total emission cross section of fission neutrons (which are measured in coincidence with fission events, i.e. including pre-fission neutrons with the spectral distribution $S_j(E)=d\sigma_j/dE$) is given by

$$\frac{d\sigma}{dE} = \sigma_{f,o} \; \bar{\nu}_o \; N_o(E) + \sum_{\substack{j \\ (j\geq 1)}} \sigma_{f,j} \; [\bar{\nu}_j \; N_j(E) + S_j(E)], \tag{6}$$

where $S_j(E)$ is normalized to 1. in the energy interval allowed because of energy conservation restrictions:

$$\int_o^{E'_j} dE \; S_j(E) = 1, \tag{7}$$

where

$$E'_j = E_i - \sum_{j'=1}^{j-1} B_{n,j'} - E_{f,j} \tag{8}$$

($B_{n,j}$ - neutron binding energy for the j-th emission step, $E_{f,j}$ - effective value of the fission barrier for chance j).

The following nuclear models were applied:

Scission point model /7/ for solving the energy partition problem: It is based on potential energy minimization at scission point. In connection with a detailed energy balance equation at scission with reference to saddle B conditions, the model is suitable to predict the partition of total available energy on both complementary fragments (E_k and E^*) as function of mass asymmetry. Microscopic effects (influencing the stiffness of the fragments at scission point strongly) are considered in a phenomenological way, i.e. shell correction energies as function of A were deduced within the model on the basis of well-known experimental data. Further, their dependence on nuclear temperature is taken into account.

5-Gaussian approach for calculating mass yield curves $Y(A:E_i)$:
As found phenomenologically /8/ as well as theoretically /9/, mass yield curves can be well represented by a 5-Gaussian-approach corresponding to two asymmetric and one symmetric fission mode. On the basis of experimental data the parameters average mass number, width, and weight of the five Gaussians were deduced as function of E_i (and separately for all possible fission chances at $E_i > 6$ MeV) for fission reactions in the Th-Cf region. The dependence on E_i was represented by data fits to several functions.

Temperature distribution model (code FINESSE) /10/ for describing the neutron yield and the spectral distribution of fission neutrons as function of A and in total form (Eqs. (1) and (2)):
The model relies on basic ideas of the MNM, but accounts for

- the explicit dependence of fission neutron characteristics on A, e.g. a realistic distribution in rest-nucleus temperature deduced from Gaussian distribution in E^*,
- model parameter averages over the charge distribution for given A,
- a modified evaporation ansatz including higher-order terms of entropy expansion in powers of excitation energy,
- emission anisotropy in the centre-of-mass system due to fragment angular momentum,
- competition of neutron and γ-ray emission (simulation),
- angular distribution of fission neutrons in the laboratory frame (with reference to fission axis and incidence beam direction, etc.

Reaction theory (Hauser-Feshbach theory with account for pre-equilibrium effects and fission, code STAPRE /11/) for predicting fission cross sections; statistical multistep (direct/compound) reaction theory (SMD/SMC), code EXIFON /12/ with fission channel renormalization on the basis of STAPRE results for calculating the spectra of pre-fission neutrons:

At present, the statistical multistep reaction theory with the direct incorporation of the fission channel /13/ is tested. It will probably considered as the theoretical basis for further calculations (cf. /4/).

The theoretical scheme outlined above was applied to calculate fission neutron data for important actinide nuclei in the energy range from thermal energy (or threshold) to 20 MeV. The results are presented and discussed in the following sections.

3. SPECTRAL SHAPES AND AVERAGE EMISSION ENERGIES

Post-fission neutron spectra are neither Maxwellian nor Watt distributions /5,10/. Nevertheless, most of the experimental spectra were approximated by at least one of both for data reduction. The spectral shape of the ^{252}Cf(sf) neutron spectra was carefully investigated experimentally as well as theoretically /1-3/. This nuclear standard can now be considered as well-established /14/.

As shown in Ref. /10/, FINESSE calculations reproduce the ^{252}Cf(sf) standards N(E) and $\bar{\nu}$ within experimental uncertainties. In the present work, some of the calculational results are represented with reference to the standard spectrum, i.e. the spectral ratio

$$R(E,E_i) = N(E,E_i) \ / \ N_{Cf}(E) \tag{9}$$

is analyzed. Note that both spectra are normalized to 1, so that neutron yield differences are eliminated (see definitions above). The matrix $R(E,E_i)$ calculated for ^{238}U fission induced by neutrons with energies up to 20 MeV is represented in Fig. 1. Note the remarkable influence of the multiple-chance fission at the thresholds 6.5 (j=1) and 12 MeV (j=2). Here, the emission of pre-fission neutrons reduces the total excitation energy of the fragments from higher-order fission chances and, consequently, the average emission energy for $j \geq 1$.

In the following, FINESSE results obtained without any parameter fit are shown in comparison with recent experimental data for the incidence energy ranges

- thermal neutron energy,
- 1.5 - 2.0) MeV and 2.9 MeV (DD-neutrons),
- about 7 MeV (just above the (n,n′f)-threshold),
- around 14 MeV (DT-neutrons).

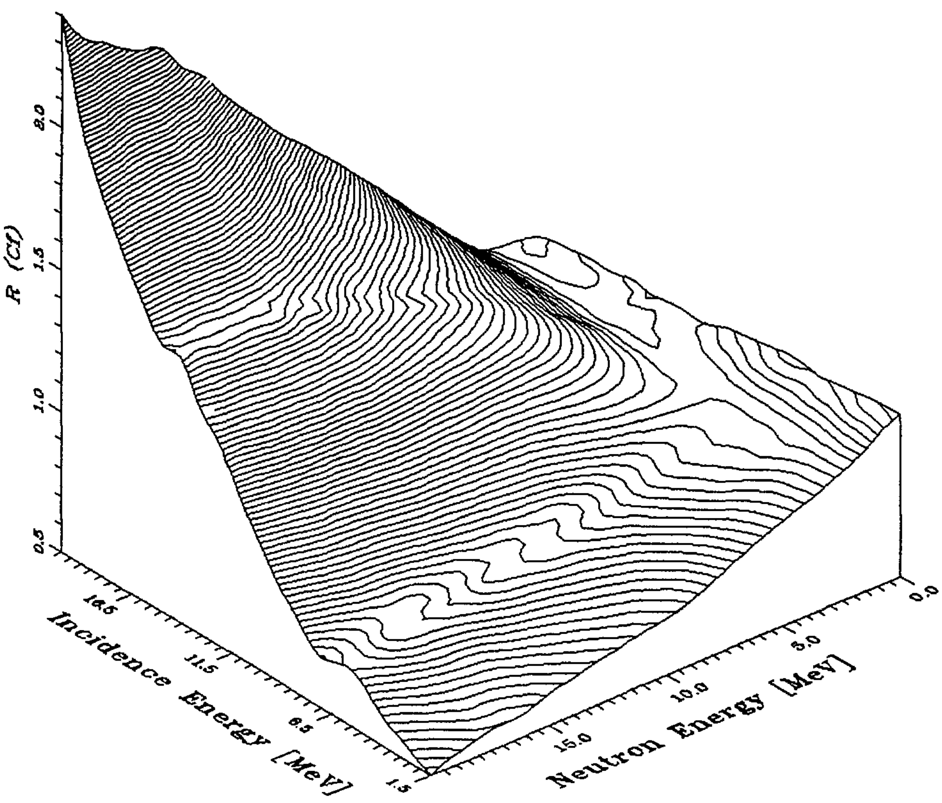

Fig. 1 The spectral matrix of ^{238}U(n,jnf) neutrons (here, only post-fission neutrons) with reference to the ^{252}Cf(sf) spectrum (FINESSE/STAPRE/EXIFON calculation)

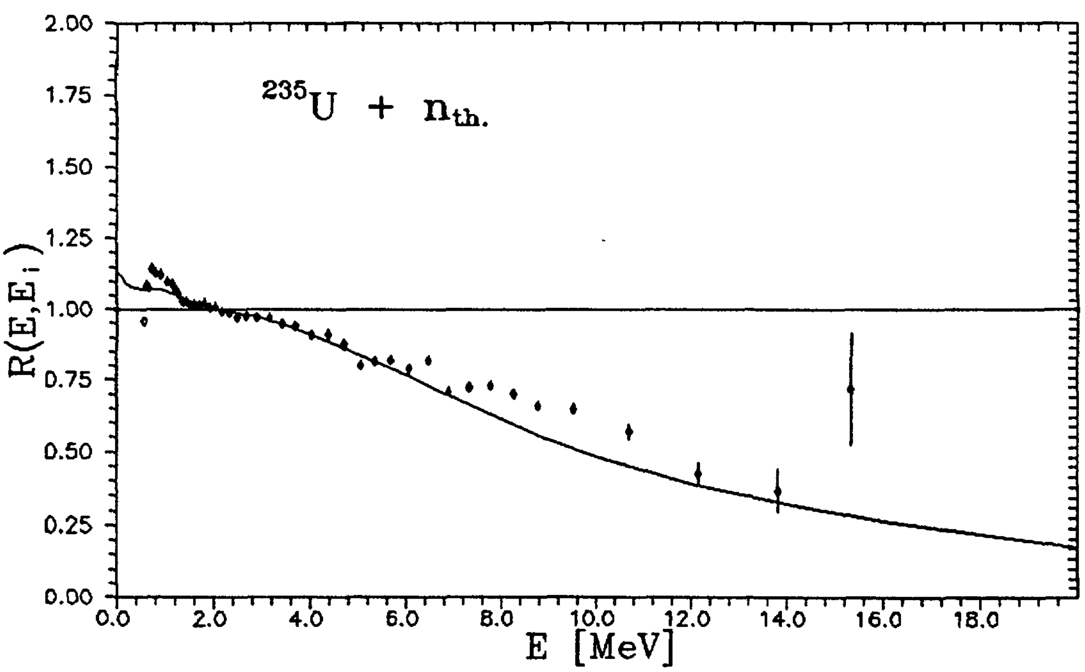

Fig. 2 Spectral ratio to the ^{252}Cf(sf) standard for the fission reaction specified (experimental data - /15/)

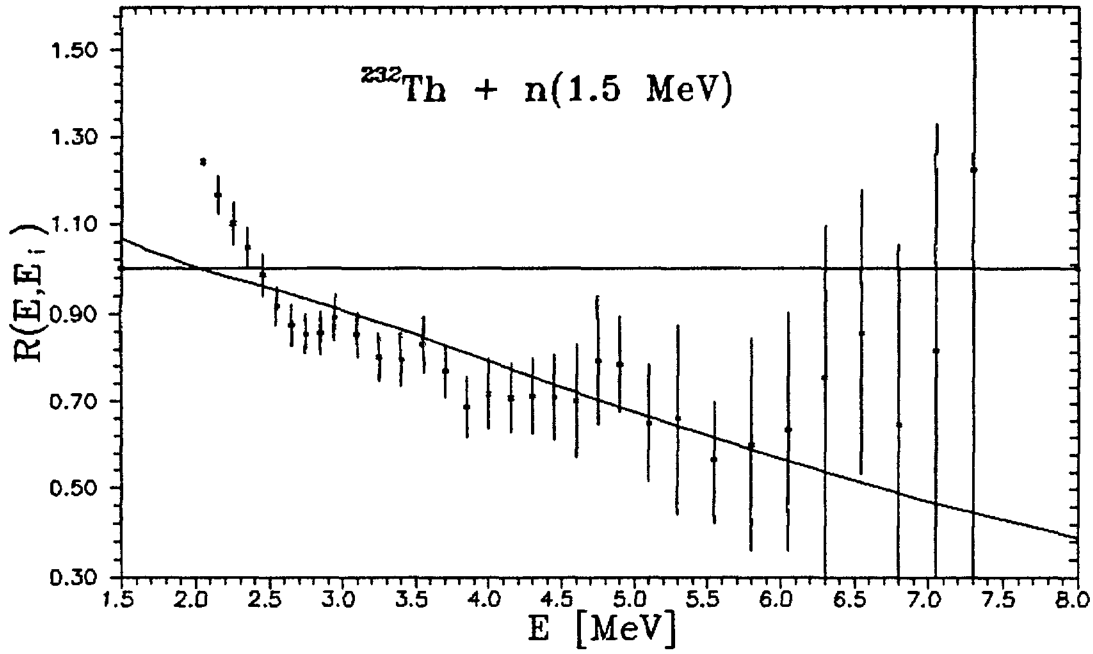

Fig. 3 As for Fig. 2 (experimental data - /16/)

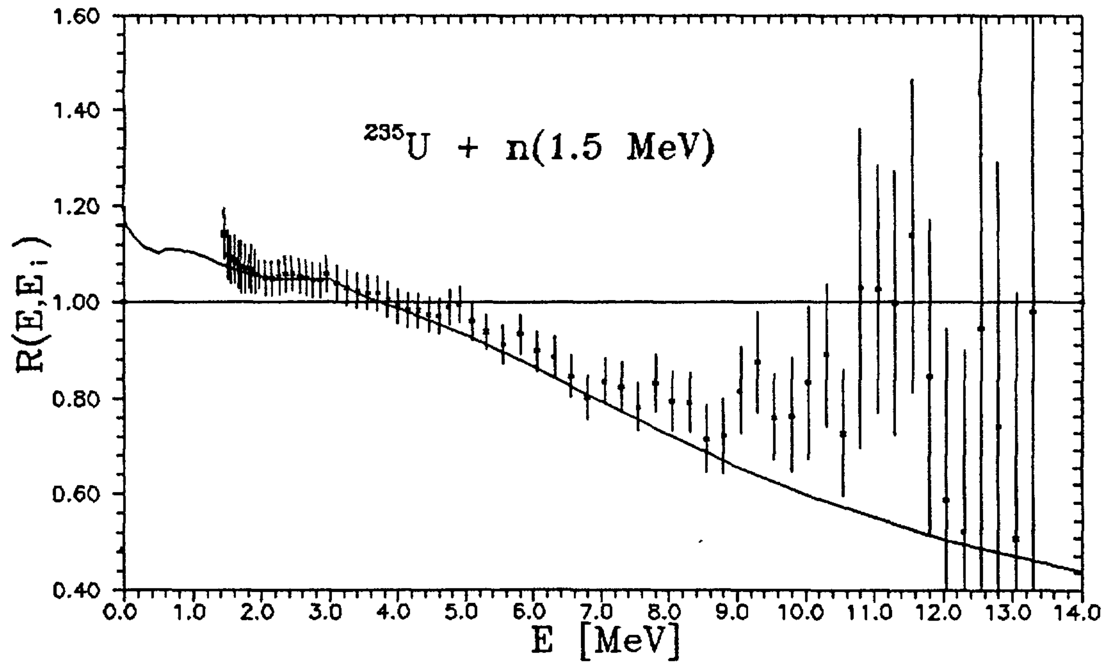

Fig. 4 As for Fig. 2 (experimental data - /16/)

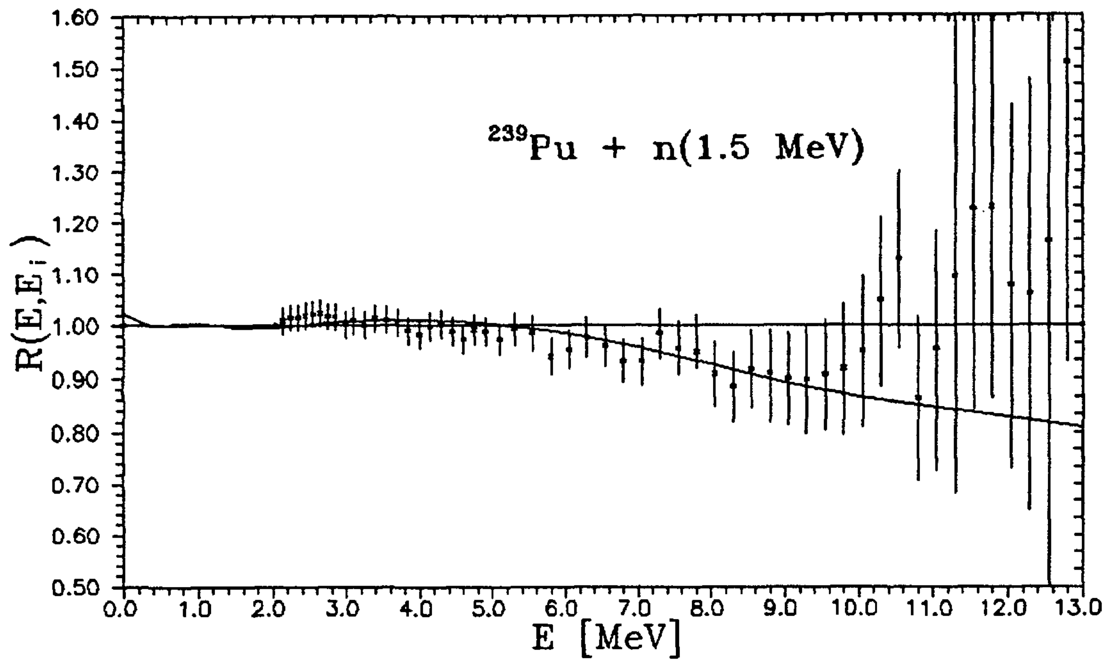

Fig. 5 As for Fig. 2 (experimental data - /16/)

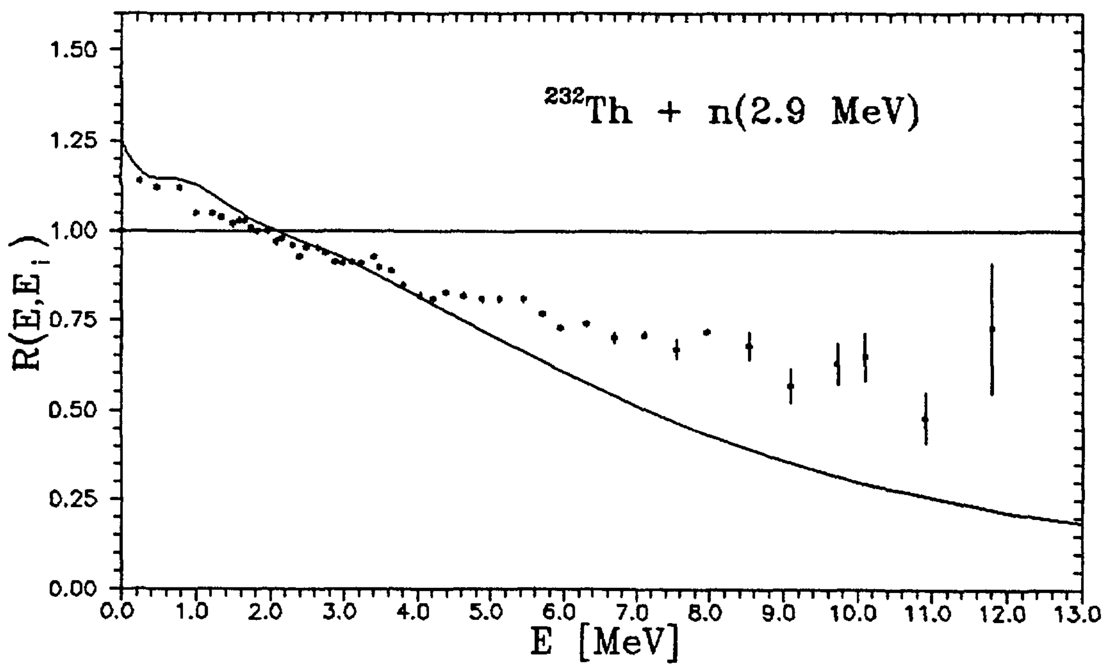

Fig. 6 As for Fig. 2 (experimental data - /17/)

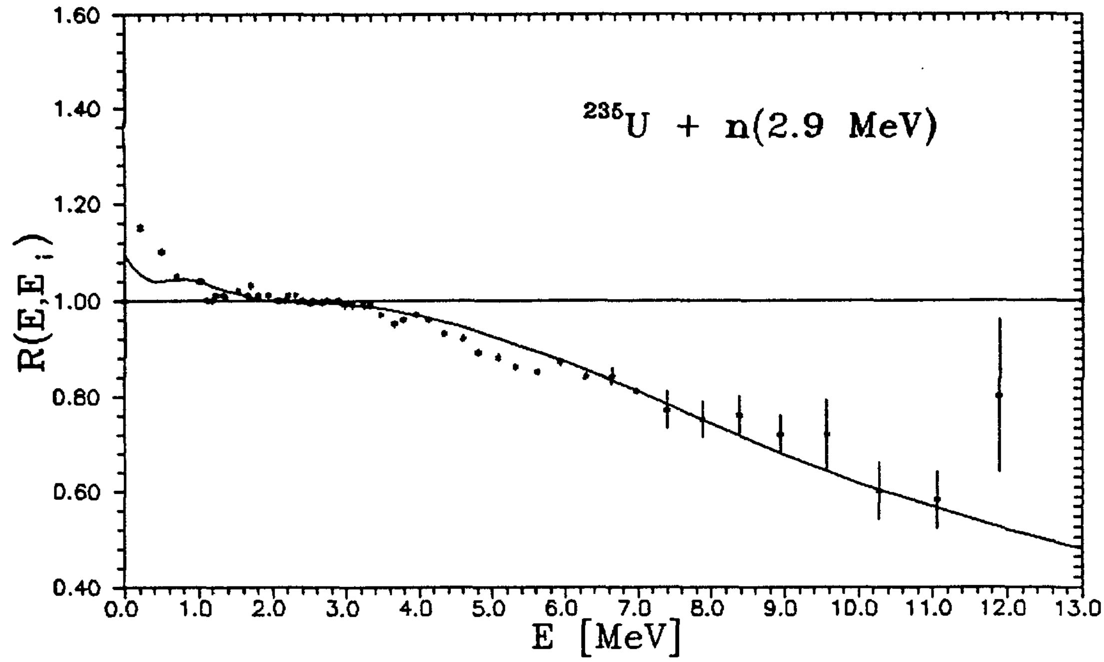

Fig. 7 As for Fig. 2 (experimental data - /17/)

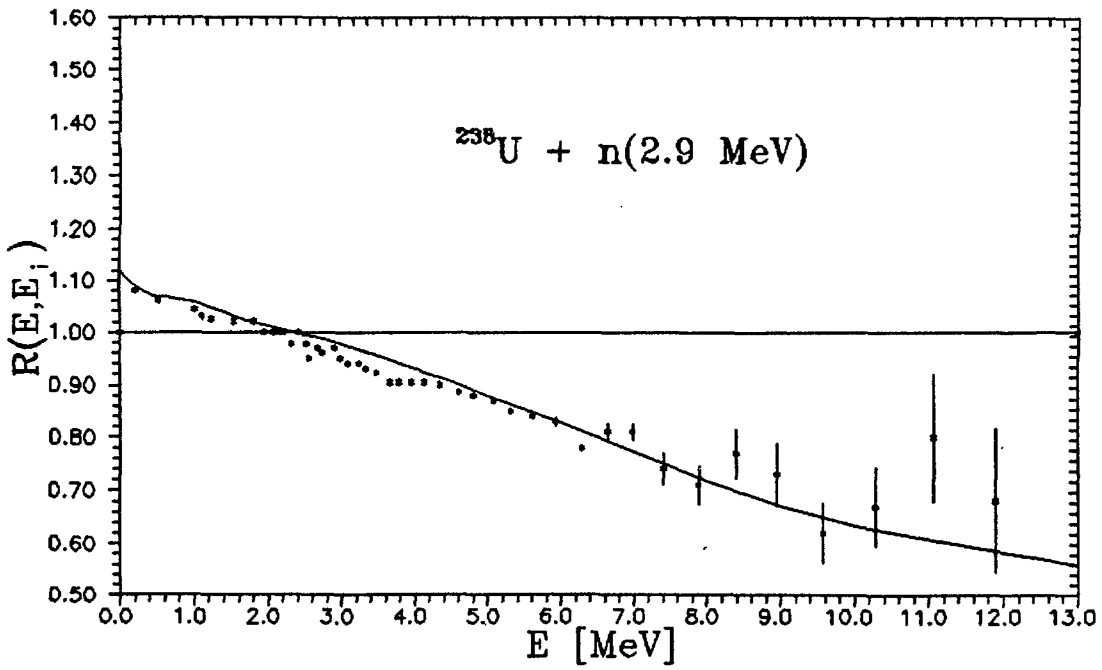

Fig. 8 As for Fig. 2 (experimental data - /17/)

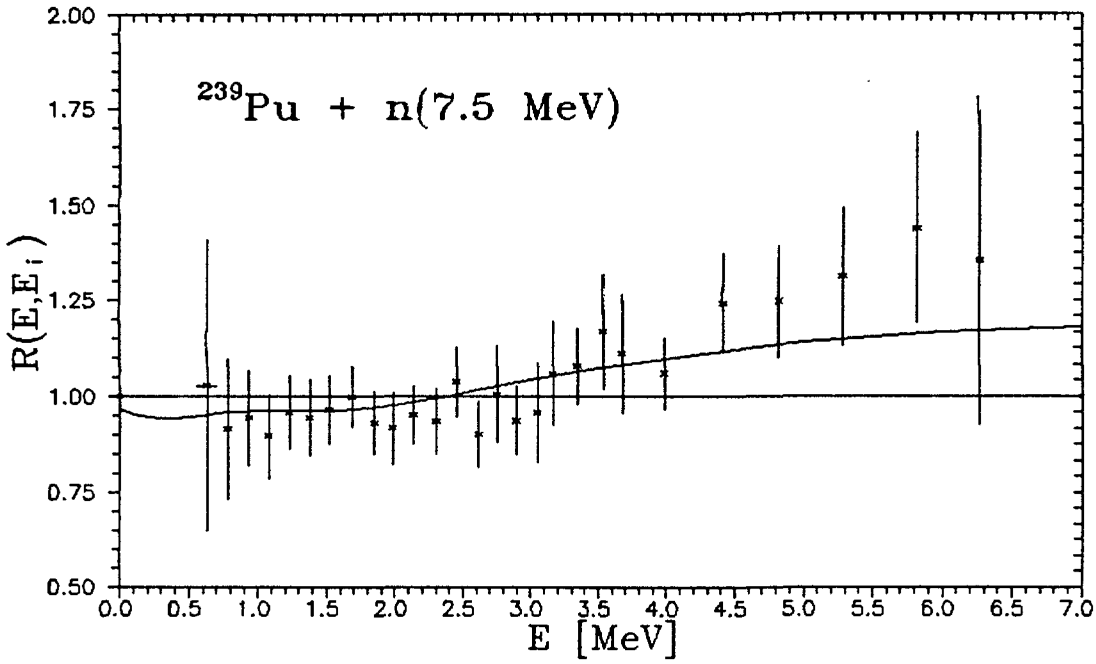

Fig. 9   As for Fig. 2 (experimental data - /18/)

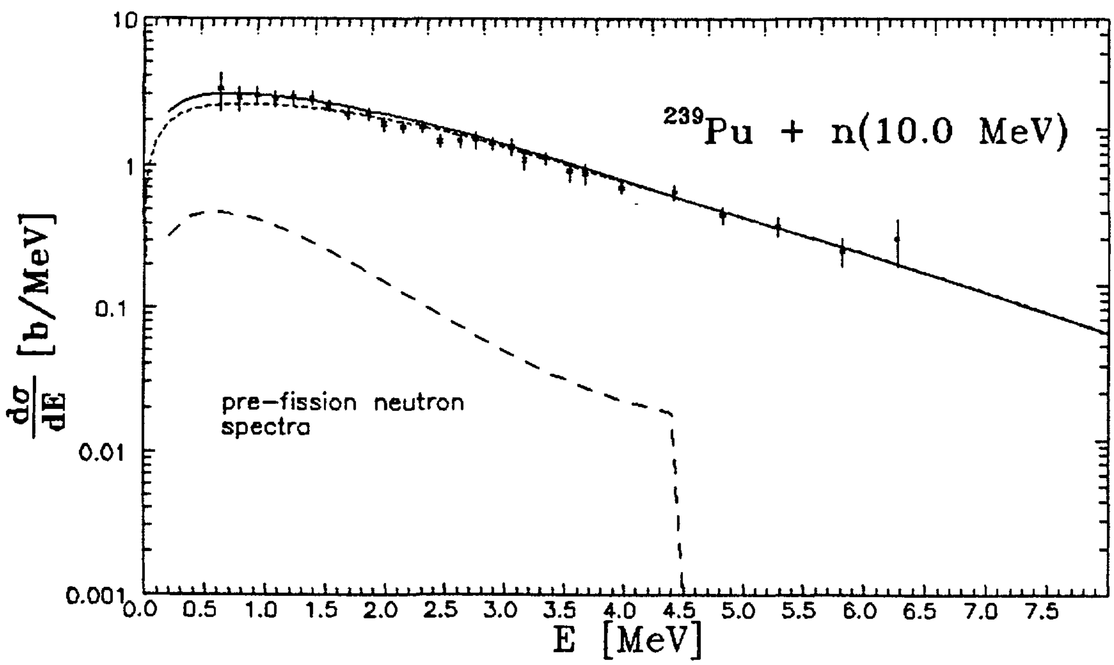

Fig. 10   Emission cross section of fission neutrons for the reaction specified (experimental data - /18/)

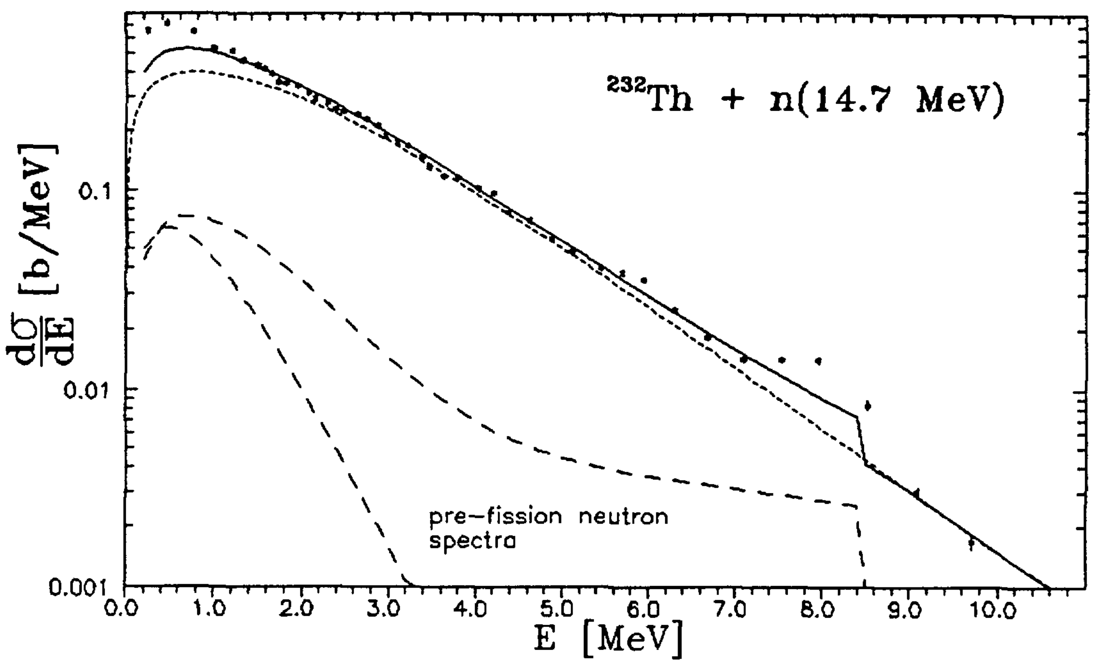

Fig. 11 As for Fig. 10 (experimental data - /17/)

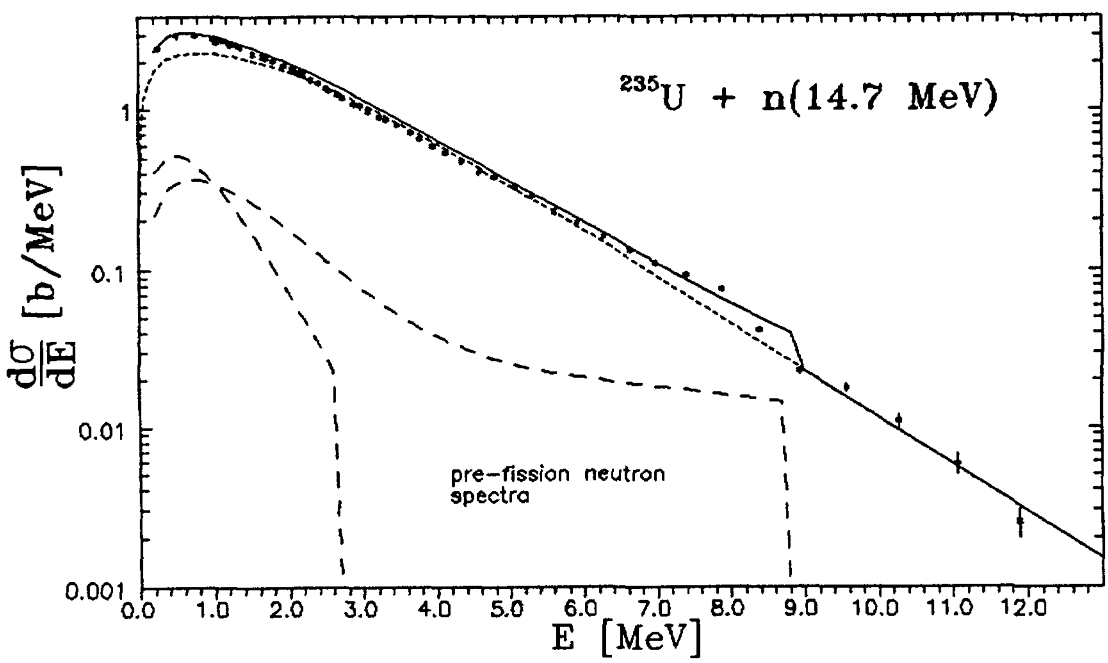

Fig. 12 As for Fig. 10 (experimental data - /17/)

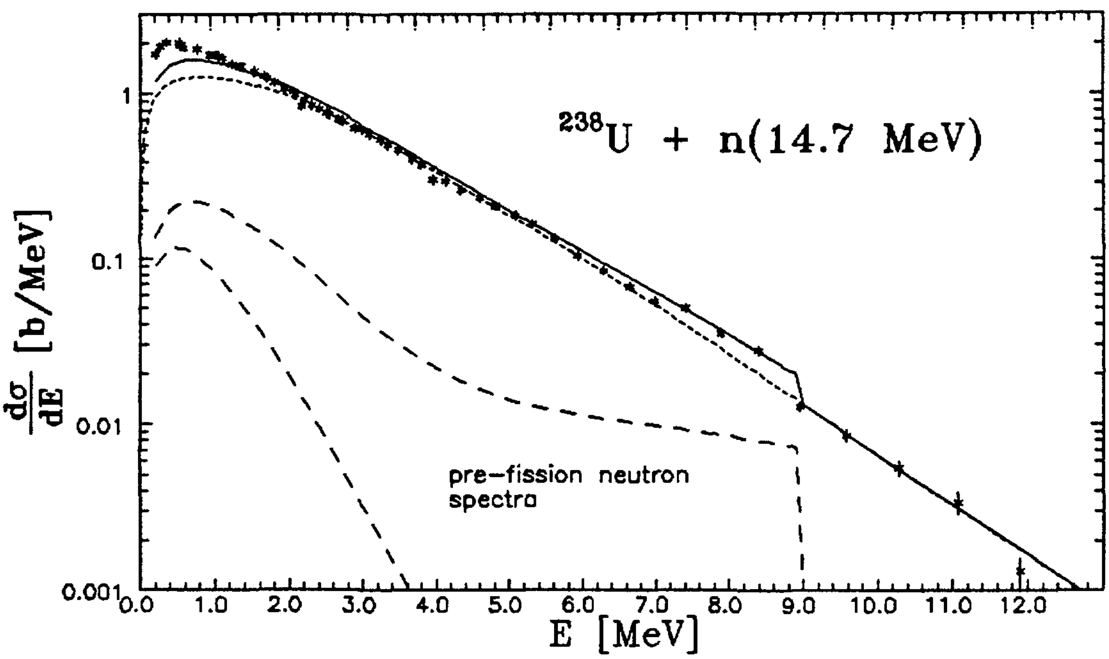

Fig. 13 As for Fig. 10 (experimental data - /17/)

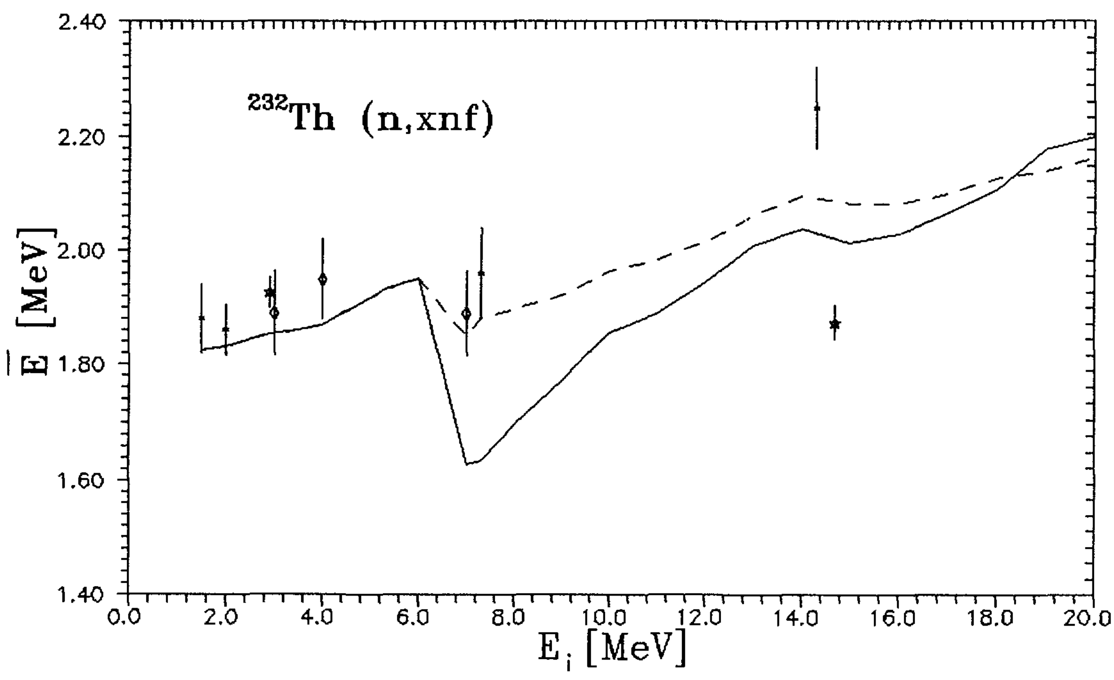

Fig. 14 Average emission energy of fission neutrons as function of neutron incidence energy for the fission reaction specified. Experimental data were taken from references listed in CINDA and from /15-18/. Calculational results are represented for pure post-fission neutrons (dashed line) as well for all fission neutrons (pre-fission and post-fission neutrons - solid line).

The Figs. 10-13 show the spectra of pre-fission neutrons explicitly. As known from nuclear reaction studies, equilibrium, pre-equilibrium as well as direct processes are the mechanisms of their emission /4,13/.

Besides $\bar{\nu}$, the average emission energy $\bar{E}$ is an essential parameter characterizing fission neutron emission. Since the calculations are performed for the full energy region, it can be obtained by direct averaging:

$$\bar{E} = \int_0^\infty dE\ E\ N(E) \tag{10}$$

In contrast to this theoretical treatment, experimental fission neutron spectra are commonly fitted to either a Maxwellian or a Watt distribution yielding $\bar{E}$ from the spectrum parameters. However, the values deduced depend on the energy range covered in the experiment. Therefore, a direct comparison between experimental and theoretical spectra is inevitable. Experimental $\bar{E}$ data are systematically to high (slow) if the low-energy (high-energy) range is preferentially covered in the experiment. This is a consequence of the typical spectral shape of fission neutron spectra /5,10/. The influence of the experimental energy range is much more crucial in the case of multiple-chance fission reactions, e.g. just above the chance thresholds, where the spectrum of the pre-fission neutrons is limited to low energy (cf. Figs. 14-18). At E_i < 6 MeV, $\bar{E} = f(E_i)$ is a (approximately) linearly increasing function. At E_i > 6 MeV, $\bar{E}$ is drastically reduced due to the influence of the pre-fission neutrons yielding a step-like behaviour of $\bar{E} = f(E_i)$. Average emission energies of fission neutrons were analyzed on the basis of the present calculations. The Figs. 14-18 represent calculational results in comparison with experimental data (cf. CINDA, /15-18/). For comparison, the $\bar{E}$ values for pure post-fission neutrons at E_i > 6 MeV are included.

4. AVERAGE EMISSION ENERGY VERSUS AVERAGE NUMBER OF NEUTRONS

The average number of neutrons is a direct measure of the total excitation energy of the fragments. As higher $\bar{E}^*_{tot}$ as higher $\bar{\nu}$ and, consequently, as higher $\bar{E}$. The correlation function $\bar{E}$ =

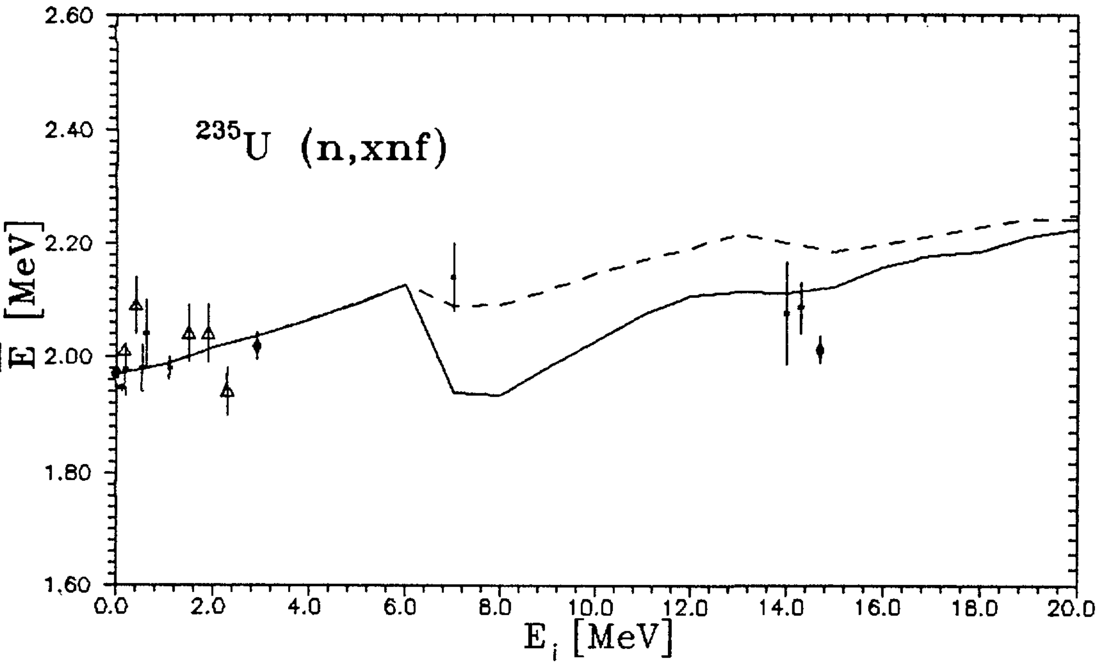

Fig. 15 As for Fig. 14.

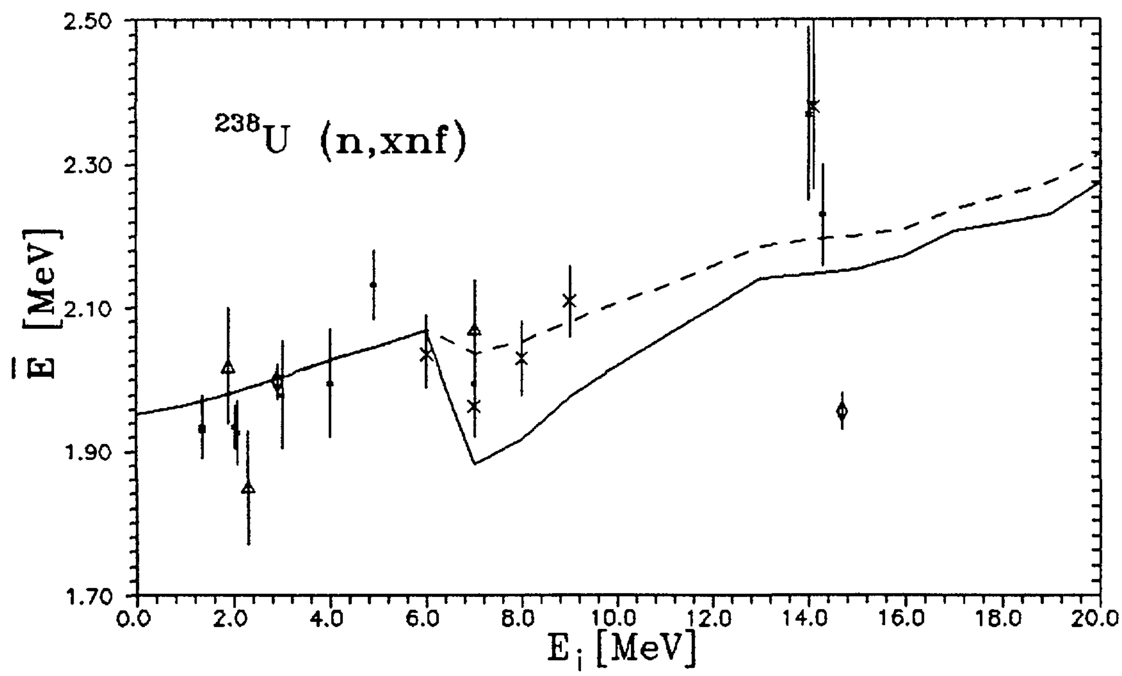

Fig. 16 As for Fig. 14.

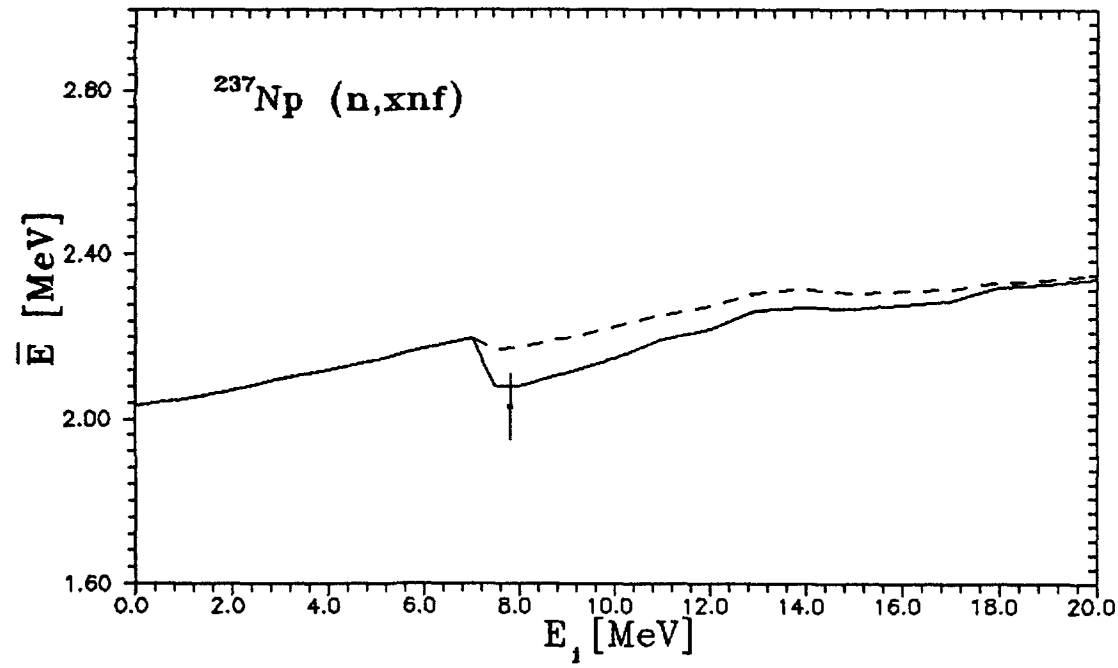

Fig. 17 As for Fig. 14

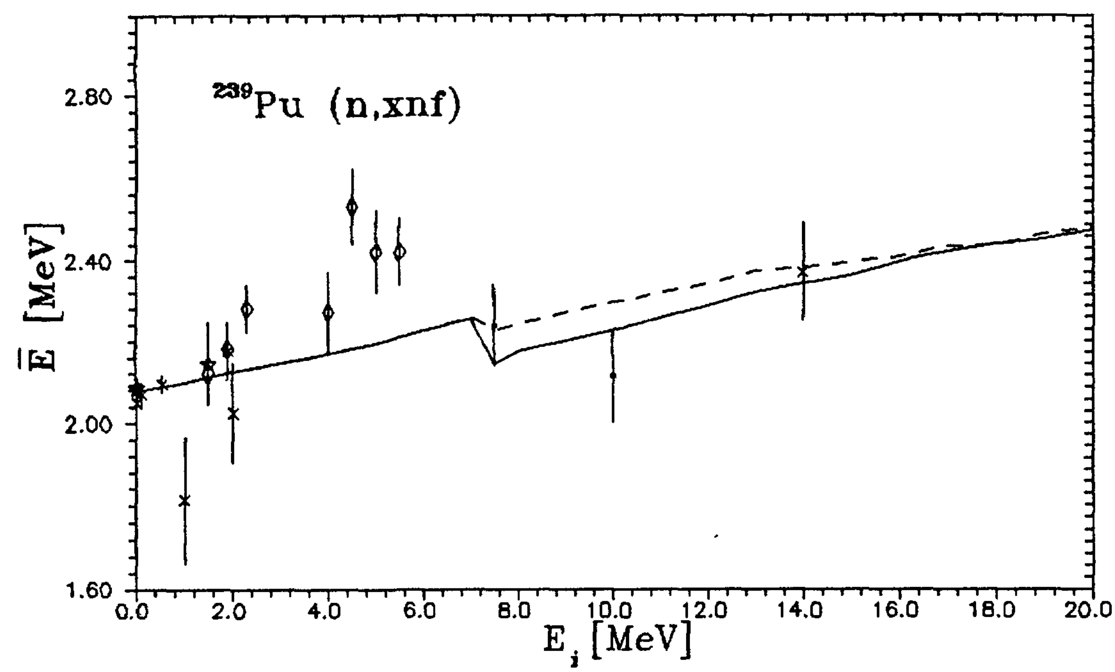

Fig. 18 As for Fig. 14

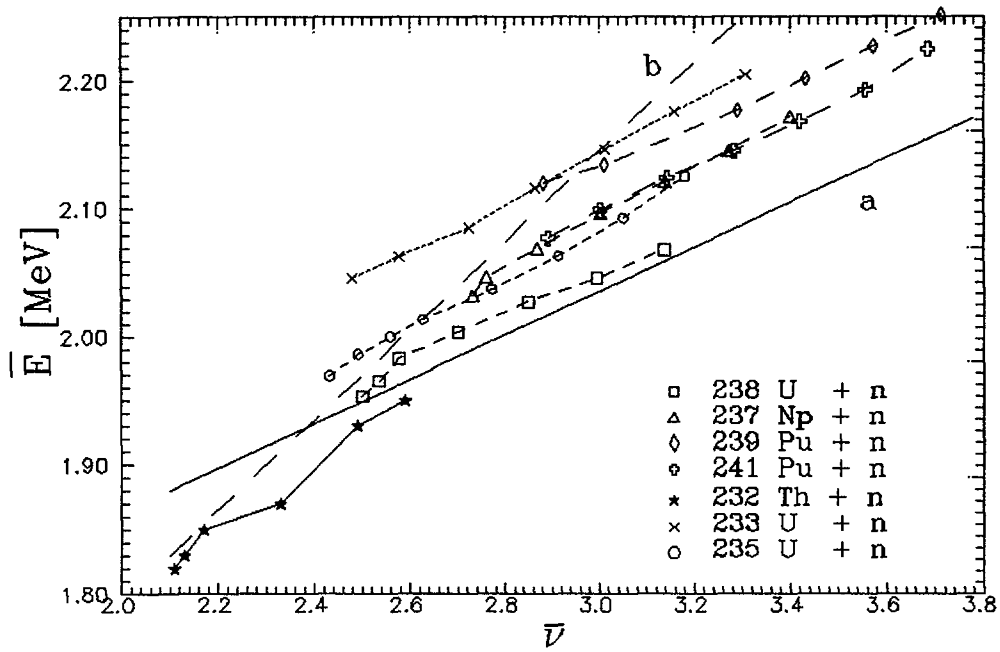

Fig. 19 The $\bar{E}(\bar{\nu})$ correlation: Calculational results for various fission reactions as specified [a - Eq. (11), b - Eq. (12)]

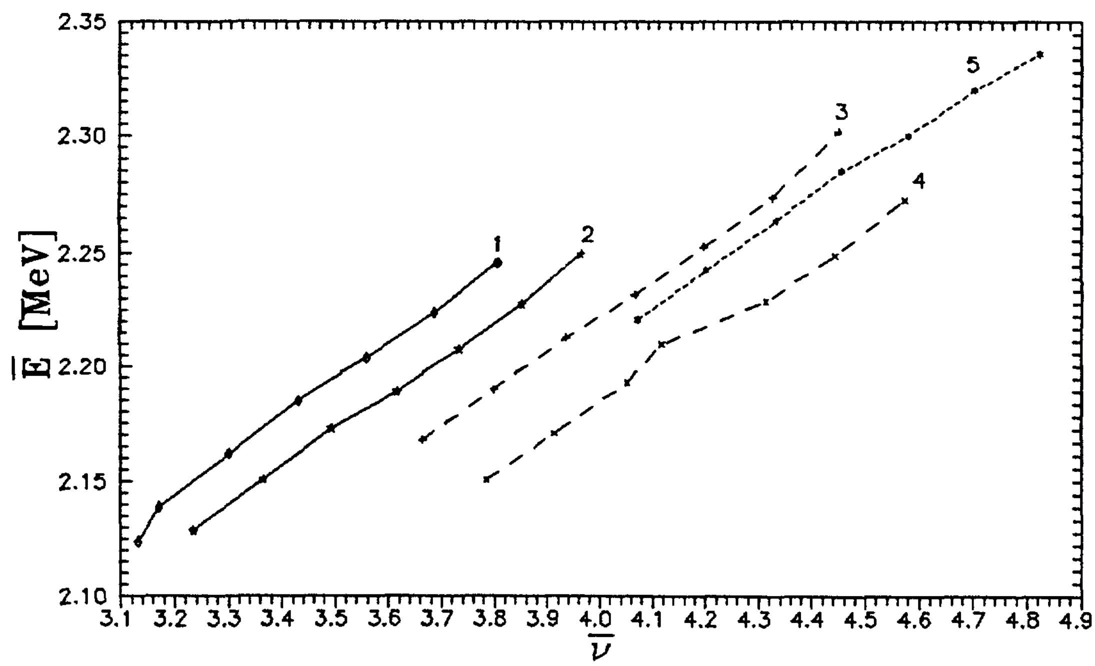

1– ^{241}Am, 2– ^{242}Am, 3– ^{245}Cm, 4– ^{247}Cm, 5– ^{249}Cf

Fig. 20 The $\bar{E}(\bar{\nu})$ correlation: Calculational results for various fission reactions as specified

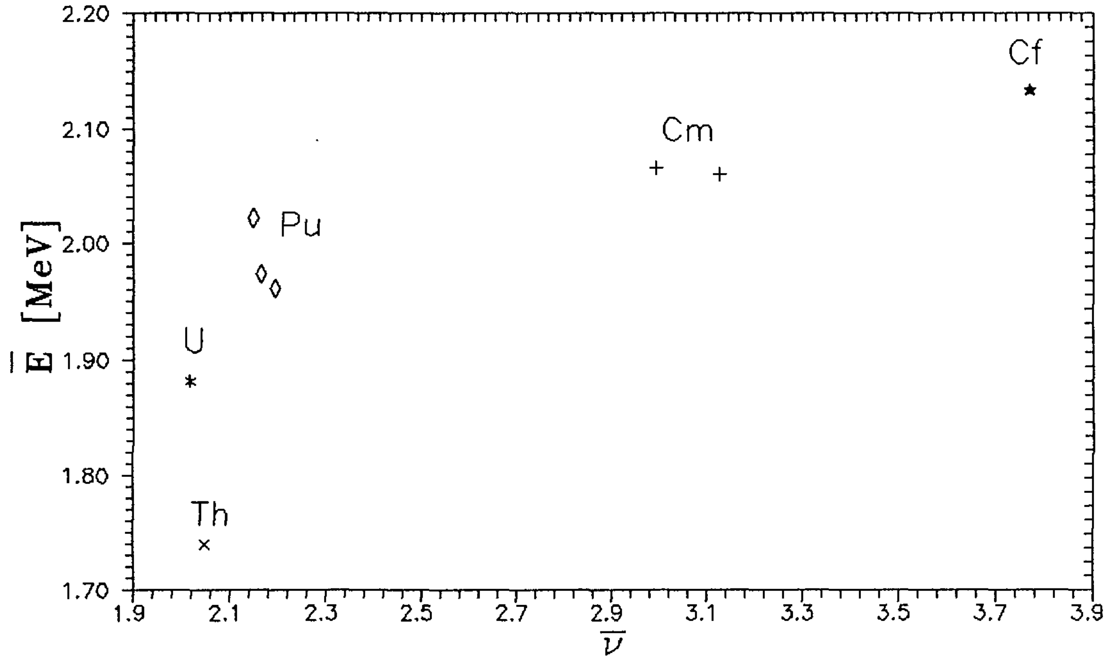

Fig. 21 The $\bar{E}(\bar{\nu})$ correlation for spontaneous fission of various nuclei as specified (present calculations)

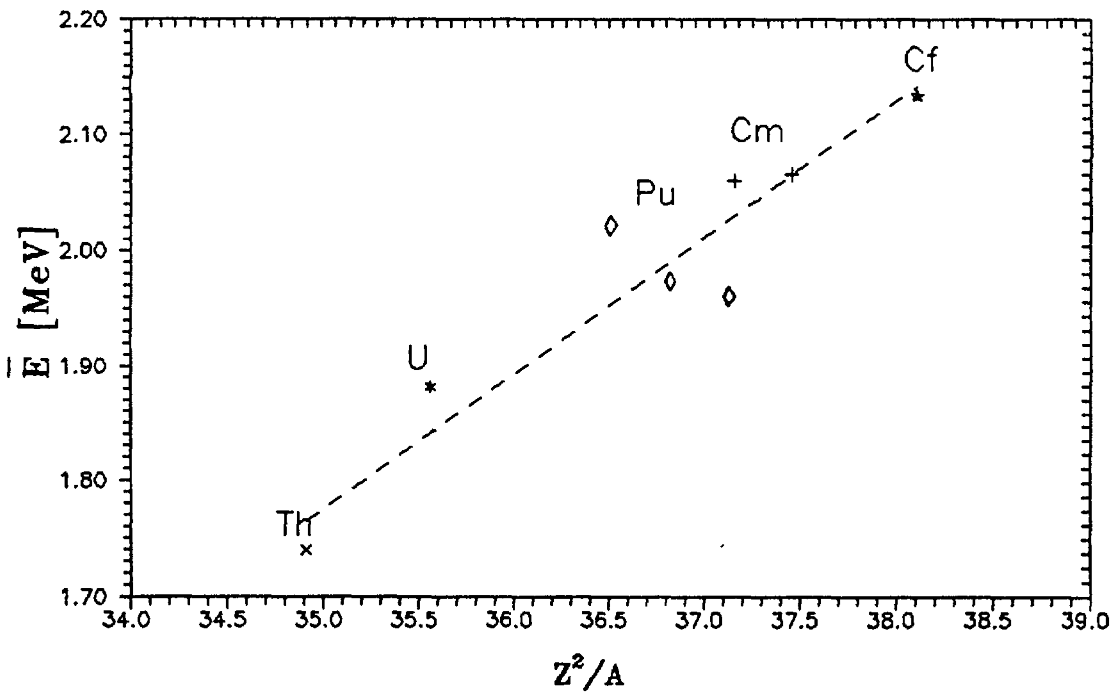

Fig. 22 The $\bar{E}(Z^2/A)$ correlation for spontaneous fission of various nuclei specified (present calculations)

$f(\bar{\nu})$, which is of essential importance in the field of fission neutron data, was postulated as an universal function by Terrell /19/,

$$\bar{E} = 0.74 + 0.645\ (\bar{\nu} + 1)^{1/2}, \qquad (11)$$

and later modified by Knitter et al. /20/,

$$\bar{E} = 0.74 + 0.35\ (\bar{\nu} + 1). \qquad (12)$$

However, the present systematic calculations do not confirm the above relations. As firstly discussed in Ref. /21/, the $\bar{E}(\bar{\nu})$ relation is different for the (n,f)-reactions studied. The Figs. 19 and 20 show calculational results for various reactions. The following parameterization, which reproduces the calculational results within (1-2) % accuracy, includes the dependence on the fissility parameter $x = Z^2/A$:

$$\bar{E} = (0.0698\ x - 0.8825) + (0.641 - 0.0133\ x)\ \bar{\nu} \qquad (13)$$

(valid for (n,f)-reactions). Spontaneous fission neutron data do not follow this relation (Fig. 21), but can be well reproduced by

$$\bar{E} = 0.1181\ x - 2.35907, \qquad (14)$$

i.e. their is no explicit dependence on $\bar{\nu}$ (cf. Fig. 22).

It is emphasized that the fission neutron data at $E_i > 6$ MeV cannot be parameterized in a simplifying manner. Here, the spectral shape as well as $\bar{E}(\bar{\nu})$ relation are strongly influenced by pre-fission neutron emission. New evaluations of neutron data for actinide nuclei should account for this fact adequately, i.e. inclusion of post-fission and pre-fission neutron data in complex form.

5. GROUP CONSTANTS

Finally, we present a comparison of calculated group constants

$$N^g(E_1^g, E_2^g) = \int_{E_1^g}^{E_2^g} N(E)\ dE \qquad (15)$$

for thermal-neutron induced fission of ^{233}U, ^{235}U, and ^{239}Pu with

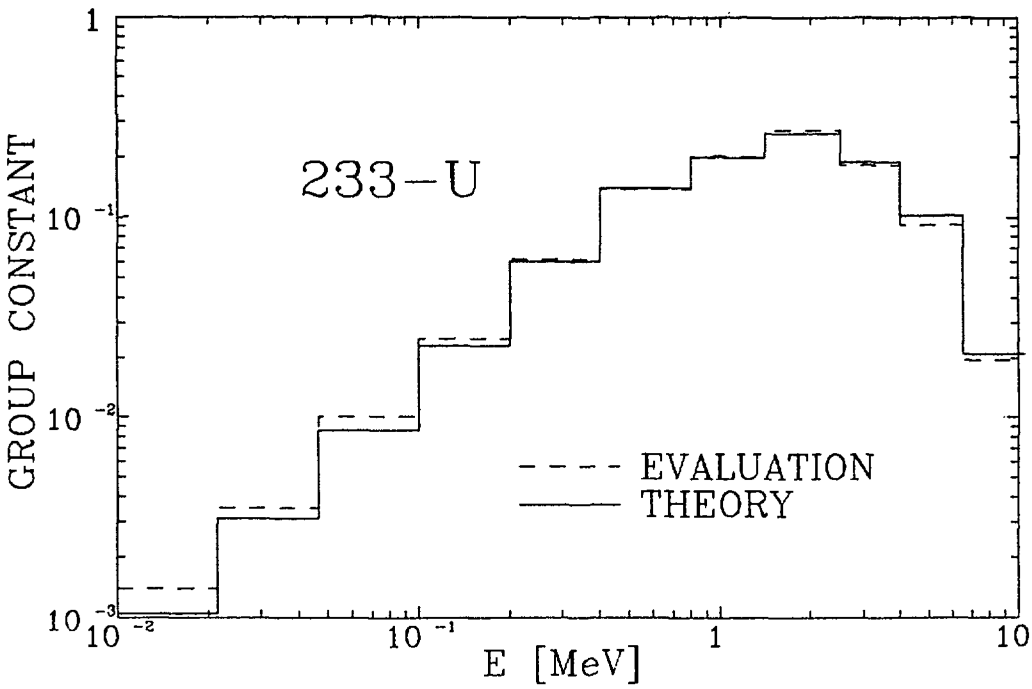

Fig. 23 Calculated group data (Eq. 15) in comparison with an evaluation /22/

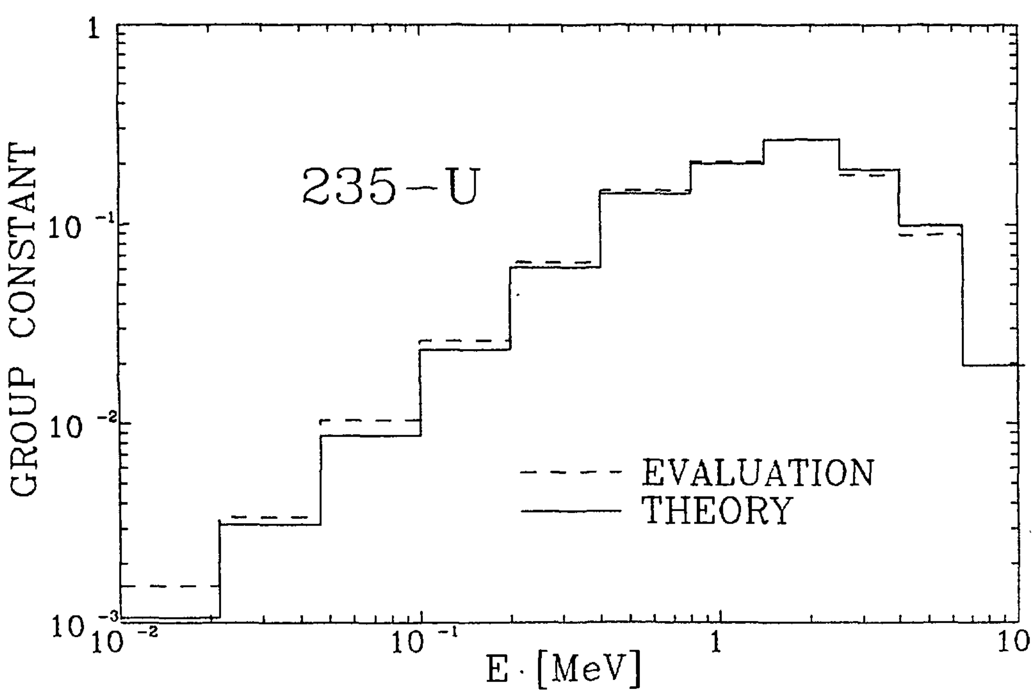

Fig. 24 Calculated group data (Eq. 15) in comparison with an evaluation /22/

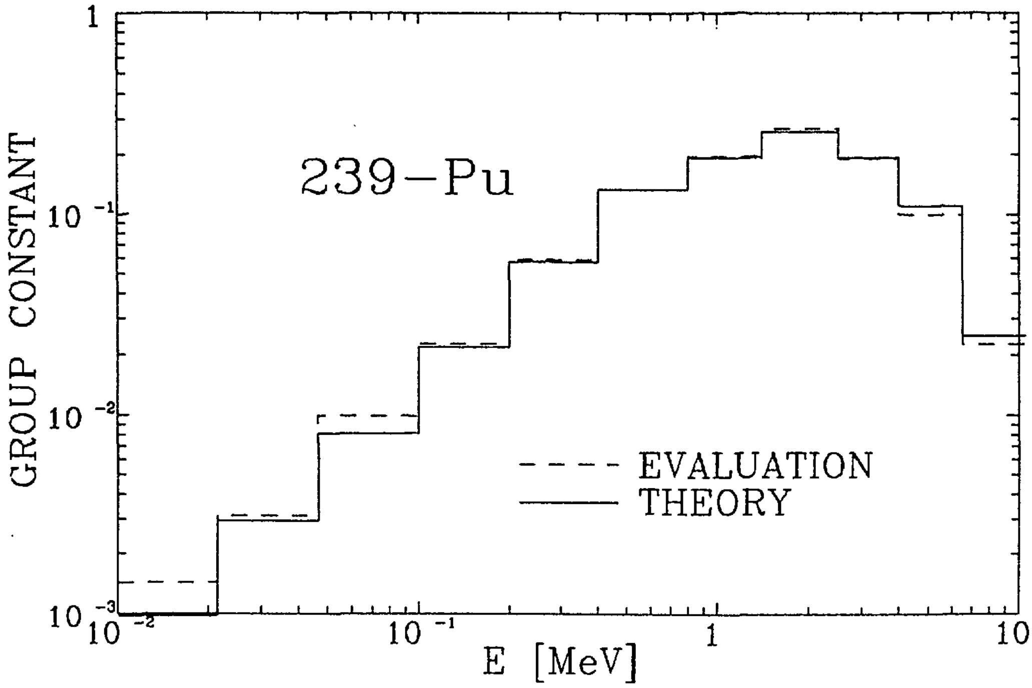

Fig. 25 Calculated group data (Eq. 15) in comparison with an evaluation /22/

an evaluation /22/. The FINESSE results obtained on the basis of the scission point model calculations reproduce the evaluated data (again without any parameter fit!). The group data are represented in the Figs. 23-25. The calculations performed for ^{233}U, ^{235}U, and ^{239}Pu fission induced by thermal neutrons yielded the following $\bar{E}$ values: 2.047, 1.969, and 2.078 MeV, respectively (cf. /22/: 2.015 $\pm$ 0.015, 1.970 $\pm$ 0.015, 2.087 $\pm$ 0.015 MeV, respectively)

6. SUMMARY

The present work shows the predictive power of recent nuclear model approaches to fission neutron emission. All calculations were performed in the framework of a model complex which has successfully been tested in the case of well-investigated fission reactions. The calculations are consistent in regard of energy conservation. As already described in /7/, the scission point model reproduces average TKE data as function of E_i for major actinides. Exact consideration of energy conservation means that the total excitation energy of the fragments is fixed correctly. The scission point model describes the partition of $\bar{E}^*_{tot}$ on both complementary fragments including the temperature dependence of shell effects so that the E^* data for individual fragments are quite reliable. Note that the solution of the energy partition problem is given as function of mass asymmetry. Accordingly, the evaporation model approach (temperature distribution model) includes the full dependence of fission neutron observables on fragment mass number.

A further point is that the calculations of neutron multiplicity as function of E_i are in good agreement with experimental/evaluated data /7/. This indicates again the reliable description of the energetic conditions in nuclear fission.

All calculations performed reproduce recent experimental fission neutron spectra without parameter fit.

Based on the calculations a new systematics of average fission neutron energies in correlation with the average number of fission neutrons was presented. It includes the dependence on fissility parameter $x = Z^2/A$. In the case of spontaneous fission, $\bar{E}$ data are best reproduced if considering only the dependence on x, i.e. without a further correlation with $\bar{\nu}$.

REFERENCES

/ 1/ Proc. IAEA Consultants' Meeting on the U-235 Fast-Neutron Fission Cross-Section, and the Cf-252 Fission Neutron Spectrum, Smolenice, 28 March - 1 April, 1983, ed. by H.D. Lemmel and D.E. Cullen (IAEA, Vienna, 1983) INDC(NDS-146/L

/ 2/ Proc. IAEA Advisory Group Meeting on Properties of Neutron Sources, Leningrad, 9-13 June, 1986 (IAEA, Vienna, 1987) IAEA-TECDOC-410

/ 3/ Proc. IAEA Consultants' Meeting on Physics of Neutron Emission in Fission, Mito City, 24-27 May, 1988, ed. by H.D. Lemmel (IAEA, Vienna, 1989) INDC(NDS)-220

/ 4/ H. Märten, these proceedings and references therein

/ 5/ D.G. Madland and J.R. Nix, Nucl. Sci. Eng. 81 (1982) 213

/ 6/ D.G. Madland et al., loc. cit. (3), p. 259

/ 7/ A. Ruben et al., Z. Phys. A338 (1991) 67, and these proceedings

/ 8/ S. Nagy et al., Nucl. Sci. Eng. 88 (1984) 154

/ 9/ U. Brosa et al., Z. Naturforschung 41a (1986) 1341

/10/ H. Märten et al., Proc. Int. Conf. on 50 Years with Nuclear Fission, 25-28 April, 1989, Gaithersburg, ed. by J.W. Behrens and A.D. Carlson (American Nuclear Society, 1989) Vol. II, p. 743

/11/ M. Uhl and B. Strohmaier, Report IRK-76/01, IRK Vienna (1976) and Program Manual for STAPRE code, NEA Data Bank (1981)

/12/ H. Kalka et al., Z. Phys. A329 (1988) 331

/13/ D. Polster, Proc. Int. Conf. on Nucl. Phys., Gaussig, 12-16 Nov, 1990, in print, and D. Polster and H. Kalka, submitted to Z. Phys. A

/14/ W. Mannhart, Handbook of Nuclear Activation Data, Technical Report Ser.273 (IAEA, Vienna, 1987) 163
/15/ W. Yufeng et al., Chin. J. of Nucl. Phys. 11 (1989) 47
/16/ G.N. Lovchikova et al., Proc. Int. Conf. on 50th Anniversary of Nuclear Fission, Leningrad, 1989, in print
/17/ G.S. Boykov et al., ibid.
/18/ I. Düring, Diploma Thesis, TU Dresden, 1990, and to be published
/19/ J. Terrell, Proc. IAEA Symp. on Physics and Chemistry of Fission, Salzburg, 1965 (IAEA, Vienna, 1965) Vol. II, p. 3
/20/ H.H. Knitter et al., Proc. IAEA Consultants' Meeting on Prompt Fission Neutron Spectra, Vienna, 1971 (IAEA, Vienna, 1972) 41
/21/ H. Märten et al., Proc. Int. Conf. on Nuclear Data for Science and Technology, Mito, 1988, ed. by S. Igarasi (JAERI, Saikon Publ. Co., Ltd. (1988) 683
/22/ B.I. Starostov et al., Yad. Const. 3 (1985) 16 (identical to INDC(CCR)-252/G)

Neutron emission during acceleration of ^{252}Cf fission fragments

O.I.Batenkov, M.V.Blinov, A.B.Blinov, S.N.Smirnov
V.G.Khlopin Radium Institute, Leningrad, USSR

Abstract

We investigate neutron emission during acceleration of fission fragments in the process of spontaneous fission of ^{252}Cf. Experimental angular and energy distributions of neutrons are compared with the results of calculations of neutron evaporation during fragment acceleration.

The probability of the neutron emission during fission fragment acceleration is determined by the correlation of the time of neutron emission (t_n) and of the time of the fragment acceleration (t_a),. Eismont was the first who discussed this problem [1]. He found that this effect could be important espessially in the case of the fission of the highexcited nuclei. The role of the neutron emission during acceleration of the ^{252}Cf spontaneously fission was determined in the ref. [2-5]. In these works it was obtained, that even for spontaneous fission the effect investigated could be rather large. However theoretical predictions of the emission during fragment acceleration differ from each other by the value of the contribution of this process, both because of the simplification of the calculations and of the use of the different input parameters. At this time the experimental investigation of this effect is very interesting and valuable not only from point of view of the understanding of fission neutron emission mechanism, but also for determination of the life-time of the excited fission fragments.

In this work the search of neutron emission during fragment acceleration at ^{252}Cf spontaneous fission was carried out by comparison of experimental neutron angular and energy distributions [6,7] with the results of the calculations.

Experimental set-up and method of measurements of neutron energies and fragments characteristics were described in the ref. [6,7]. Fragment energies were determined by use of the semiconducter detectors, and their velocities- by fragment detectors on the base of the microchannel plates (MCP). The construction of detecting system allowed to carry on the measurements simulteneously both in narrow solid angle and in the angle 2π This gave a possibility to measure the eff#ciency of the neutron detector constanly in the course of the experiment.

The results of the angular distribution measurements of neutrons of various energies [6,7] showed that the deviations from standard model of neutron evaporation from fully accelerated fragments (MNEFAF) were observed for neutrons of low energies in the region of the low angles, and for neutrons of medium and high energies in the region of the big angles (near 90). In fig.1 the deviations from MNEFAF are .hown for various masses and total kinetic energies (energy region above 0.7 MeV).

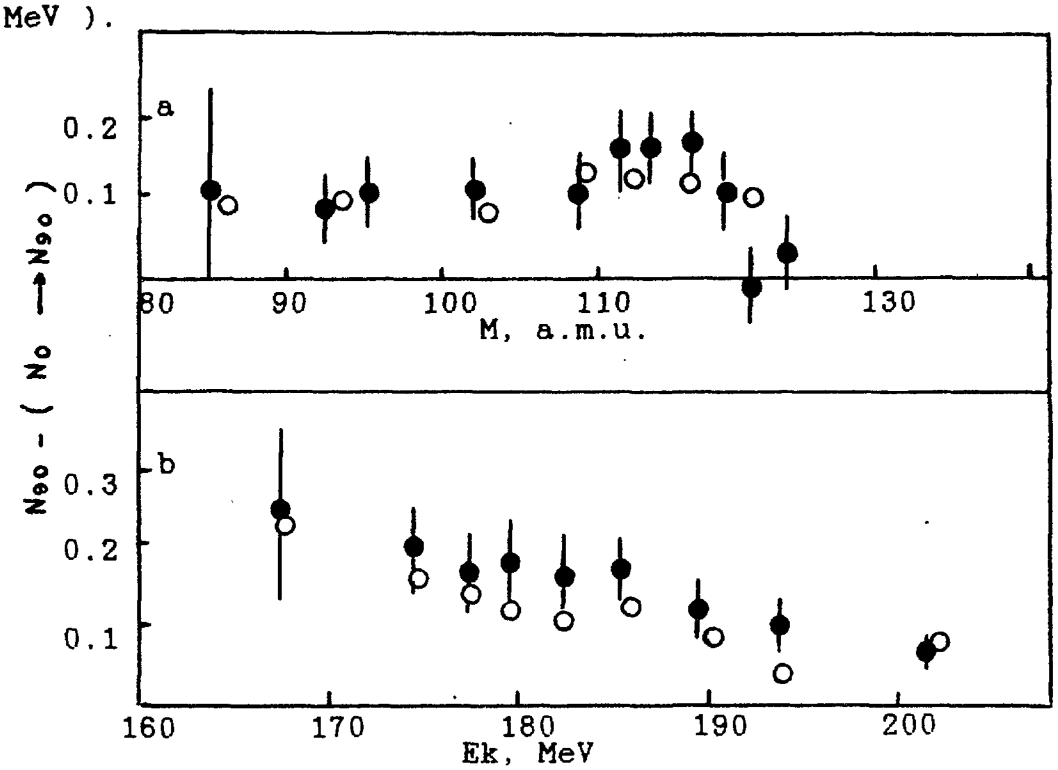

FIG.1 The difference of neutron number at the angle 90° in dependence on mass (a) and total kinetic energy (Ek) (b)

● - directy measured one at the angle 90 (N_{90}) and calculated from the data for the angle 0° ($N_0 \rightarrow N_{90}^{\#}$) without taking into account of the neutron emission during fragment acceleration.

O - calculated from the data for the angle 0 ($N_0 \rightarrow N_{90}^{\gamma}$) with taking into account of the neutron emission during fragment acceleration and without this effect.

For clearing up the reason of the deviation of the data from standard model MNEFAF, we carried out the calculations of neutron evaporation during fragment acceleration. The calculation was made supposing that the time of dissipation of collective fragment energy (t_d) essentially less than the acceleration time $t_d << t_a$. Experimental evidence for that was given in the work [6].

We considered the acceleration of the two rigid spherial fragments in mutual Coulomb fields. In fig. 2 the dependence of fragment velocity on acceleration time after scission point is shown.

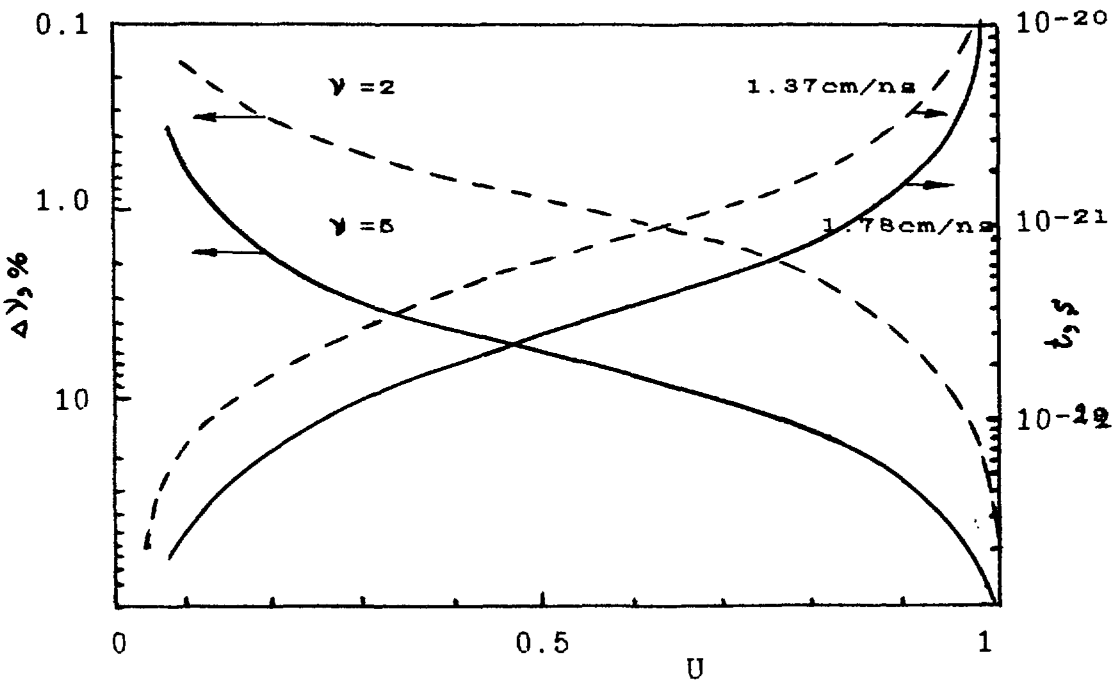

FIG.2 The dependence of fragment velocity $U=(V/V_\infty)$ on the acceleration time t.
The share of neutrons ($\Delta\nu$), emitted during the time t.

At the calculation of the number of emitted neutrons the exponential decay of excited fragments, continuous character of the emission, characteristics of the neutron cascade were taken into account. We used experimental values of fragment temperatures. As these values are averaged over the cascades, so on their base the temperatures on various stages of the cascade were calculated. The parameters of level density were determined in accordance to the results of the ref.[8]. In fig.2 the results of the statistical calculations of the contribution of neutrons, evaporated during acceleration process for the cases of emission of two and five neutrons from fragment are shown.

From fig.2 it is seen, that though this effect is not large, but it is necessary to take it into account at the analysis of the experimental data. In fig.3 the ratio of the average number of neutrons (for fragment mass M = 110 a.m.u.), directly measured at the angle 90° to calculated one from the experimental data for angle 0° (N_0 --> N_{90})is presented. In this figure it the ratio the neutron numbers (N_{90} and N_0 --> N_{90}), calculated with taking into account of the neutron emission during acceleration (for the same mass of fragment) and without it is shown. The neutron number was determined only for energy range 0.7-10 MeV for excluding of low-energy component. From fig.3 it is seen, that in the fragment exitation energy region, corresponding to the emission from one up to three neutrons, the anisotropy of neutrons N_0/N_{90} equals the calculation results with taking in account of the neutron emission during acceleration.

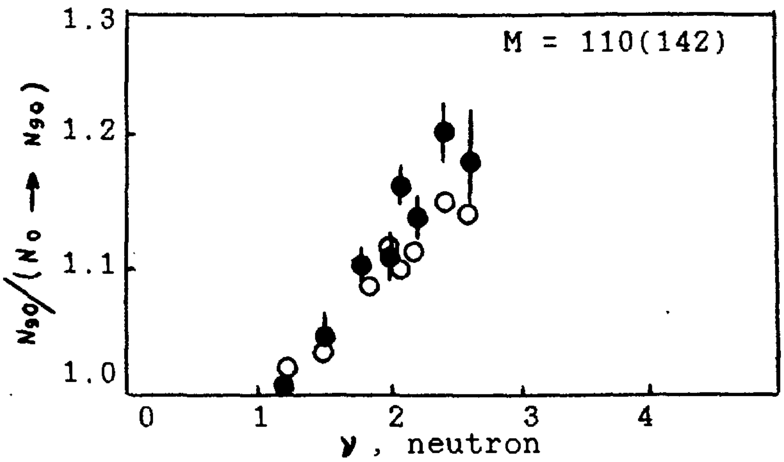

FIG.3 The ratio of the number of neutrons (energy range 0.7-10 MeV) in the l.s. for M=110 (142) a.m.u.

● - measured at the angle 90° to that calculated from the data at $\varphi=0°$ without taking into account of the neutron emission during fragment acceleration.

○ - calculated from the data at $\varphi= 0°$ with taking into account of the emission during acceleration process to the one calculated from $\varphi=0°$ without this effect.

The data, given in fig.1, for neutrons emitted by fragments of various mass and total kinetic energies show the deviation (in average 2%) from the neutron emission from the fully accelerated fragments. The calculations with the incorporation the emission during acceleration, as it is seen from fig.1, agree with the experimental data both by the absolute values and by the character of the dependence on M and Ek. Consequently at the taking into account of the effect considered the various experimental angular and energy dependences for ^{252}Cf spontaneous fission can be explained. It is quite possible the deviations, connected with low-energy component are determined by nonequilibrium emission of neutrons at the time close to scission moment.

References

1. V.P.Eismont "Atomic energy", 1965,vol.19, N.2, p.113-116,(in Rus).
2. G.A.Pik-Pichak "Nuclear physics", 1969,vol.10, N.2, p.321-327,(in Rus).
3. K.Skarsvag "Physica Scripta", 1973, vol.7, p.160-164.
4. H.Marten, D.Seeliger "J.Physics G: Nucl. phys." vol.14, 1988, P.211.
5. R.L.Walsh, G.Chircu "Physics of neutron emission in fission", (Proc. of the Intern. Conf., Mito, Japan, 1988).
6. O.I.Batenkov et. al. "Atomic energy" vol.64, N.6, 1988, p.429-433 (in Rus).
7. O.I.Batenkov et.al. "Nuclear Data for Science and Technology" (Proc. of the Intern. Conf., Mito, Japan, 1988) p. 771.
8. A.B.Ignatyuk et.al. "Nuclear physics" vol.21, N.3, p.485-490.(in Rus).

New Data on Prefission Neutrons

G.S.Boikov[1], V.D.Dmitriev[1], G.A.Kudyaev[2], Yu.B.Ostapenko[2], M.I.Svirin[2], G.N.Smirenkin[2]

[1]V.G.Khlopin's Radium Institute, Leningrad, USSR

[2]Institute of Physiks and Power Engineering, Obninsk, USSR

Abstract

The spectra of neutrons emitted in fission of ^{232}Th, ^{235}U and ^{238}U induced by 2.9- and 14.7- MeV neutrons (below and above the chance fission threshold, respectively) were measured by the time-of-flight method. Two effects were observed in the prefission neutron spectra: the high-energy wing is related to the nonequilibrium mechanism of emission up to the well pronounced upper boundary of ε_{max}=8.5 MeV; in the lower - energy wing ε < 2 MeV, neutron yield exceeds conventional statistical model description. The latter effect was attributed to the fission process dynamics.

1.Introduction

Neutron emission and fission are the dominating types of decay of excited heavy nuclei. As the excitation energy increases neutron emission becames multiple and fission becomes possible after one or more neutrons were emitted, i.e. the first - or greater chance fission occurs. The increase of incident energy is also accompanied by an enhancement of contribution from nonequilibrium emission mechanism,which draws a spectrum towards higher energies. The studies of energy distributions of neutrons emitted in the corse of 14.7 MeV neutron-induced fission of ^{235}U /1/ have shown,seemingly for the first time, that along with the conventional equilibrium (evaporative) component, the spectrum of prefission neutrons from the (n,nf) and (n,2nf) reactions includes a nonequlibrium component, and one can describe this spectrum within the statistical model assuming the mechanism of neutron emission to be universal for (n,xnf) reactions. This paper reports similar measurements on ^{232}Th and ^{238}U. These investigations have yielded quite unexpected results, not so clearly obvious from the previous studies of ^{235}U /1/.

2. Experiment.

Experiment were performed on the neutron beam from a neutron generator at incident energies of 2.9 and 14.7 MeV. The time-of-flight (TOF) method was used for measurements of energy distributions of neutrons coinciding with the fragments from fission of ^{232}Th and ^{238}U. The TOF spectrometer of 205 cm base was located at an angle of 90° with respect to the beam direction. The measurements covered 0.2 to 12 MeV neutron energy interval. The reference spectrum of the prompt neutrons from the spontaneous fission of ^{252}Cf, $N_{Cf}(\varepsilon)$ was recorded simultaneosly with the spectrum under investigation, $N(\varepsilon, E_n)$.

The TOF spectrometer consisted of a fission fragment detector, a neutron detector protected from the background neutrons, and electronics for running and preliminary processing of experimental information. The fission fragments were detected with the four-sectional multilayer ionization chamber located at the distance of 15 cm from the incindent neutron source. The pulse from each section was fed to a separate time pick-off unit. Three sections consisted of twelve bilateral targets of 10 cm diameter and 2mg cm^{-2} thickness at a total amount of isotope about 5 g. The fourth section consisted of two layers of 2 mg cm^{-2} thickness which were prepared of a homogeneous mixture of isotope under investigation and a small quantity of ^{252}Cf. The count and amplitude characteristics of all the sections were tested for identity by concurrent measurement of a fission fragment spectrum. The recorded spectra coincided within uncertainties of 5%. Each section provided the time resolution of 1.5 ns.

Neutrons were detected by the monocrystal stilbene scintillator of 10 cm diam and 4 cm thickness, which was connected to a photomultiplier with a light conduit.The n-γ separation circuit was used in order to protect from the γ-quantum background. The absolute efficiency of the neutron detector was estimated using the neutron spectrum from the ^{252}Cf spontaneous fission, which is known within uncertainties of 3% /2/ over the energy interval of interest.The TOF spectrometer provided the time resolution of 2.5 ns. The experimental apparatus and methods are discussed in greater detail in the previous paper /1/.

3.Results.

Characteristics of the prompt neutrons from the ^{252}Cf spontaneous fission,spectrum $N_{Cf}(\varepsilon)$ and yeild $\bar{\nu}_{Cf}$, are commonly regarded in a rank of standards /2/. Making use of them one can deduce from the measured coincidence spectra $n(\varepsilon,E_n)$ and $n_{Cf}(\varepsilon)$ the energy dependence of neutron detection efficiency

$$\frac{\eta(\varepsilon)}{\bar{\eta}} = \frac{1}{N_{Cf}(\varepsilon)} \frac{n_{Cf}(\varepsilon)}{\int n_{Cf}(\varepsilon)d\varepsilon} , \quad \bar{\eta}=\int\eta(\varepsilon)N_{Cf}(\varepsilon)d\varepsilon , \qquad (1)$$

neutron spectra tmemselves (in normalized form)

$$N(\varepsilon,E_n) = \frac{\bar{\eta}}{\eta(\varepsilon)} \frac{n(\varepsilon,E_n)}{\int n(\varepsilon,E_n)d\varepsilon} , \qquad (2)$$

integral and differential neutron yields

$$\bar{\nu}(E_n) = \bar{\nu}_{Cf} \frac{\int n(\varepsilon, E_n) d\varepsilon}{\int n_{Cf}(\varepsilon) d\varepsilon} , \qquad (3)$$

$$\frac{d\bar{\nu}(\varepsilon, E_n)}{d\varepsilon} = \bar{\nu}(E_n) \; N(\varepsilon, E_n) \qquad (4)$$

The results obtained are listed in table 1.

Figure 1 shows the spectra ratios

$$R(\varepsilon, E_n) = \frac{N(\varepsilon, E_n)}{N_{Cf}(\varepsilon)} = \frac{d\bar{\nu}(\varepsilon, E_n)/d\varepsilon}{\bar{\nu}(E_n) \; N_{Cf}(\varepsilon)} , \qquad (5)$$

normalized to 1. Universal shape of the prompt heutron spectra explains similarity of the $R(\varepsilon, E_n)$ energy dependences for "pure" (n,f) reaction at E_n=2.9 MeV. The dashed lines represent approximations in the Maxwellian form /3/

$$N(\varepsilon)=2(\varepsilon/\pi T^3)^{1/2}\exp(-\varepsilon/T) \qquad (6)$$

where temperatures T are as listed in table 1 and T_{Cf}=1.42 MeV /2/. These approximations are almost the stright lines with slopes given by the difference T_{Cf}-T.

In the case of E_n=14.7 MeV the ratios $R(\varepsilon, E_n)$ all are also very similar but to each other quite different from those in fig.1a. The difference is due to the prefission neutron contribution in the (n,nf) and (n,2nf) reactions at E_n=14.7 MeV. An increase at ε < 2 MeV and the maximum at 8 MeV are related to the evaporated neutrons and nonequilibrium component of prefission neutrons, respectively. The right-hand slope of the maximum corresponds to the cut-off in the nonequilibrium spectra due to the first-chance fission threshold. Thus, the prompt neutron spectrum is "pure" only at ε > 9 MeV where the neutron yield substantially falls, whereas at lower energies it apreciably affected by prefission neutrons. Neutrons of evaporation

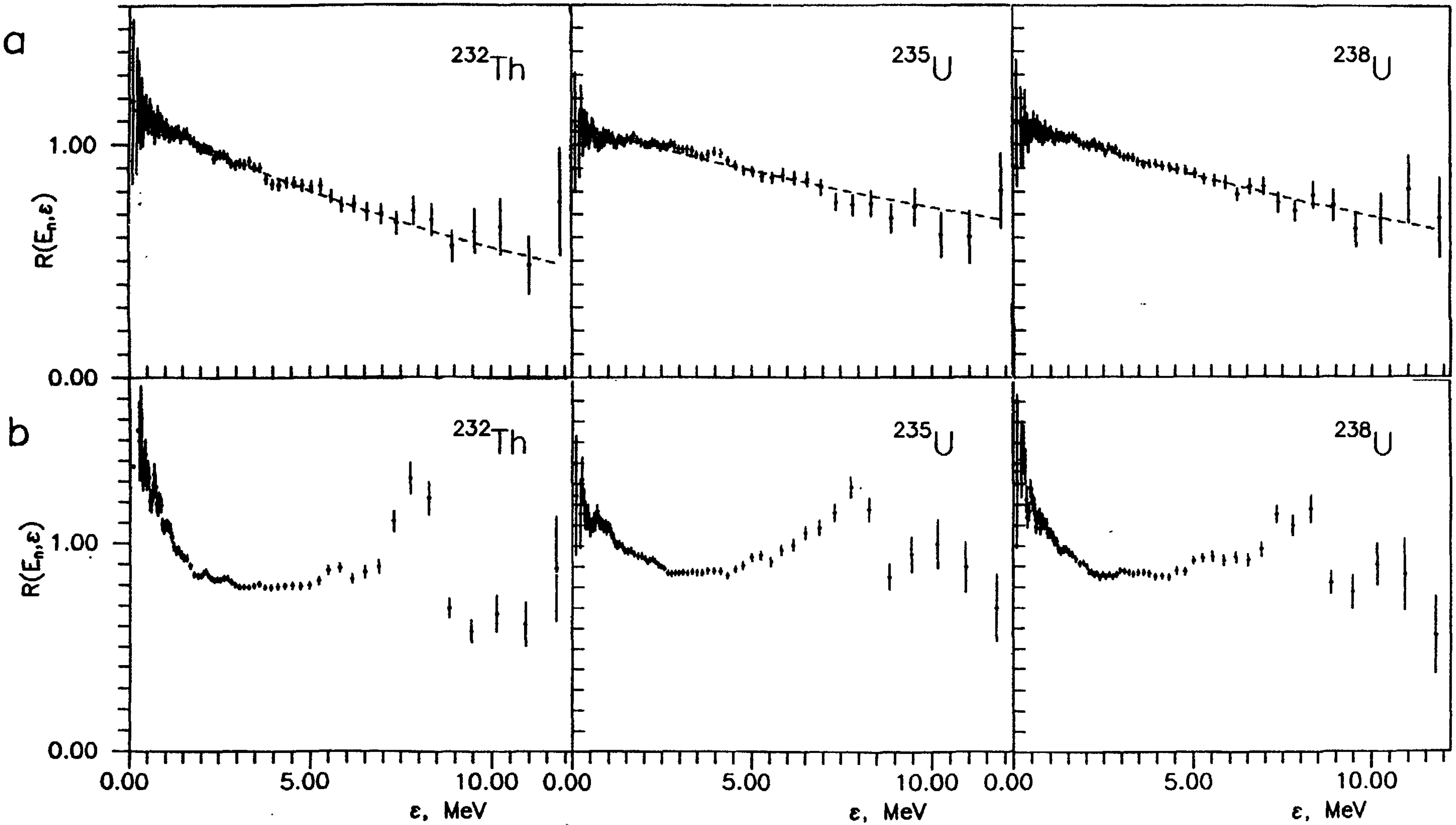

Fig.1. Ratios of spectra $R(\varepsilon,E_n)$ for ^{232}Th, ^{235}U, ^{238}U versus energy ε for E_n=2.9 MeV (a) and E_n=14.7 MeV (b). Points - present experiment, dashed lines - calculation for E_n-2.9 MeV.

Table 1.

Experimental results.

Target-nuclei	E_n, Mev	$\bar{\varepsilon}$, MeV	T, MeV	$\bar{\nu}$
^{232}Th	2.9	1.928 ± 0.027	1.285 ± 0.018	2.27 ± 0.06
	14.7	1.874 ± 0.030	———	3.92 ± 0.09
^{235}U	2.9	2.016 ± 0.023	1.344 ± 0.015	2.77 ± 0.07
	14.7	2.011 ± 0.023	———	4.39 ± 0.11
^{238}U	2.9	1.998 ± 0.024	1.332 ± 0.016	2.71 ± 0.07
	14.7	1.957 ± 0.026	———	4.25 ± 0.10

draw spectrum towards lower energies and nonequilibrium neutrons produce opposite effect, but the former influence is much stronger. This is confirmed by table 1, where one can see close values of average spectrum energy for both cases of E_n energies, in spite of substantially higher neutron yield $\bar{\nu}(E_n)$ at E_n=14.7 MeV.

Within the overlapping region $\varepsilon \lesssim 5$ MeV our results reasonably agree with the earlier $N(\varepsilon,E_n)$ measurements on the same nuclei at E_n=14.3 MeV /4/. These data were fairly well approximated with a superposition of the Watt distribution for prompt neutrons (resembles (6)) and Weisscopf distribution for prefission neutrons. Measurements within a broader ε interval /5/ have shown that since this approximation ignored the nonequilibrium contribution over $5 < \varepsilon < 9$ MeV interval, it distorted the real $T(E_n)$ dependence and thus was invalid. In the case of chance fission one should employ more complicated calculations of $N(\varepsilon,E_n)$ rather than conventional empirical approaches in order to take into account the contributions from various (n,xnf) reactions, that is from first- and greater chance fission, $\sigma_{fx}(E_n)$, into the total fission cross section

$$\sigma_f(E_n) = \sum_{x=0}^{x_{max}} \sigma_{fx}(E_n) \qquad (7)$$

and various mechanisms of neutron emission as well.

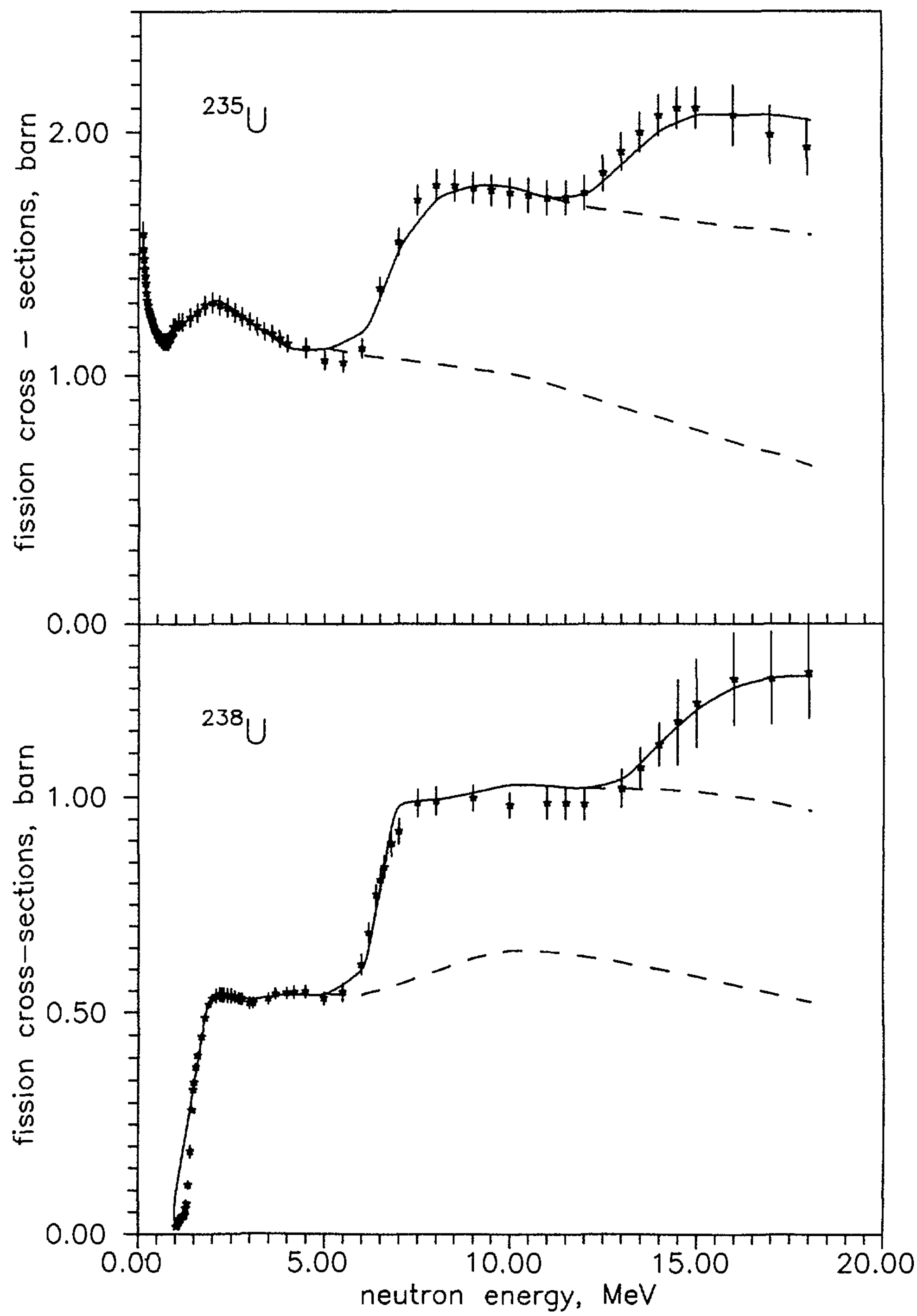

Fig.2. Fission cross-sections versus incindent neutron energy for target-nuclei ^{235}U and ^{238}U. Points - standart values /2/, full lines - σ_f calculation, dashed lines - σ_{fx} calculation.

4.Analysis of fission neutron spectra of ^{235}U and ^{238}U.

Figure 2 shows the fission cross sections as taken from /2/. The curves represent calculations of $\sigma_f(E_n)$ and contributions from first- and second-chance fission for target nuclei $^{235,238}U$. Description of cross sections included such components as:

i) the code STAPRE (the Hauser-Feshbach model) /6/ with neutron transmission coefficients from /7/ and the exciton-model description of nonequilibrium emission /8/, both tested in calculations of (n,xn) and (n,xnf)-reaction /9/;

ii) single-particle spectra calculations and quasi-particle level density and potential energy as a function of nuclear deformation based on them (in regards of /10/);

iii) the adiabatic description of collective enhancement of level density /11,12/.

The main fitting parameters were the heights of humps B and A of fission barrier, which we variated keeping in mind the systematics in /13/. In addition, small variations were allowed for parameters of the energy dependence of level density. We were seeking for approximation of cross- sections $\sigma_f=\sigma_{f0}+\sigma_{f1}+\sigma_{f2}$ for nuclei A (^{236,239}U) as well as $\sigma_{f0}+\sigma_{f1}$ for nuclei A-1 (^{235,238}U) and σ_{f0} for nuclei A-2 (^{234,237}U).

Figure 3a shows the observed neutron yields distributions $\frac{d\bar{\nu}}{d\varepsilon} = \bar{\nu}N(\varepsilon,E_n)$ for chance fission at E_n=14.7 MeV obtained with $N_{Cf}(\varepsilon)$ as in eq.(6) for T_{Cf} = 1.42 MeV. The curves represent the total distribution (V)

$$\frac{d\bar{\nu}}{d\varepsilon} = \frac{d\bar{\nu}_f}{d\varepsilon} + \frac{d\bar{\nu}_{pre}}{d\varepsilon} = C \sum_{x=0}^{2} \alpha_x \bar{\nu}_{fx} N(\varepsilon,T_x) + \sum_{i=I,II,III} \frac{d\bar{\nu}^i_{pre}}{d\varepsilon} \qquad (8)$$

and its components as well:

IV - the prompt neutron distribution, which is a superposition of three Maxwellians (6). Their weights $\alpha_x\bar{\nu}_{fx}= (\sigma_{fx}/\sigma_f)\bar{\nu}_{fx}$ were deduced from the calculated cross sections (fig.2) and systematics of $\bar{\nu}(E_n)$ /14/ and $T(E_n)$ /15/ (see /1/ for detail). Close to unity fitting parameter compensate inaccuracies of used semiempirical approach in description of $d\bar{\nu}_f/d\varepsilon$, particularly, the fact that this approach neglects the fission fragment angle anisotropy due to which the yield $\bar{\nu}_f$ gains a week angle dependence (within the error bars as seen from

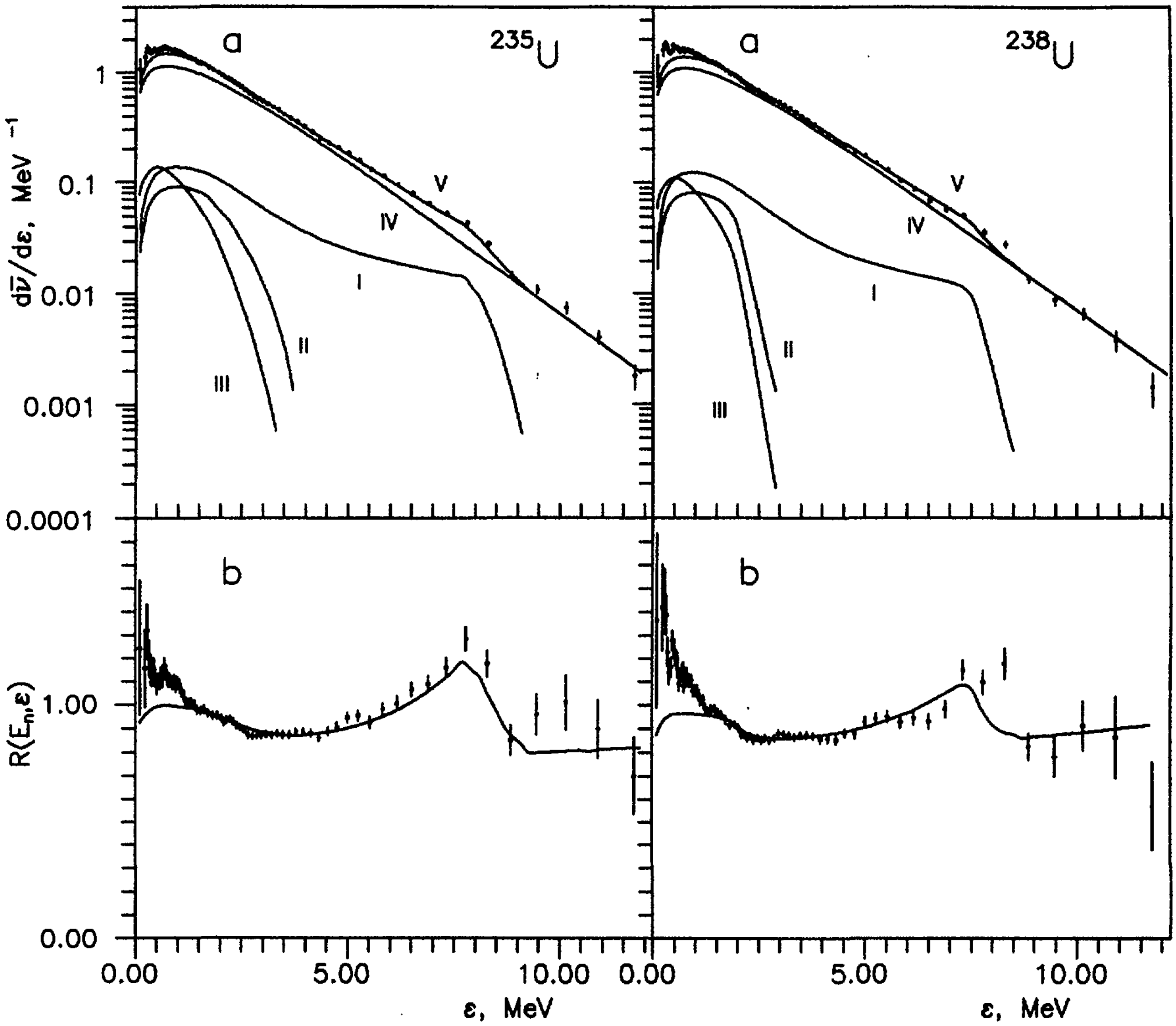

Fig.3. a) Neutron yield energy distributions $d\bar{\nu}/d\varepsilon = \bar{\nu}\ N(\varepsilon,E_n)$ for chance fission (E_n= 14.7 MeV) of target nuclei ^{235}U and ^{238}U. Points - present experiment. Lines - calculation results: V - total distribution, I-IV - its components (see text).

b) Energy distribution of ratios $R(\varepsilon,E_n)$ for E_n= 14.7 MeV for ^{235}U and ^{238}U. Points - present experiment, line - calculations results.

evaluations), and also anaccuracy of $\bar{\nu}_f(E_n)$ extrapolation for $E_n > 6$ Mev /14/.

I-III - the distributions of neutron yields

$$\frac{d\bar{\nu}^{I}_{pre}}{d\varepsilon} = \frac{\alpha_1}{\sigma_{n1}}\frac{d\sigma_{n1}}{d\varepsilon}\ ,\quad \frac{d\bar{\nu}^{II}_{pre}}{d\varepsilon} = \frac{\alpha_2}{\sigma_{n1}}\frac{d\sigma_{n1}}{d\varepsilon}\ ,\quad \frac{d\bar{\nu}^{III}_{pre}}{d\varepsilon} = \frac{\alpha_2}{\sigma_{n2}}\frac{d\sigma_{n2}}{d\varepsilon} \qquad (9)$$

for first neutron coincident with the fission act of nucleus A-1 (I),

Table 2.

Average neutron yields and its components.

Target-nuclei	$\bar{\nu}$	$\bar{\nu}_f$	$\bar{\nu}_{pre}$	$\delta\bar{\nu}_{pre}$
^{235}U	4.39 ± 0.11	3.35	0.80	0.24
^{238}U	4.25 ± 0.10	3.27	0.64	0.34

first neutron coincident with the fission act of nucleus A-2 (II), and second neutron coincident with the fission act of nucleus A-2 (III). Here $d\sigma_{n1}/d\varepsilon$ and $d\sigma_{n2}/d\varepsilon$ are the appropriate spectra parts of the first and second neutrons calculated with the code STAPRE in an assumption that the mechanism of nonequilibrium emission is only valid during the first stage of neutron cascade,

$$\sigma_{nj} = \int (d\sigma_{nj}/d\varepsilon)d\varepsilon \ , \quad j = 1,2 \tag{10}$$

Some important details of description is seen better in fig.3b which shows the experimental results as ratios $R(\varepsilon,E_n)$ and the curves on it are calculated as in (5) from distributions V with experimental values of $\bar{\nu}(E_n)$.

5.Discussion and conclusions.

The calculated curves repoduce fairly well the form of the observed spectra in the broad range of energies (ε > 2 MeV), thus indicating validity of considering ones to be of the nonequilibrium emission origin. However at lower energies ε < 2 MeV the curves are well below the data points, especially for ^{238}U. This disagreement was attempted to remove for ^{235}U /1/ but this appeared to be followed by a falure in approximation of first- and second-chance fission cross sections for ^{235}U and ^{234}U, respectively. This is impossible at all in the case of ^{238}U due to lesser cross section of the (n,2nf) reaction σ_{f2} which with regard to (9) and (10) affects the yield of prefission neutrons at the lowest energies.

Thus we may conclude that the model employed here falured to explain the low-energy wing of the prefission neutron spectra. The spectrum of "excessive" neutrons may be reasonably reproduced with the Weisscopf distribution at a temperature $\tau \cong 0.4$ MeV as in /4/. Integral characteristics of fission neutron multiplicities are listed in table 2. Here the total yield $\bar{\nu}$ are as taken from table 1 and the contributing components $\bar{\nu}_f$, $\bar{\nu}_{pre}$ and $\delta\bar{\nu}_{pre} = \bar{\nu} - \bar{\nu}_f - \bar{\nu}_{pre}$ are deduced from the calculated distributions shown in fig.3.

The situation we faced to is a typical one for similar studies on heavy ion projectiles at energies of several tens of MeV (e.g., see /15,16/) which were intensified in recent years. In this case $\bar{\nu}_{pre}$ increases as well as $\delta\bar{\nu}_{pre}$ which accesses a value of several units. However, qualitative result is the same, namely, inadequacy of the conventional statistical model which assumes the neutron emission to occur solely at the earliest stages of fission, that is at the first potential well. In reality, due to fission dynamics and viscosity of nuclear matter, neutron emission may occur through the whole duration of the process of nuclear deformation (see, e. g. /17/).

We consider the light-particle induced reaction to be appreciably helpful in investigations of the nuclear fission dynamics being performed at low energies inaccessible with the heavy-ion induced reaction. It should be noted in conclusion that the questions we faced have already arisen, e. g. in studies of fission neutron spectra from 10- to 20- MeV-proton-induced reactions /18/.

References.

1. Boikov G. et al.- Atomnaya Energiya,1990,v.1, to be published.
2. 1982 INDC/NEANDC Nuclear Standards File. Tech. Reports, 227, IAEA, Vienna,1983.
3. Terrell J. - Phys.Rev.,1959, v.113,p.527.

4. Vasilyev Yu.A. et al.-ZhETF,1960, v.38, p.671; in book : "Fizika deleniya atomnykh yader", M., Gosatomizdat, 1962, p.121.

5. Kornilov N.V. - Voprosy atomnoj nauki i tekhniki. Ser.:Yadernye konstanty, 1985, vyp.4, p.46.

6. Uhl M., Strohmier B. - Report IRK-76/01, Vienna, 1976, Addenda, 1978.

7. Lagrange Ch. - Report INDC(FR)-56/L (NEANDC-228-L), 1982.

8. Blann M. - Phys.Rev.Lett., 1970,v.21, p.1357; v.22, p.337; Ann. Rev. Nucl. Sci., 1975, v.25, p.1231.

9. Ignatyuk A.V. et al. - Yad Fiz., 1988, v.47, p.355.

10. Pashkevich V.V. - Nucl. Phys.A, 1971, v.169, p.275; Intern. School-Seminar on Heavy Ion Physics, Alushta, 1983; Dubna, 1983, p.405.

11. Bjornholm S., Bohr A., Mottelson B.R. - Phys. and Chem. of Fission (Proc. Simp., Rochester, 1973), Vienna: IAEA, 1974, v.1, p.361.

12. Kudyaev G.A. et al. - Yad Fiz., 1987, v.45, p.1534.

13. Bjornholm S., Lynn J.E. -Rev.Mod.Phys., 1980, v.52, p.725.

14. Howerton R.J. - Nucl.Sci. Eng., 1977, v.62, p.438.

15. Gavron A., Gayer A., Boissevain J. et. al. - Phys.Rev., 1987, v.C35, p.579.

16. Hinde D.J., Charity R.J., Foote G.S. et.al.-Nucl.Phys., 1986, v.A452, p.550

17. Gregoire C. et.al. - Z.Phys.A., 1988, v.329, p.497.

18. Bishop C.J., Halpern I., Shaw R.W., Jr., Vandenbosch R. Nucl.Phys., 1972, v.A198, p.161.

THEORETICAL DESCRIPTIONS OF NEUTRON EMISSION IN FISSION

David G. Madland
Theoretical Division, Los Alamos National Laboratory
Los Alamos, New Mexico 87545, USA

ABSTRACT

Brief descriptions are given of the observables in neutron emission in fission together with early theoretical representations of two of these observables, namely, the prompt fission neutron spectrum N(E) and the average prompt neutron multiplicity $\bar{\nu}_p$. This is followed by summaries, together with examples, of modern approaches to the calculation of these two quantities. Here, emphasis is placed upon the predictability and accuracy of the new approaches. In particular, the dependencies of N(E) and $\bar{\nu}_p$ upon the fissioning nucleus and its excitation energy are discussed. Then, recent work in multiple-chance fission and other recent work involving new measurements are presented and discussed. Following this, some properties of fission fragments are mentioned that must be better known and better understood in order to calculate N(E) and $\bar{\nu}_p$ with higher accuracy than is currently possible. In conclusion, some measurements are recommended for the purpose of benchmarking *simultaneous* calculations of neutron emission *and* gamma emission in fission.

I. INTRODUCTION AND EARLY REPRESENTATIONS

Neutron emission in fission can be described in terms of several experimental observables. These include the following:

- neutron emission times during the fission process (in principle),
- the energy spectrum of prompt fission neutrons N(E), where E is the laboratory energy of the emitted neutron and "prompt" refers to neutron emission prior to the onset of fission-fragment β-decay processes,
- the average number (multiplicity) of prompt neutrons emitted per fission $\bar{\nu}_p$,
- the various components of N(E) and $\bar{\nu}_p$ for fixed values of the fission-fragment total kinetic energy and/or fission-fragment mass number and/or neutron emission angle,
- the prompt fission neutron multiplicity distribution P(ν),
- the correlations and/or anti-correlations in neutron emission from complementary fragments,
- the energy spectrum of pre-fission neutrons ϕ(E) emitted prior to fission in multiple-chance fission,
- scission neutrons,
- neutron emission in ternary fission, and
- neutron emission from *accelerating* fragments in contrast to neutron emission from *fully accelerated* fragments.

While this list is not exhaustive, it does include most of the types of neutron emission measurements that have been performed or attempted. In this paper, the second and third items, the prompt fission neutron spectrum N(E) and the average prompt neutron multiplicity $\bar{\nu}_p$, will be discussed for both spontaneous and neutron-induced fission.

Two early representations of the prompt fission neutron spectrum, which are still used today, are the Maxwellian and Watt spectrum representations, with parameters that are adjusted to optimally reproduce the experimental spectrum for a given fissioning system. The Maxwellian spectrum is given by

$$N(E) = (2/\pi^{1/2} T_M^{3/2}) \, E^{1/2} \exp(-E/T_M) \, , \tag{1}$$

where the single (temperature) parameter appearing, T_M, is related to the average energy of the spectrum <E> by

$$<E> = (3/2)T_M \; . \tag{2}$$

The Maxwellian spectrum neglects the distribution of fission-fragment excitation energy, the energy dependence of the inverse process of compound nucleus formation, and the center-of-mass motion of the fragments from which the neutrons are emitted. Thus, the single temperature parameter T_M must simultaneously account for all of these physical effects. Accordingly, there is no predictive power in a Maxwellian approach.

The two-parameter Watt spectrum[1] consists of a center-of-mass Maxwellian spectrum that has been transformed[2] to the laboratory system, for an average fission fragment moving with an average kinetic energy per nucleon E_f. This spectrum is given by

$$N(E) = \frac{\exp(-E_f/T_W)}{(\pi E_f T_W)^{1/2}} \exp(-E/T_W) \sinh[2(E_f E)^{1/2}/T_W] \, , \tag{3}$$

where E_f and the Watt temperature T_W are related to the average energy of the spectrum <E> by

$$<E> = E_f + (3/2)T_W \, . \tag{4}$$

The Watt spectrum also neglects the distribution of fission-fragment excitation energy and the energy dependence of the inverse process of compound nucleus formation, but does account for the center-of-mass motion of an average fragment. However, for spontaneous and low-energy neutron-induced ($E_n < 15$ MeV) fission, the concept of an average fragment is usually not a good one because there are ordinarily two average fragments due to the double-humped fragment mass distribution. For these reasons, the Watt spectrum, although it is more physical than the Maxwellian spectrum, has little predictive power in most applications. [If one insists on using a Watt spectrum representation, the average of the separate Watt spectra for the light and heavy mass peaks should be taken to represent the total laboratory spectrum N(E). This amounts to a three-parameter representation, assuming the existence of statistical equilibrium between the nascent fragments.]

At the same time that these early representations were introduced for N(E), the average prompt neutron multiplicity $\bar{\nu}_p$ was modeled[3] by a simple polynomial (usually linear) in incident neutron energy E_n, for each fissioning system considered: $\bar{\nu}_p = \nu_0 + \alpha E_n$, and again, the parameters appearing were, and are, adjusted to optimally reproduce the experimental average multiplicity.

To summarize, it is clear that none of the approaches described above can be used to predict N(E) and/or $\bar{\nu}_p$ (E_n) for a different fissioning nucleus or for a different excitation energy from what has been experimentally measured. Therefore, in Sec. II three modern approaches to the calculation of N(E) and $\bar{\nu}_p$ are described and examples given. More recent work with these approaches is described in Secs. III and IV, and some conclusions and recommendations are presented in Sec. V.

II. MODERN APPROACHES TO THE CALCULATION OF N(E) AND $\bar{\nu}_p$

In recent years three new theoretical approaches have evolved for the calculation of the prompt fission neutron spectrum N(E). These are the following:

- The Los Alamos approach,[4] begun in 1979, which is based upon standard nuclear evaporation theory[5] and simultaneously treats the average prompt neutron multiplicity $\bar{\nu}_p$. This approach emphasizes predictive capabilities while requiring minimal input. Refinements to this approach that treat the entire fission-fragment mass and charge distributions, instead of averages over their peak regions, have also been performed.[6-8]

- The Dresden approach,[9] begun in 1982, which is also based upon standard nuclear evaporation theory,[5] but accounts explicitly for neutron cascade emission. This approach emphasizes a complete description, requiring a substantial amount of experimental information. The Dresden group has also employed the Los Alamos approach including the refinements mentioned above.[6,10]

- The Hauser-Feshbach statistical model approach, which is based upon Hauser-Feshbach theory[11] and accounts explicitly for the competition between neutron emission and gamma-ray emission in a given fission fragment. This approach, if properly applied, accounts for the influence of angular momentum on neutron and gamma-ray emission, whereas the Los Alamos and Dresden approaches do not. Accordingly, the Hauser-Feshbach approach may, ultimately, become the best theoretical approach.

II.A. Summary of Los Alamos Model.

The original Los Alamos model[4] addresses both neutron-induced and spontaneous fission and accounts for the physical effects of

(1) the distribution of fission-fragment excitation energy,
(2) the energy dependence of the inverse process of compound nucleus formation,
(3) the center-of-mass motion of the fission fragments, and
(4) multiple-chance fission at high incident neutron energy.

In particular, to simulate the initial distribution of fission-fragment excitation energy and subsequent cooling as neutrons are emitted, a triangular approximation to the corresponding fission-fragment residual nuclear temperature distribution is used. This approximation, based upon the observations of Terrell,[12] is given by

$$P(T) = \begin{cases} 2T/T_m^{\,2} & T \le T_m \\ 0 & T > T_m \, , \end{cases} \tag{5}$$

where the maximum temperature T_m is related to the initial total average fission-fragment excitation energy $\langle E^* \rangle$ by

$$T_m = (\langle E^* \rangle / a)^{1/2} \, , \tag{6}$$

and where a is the nuclear level density parameter. In Eq. (6), the initial total average fission-fragment excitation energy is given by

$$\langle E^* \rangle = \langle E_r \rangle + E_n + B_n - \langle E_f^{tot} \rangle \, , \tag{7}$$

where $\langle E_r \rangle$ is the average energy release in fission, B_n and E_n are the separation and kinetic energies of the neutron inducing fission (set to zero for spontaneous fission), and $\langle E_f^{tot} \rangle$ is the total average fission-fragment kinetic energy. These quantities are either known or can be calculated.

The energy dependence of the inverse process is treated in the center-of-mass frame by calculating the compound nucleus formation cross section $\sigma_c(\varepsilon)$ for the inverse process using an optical-model potential with explicit isospin dependence so as to describe (neutron rich) fission fragments more correctly. It is the *shape of* $\sigma_c(\varepsilon)$ with ε that affects N(E).

The values of the average kinetic energy per nucleon of the average light fragment A_L and average heavy fragment A_H are obtained using momentum conservation and are given by

$$E_f^L = (A_H/A_L)(\langle E_f^{tot}\rangle/A) ,$$

$$E_f^H = (A_L/A_H)(\langle E_f^{tot}\rangle/A) , \tag{8}$$

where A is the mass number of the fissioning nucleus.

With the inclusion of these physical effects, the prompt fission neutron spectrum in the laboratory system is given by

$$N(E) = \frac{1}{2}\left[N(E,E_f^L,\sigma_c^L) + N(E,E_f^H,\sigma_c^H)\right] , \tag{9}$$

where

$$N(E,E_f,\sigma_c) = \frac{1}{2\sqrt{E_f}\,T_m^2}\int_{(\sqrt{E}-\sqrt{E_f})^2}^{(\sqrt{E}+\sqrt{E_f})^2} \sigma_c(\varepsilon)\sqrt{\varepsilon}\,d\varepsilon \int_0^{T_m} k(T)\,T\exp(-\varepsilon/T)\,dT . \tag{10}$$

In this equation, ε is the center-of-mass neutron energy and the temperature-dependent normalization k(T) is given by

$$k(T) = \left[\int_0^{\infty} \sigma_c(\varepsilon)\,\varepsilon\exp(-\varepsilon/T)\,d\varepsilon\right]^{-1} . \tag{11}$$

If $\sigma_c(\varepsilon)$ is constant, Eq. (10) reduces to the closed form expression

$$N(E,E_f) = \frac{1}{3(E_fT_m)^{1/2}}\left[u_2^{3/2}E_1(u_2) - u_1^{3/2}E_1(u_1) + \gamma(\tfrac{3}{2},u_2) - \gamma(\tfrac{3}{2},u_1)\right] , \tag{12}$$

where $$u_1 = (\sqrt{E} - \sqrt{E_f})^2/T_m ,$$

$$u_2 = (\sqrt{E} + \sqrt{E_f})^2/T_m ,$$

$E_1(x)$ is the exponential integral function, and

$\gamma(a,x)$ is the incomplete gamma function.

Similarly, the average prompt fission neutron multiplicity $\bar{\nu}_p$ is obtained from considerations of energy conservation and is given by

$$\bar{\nu}_p = \frac{\langle E^* \rangle - \langle E_\gamma^{tot} \rangle}{\langle S_n \rangle + \langle \varepsilon \rangle} , \qquad (13)$$

where $\langle E_\gamma^{tot} \rangle$ is the total average prompt gamma-ray energy, $\langle S_n \rangle$ is the average fission-fragment neutron separation energy, and $\langle \varepsilon \rangle$ is the average center-of-mass energy of the emitted neutrons.

There are two specific connections between N(E) and $\bar{\nu}_p$ that are worth noting. The first is that the maximum temperature T_m appearing as one of three parameters in N(E) also appears in $\bar{\nu}_p$ as T_m^2, through Eq. (6). The second is that the average center-of-mass neutron energy $\langle \varepsilon \rangle$ appearing in $\bar{\nu}_p$ is also the first moment of the center-of-mass spectrum $\phi(\varepsilon)$ corresponding to the laboratory spectrum N(E). These two connections are very important because they mean that if one has experimental information on either N(E) or $\bar{\nu}_p$ for a given fissioning system, then that information can be used as a constraint in the calculation of the other, unmeasured, observable.

If the complete fission-fragment mass and charge distributions are treated, instead of averages over their peak regions, Eq. (9) becomes

$$N(E) = \sum_A \frac{\bar{\nu}(A)}{\bar{\nu}_{tot}} Y(A) \sum_Z P(Z)\, N\Big[E, E_f(A), \sigma_c(Z,A), T_m(Z,A) \Big] , \qquad (14)$$

where (A,Z) are fragment mass and charge numbers,

$\bar{\nu}(A)$ is the average prompt neutron multiplicity for each fragment mass,

Y(A) is the fragment mass yield,

$\bar{\nu}_{tot} = \sum_A Y(A)\,\bar{\nu}(A)$ is the total average prompt neutron multiplicity ,

P(Z) is the fragment charge distribution,

and $E_f(A)$ and $T_m(Z,A)$ are calculated as in Eqs. (8) and (6), respectively, but without the use of any averaged quantities [see Ref. 7]. Similarly, if experimental values for $\bar{\nu}(A)$ do not exist, they are calculated as in Eq. (13), but without the use of corresponding averaged quantities.

Examples of calculations performed using the original Los Alamos model are shown in Figs. 1-7. The numerical details and evaluation of the constants appearing in these calculations are found in Ref. 4 so they are not repeated here. First, comparisons of the Los Alamos spectrum for a constant cross section to Maxwellian and Watt spectra for the same fissioning system are shown in Figs. 1 and 2. The first moments (average laboratory neutron energies) of the three spectra have been constrained to be identical by determining the Maxwellian and Watt temperatures, T_M and T_W, in terms of the physically based value of T_m. Using this basis for comparison, the Los Alamos spectrum lies between the Maxwellian and Watt spectra. The fact that T_M includes the effects of fragment motion is evident in Fig. 2, where the tail of the Maxwellian spectrum is clearly too hard due to the overly large value of T_M. The converse is true for the tail of the Watt spectrum, which is too soft because T_W is less than T_m.

The dependence of N(E) on the fissioning nucleus and its excitation energy is shown for the constant cross section Los Alamos model in Figs. 3 and 4. Figure 3 shows how the spectrum increases at high energy and decreases at low energy as the mass and charge of the fissioning nucleus increases, for thermal-neutron-induced fission. Thus, $\langle E_r \rangle$ is increasing faster with the mass of the fissioning nucleus than $\langle E_f^{tot} \rangle$ is increasing with the charge of the fissioning nucleus [see Eqs. (6) and (7)]. Similarly, Fig. 4 shows how the spectrum increases at high energy and decreases at low energy as the kinetic energy of the incident neutron increases, for the first-chance fission of ^{235}U.

Figures 5 and 6 compare both the exact and approximate versions of the Los Alamos spectrum with experimental data. Clearly, there is a preference for the exact energy-dependent cross-section calculation, although both agree well with the experiment. Thus, given the quality of the experimental data, the Los Alamos exact spectrum given by Eqs. (9) and (10) is to be used when high accuracy is required. In such cases, the energy dependence of the inverse process of compound nucleus formation cannot be ignored.

Turning to the calculation of the average prompt neutron multiplicity $\bar{\nu}_p$ using the Los Alamos model, Fig. 7 shows a comparison of calculated and experimental values of $\bar{\nu}_p$ for the neutron-induced fission of ^{235}U. The agreement is better than 1% at energies below 1 MeV and at 6 MeV. In the region from ~ 1.5 to 5.5 MeV, however, the experimental values are somewhat less than the calculated values, ~ 3% differences at 4.5 MeV. Nevertheless, the agreement between experiment and calculation is quite good, given the approximations implied by the use of averaged quantities in Eq. (13).

A comparison of the original and (preliminary) refined Los Alamos models, corresponding to Eqs. (9) and (10) and Eqs. (14) and (10), respectively, is shown in Fig. 8 for the spontaneous fission of ^{252}Cf. The refined calculation agrees even better with experiment than does the original calculation [see Refs. 7-8], but there is still room for further improvement. This is presumably accomplished by increasing the number of calculated fragments from 28 (two fragments every sixth mass number) to say, 56 (two fragments every third mass number), or perhaps even more. This work is currently in progress.

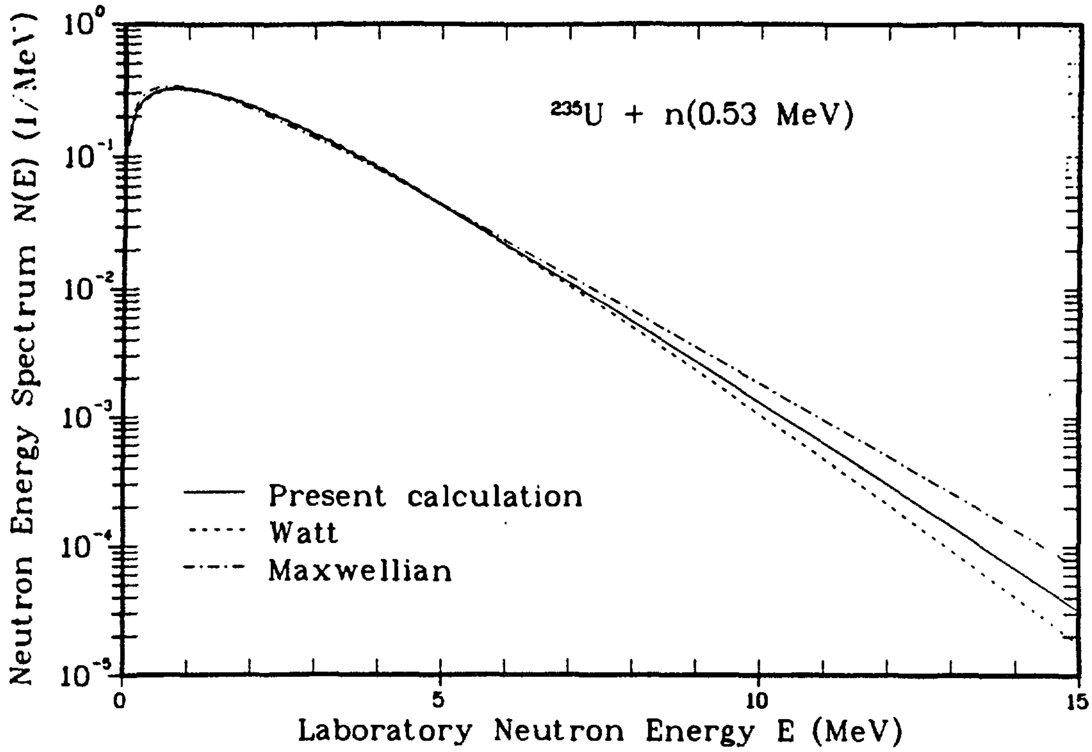

Fig. 1. Prompt fission neutron spectrum for the fission of ^{235}U induced by 0.53-MeV neutrons. The solid curve gives the Los Alamos spectrum calculated from Eqs. (9) and (12), the dashed curve gives the Watt spectrum calculated from Eq. (3), and the dot-dashed curve gives the Maxwellian spectrum calculated from Eq. (1). The average neutron energies of the three spectra are identical.

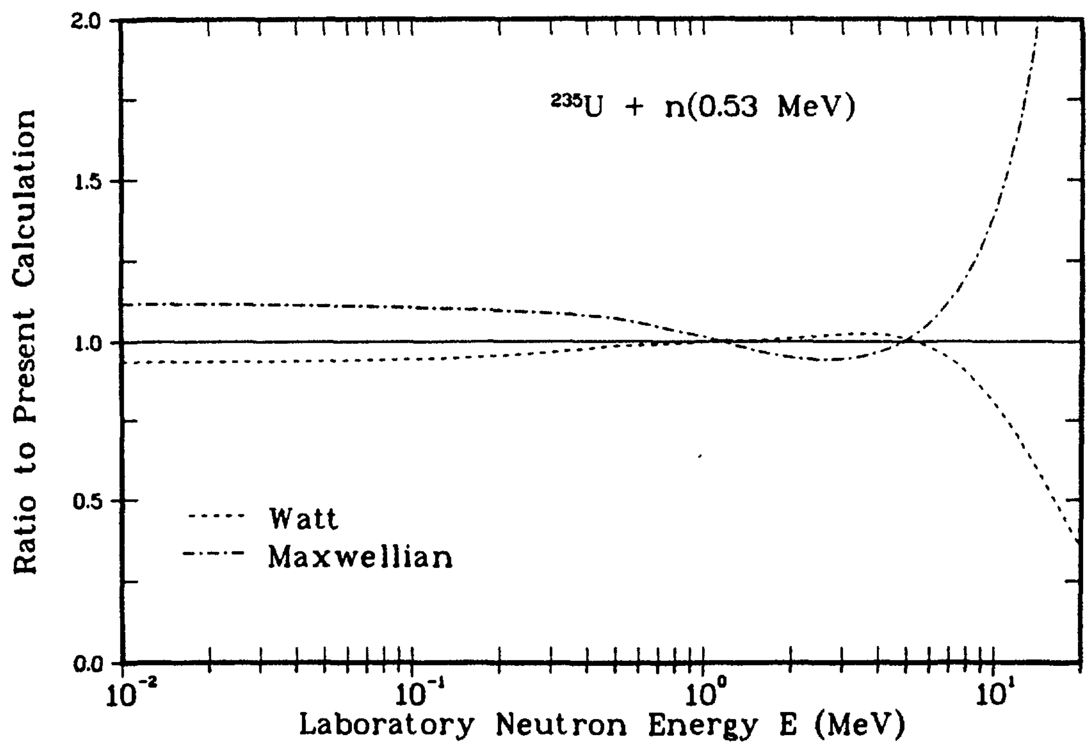

Fig. 2. Ratio of the Watt spectrum and the Maxwellian spectrum to the Los Alamos spectrum, corresponding to the curves shown in Fig. 1.

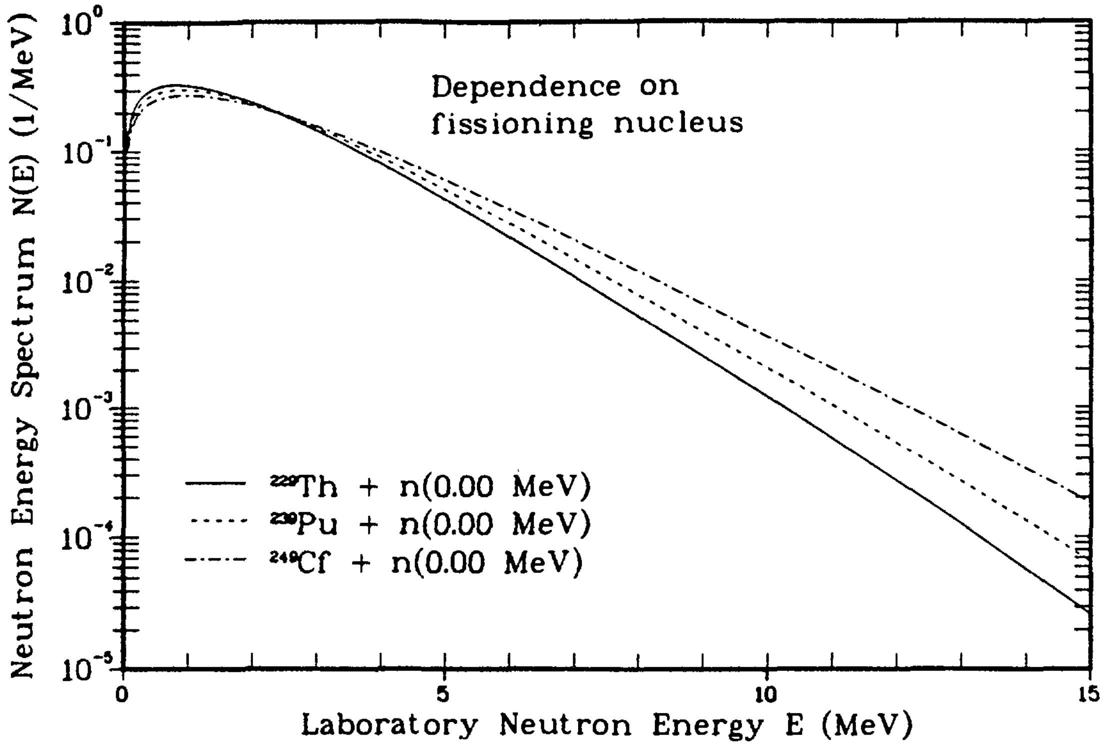

Fig. 3. Dependence of the prompt fission neutron spectrum on the fissioning nucleus, for thermal-neutron-induced fission, calculated using the Los Alamos model, Eqs. (9) and (12), for $\sigma_c(\varepsilon)$ = constant.

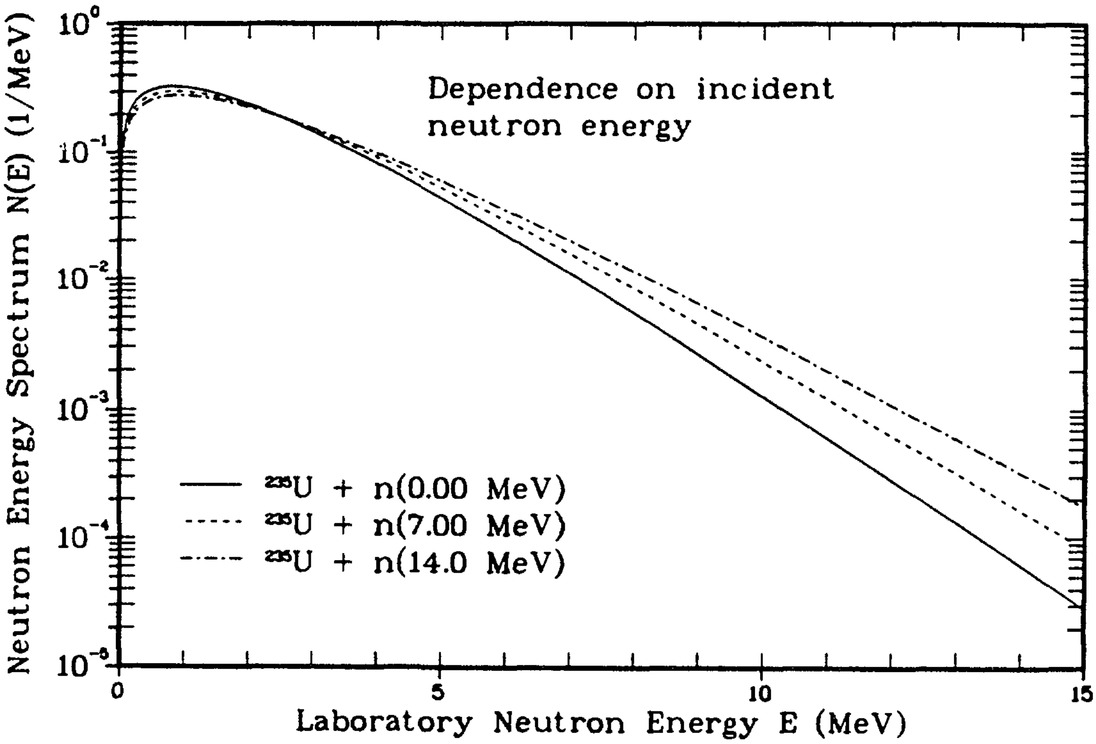

Fig. 4. Dependence of the prompt fission neutron spectrum on the kinetic energy of the incident neutron for the fission of ^{235}U, calculated using the Los Alamos model, Eqs. (9) and (12), for $\sigma_c(\varepsilon)$ = constant and assuming first-chance fission only.

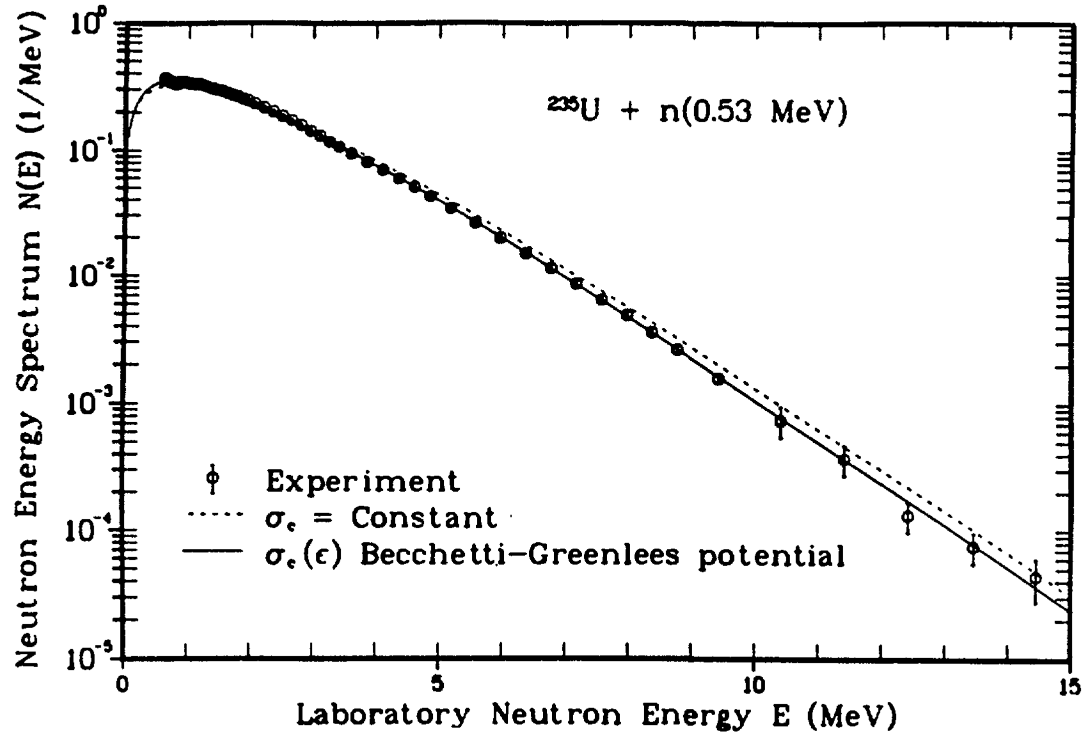

Fig. 5. Prompt fission neutron spectrum for the fission of ^{235}U induced by 0.53-MeV neutrons. The dashed curve gives the Los Alamos spectrum calculated from Eqs. (9) and (12), for $\sigma_c(\varepsilon)$ = constant, whereas the solid curve gives the Los Alamos spectrum calculated from Eqs. (9)-(11), for $\sigma_c(\varepsilon)$ obtained using the optical-model potential of Becchetti and Greenlees (Ref. 31). The experimental data are those of Johansson and Holmqvist (Ref. 26).

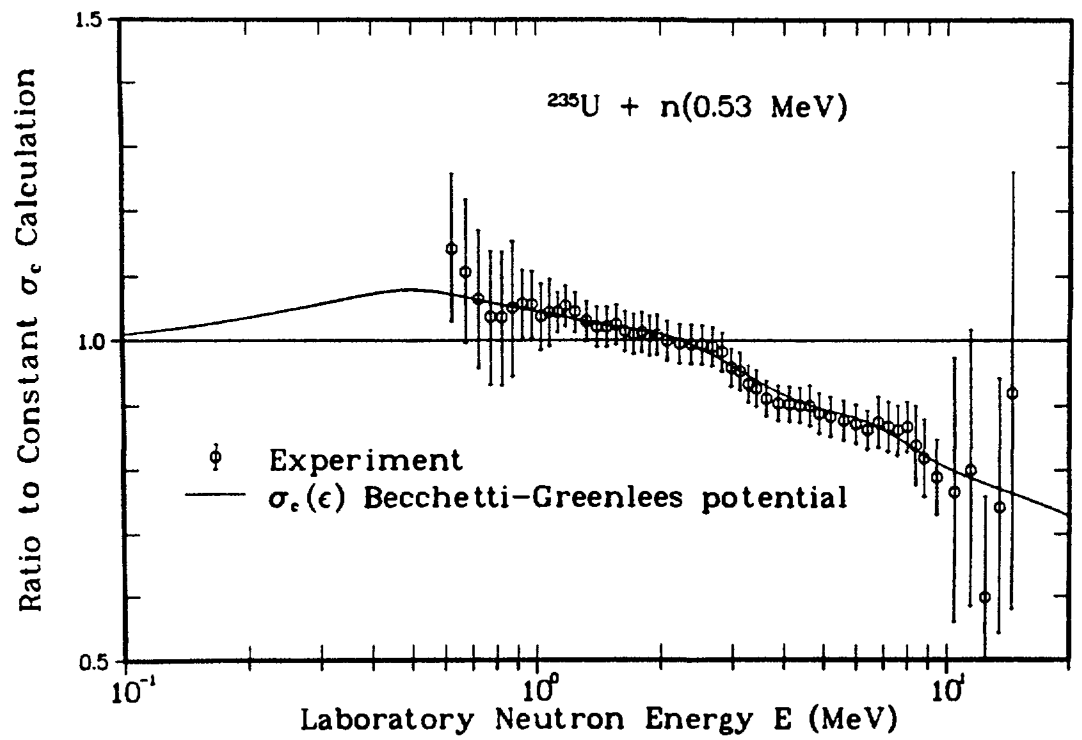

Fig. 6. Ratio of the Los Alamos spectrum calculated using energy-dependent cross sections and the experimental spectrum to the Los Alamos spectrum calculated using a constant cross section, corresponding to the curves shown in Fig. 5.

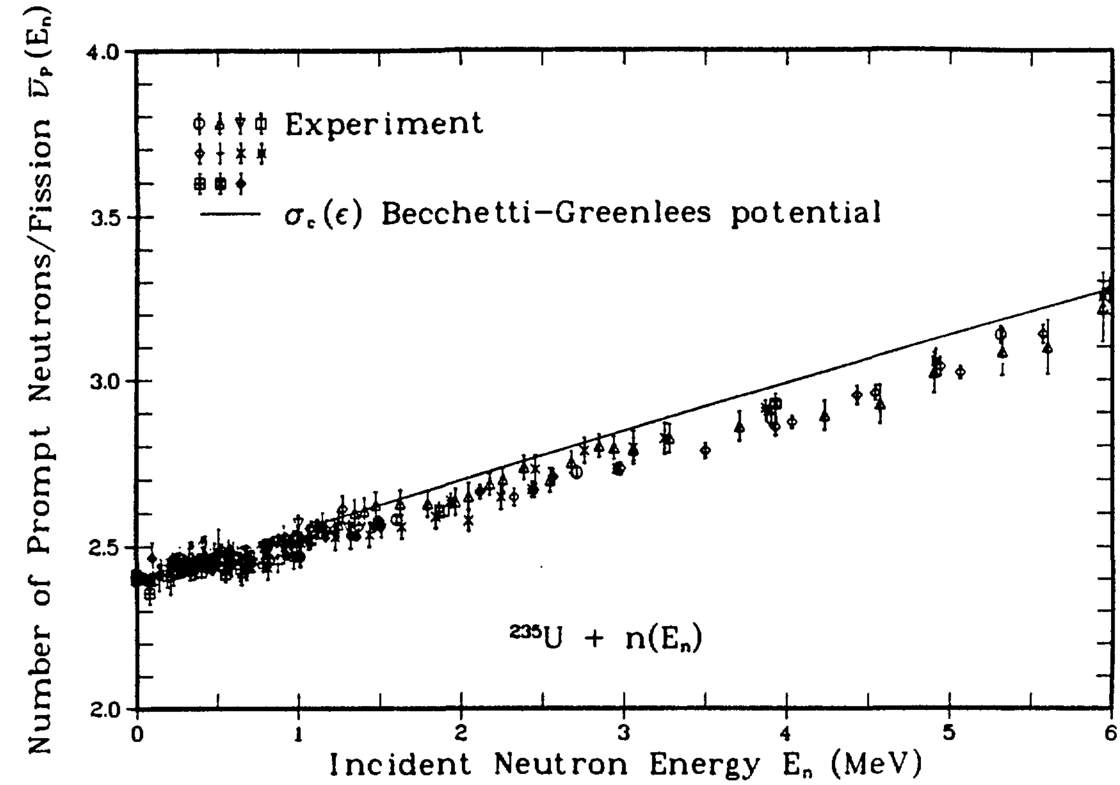

Fig. 7. Average prompt neutron multiplicity as a function of the incident neutron energy for the neutron-induced fission of ^{235}U. The solid curve gives the Los Alamos multiplicity calculated with Eq. (13) using the optical-model potential of Becchetti and Greenlees (Ref. 31) to calculate the average center-of-mass energy $<\varepsilon>$. The experimental data are listed in Ref. 4.

II.B. Summary of Dresden Model.

The Dresden model,[9] currently known as the Complex Cascade Evaporation Model, accounts for the physical effects of

(1) the distribution of fission-fragment excitation energy in each step of the cascade evaporation of neutrons,
(2) the energy dependence of the inverse process of compound nucleus formation,
(3) the center-of-mass motion of the fission fragments,
(4) the anisotropy of the center-of-mass neutron spectrum,
(5) the complete fission-fragment mass and kinetic energy distributions, and
(6) semi-empirical fission-fragment nuclear level densities.

With knowledge of the above physical effects in sufficient detail, the prompt fission neutron spectrum in the laboratory system is given by

$$N(E) = \sum_A \int P(A,TKE)\, N(E,A,TKE)\, dTKE \ , \tag{15}$$

where P(A,TKE) is the normalized fission-fragment mass distribution for a fixed value of

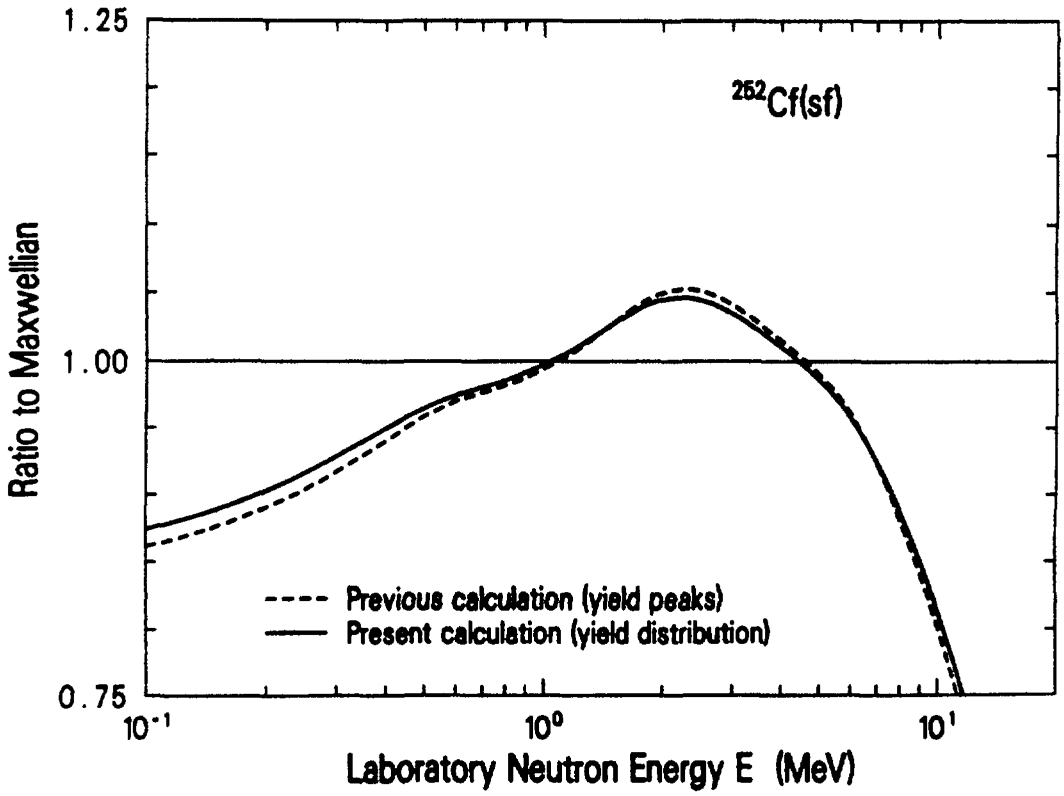

Fig. 8. Ratio of the original Los Alamos spectrum, based upon considerations of the *peaks* of the fission-fragment mass and charge distributions, and the (preliminary) refined Los Alamos spectrum, based on considerations of the *entire* fission-fragment mass and charge distributions, to a Maxwellian spectrum with $T_M = 1.42$ MeV. The nuclear level-density parameter is identical in both calculations.

the total fission-fragment kinetic energy TKE, and N(E,A,TKE) is the laboratory spectrum for fixed fragment mass A and fixed TKE. The sum and integral are over all contributing fragment mass numbers and total kinetic energies, respectively. The fragment spectrum N(E,A,TKE) is given by

$$N(E,A,TKE) = \int_{(\sqrt{E}-\sqrt{E_f})^2}^{(\sqrt{E}+\sqrt{E_f})^2} \frac{\phi(\varepsilon,A,TKE)}{4\sqrt{\varepsilon E_f}} \left\{ \frac{1 + b\,[(E - E_f - \varepsilon)^2/4\varepsilon E_f]}{[1 + (b/3)]} \right\} d\varepsilon\ , \qquad (16)$$

where E_f is the kinetic energy per nucleon of the fragment, b is the anistropy coefficient, ε is the center-of-mass neutron energy, and $\phi(\varepsilon$,A,TKE) is the center-of-mass spectrum for fixed fragment mass and fixed TKE, given by

$$\phi(\varepsilon,A,TKE) = \sum_i \int_{B_i}^{\infty} \phi_i(\varepsilon,E^*,A-i)\, P_i\,(E^*,A,TKE)\, dE^*\ . \qquad (17)$$

In this equation, the sum is over the steps i of the cascade while the integral is over the fragment excitation energy E*, and B_i is the neutron binding energy in a fragment that has

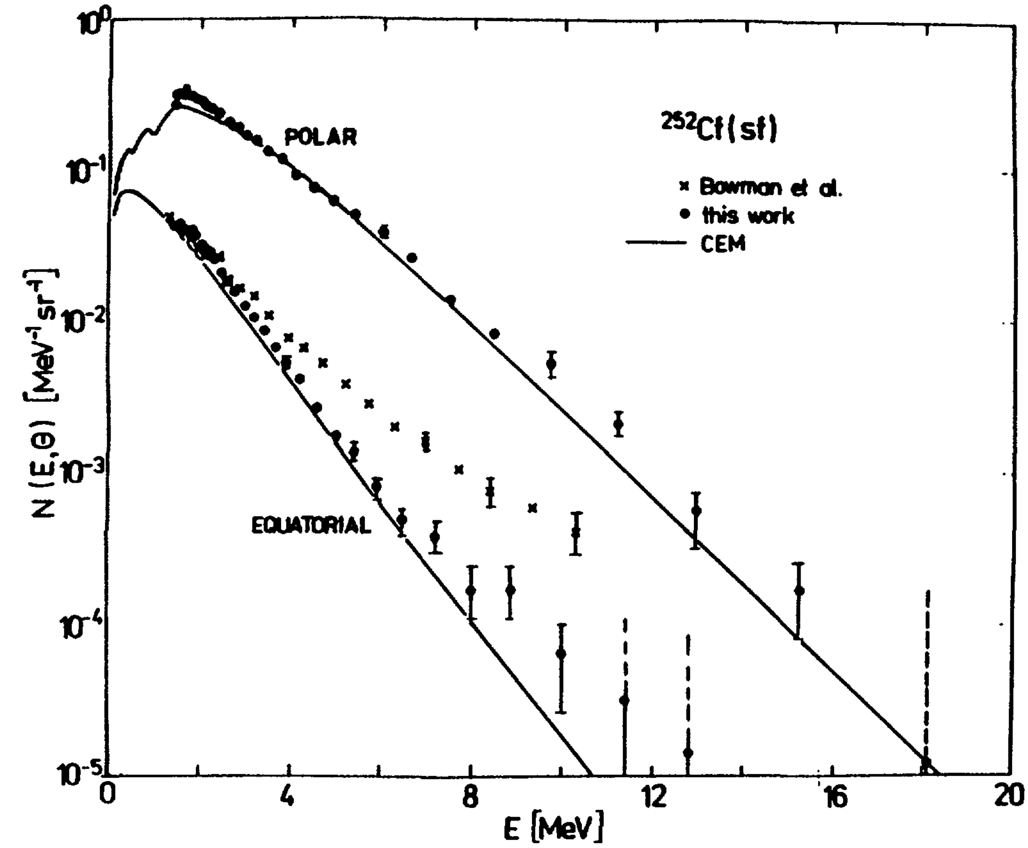

Fig. 9. Prompt fission neutron spectra for the spontaneous fission of ^{252}Cf in the parallel (polar) and perpendicular (equatorial) directions with respect to the fission axis, calculated using the Dresden model (CEM), Eqs. (15)-(18), but prior to integration over angle. The experimental data are from Ref. 13 (closed circles) and Ref. 32 (crosses). [Figure is from Ref. 13.]

emitted i neutrons. Also, P_i (E*,A,TKE) is the excitation energy distribution *before* step i and is expressed in terms of P_{i-1} and, ultimately, P_0, which is assumed Gaussian. Finally, $\phi(\varepsilon,E^*,A)$ is the Weisskopf[5] center-of-mass neutron energy spectrum for fixed E* and A, given by

$$\phi(\varepsilon,E^*,A) = C\,\sigma_c(\varepsilon,A-1)\,\varepsilon\,\rho\,(E^* - B_n - \varepsilon,\, A-1)\ , \qquad (18)$$

where ρ is the level density of the residual nucleus for zero angular momentum states and C is the normalization constant.

Examples of calculations performed using the Dresden model are shown in Figs. 9 and 10 for the spontaneous fission of ^{252}Cf. The numerical details and evaluation of the constants appearing in these calculations are found in Refs. 13 and 14 so they are not repeated here. The reality of anisotropy effects in the prompt fission neutron spectrum is demonstrated in Fig. 9 where recent experimental data for polar and equatorial emission, and calculations using the Dresden model with an anisotropy coefficient b = 0.1, agree well with each other. The experimental and calculated spectra for the same fissioning system, but integrated over all angles of neutron emission, are shown in Fig. 10 as deviations from

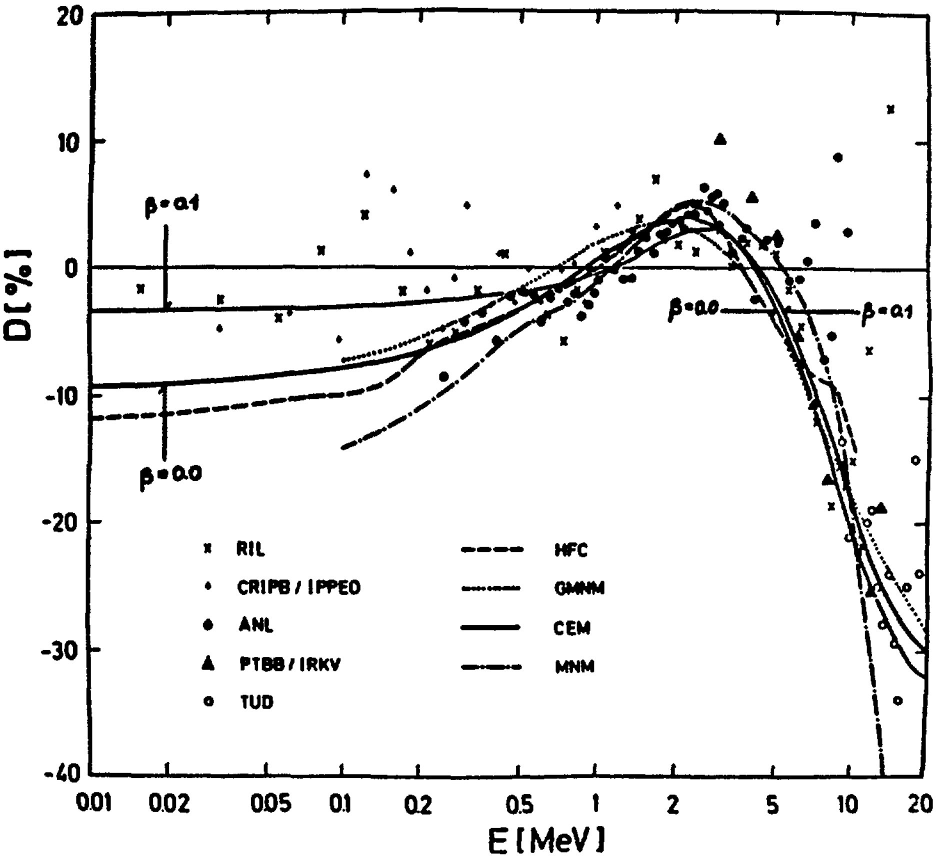

Fig. 10. Prompt fission neutron spectra for the spontaneous fission of ^{252}Cf shown as the deviation, in per cent, from a Maxwellian spectrum with $T_M = 1.42$ MeV. The solid curves are calculated using the Dresden model (CEM), Eqs. (15)-(18), for two values of the anisotropy coefficient b (β in the figure). Calculations are also shown for the Hauser-Feshbach (HFC) and Los Alamos (GMNM and MNM) models. The experimental data points are from the indicated laboratories, but with error deleted for clarity. [Figure is from Ref. 14.]

a Maxwellian spectrum. Again, the Dresden model (CEM), solid curve for b = 0.1 (β = 0.1), yields quite good agreement with experiment, especially at the low energy end of the spectrum. Clearly, the anisotropy of the center-of-mass spectrum must be taken into account to obtain the most realistic representation of the experimental spectrum.

The Dresden group has also employed[6,10] the Los Alamos model and has refined it (GMNM model) to include dependence on fragment mass and center-of-mass emission angle.[15]

II.C. Summary of Hauser-Feshbach Approach.

This approach consists of Hauser-Feshbach statistical model calculations of the de-excitation of representative nuclei of the fission-fragment mass and charge distributions. This model applied to fission fragments accounts for the physical effects included in the Los Alamos and Dresden models and, *in addition*, accounts for

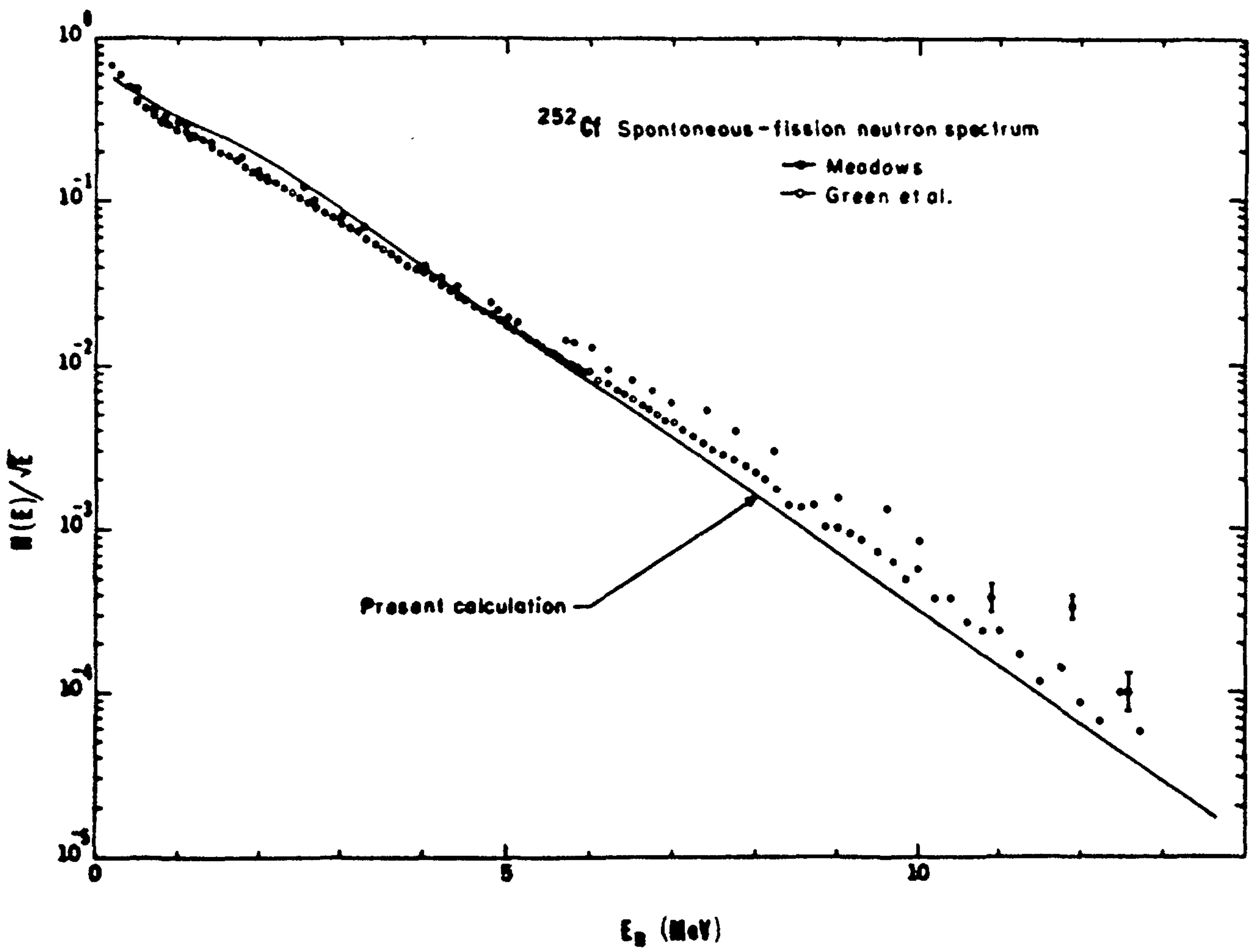

Fig. 11. Prompt fission neutron spectrum for the spontaneous fission of ^{252}Cf, calculated by Browne and Dietrich (Ref. 16) using the Hauser-Feshbach approach, together with experimental data from Meadows (Ref. 19) and Greene *et al.* (Ref. 20). [Figure is from Ref. 16.]

(1) Neutron and gamma-ray *competition* in the de-excitation of a given fission fragment,

(2) neutron transmission coefficients T_{lj} from an optical-model potential for each fragment considered [for each value of ε, these T_{lj} are essentially the angular momentum decomposition of the $\sigma_c(\varepsilon)$ used in the Los Alamos and Dresden models],

(3) gamma-ray transmission coefficients T_γ for each fragment considered, and

(4) the angular momentum distribution P(J) for each fragment considered.

A detailed description of the Hauser-Feshbach formalism for de-excitation of fission fragments is not presented here, due to space limitations. Crucial aspects of such calculations, however, include fragment nuclear level densities, initial excitation energy and angular momentum distributions, neutron optical-model potentials for fragments, and the partition of available excitation energies between light and heavy fragments. These subjects are discussed by Browne and Dietrich,[16] who performed a H-F calculation of the neutron

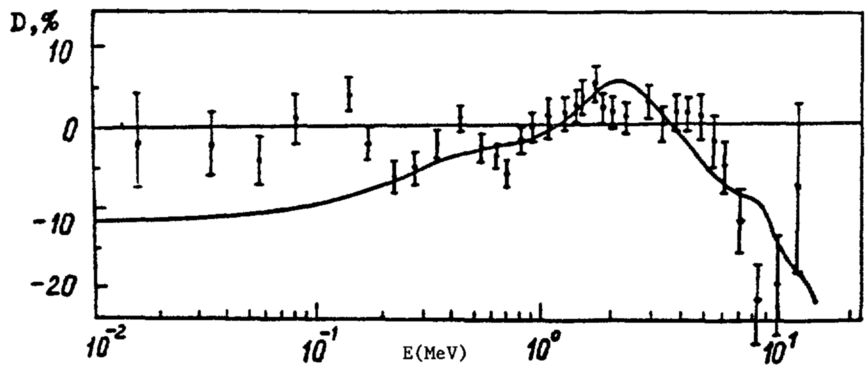

Fig. 12. Prompt fission neutron spectrum for the spontaneous fission of ^{252}Cf shown as the deviation, in per cent, from a Maxwellian spectrum with $T_M = 1.42$ MeV. The calculated spectrum using the Hauser-Feshbach approach has been obtained by Gerasimenko and Rubchenya (Ref. 17) and the experimental data are from Balenkov *et al.* (Ref. 21). [Figure is from Ref. 17.]

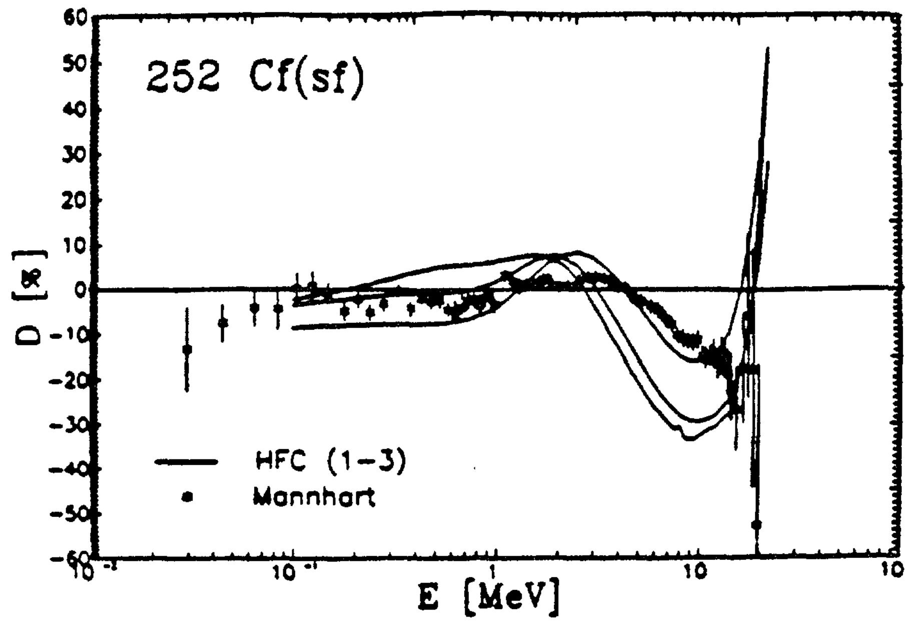

Fig. 13. Prompt fission neutron spectrum for the spontaneous fission of ^{252}Cf shown as the deviation, in per cent, from a Maxwellian spectrum with $T_M = 1.42$ MeV. The Hauser-Feshbach calculations of the spectra, performed by Seeliger *et al.* (Ref. 22) are shown for three values of a "scaling factor" on the gamma-emission width. The evaluated data are from Mannhart (Ref. 23). [Figure is from Ref. 22.]

spectrum N(E) for the $^{252}Cf(sf)$ reaction. Their results are compared with two experimental spectra (that were available in 1974) in Fig. 11. Gerasimenko and Rubchenya[17-18] have also performed H-F calculations of N(E), for the same $^{252}Cf(sf)$ reaction, beginning in 1980. They consider 18 representative fission fragments, and use a Fermi-gas level density and a Gaussian distribution of initial excitation energy, to obtain the total spectrum shown in good agreement with experiment in Fig. 12. They obtain even better agreement when including a center-of-mass anisotropy coefficient of b = 0.15, although this effect is still under study.[18]

More recent H-F calculations have been performed by Seeliger *et al.*[22], again, for the ^{252}Cf(sf) prompt neutron spectrum N(E). In these calculations, shown in Figs. 13 and 14, good agreement is obtained with evaluation and experiment. In particular, for the right value of a "scaling factor" on the gamma-emission width, the laboratory neutron energy spectrum and neutron total angular distribution are well reproduced. On the other hand, calculational difficulties remain with the average center-of-mass neutron emission energy as a function of fragment mass. This work is continuing.

III. RECENT WORK ON MULTIPLE-CHANCE FISSION

Two examples of recent work on the effects of neutron-induced multiple-chance fission upon the prompt fission neutron spectrum N(E) and average prompt neutron multiplicity $\bar{\nu}_p$ are discussed in this section. The major physical effect here is that when the incident neutron energy is sufficiently high (above the neutron binding energy, say), then two or more reaction channels resulting in fission can be open *simultaneously*. For example, the first-chance fission (n,f) reaction in competition with the second-chance fission (n,n'f) reaction. The *competition* between the open fission channels affects the observables N(E) and $\bar{\nu}_p$.

III.A. Neutron-Induced Multiple-Chance Fission of ^{235}U.

The Los Alamos model has been used to calculate the neutron-induced multiple-chance fission neutron spectrum and average multiplicity for ^{235}U up through third-chance fission. The exact energy-dependent spectra, given by Eqs. (9)-(11), together with evaporation spectra $\phi_j(E,\sigma_c)$ to describe neutron emission prior to fission, are combined in proportion to multiple-chance fission probabilities $P^A_{f_i}$ and average prompt neutron multiplicities $\bar{\nu}_{p_i}$ for the fissioning nuclei involved. This yields the total prompt fission neutron spectrum due to first-, second-, and third-chance fission events in the laboratory system:

$$N(E) = \Big\{ P^A_{f_1}\bar{\nu}_{p_1}N_1(E) + P^A_{f_2}\left[\phi_1(E)+\bar{\nu}_{p_2}N_2(E)\right] + P^A_{f_3}\left[\phi_1(E)+\phi_2(E)+\bar{\nu}_{p_3}N_3(E)\right]\Big\} \Big/ \left[P^A_{f_1}\bar{\nu}_{p_1} + P^A_{f_2}(1+\bar{\nu}_{p_2}) + P^A_{f_3}(2+\bar{\nu}_{p_3})\right], \tag{19}$$

where the index "i" on P^A_f and $\bar{\nu}_p$ refers to first-, second-, or third-chance fission and the

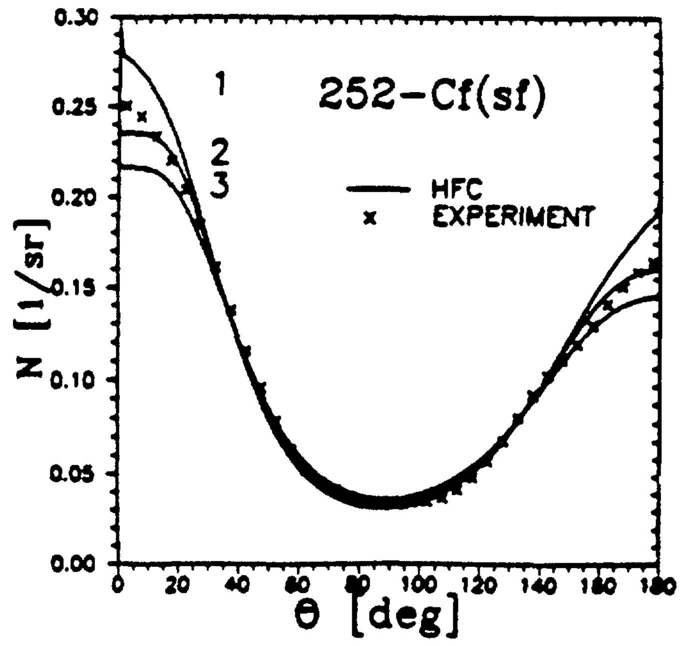

Fig. 14. Neutron total angular distribution from the spontaneous fission of ^{252}Cf. The Hauser-Feshbach calculations of the angular distribution, performed by Seeliger *et al.* (Ref. 22) are shown for three values of a "scaling factor" on the gamma-emission width. The experimental data are from Märten *et al.* (Ref. 24). [Figure is from Ref. 22.]

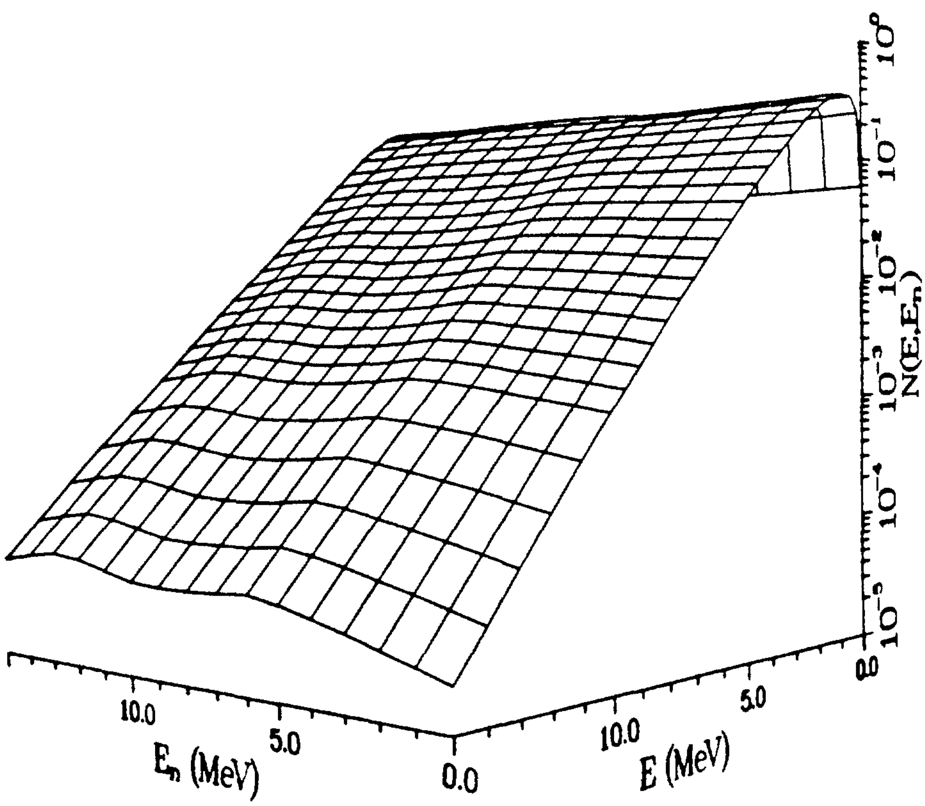

Fig. 15. Prompt fission neutron spectrum matrix N(E,E_n) for the neutron-induced fission of ^{235}U as a function of incident neutron energy E_n and emitted neutron energy E, and calculated using the Los Alamos model, Eqs. (9)-(11), and (19).

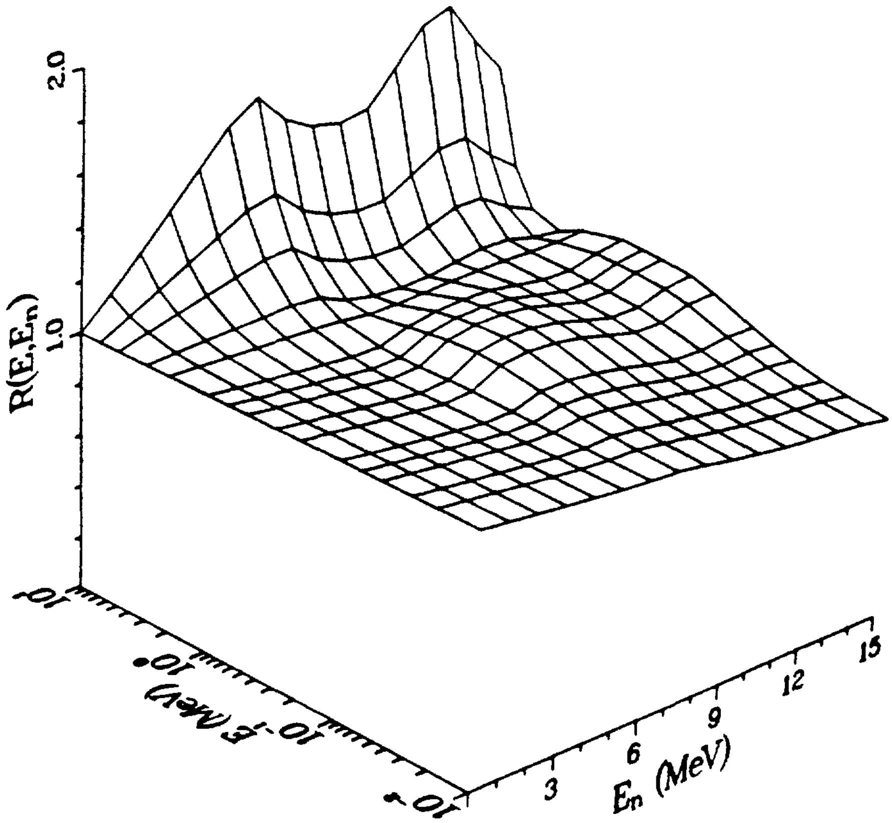

Fig. 16. Prompt fission neutron spectrum ratio matrix $R(E,E_n) = N(E,E_n)/N(E,0)$, corresponding to the matrix shown in Fig. 15.

index "j" on ϕ refers to the corresponding neutron evaporation spectra prior to fission. [Note that these "ϕ" are different from the "ϕ" of the Dresden model described above.]

Similarly, the total average prompt neutron multiplicity due to first-, second-, and third-chance fission events is given by

$$\bar{\nu}_p = \left[P^A_{f_1} \bar{\nu}_{p_1} + P^A_{f_2}(1 + \bar{\nu}_{p_2}) + P^A_{f_3}(2 + \bar{\nu}_{p_3}) \right] / (P^A_{f_1} + P^A_{f_2} + P^A_{f_3}) \,, \qquad (20)$$

where the indices have the same meaning as in Eq. (19).

The evaluation of Eq. (19) and Eq. (20) as a function of incident neutron energy E_n leads to the prompt fission neutron spectrum matrix $N(E,E_n)$ and the average prompt neutron multiplicity vector $\bar{\nu}_p(E_n)$. These are shown for n + ^{235}U in Figs. 15 and 16 for $N(E,E_n)$, and in Fig. 17 for $\bar{\nu}_p(E_n)$. Detailed features of these calculations are discussed in Ref. 4 and in Ref. 7. Figures 15 and 16 clearly illustrate the dependence of the matrix $N(E,E_n)$ upon the incident neutron energy E_n. In particular, the partition of the total available excitation energy into neutron emission prior to fission and neutron emission from fission fragments leads to suggestions of a *staircase effect* in the peak regions of the matrix and an *oscillatory effect* in the tail regions of the matrix. The staircase effect is due largely to the pre-fission evaporation neutrons while the oscillatory effect is due largely to the oc-

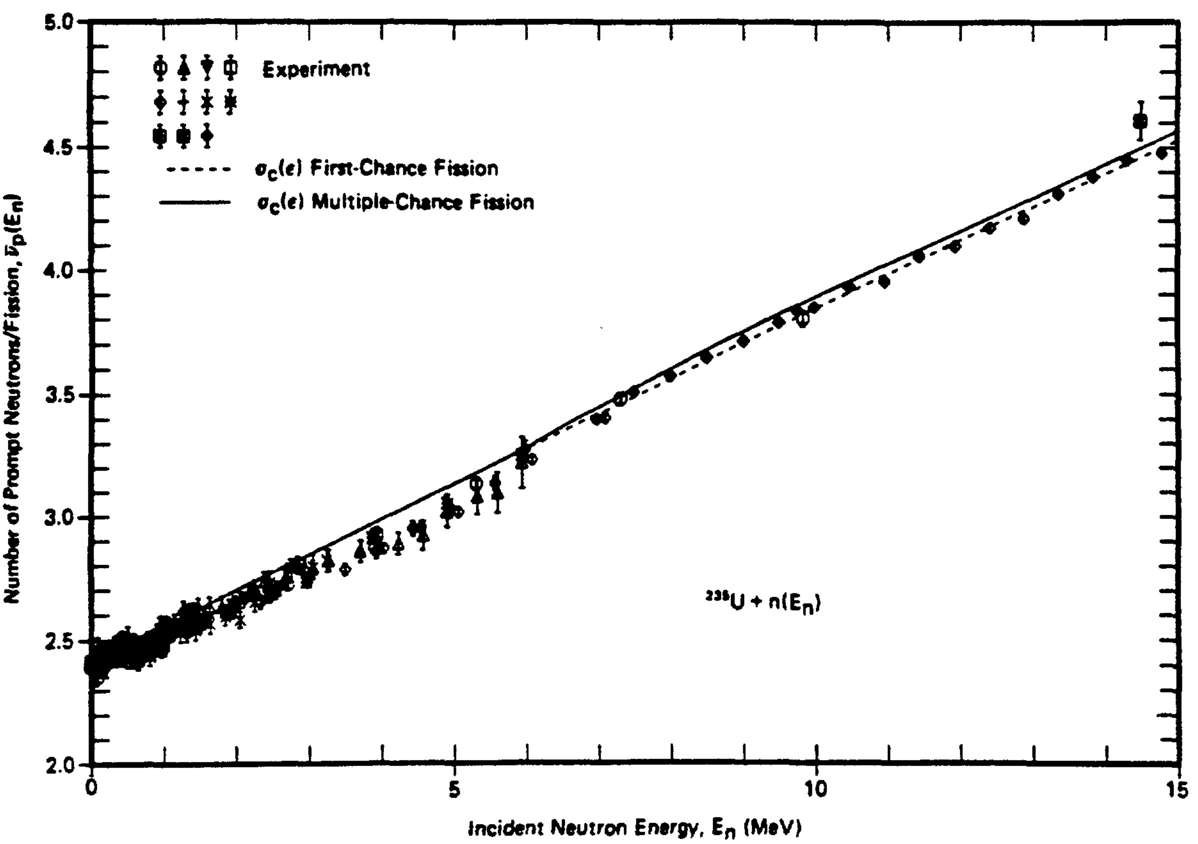

Fig. 17. Average prompt neutron multiplicity for the neutron-induced fission of ^{235}U. The dashed curve gives the multiplicity calculated with Eq. (13) assuming first-chance fission, whereas the solid curve gives the multiplicity calculated with Eq. (20) assuming multiple-chance fission. In both cases, the optical-model potential of Becchetti and Greenlees (Ref. 31) is used to calculate the average center-of-mass energy $<\varepsilon>$. The experimental data are listed in Ref. 4.

currence of cooler fission fragments following the emission of a neutron, or two neutrons, prior to fission. Figure 17 illustrates the calculated vector $\bar{\nu}_p(E_n)$, under the assumptions of multiple-chance fission and first-chance fission only, in comparison with experiment. Surprisingly, there are only slight differences between the two calculations for the n + ^{235}U system. This means that the combined incident energy dependencies of the components of Eq. (20) and those of Eq. (13) are very similar, perhaps fortuitously so.

III.B. Neutron-Induced Multiple-Chance Fission of ^{232}Th.

The Dresden group has employed a refined version of the Los Alamos model (their GMNM model[6]) to calculate the neutron-induced multiple-chance fission neutron spectrum and average neutron multiplicity for ^{232}Th. The spectrum N(E) is calculated for $E_n = 7.3$ MeV, at which the Dresden group also measured the spectrum.[25] The average multiplicity is calculated[15] from threshold to 10 MeV. The calculations of these two observables then require inclusion of first- and second-chance fission effects from the standpoint of energetics. A comparison of the measured and calculated spectra is shown in Fig. 18, without illustration of first- and second-chance components, because the spectrum is "not influ-

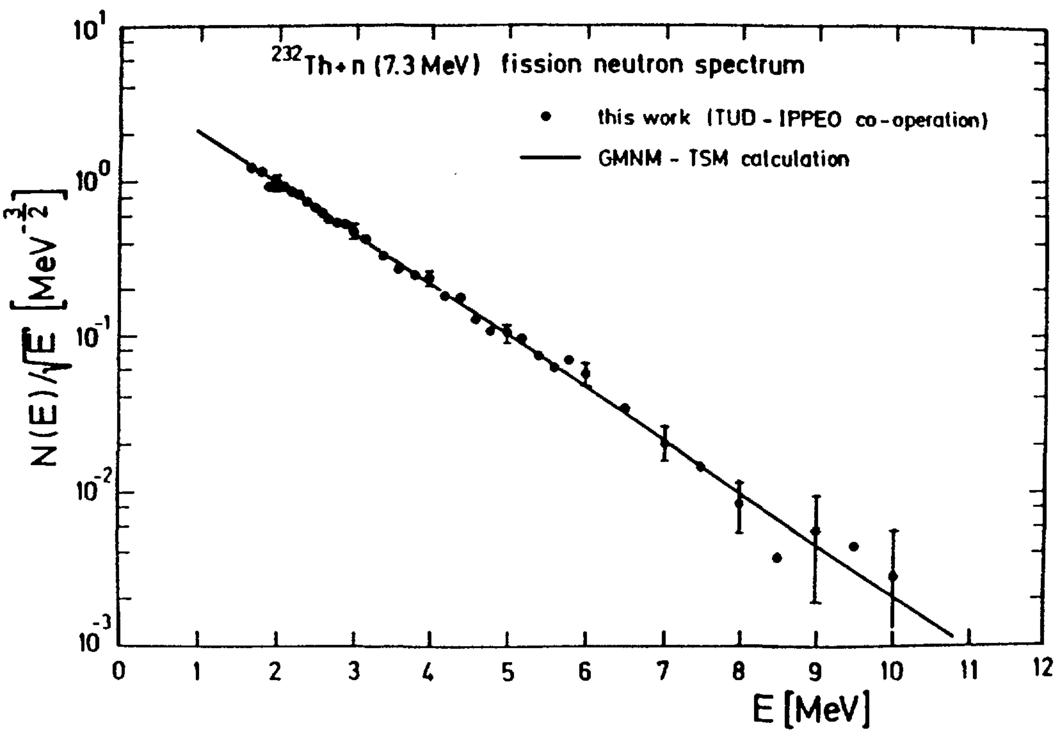

Fig. 18. Prompt fission neutron spectrum from the neutron-induced fission of ^{232}Th calculated, using the Dresden version (GMNM) of the Los Alamos model, and measured by Märten *et al.* (Ref. 25). [Figure is from Ref. 25.]

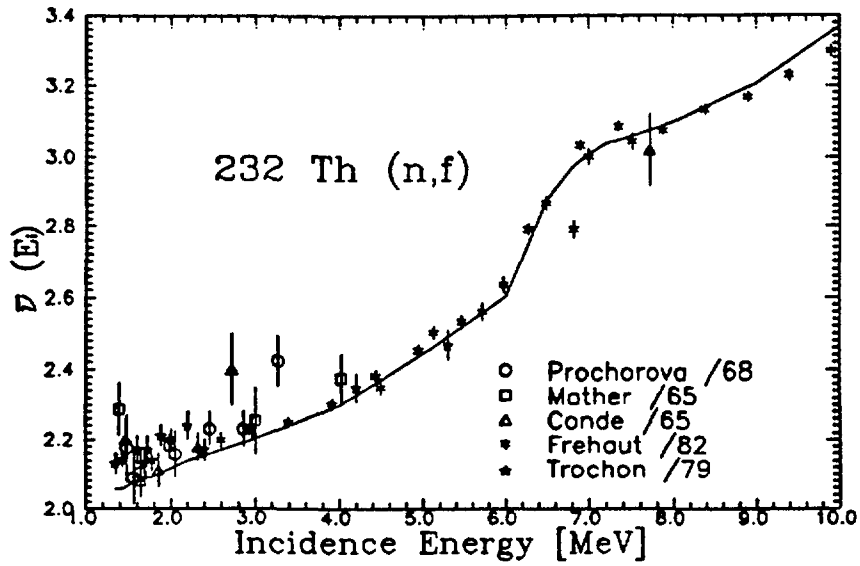

Fig. 19. Average prompt multiplicity as a function of the incident neutron energy for the neutron-induced fission of ^{232}Th. The solid curve gives the calculation (Ref. 15) using the Dresden version (GMNM) of the Los Alamos model. [Figure is from Ref. 15.]

enced by pre-fission neutrons above 1 MeV." This implies that, for this case, multiple-chance fission effects are found to be negligible. On the other hand, the measured and calculated average neutron multiplicities, shown in Fig. 19, indicate the presence of second-chance fission effects just above 6 MeV and a very strong second-chance fission component at ~ 7 MeV. Comparing with the ^{235}U case for both observables, one sees that

N(E, 7 MeV) for ^{235}U, Fig. 16, shows a reasonably strong second-chance fission presence in sharp contrast to N(E, 7.3 MeV) for ^{232}Th, shown in Fig. 18, whereas the converse is true for $\bar{\nu}_p$ in the same energy region, as shown in Figs. 17 and 19. Although differences in both macroscopic and microscopic components of the respective potential energy surfaces, together with differences in the energetics, are responsible for this circumstance, it is nevertheless difficult to isolate a dominant cause. Clearly, there is a need for further studies in multiple-chance fission.

IV. OTHER RECENT WORK

In this section other recent work is presented on the calculation of the prompt fission neutron spectrum N(E). Some of these calculations are due to the completion of very recent measurements.

IV.A. N(E,θ) for $^{252}Cf(sf)$.

The Dresden group has applied the Los Alamos model to the calculation of the energy and angle spectrum, N(E,θ), for the $^{252}Cf(sf)$ reaction. To accomplish this, they have written a new computer code,[15] FINESSE, which is based upon a refined Los Alamos model (their GMNM model[6]). The calculated[15] spectrum is shown in the upper portion of Fig. 20 in comparison with smoothed experimental data[24] shown in the lower portion of the figure. The good overall agreement is a rather remarkable achievement, despite the reported strong sensitivity of the tail of the spectrum to the optical potential employed.

IV.B. N(E, 0.53 MeV) for the n + ^{235}U and n + ^{239}Pu Reactions.

Calculations for the identical fission reactions are compared here for the original Los Alamos model (Ref. 4, 1982) and the Los Alamos model refined by the Dresden group (Ref. 15, 1990). The experimental data for the n + ^{235}U and n + ^{239}Pu reactions, at E_n = 0.53 MeV, are those of Johansson and Holmqvist[26] and Johansson *et al.*,[27] respectively. The comparisons are shown in Figs. 21 and 22, wherein the calculations (and data) for the original Los Alamos model[4] are referenced to the constant cross-section calculation (Eqs. 9 and 12), while the calculations (and data) for the Los Alamos model refined[15] by the Dresden group are referenced to best-fit Maxwellian spectra. The figures show that the original Los Alamos model agrees better with the ^{235}U data, although the refined Los Alamos model calculation is in reasonable agreement. On the other hand, neither calculation agrees well with the ^{239}Pu experiment. This means that the calculations are in error, or that the experimental data are suspect, or both. Clearly, existing ^{239}Pu data at other incident energies should be calculated as the first step in resolving this discrepancy.

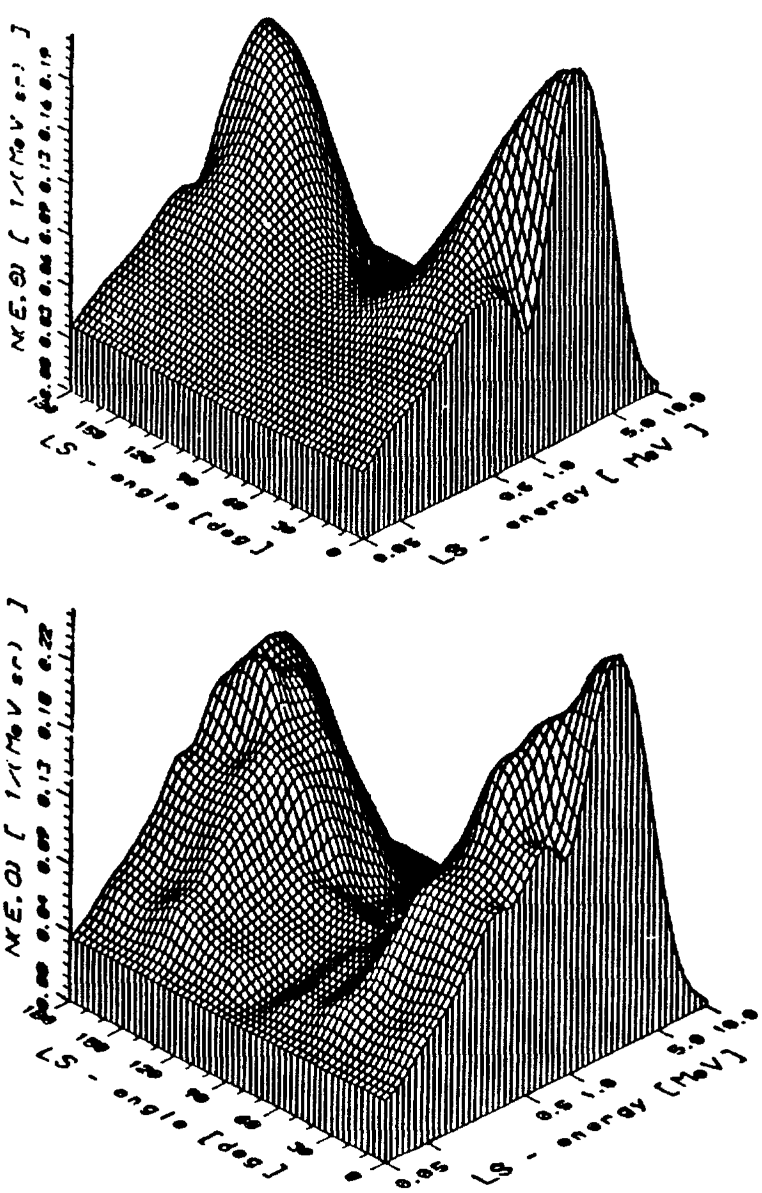

Fig. 20. Prompt fission neutron spectrum energy and angle matrix N(E,θ) for the ^{252}Cf(sf) reaction, calculated (Ref. 15) using the Dresden version (GMNM) of the Los Alamos model (upper portion of figure), and compared with the smoothed experimental data of Märten *et al.* (Ref. 24) (lower portion of figure). [Figure is from Ref. 15.]

IV.C. N(E, 0 MeV) for the n + ^{235}U Reaction.

A new measurement of the prompt fission neutron spectrum for the thermal-neutron-induced fission of ^{235}U has been reported by Wang *et al.*[28] in 1989. This spectrum was calculated[29] in 1983 using the Los Alamos model, Eqs. (9)-(11), and is identical to the thermal spectrum shown in Figs. 15 and 16. The comparison with the new data is shown in Figs. 23 and 24. Since the measurement occurred six years after the calculation, the comparison is certainly one without parameter adjustment. Although the agreement is reasonably good, the low energy (E < ~ 1 MeV) end of the spectrum is underpredicted. This may be further evidence for center-of-mass anisotropy, which is not included in the calculation.

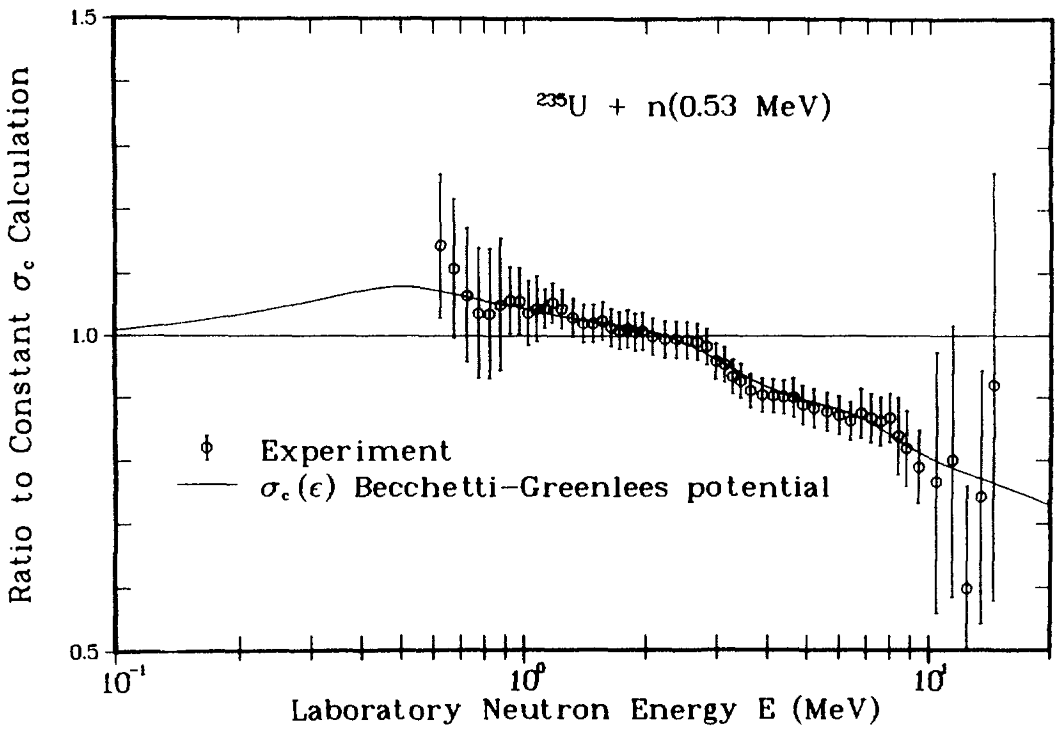

Fig. 21(a).

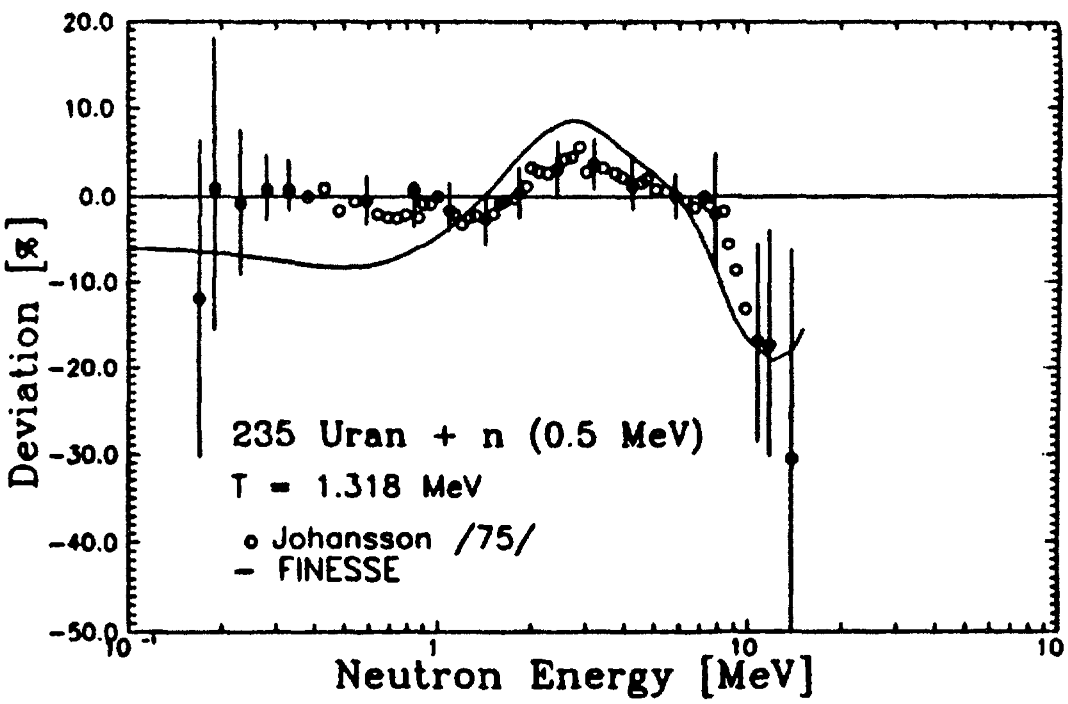

Fig. 21(b).

Fig. 21. (a) Prompt fission neutron spectrum for the fission of ^{235}U induced by 0.53-MeV neutrons. The solid curve gives the ratio of the Los Alamos spectrum calculated (Ref. 4) using energy-dependent cross sections and the experimental spectrum to the Los Alamos spectrum calculated using a constant cross section. The experimental data are those of Johansson and Holmqvist (Ref. 26). (b) Identical to (a) except that the calculation (Ref. 15) is the Dresden version (GMNM) of the Los Alamos model and the reference spectrum is the best-fit Maxwellian with T_M = 1.318 MeV.

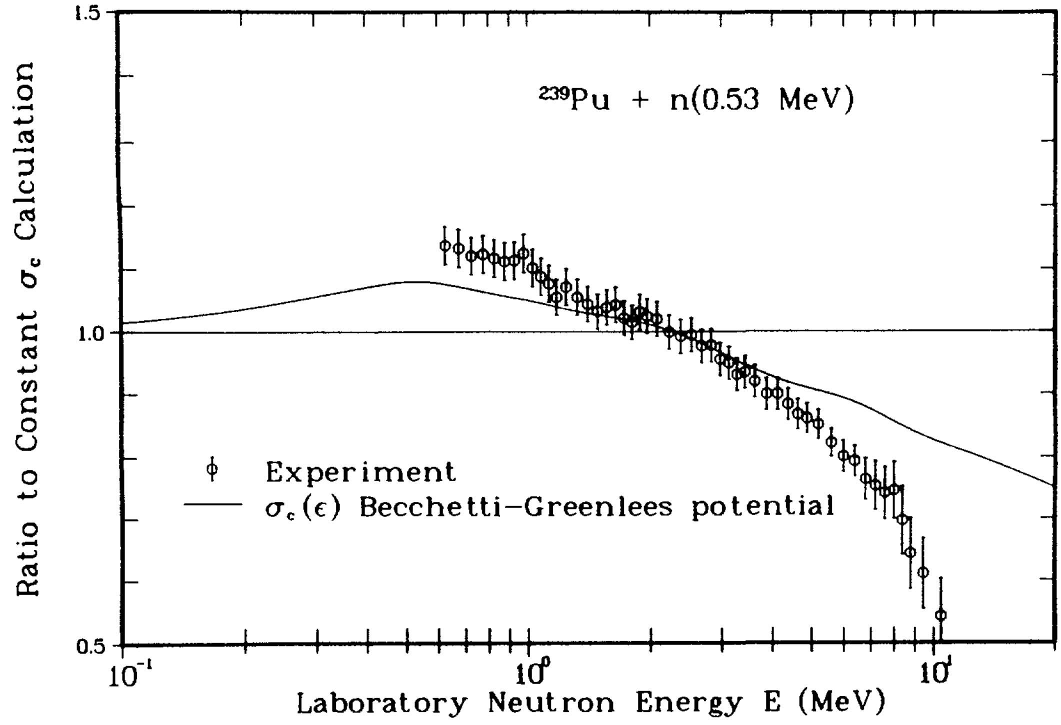

Fig. 22(a).

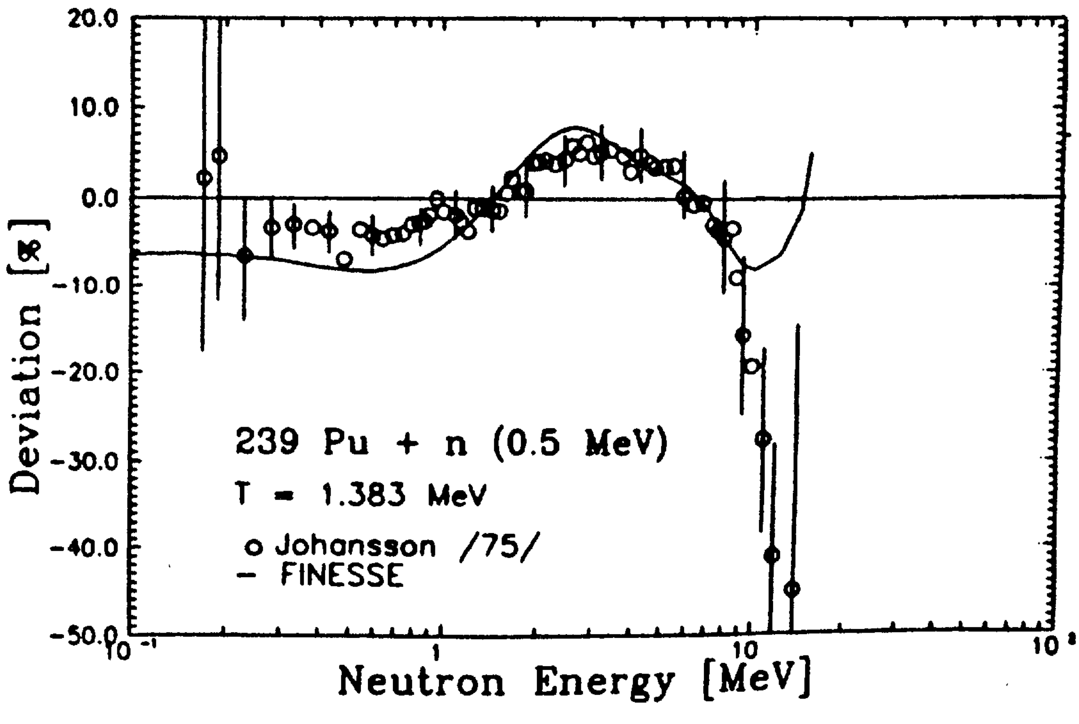

Fig. 22(b).

Fig. 22. (a) Identical to Fig. 21(a) except for ^{239}Pu, and where the experimental data are those of Johansson *et al.* (Ref. 27). (b) Identical to Fig. 21(b) except for ^{239}Pu, and where the experimental data are those of Johansson *et al.* (Ref. 27).

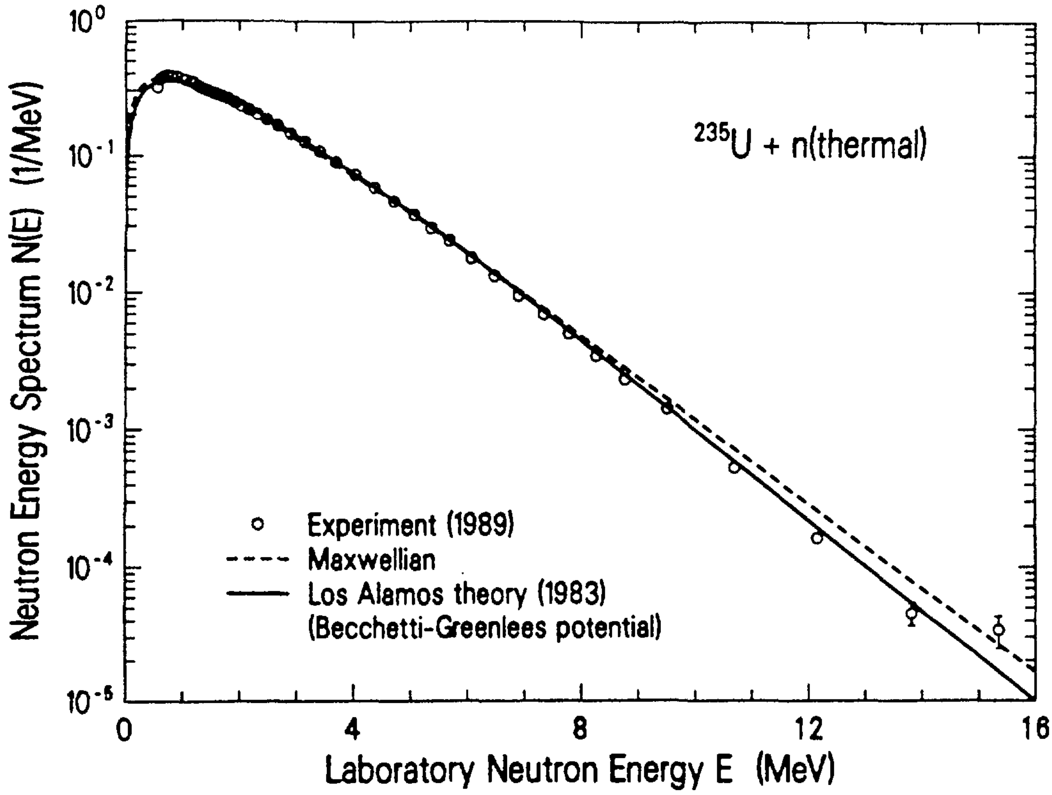

Fig. 23. Prompt fission neutron spectrum for the fission of ^{235}U induced by thermal neutrons. The dashed curve gives the best-fit Maxwellian spectrum (T_M = 1.321 MeV) determined in Ref. 28, and the solid curve gives the Los Alamos spectrum calculated from Eqs. (9)-(11) for $\sigma_c(\varepsilon)$ obtained using the optical-model potential of Becchetti and Greenlees (Ref. 31). The experimental data are those of Wang *et al.* (Ref. 28).

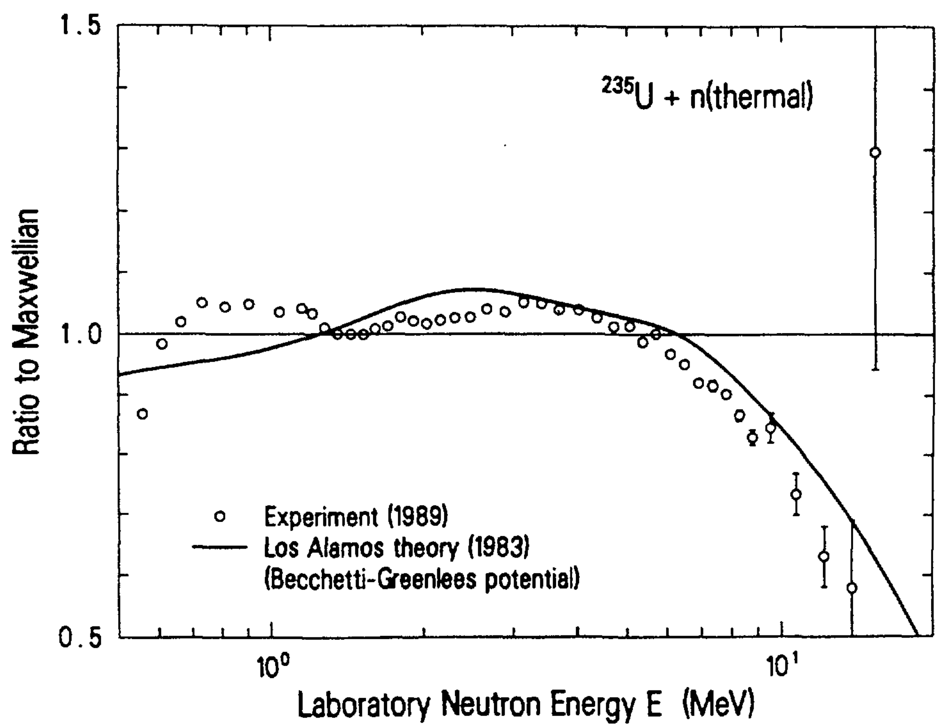

Fig. 24. Ratio of the Los Alamos spectrum and the experimental spectrum to the best-fit Maxwellian spectrum, corresponding to the curves shown in Fig. 23.

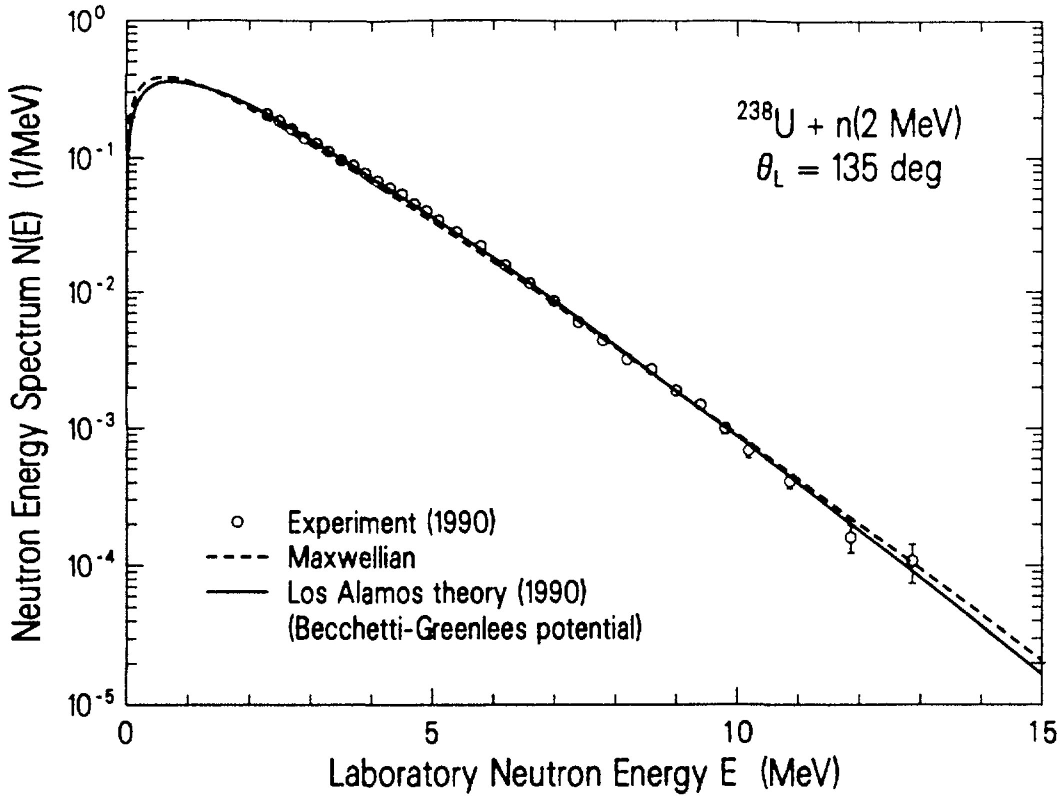

Fig. 25. Prompt fission neutron spectrum for the fission of ^{238}U induced by 2-MeV neutrons. The dashed curve gives the best-fit Maxwellian (T_M = 1.24 MeV) determined in Ref. 30, and the solid curve gives the Los Alamos spectrum calculated from Eqs. (9)-(11) for $\sigma_c(\varepsilon)$ obtained using the optical-model potential of Becchetti and Greenlees (Ref. 31). The experimental data are those of Baba *et al.* (Ref. 30).

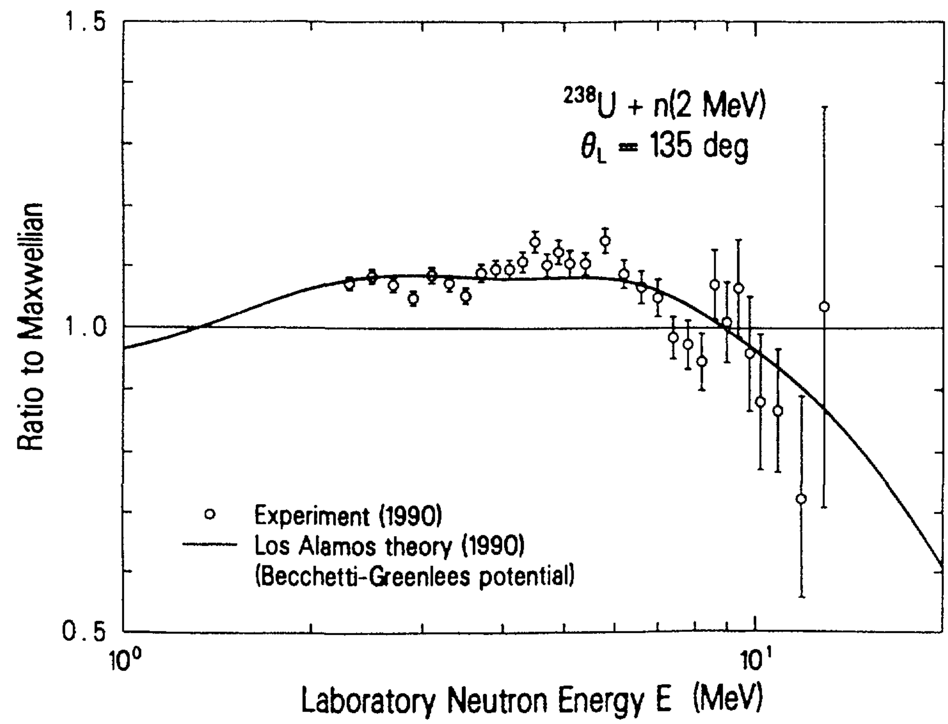

Fig. 26. Ratio of the Los Alamos spectrum and the experimental spectrum to the best-fit Maxwellian spectrum, corresponding to the curves shown in Fig. 25.

IV.D. N(E, 2 MeV) for the n + ^{238}U Reaction.

A new measurement of the prompt fission neutron spectrum has also been reported[30] for 2-MeV neutrons incident on ^{238}U. The spectrum was calculated with the Los Alamos model, Eqs. (9)-(11), using input parameters, except the value of E_n, determined in 1982 (Ref. 4), and is compared with the new data of Baba *et al.*[30] in Figs. 25 and 26. Here also, the agreement is reasonably good, especially given that no parameter adjustments have been made. However, the constant cross-section version of the Los Alamos model, Eqs. (9) and (12), was also used to calculate this spectrum (JENDL-3) and is shown in Ref. 30 (Fig. 6). A comparison of the two different calculations clearly shows that, in this case, the energy-dependent cross section calculation is the preferred one. It should be noted here that an adjustment in the effective level density parameter of the JENDL-3 calculation would improve the agreement.

V. CONCLUSIONS AND RECOMMENDATIONS

It is concluded that prompt fission neutron spectra and average prompt neutron multiplicities can be calculated with reasonably good confidence

- for unmeasured as well as measured systems, and
- for spontaneous as well as neutron-induced fission.

A high-quality measurement of the prompt fission neutron spectrum matrix from neutron-induced multiple-chance fission, a fission coincidence measurement, would crucially test the already existing calculations for multiple-chance fission effects. This would undoubtedly lead to a better understanding of multiple-chance fission effects, especially in their competition.

The current limitations to calculating N(E), $N(E,E_n)$, and $\bar{\nu}_p(E_n)$ with higher accuracy than is now possible include insufficient knowledge of

- excitation energy partition in fission,
- fission-fragment nuclear level densities,
- isospin dependence of global neutron optical-model potentials,
- fission-fragment ground-state masses (for the calculation of fission energy release),
- fission-fragment mass and charge distributions (as opposed to these distributions for fission products), and
- fission-fragment initial excitation energy and initial angular momentum distributions.

It is believed that, ultimately, the Hauser-Feshbach approach will probably yield the most accurate results in the calculation of N(E), $N(E,E_n)$, and $\bar{\nu}_p(E_n)$. One of the reasons for this belief is that simultaneous calculation of neutron and gamma-ray competition is the best way to account for the available fission-fragment excitation energy. Another reason is the explicit treatment of each fragment pair in the calculation. To benchmark such calculations, it is recommended that the following measurements be performed with high accuracy and over the widest possible secondary energy range, if they do not already exist:

- The prompt fission neutron and gamma-ray spectra for the thermal-neutron-induced fission of ^{235}U (leading to compound nucleus spin/parity of 3^- and 4^- only), and

- the prompt fission neutron and gamma-ray spectra for the thermal-neutron-induced fission of ^{239}Pu (leading to compound nucleus spin/parity of 0^+ and 1^+ only).

It is clear that these measurements would, ideally, be performed on a fragment pair by fragment pair basis.

REFERENCES

1. B. E. Watt, Phys. Rev. **87**, 1037 (1952).
2. N. Feather, "Emission of Neutrons from Moving Fission Fragments," BM-148, British Mission (1942).
3. See, for example, F. Manero and V. A. Konshin, Atomic Energy Rev. **10**, 637 (1972).
4. D. G. Madland and J. R. Nix, Nucl. Sci. Eng. **81**, 213 (1982), and earlier references contained therein.
5. V. F. Weisskopf, Phys. Rev. **52**, 295 (1937).
6. H. Märten and D. Seeliger, Nucl. Sci. Eng. **93**, 370 (1986).
7. D. G. Madland, R. J. LaBauve, and J. R. Nix, *Proceedings of the IAEA Consultants' Meeting on the Physics of Neutron Emission in Fission, Mito, Japan, 1988,* H. D. Lemmel, Ed. [IAEA, INDC(NDS)-220, 1989], p. 259.
8. D. G. Madland, *Proceedings of the International Conference Nuclear Data for Science and Technology, Mito, Japan, 1988,* S. Igarasi, Ed. (Saikon Publishing, Tokyo, 1988), p. 759.
9. H. Märten and D. Seeliger, J. Phys. G **10**, 349 (1984), and earlier references contained therein.
10. H. Märten, A. Ruben, and D. Seeliger, *Proceedings of the IAEA Consultants' Meeting on the Physics of Neutron Emission in Fission, Mito, Japan, 1988,* H. D. Lemmel, Ed. [IAEA, INDC(NDS)-220, 1989], p. 245.

11. W. Hauser and H. Feshbach, Phys. Rev. **87**, 366 (1952).

12. J. Terrell, Phys. Rev. **113**, 527 (1959).

13. D. Seeliger, H. Märten, W. Neubert, and D. Richter, Sov. J. Nucl. Phys. **47**, 403 (1988).

14. H. Märten and D. Seeliger, *Proceedings of the Advisory Group Meeting on Nuclear Standard Reference Data, Geel, Belgium, 1984* (IAEA-TECDOC-335, Vienna, 1985), p. 255.

15. D. Seeliger, H. Märten, and A. Ruben, *Contributions to the Theory of Fission Neutron Emission* [INDC(GDR)-057, Vienna, 1990].

16. J. C. Browne and F. S. Dietrich, Phys. Rev. C. **10**, 2545 (1974).

17. B. F. Gerasimenko and V. A. Rubchenya, *Proceedings of the Advisory Group Meeting on Properties of Neutron Sources, Leningrad, USSR, 1986* (IAEA-TECDOC-410, Vienna, 1987), p. 208, and earlier references contained therein.

18. B. F. Gerasimenko and V. A. Rubchenya, *Proceedings of the IAEA Consultants' Meeting on the Physics of Neutron Emission in Fission, Mito, Japan, 1988*, H. D. Lemmel, Ed. [IAEA, INDC(NDS)-220, 1989], p. 283.

19. J. W. Meadows, Phys. Rev. **157**, 1076 (1967).

20. L. Green, J. A. Mitchell, and N. M. Steen, Nucl. Sci. Eng. **50**, 257 (1973).

21. O. Balenkov *et al.*, *"Proceedings of the IAEA Consultants' Meeting on the U-235 Fast-Neutron Fission Cross Section and the Cf-252 Fission Neutron Spectrum, Smolenice, Czechoslovakia, 1983*, H. D. Lemmel and D. E. Cullen, Eds. [IAEA, INDC(NDS)-146, 1983], p. 161.

22. D. Seeliger, *et al.*, *Prompt Neutron Emission in Nuclear Fission* [INDC(GDR)-056/L, Vienna, 1989], p. 8.

23. W. Mannhart, *Proceedings of the Advisory Group Meeting on Properties of Neutron Sources, Leningrad, USSR, 1986* (IAEA-TECDOC-410, Vienna, 1987), p. 158.

24. H. Märten *et al.*, Nucl. Instr. Meth. **A264**, 375 (1988).

25. H. Märten *et al.*, *Proceedings of the IAEA Consultants' Meeting on the Physics of Neutron Emission in Fission, Mito, Japan, 1988*, H. D. Lemmel, Ed. [IAEA, INDC(NDS)-220, 1989], p. 169.

26. P. I. Johansson and B. Holmqvist, Nucl. Sci. Eng. **62**, 695 (1977).

27. P. I. Johansson *et al.*, *Proceedings of the Conference on Nuclear Cross Sections and Technology, Washington, DC, 1975* (NBS Special Publication 425, U.S. National Bureau of Standards, 1975) Vol. II, p. 572.

28. Wang Yufeng *et al.*, Chin. Jour. Nucl. Phys. **11**, 47 (1989).

29. D. G. Madland and J. R. Nix, *Proceedings of the NEANDC Specialists' Meeting on Yields and Decay Data of Fission Product Nuclides, Brookhaven National Laboratory, Upton, NY, 1983*, R. E. Chrien and T. W. Burrows, Eds. (BNL 51778, 1984), p. 423.

30. M. Baba *et al.*, J. Nucl. Sci. Technol. **27**, 601 (1990).

31. F. D. Becchetti, Jr. and G. W. Greenlees, Phys. Rev. **182**, 1190 (1969).

32. H. R. Bowman *et al.*, Phys. Rev. **126**, 2120 (1962).

NEW RESULTS AND INTERPRETATIONS OF COLD FISSION DATA FROM ^{252}CF.

F.- J. Hambsch, H.- H. Knitter[1] and C. Budtz-Jørgensen[2]
Commission of the European Communities
Central Bureau for Nuclear Measurements, JRC-Geel,
Steenweg op Retie, B - 2440 Geel, Belgium

[1] present address : Gerststraat 8, B-2490 Balen
[2] present address : Danish Space Research Institute, DK-2800 Lyngby

Abstract :
The spontaneous fission of ^{252}Cf was investigated experimentally in the cold fission region. The fission fragment mass- and nuclear charge distributions were determined in total kinetic energy bins of 2 MeV width parallel to the average Q_{max}-value as a function of mass from 1 to 15 MeV.
In evaluation bin 6 [($\bar{Q}_{max}$-TKE) = 11 MeV] 220 nuclides were identified, whereof 59 are lying outside the Karlsruhe Chart of Nuclides. Proton, neutron and mass odd-even effects were evaluated. There is no odd-even effect in the mass yield, whereas proton and neutron odd-even effects δ_Z and δ_N show linear dependence as function of ($\bar{Q}_{max}$-TKE), however with different slopes. The local proton odd-even effect $\delta_Z(A)$ at constant ($\bar{Q}_{max}$-TKE) shows an undulatory behaviour with a period of about five mass units. This structure persists even at ($\bar{Q}_{max}$-TKE)=15 MeV, where δ_Z, the average, is largely reduced. The neutron odd-even effect $\delta_N(A)$ shows vehement changes with fragment mass from positive to negative values and from small to large amplitudes.
The conclusion from the present results is that δ_Z and δ_N cannot be interpreted as indicators of the intrinsic excitation energy at scission, and that the structure of five to six mass units observed in many fission parameters finds its explanation in the shape of the fission energy surface for the Q-value as a function of mass and nuclear charge.

Introduction :

Nuclear mass and charge distributions close to the reaction Q-values were measured for the spontaneous fission of ^{252}Cf. In these high energy outskirts of the fission fragment distribution the yield has decreased by several orders of magnitude and therefore an efficient detection system with a high energy resolution is needed. The interesting fact for such fragmentations is that those fragments carry nearly no excitation energy, which makes neutron emission unlikely. The scission configuration as well as the fragments are close to their ground state. Nuclear fission is a large rearrangement of nuclear matter which results normally in two highly excited fragments. Investigation of the rare events close to the reaction Q-values, therefore, gives unique information about the roles of nuclear pairing, shell and liquid drop effects as well as on the possible ground state deformations of nuclei in the large range covered by the fission fragments.

The Experiment

The fission fragment detection is done with a Frisch-gridded twin ionization chamber /1/, which permits the measurement of the energies of both fragments with a resolution of <500 keV and allows also to determine the nuclear charge distributions.

For the whole fragment distribution $1.4 \cdot 10^8$ fission events were measured. However only the outskirts of the distribution were collected on magnetic tape. Fragment energies were corrected for the energy loss of the fragments in the source carrier and for the pulse height mass defect which is energy, mass and charge dependent. Both corrections were determined experimentally in separate measurements.

The nuclear charge information has been obtained from the experimental double-ratio $R(Z_L) = \frac{(P_{anode,L} - P_{sum,L})/P_{anode,L}}{(P_{anode,H} - P_{sum,H})/P_{anode,H}} = \frac{\bar{X}_L(E_L, A_L, Z_L)}{\bar{X}_H(E_H, A_H, Z_H)}$

$\bar{X}$ is the distance of the centre of gravity of the charge distribution of the fragments' ion trace in the detector gas from its origin. $\bar{X}(E)$ can be determined independently from the experiment /1/. P_{anode} is the anode signal and P_{sum} the sum signal of anode and grid /1/.

Evaluation and Results :

The scheme of the data evaluation is illustrated by fig. 1. This figure shows on the left hand side an energy scale in MeV and a percentage scale on the right hand side. Both scales are correlated with the light fragment mass scale as abscissa. The open and full circles represent the maximum Q-values as a function of mass split as calculated using the mass tables of Möller and Nix /2/ and of Möller et al. /3/, respectively.

The thick line through the open points is a kind of average Q_{max}-value between the odd and even mass splits. Parallel to this line in steps of 2 MeV eight fragment total kinetic energy bins are defined as indicated by the thin lines. For each total kinetic energy bin the nuclide yields were evaluated. Thus, the nuclide yields as a function of the total excitation energy available to both fragments are obtained.

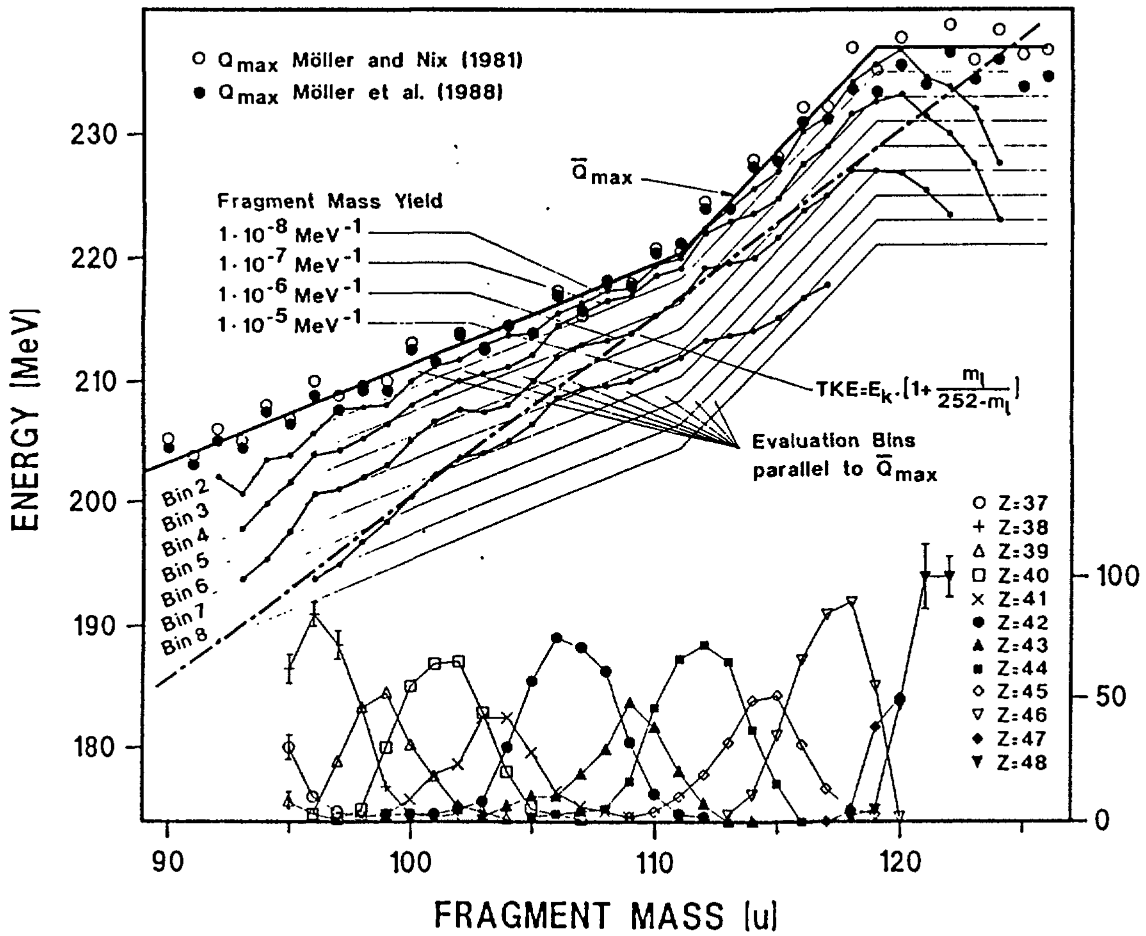

Fig. 1 : Maximum Q-values of $^{252}Cf(SF)$. TKE-evaluation bins. Lower part : Nuclear charge distributions versus light fragments mass.

Other cuts through the two-dimensional yield Y(A,TKE), like they are often used, e.g. for constant kinetic energy values, are arbitrary in the sense that they are not related to the same excitation energy available to both fragments as shown in fig. 1. Therefore comparisons between different fission nuclides are not possible.

The isobaric yields for these total kinetic energy bins are shown in scaled form in fig. 2. One may observe that the mass resolution decreases with increasing difference between the Q_{max}-value and the total kinetic energy. This is well understood by the onset of the neutron evaporation with increasing availability of excitation energy to the fragments.

The experimental nuclear charge distribution as measured for $\bar{Q}_{max}$-TKE = 11 MeV is shown in fig. 3. On the left side is the logarithmic contour-image plot of the mass charge correlation data array, where the highest intensities show even charges, and on the right side are the elemental compositions of two selected mass splits $A_L/A_H = 106/146$ and 109/143. The elemental yields as obtained from bin 6 are plotted in the lower part of fig. 1 with its scale in percent on the right hand side.

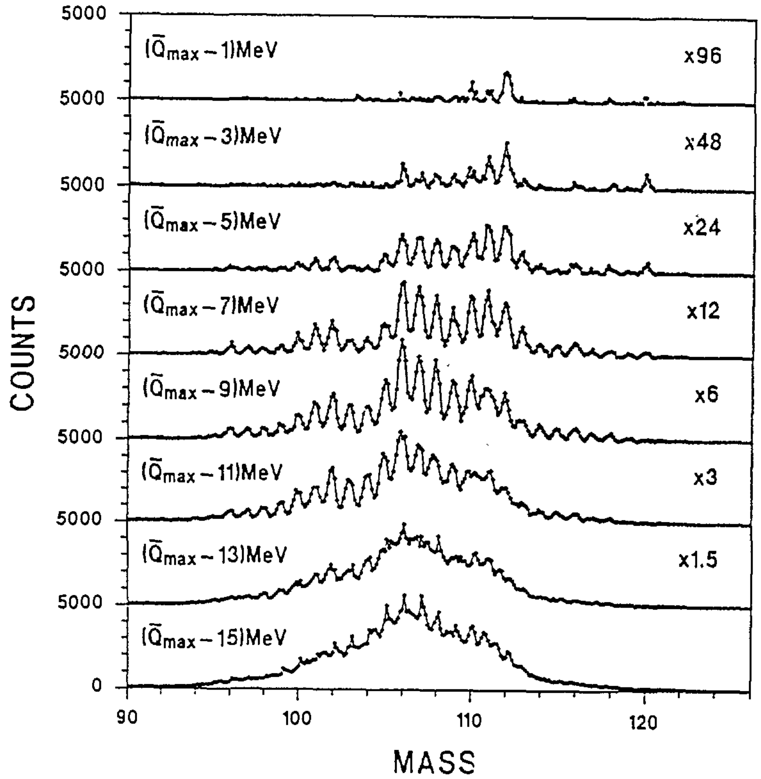

Fig. 2 : Scaled light fragment mass distributions for different evaluation bins.

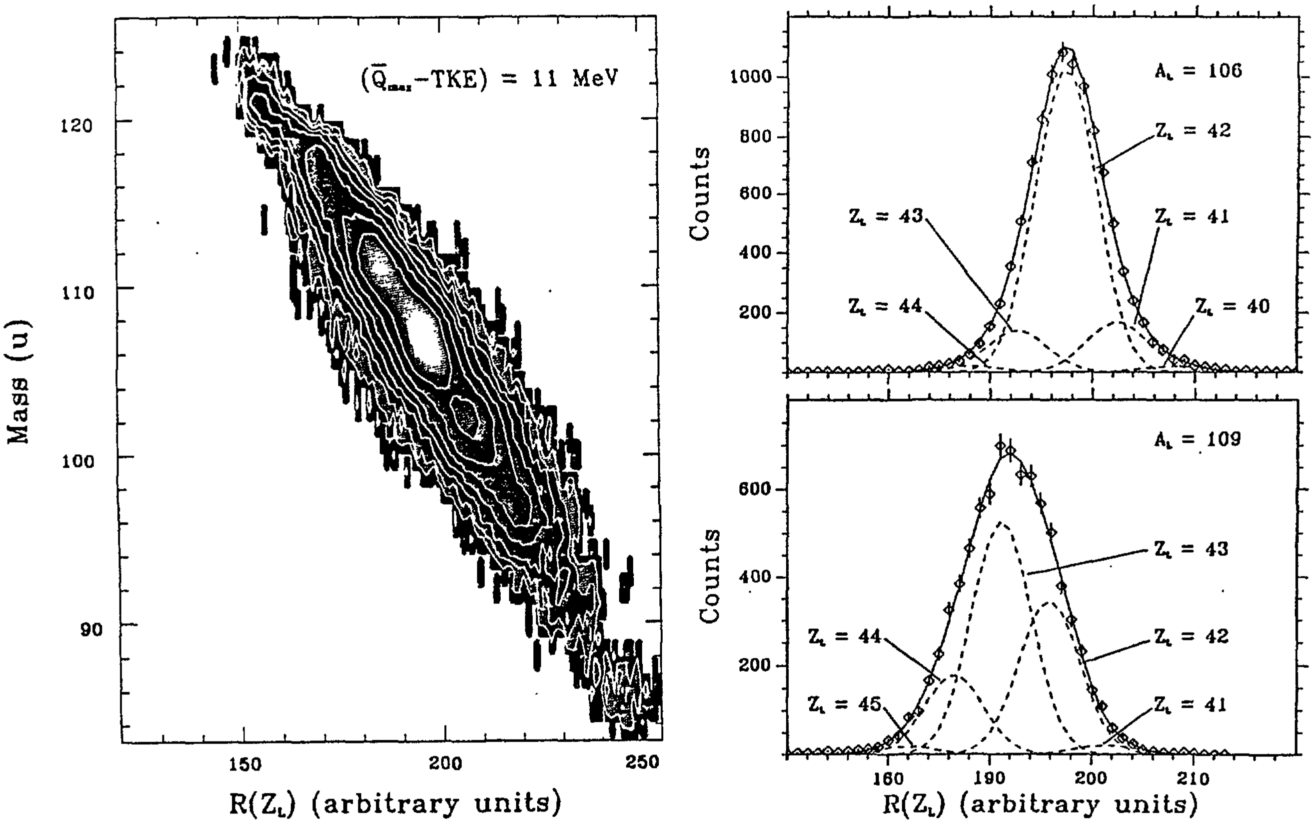

Fig. 3 : Experimental nuclear charge distribution for $\bar{Q}_{max}$-TKE = 11 MeV . Left side : Contour-image representation of the mass-charge correlation. Right side : Cut through the left picture for two selected masses and convolution of individual charges (dashed lines).

Table 1 : The odd-even effects for fragment mass, nuclear charge and neutron number as well as the nuclear charge variance, are given for the different TKE-evaluation bins. The four lower lines give the relative yields for even-even, odd-odd, even-odd and odd-even nuclear charge and neutron number respectively.

	BIN 1 (0-2)MeV	BIN 2 (2-4)MeV	BIN 3 (4-6)MeV	BIN 4 (6-8)MeV	BIN 5 (8-10)MeV	BIN 6 (10-12)MeV	BIN 7 (12-14)MeV	BIN 8 (14-16)MeV
δ_A	0.19±0.06	0.06±0.03	0.014±0.014	-0.007±0.008	0.000±0.005	0.009±0.003	0.000±0.002	-0.003±0.002
δ_Z	-	0.48±0.04	0.45±0.01	0.506±0.007	0.370±0.005	0.304±0.003	0.238±0.002	0.183±0.002
δ_N	-	0.13±0.05	0.06±0.02	0.068±0.008	0.045±0.005	0.033±0.003	0.018±0.002	0.013±0.002
$<\sigma_Z^2>$	-	0.16±0.09	0.32±0.11	0.33 ±0.66	0.40 ±0.04	0.45 ±0.03	0.48 ±0.02	0.50 ±0.02
EE[%]	(59)	37.6 ±4	36.9 ±1.2	40.7 ±0.6	35.1 ±0.3	36.6 ±0.2	31.4 ±0.2	29.7 ±0.2
OO[%]	(0)	6.7 ±2	11.4 ±0.5	12.0 ±0.3	14.8 ±0.2	16.8 ±0.1	18.6 ±0.1	19.8 ±0.1
EO[%]	(33)	36.7 ±3	35.6 ±1.0	34.6 ±0.5	32.9 ±0.3	31.6 ±0.2	30.5 ±0.2	9.5 ±0.1
OE[%]	(7)	19.8 ±1	16.1 ±0.6	12.7 ±0.3	17.1 ±0.2	18.0 ±0.2	19.5 ±0.1	21.0 ±0.1

Since the nuclide yields for each bin are measured, it is possible to sum up the nuclides with even-even, odd-odd, even-odd and odd-even proton and neutron numbers, respectively. These numerical values are given in table 1. It is evident that also the odd-even effects for the mass, δ_A, nuclear charge δ_Z and neutron number, δ_N can be obtained. They are given in table 1 also.

δ_A is essentially zero which gives evidence for the randomness of the neck-rupture at scission even at very small excitation energy, whereas δ_Z and δ_N reveal linear dependence with ($\bar{Q}_{max}$-TKE). However the magnitude of δ_Z is about five times larger than of δ_N. The slopes for δ_Z and δ_N are -(0.032±0.003)MeV^{-1} and -(0.0057±0.0008)MeV^{-1}, respectively. Table 1 gives the numerical values of the odd-even effects δ_A, δ_Z, δ_N and the relative yields for even-even (EE), odd-odd (OO), even-odd (EO) and odd-even (OE) fragmentations for the different evaluation bins. From table 1 it is clear that even fragmentation is favoured and odd fragmentation is dying out. This is a well known fact found also for other fissioning systems.

Up to now only results of the odd-even effect integrated over all fragments were presented. However the measurement permitted to evaluate proton and neutron odd-even effects also as function of mass split. This is done in the same way as for the integrated values and as an example shown in fig. 4.

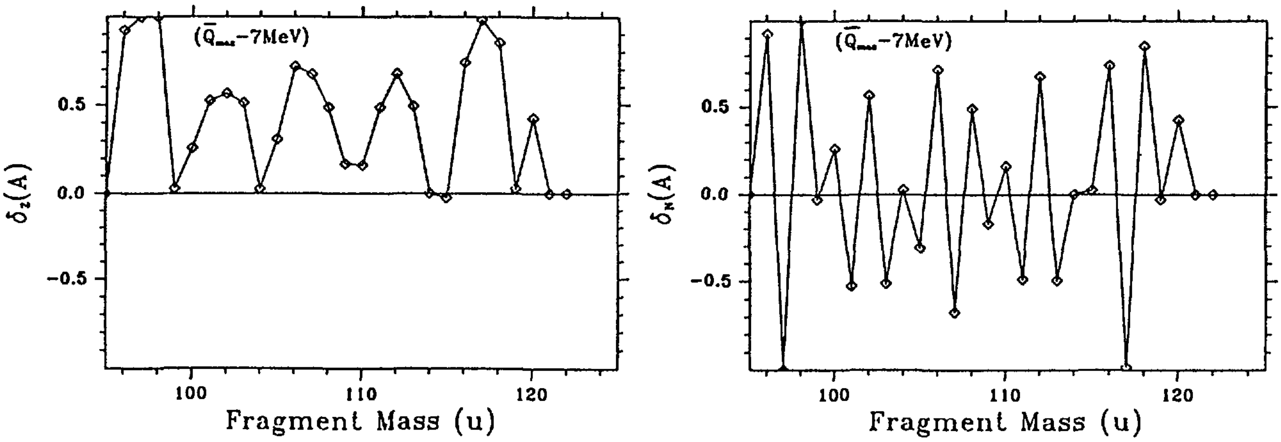

Fig. 4 : Local odd-even effects for protons (left) and neutrons (right) as function of fragment mass.

A clear undulatory structure with a period of five to six mass units is seen in $\delta_Z(A)$, whereas $\delta_N(A)$ shows strong fluctuations from one mass to the other. This is due to the fact that $\delta_Z(A)$ and $\delta_N(A)$ are directly dependent on one another /4/. Such structures can also be seen in other fissioning nuclides /4/.
The experimentally measured nuclide yields are a direct picture of the structures visible in the Q-value energy surface $Q(A_L, Z_L)$ shown in fig. 5.
This figure explains the behaviour of $\delta_Z(A)$ and other parameters showing structures of five to six mass units.

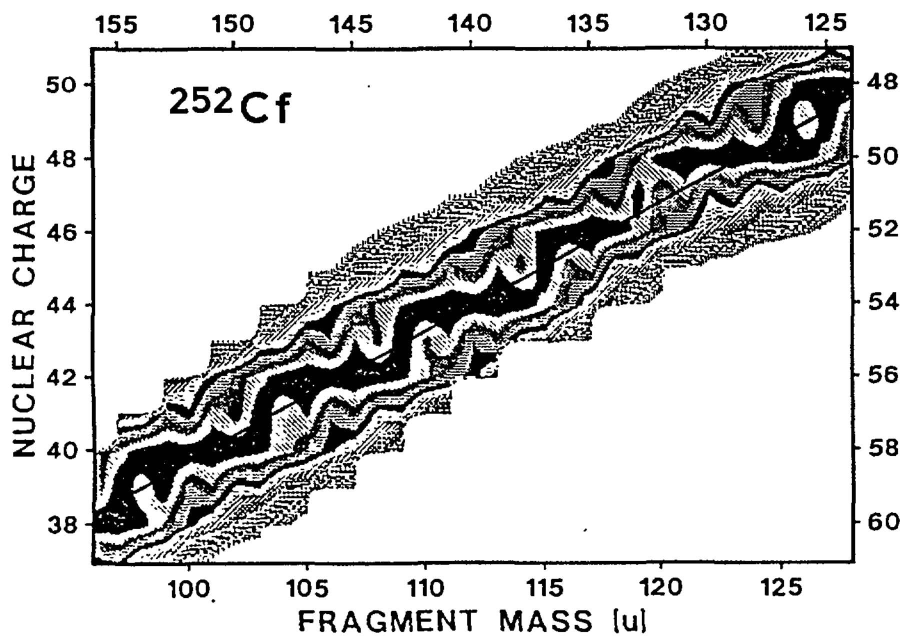

Fig. 5 : The Q-value energy surface Q(A,Z) in a grey-shaded representation

Also the dying out of the odd- fragmentations can be understood due to the fact that mostly the even- charge fragmentations have the highest Q-value and the evaluation bins follow parallel to this Q-value and not parallel to individual Q-values of single charges. However, the measured data allow also the correction for the same excitation energy of even or odd- charge fragmentations and then allow to calculate a similar table as table 1. Fig. 6 shows the result.

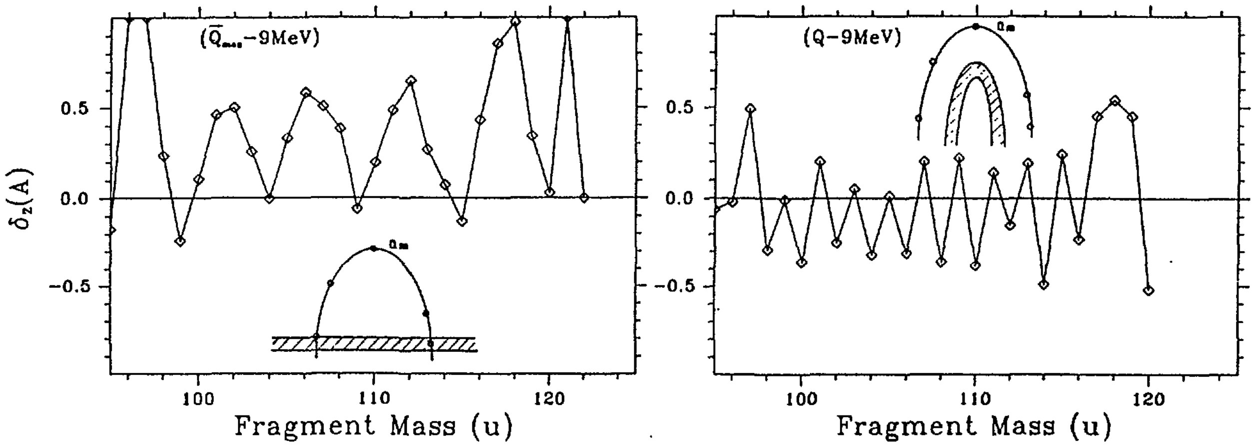

Fig. 6 Local proton odd-even effect at (Q-9 MeV). Left : for cuts parallel to $\bar{Q}_{max}$. Right : for cuts with constant distance from Q(A, Z).

The undulatory structure seen before essentially disappears when $\delta_Z(A)$ is evaluated for a constant excitation energy TXE (A, Z). Summing the local odd even effects over all masses, gives slightly negative values for δ_A, δ_Z and δ_N. Also the abundancy of OO, EE, OE, and EO changes drastically giving now higher probability for odd-odd (OO) than for EE fragmentations.
The structure left over in the right picture of fig. 6 can be understood by level density considerations. The level densities close to the ground state are larger for OO- fragments than for EE-fragments and therefore favour fragmentations with broken nucleon pair.
The only physical cut through the landscape Y(A, Z, TKE) is the one evaluating the yields for constant Q(A, Z)-TKE. Doing so, the evaluation is performed for constant TXE(A, Z). The models proposed in the past, e.g. /5/, linking odd-even effects to pair breaking and excitation energy (TXE ~ ln δ)are no longer valid, because δ_Z and δ_N close to zero, as shown in fig. 6, would imply intrinsic excitation energy close to infinity. Negative values for δ_Z and δ_N, may not occur either. So δ_Z or δ_N cannot be interpreted as being a measure of the excitation energy of the fissioning nucleus at the moment of scission.

References :

/1/ C. Budtz-Jørgensen, H.- H. Knitter, Ch. Straede, F.- J. Hambsch and R. Vogt,
Nucl. Instr. Meth. A258, (1987)209

/2/ P. Möller and J.R. Nix,
Atomic Data and Nucl. Data Tables 26, (1981) 165

/3/ P. Möller, W. D. Myers, J. W. Swiatecki and J. Treiner,
Atomic Data and Nucl. Data Tables 39, (1988) 225

/4/ H.- H. Knitter, F.- J. Hambsch and C. Budtz-Jørgensen
submitted to Nucl. Physics.

/5/ H. Nifenecker, G. Mariolopoulos, J.P. Bocquet, R. Brissot,
Mme Ch. Hamelin, J. Crançon and Ch. Ristori
Z. Phys. A308, (1982)39

EVALUATION OF TOTAL FISSION CHARACTERISTICS FOR URANIUM-235 IN THE RESONANCE REGION

U. Gohs+) and H. Märten
Technische Universität Dresden
Institut für Kern- und Atomphysik
Mommsenstraße 13, O-8027 Dresden, Germany

Abstract: *An energy conservation consistent evaluation of total fission characteristics for $J^{\pi}=4^{-}$ resonances of uranium-235 has been carried out on the basis of a combined fission path/fission channel representation. Experimental fission characteristics (total kinetic energy and neutron multiplicity) as function of fragment mass number for thermal-neutron induced fission of U-235 were used to define the parameters of energy partition at scission point. Applying a scission point model including semi-empirical, energy-dependent shell correction energies and a phenomenological description of the $(n,\gamma f)$-process, average values of total kinetic energy, total number of neutrons, total number of γ-rays and total energy of γ-rays for different resonances of uranium were calculated and compared with experimental data.*

1. Introduction

Hambsch et al. /1/ measured total fission yields Y(A) as function of fragment mass number A and total kinetic energies $\overline{TKE}(A_1/A_2)$ for resolved neutron resonances of uranium-235. The observed fluctuations in $\overline{TKE}$ were related to fluctuations in the yield of fission modes (standard 1, standard 2, superlong) /2/. However, measured fluctuations can not exactly be reproduced on the basis of fission mode parameters deduced by Hambsch et al. /1/.
According to Furman et al. /3/, the occupation probability $W_{d\lambda}$ of the fission path d for resonances numbered by λ is related to the relative contribution $P_{k\lambda}$ of fission channels k as

$$W_{d\lambda} = \sum_{k} P_{k\lambda} W_d^k . \tag{1}$$

W_d^k denotes the contribution of channel k to a given fission path d. Following this idea, the total characteristic X_λ of the resonance λ can be expressed by

+) Present Address: Joint Institute for Nuclear Research Dubna, Laboratory for Neutron Physics, Dubna 141980, USSR

$$X_\lambda = \sum_d \sum_k P_{k\lambda}\, W_d^k\, X_d^k \tag{2}$$

with

$$X_d^k = \sum_A Y_d(A)\; X_d^k(A). \tag{3}$$

X stands for $\overline{TKE}$, average number of neutrons $\tilde{\nu}_n$ and γ-rays $\bar{N}_\gamma$, or average total energy of γ-rays $\bar{E}_\gamma$. The mass yield of fission mode d, i.e. $Y_d(A)$, is represented by a Gaussian. Neglecting channel effects in describing fission characteristics X, equation (2) reduces to

$$X_\lambda = \sum_d W_{d\lambda}\, X_d \tag{4}$$

with

$$X_d = \sum_A Y_d(A)\; X_d(A). \tag{5}$$

In the present work, the fission characteristics $X_d(A)$ and $X_d^k(A)$ are calculated within the scission point model of Ruben at el. /4/, but introducing the modifications outlined in Section 2. These data are used to describe the total characteristics on the basis of equations (2) and (4), i.e. with and without account for channel effects on energy partition in fission, respectively.

2. Energy balance

The general energy balance in fission reads

$$\bar{Q}(A_L/A_H) + B_n + E_n = \overline{TKE}_d^k(A_L/A_H) + \overline{TXE}_d^k(A_L,A_H), \tag{6}$$

where $\bar{Q}$ is the energy release in fission for a given mass split A_L/A_H (averaged over charge distribution). B_n and E_n are the binding energy and the kinetic energy of the incidence neutron, respectively. $\overline{TXE}_d^k$ denotes the total fragment excitation energy for given mass split, fission channel k, and fission mode d. Both terms in the right-hand side of equation (6) can be expressed with reference to scission point considering pre-scission kinetic energy $\bar{E}_{pre}$ as well as intrinsic excitation energy (assumed as sum of excitation energy at saddle B, XE_d^k, of fission barrier and dissipative energy $\bar{E}_{dis,d}$):

$$\overline{TKE}_d^k(A_L/A_H) = \bar{E}_{c,d}(A_L/A_H) + \bar{E}_{pre,d}^{k} , \tag{7}$$

$$\overline{TXE}_d^k(A_L/A_H) = \bar{E}_{def,d}(A_L) + \bar{E}_{def,d}(A_H) + \bar{E}_{dis,d} + XE_d^k . \tag{8}$$

The fragment deformation energy $\bar{E}_{def,d}(A)$ is the main source of excitation energy (due to post-scission dissipation). $\bar{E}_{c,d}$ is the effective Coulomb potential energy at scission point corrected for nuclear interaction between both nascent fragments. XE_d^k is expressed with account for transition state energy $E_{f,d}^{k}$ of channel k (with reference to g.s. energy) by

$$XE_d^k = B_n + E_n - E_{f,d}^{k} \tag{9}$$

with the constraint $XE_d^k \geq 0$. Based on informations on transition states in U-236 fission obtained by Back et al. /5/, the values for 4^- resonances with projection K of angular momentum on fission axis were adjusted in order to reproduce $\overline{TKE}$ fluctuations. The difference between the K=1 and the K=2 transition state for 4^- resonances were found to be about 300 keV.

The calculation of fragment energies relies on a phenomenological scission point model /4/. The scission configuration is described by two spheroidally deformed fragments. The deformation energy $\bar{E}_{def,d}(A)$ is assumed to be quadratic in radius change with reference to a spherical nucleus with radius R:

$$\bar{E}_{def,d}(A) = \alpha(A)\ (D-R)^2 \tag{10}$$

D is the major semi-axis of the fission fragment. The deformability parameter $\alpha(A)$ is related to the stiffness parameter C:

$$C = \frac{5}{2\pi}\ \alpha(A)\ R^2 . \tag{11}$$

The partition of deformation energy can be expressed in terms of the deformability ratio of both fragments /4/

$$E_{def,d}(A_L)\ \alpha(A_L) = E_{def,d}(A_H)\ \alpha(A_H) . \tag{12}$$

The deformability parameter $\alpha(A)$ is related to the mean shell correction energy $\delta E_{sh}(A,E^*)$ by the empirical relation

$$\alpha(a) = \alpha_{LDM}(A) \frac{K(A)-\delta E_{sh}(A,E^*)}{K(A)-\delta E_{sh}(A,E^*)}, \tag{13}$$

where α_{LDM} is the liquid-drop model value of deformability. The energy dependence of shell correction energy on excitation energy is taken into account /6,7/.

Experimental data $\overline{TKE}(A_1/A_2)$ /1/ and $\bar{\nu}(A)$ /9/ for thermal-neutron indurced fission of uranium-235 were used to adjust the parameter K(A) as well as to compensate unceсurity of the used approximation in describing E_{def}. We obtained a mean value of (8.1 $\pm$ 1.1) MeV which agrees with the result of Kildir and Aras [(8.0 $\pm$ 0.2) MeV] quite well /10/.

The average excitation energy of a fragment $\overline{TXE}(A)$ can be calculated based on

$$\begin{aligned} \overline{TXE}_d^k(A) = {} & \bar{\nu}_{n,d}^{\,k}(A) \, [\bar{B}_n(A)+\bar{\varepsilon}_{n,d}^{\,k}(A)] + \\ & \bar{N}_{\gamma,d}^{E\,k}(A) \, \bar{E}_{\gamma,d}^{E\,k}(A) + \bar{N}_{\gamma,d}^{s\,k} \, \bar{E}_{\gamma,d}^{s\,k}(A), \end{aligned} \tag{14}$$

where $\bar{B}_n$ is the neutron binding energy averaged over the neutron cascade and the distribution in charge number Z, and $\bar{\varepsilon}_n(A)$ is the average neutron emission energy in the centre-of-mass system. $\bar{N}_{\gamma,d}^{E\,k}(A)$ stands for the number of γ-rays of E1/E2-transitions and statistical γ-rays with an energy lower than 1.6 MeV. $\bar{N}_{\gamma,d}^{s\,k}(A)$ includes statistical γ-rays with an energy above 1.6 MeV, the so-called contraction γ-rays for the superlong fission path /8/ and γ-rays of the $(n,\gamma f)$-process.

Pre-scission kinetic and dissipation energies were taken from calculations of Grossmann et al. /11/. We used the data of Tscherbakov /12/ to describe the $(n,\gamma f)$-process for uranium resonances. The occupation probabilities of the fission-paths d for 4^--resonances of uranium were taken from Hambsch et al. /1/.

3. Fluctuations of total fission characteristics

Starting point for the calculation of total fission characteristics is the thermal-neutron induced fission of U-235. Using the fitted data of K(A) we describe both $\overline{TKE}(A_1/A_2)$ and $\bar{\nu}(A)$

for thermal-neutron induced fission within the experimental errors (figures 1 and 2).

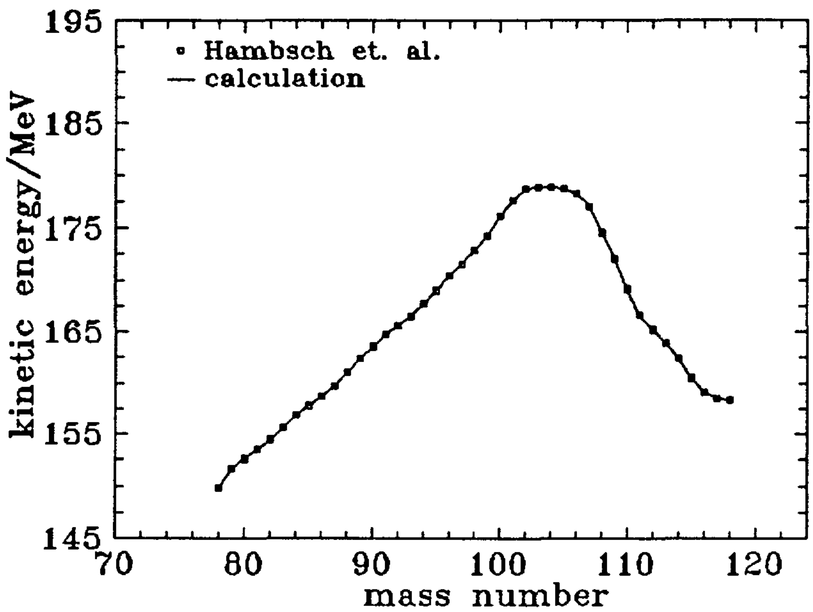

Fig. 1 Average kinetic energy for thermal-neutron induced fission of U-235

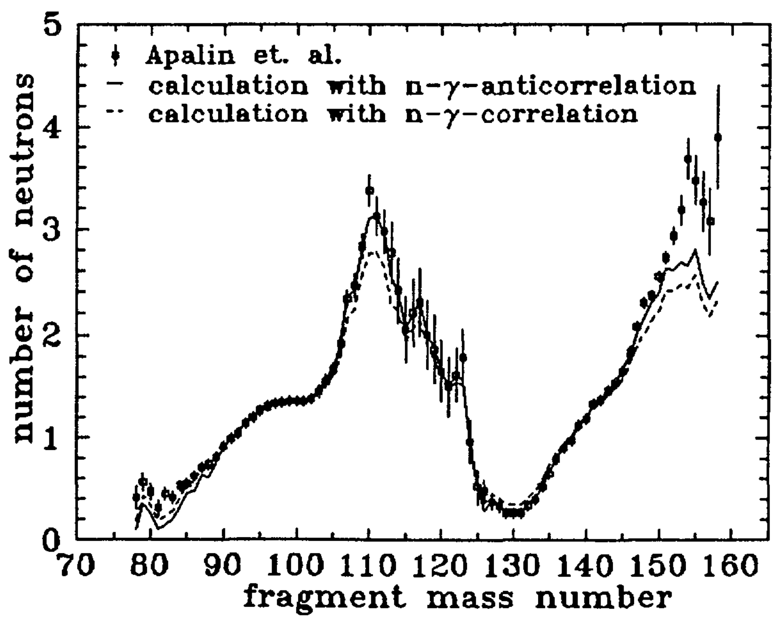

Fig. 2 Average number of neutrons for thermal-neutron induced fission of U-235

The correlation between the number of neutrons and the number of statistical γ-rays with an energy above 1.6 MeV, $\bar{N}_{sta,d}^{\,k}$, is described by

$$\bar{N}_{sta,d}^{\,k}(A) = a\ \bar{\nu}_{n,d}^{\,k}(A) + b \qquad (14)$$

Assuming an anticorrelation ($a<0$) we obtain the same mass dependence for the number of γ-rays labelled by $\bar{N}_{\gamma}^{s}$ as Schmidt-Fabian /8/.
The calculated total γ-ray energy for thermal-neutron induced fission of uranium-235 is

$$\bar{E}_{\gamma} = (4.48 \pm 0.15)\ \text{MeV} + (2.1 \pm 0.1)\ \text{MeV}. \qquad (15)$$

For comparison, we used the data of Frehaut /14/ and $\bar{\nu}_n = 2.4251$ /13/ and obtained

$$\bar{E}_{\gamma} = (4.33 \pm 0.21)\ \text{MeV} + (2.35 \pm 0.20)\ \text{MeV}. \qquad (16)$$

The first term in the right-hand side of equation (16) stands for E1/E2-transitions and statistical γ-rays with an energy lower than 1.6 MeV. The second term represents the contribution of the γ-rays labeled by $\bar{N}_{\gamma,d}^{s\ k}$.
In table 1, the calculated mean values of TKE, ν_n, N_{γ} and E_{γ} and the experimental data are shown for the thermal-neutron induced fission of uranium-235. The calculations reproduce experimental data.

Table 1 Total fission characteristics for $^{235}U(n_{th},f)$

X	calculation	experiment
$\overline{TKE}$ [MeV]	170.60 ± 0.01	170.604 ± 0.005 /1/
$\bar{\nu}_n$	2.418 ± 0.015	2.4251 ± 0.0034 /13/
$\bar{N}_{\gamma}$	6.66 ± 0.22	
$\bar{E}_{\gamma}$ [MeV]	6.51 ± 0.14	

The results of the calculation of fission characteristics for some 4^- resonances are shown in figures 3, 4, and 5. The calculation were performed within the following approaches:

combined fission path/fission-channel representation
- equation (2) - CALCULATION I -

pure fission-path representation
- equation (4) - CALCULATION II -.

It is indicated that the experimental data are better reproduced if including channel effects. Assuming equal spin of both fragments for each fission-path, an anticorrelation between $\bar{\nu}_n$ and $\bar{N}_\gamma$ is favoured. The anticorrelation between $\overline{TKE}$ and $\bar{\nu}_n$ is destroyed by the $(n,\gamma f)$-process.

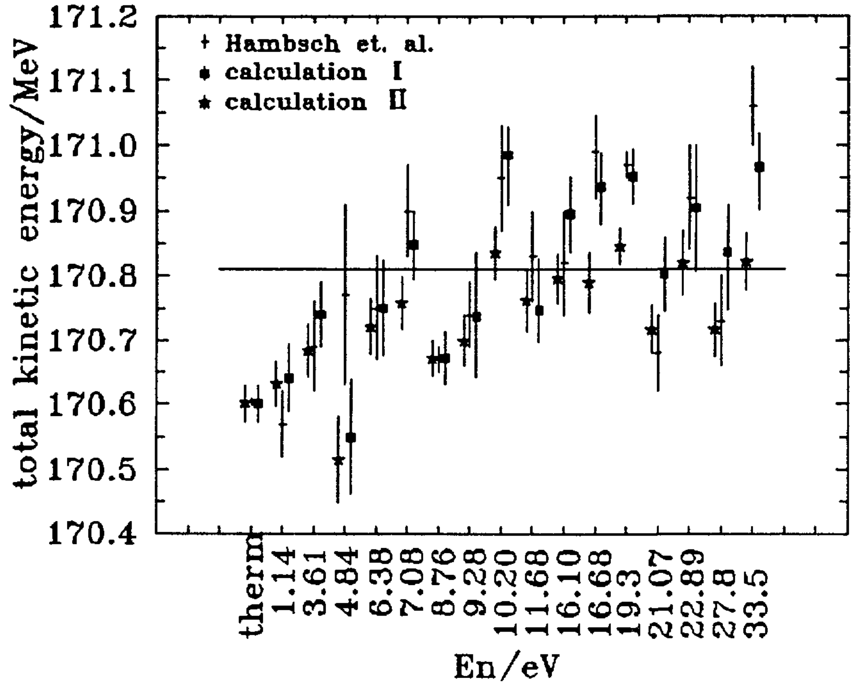

Fig. 3 $\overline{TKE}$ as function of E_n for resonance fission of ^{235}U

The fluctuation of relative neutron numbers is reproduced if including the $(n,\gamma f)$-process even. Its contribution is given by

$$P_{n,\gamma f} = \frac{\sigma^{4^-}_{n,\gamma f}}{\sigma^{\lambda}_{n,f}}. \tag{16}$$

($\sigma^{\lambda}_{n,f}$ - total fission cross section of resonance λ, $\sigma^{4^-}_{n,\gamma f}$ - cross section of $(n.\gamma f)$-process for 4^- resonances).

4. Summary

It has been shown that the calculational results of A-dependent and total fission characteristics are in agreement with experimental data. On the basis of the present model one may conclude that there is an anti-correlation between $\bar{\nu}_n$ and $\bar{N}_\gamma$.

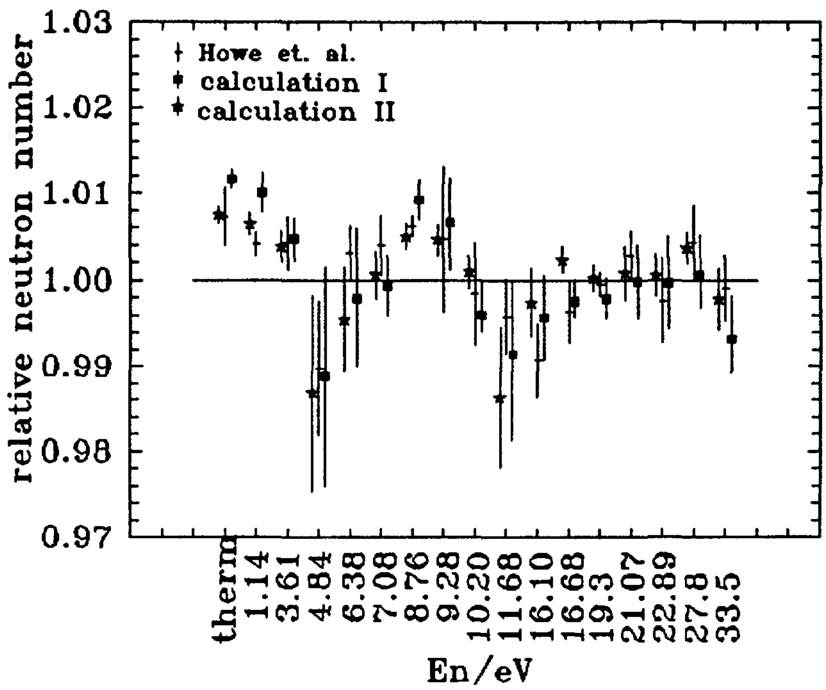

Fig. 4 Relative $\bar{\nu}_n$ as function of E_n for fission of ^{235}U

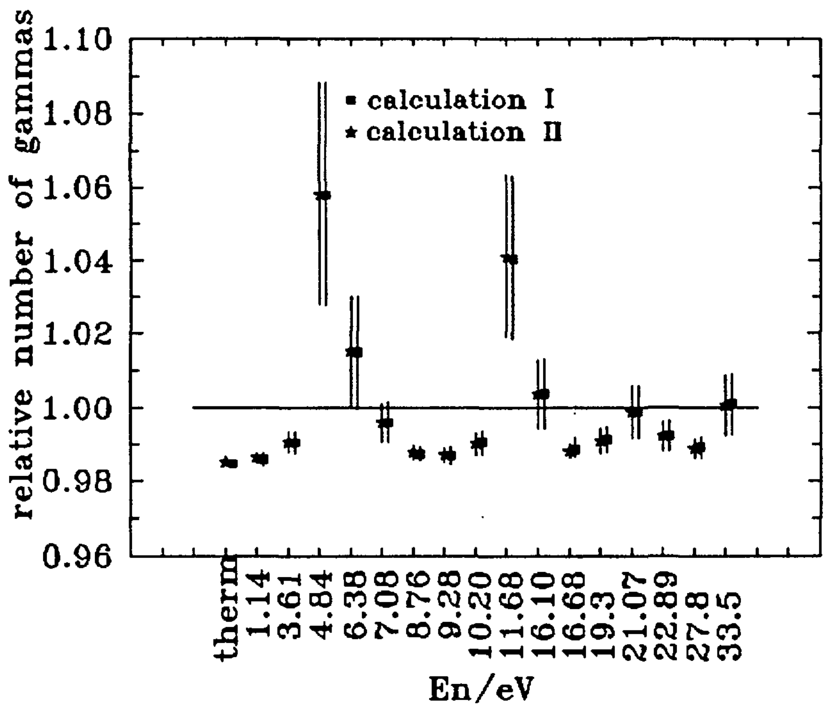

Fig. 5 Relative $\bar{N}_\gamma$ as function of E_n for fission of ^{235}U

The calculations indicate that channel effects and the $(n,\gamma f)$-process should be taken into account to explain the fluctuations of total fission characteristics. It is not excluded that the $(n,\gamma f)$-process, which runs via other transition states, influences the total mass yield because of the lower excitation energy at the second saddle.

References

/1/ F.J. Hambsch, thesis, Darmstadt, 1987

/2/ U. Brosa et al., Proc. XVIth Int. Symp. on Nucl. Phys., Gaussig, 1986, ZfK-610 (1986) 162

/3/ V.J. Furman and J. Kliman, Proc. of the XVIIth Int. Symp. on Nucl. Phys., Gaussig, 1987, ZfK-646 (1988) 142

/4/ D. Seeliger et al., INDC(GDR)-57/1 (1990), and A. Ruben et al., submitted to Z. Phys A

/5/ B.B. Back et al., Nucl. Phys. A 165 (1971) 449

/6/ A.V. Ignatyuk et al., Yad. Fiz. 21 (1975) 485

/7/ S.K. Kataria et al., Phys. Rev. C 18 (1978) 549

/8/ R. Schmidt-Fabian, thesis, Heidelberg, 1989

/9/ W.F. Apalin et al., Nucl. Phys. 71 (1965) 553

/10/ M. Kildir and N.K. Aras, Phys. Rev. C 25 (1982) 365

/11/ S. Grossmann et al., Nucl. Phys. A 481 (1988) 340

/12/ Tscherbakov, thesis, Leningrad, 1985

/13/ Neutron Cross Sections, BNL, 1984

/14/ J. Frehaut, Proc. Cons. Meet. on Physics of Neutron Emission in Fission, Mito (1988), INDC(NDS)-220/L (1989) 99

LIST OF PARTICIPANTS

AUSTRALIA

Dr. R.L. Walsh
Lucas Heights Research Laboratories
Private Mail Bag 1
Menai, N.S.W. 2234

CHINA

Huang Shengnian
Institute of Atomic Energy
P.O. Box 275 (46)
102413 Beijing

FRANCE

E. Fort
DER/SPRC/LEPH-Bâtiment 230
Centre d'Etudes Nucléaires de
Cadarache (CEN)
Boîte Postale No. 1
F-13108 Saint-Paul-lez-Durance

H. Tellier
SERMA
Commissariat à l'Engergie Atomique
Centre d'Etudes Nucléaires de Saclay
Boîte Postale No. 2
F-91191 Gif-wur-Yvette Cedex

GERMANY

H. Märten
Sektion Physik
Technische Universität Dresden
Mommsenstrasse 13
D-O 8027 Dresden

M. Mutterer
Technische Hochschule Darmstadt
Institut für Kernphysik
Schlossgartenstrasse 9
D-W 6100 Darmstadt

INDIA

S.S. Kapoor
Bhabha Atomic Research Centre
Physics Group
Trombay, Bombay 400 085

JAPAN

T. Ohsawa
Atomic Energy Research Institute
Kinki University
3-4-1 Kowakae
Higashi-osaka
Osaka 577

USSR	M.V. Blinov Radievyj Institut V.G. Khlopin Ul. Rentgena 1 SU-197 022 St. Petersburg
	B.D. Kuzminov Fiziko-Energeticheskij Institut Ploshchad Bondarenko Ul. Rentgena 1 SU-249 020 Obninsk, Kaluga Region
USA	D.G. Madland Nuclear Theory, T-2 MS/B243 Los Alamos National Laboratory P.O. Box 1663 Los Alamos, New Mexico 87545
COMMISSION OF THE EUROPEAN COMMUNITIES	F.J. Hambsch Central Bureau for Nuclear Measurements Steenweg op Retie B-2440 Geel
IAEA/NDS	V.A. Konshin J.J. Schmidt D.W. Muir S. Ganesan (Scientific Secretary) H.D. Lemmel N.P. Kocherov V. Osorio A.B. Pashchenko Wang DaHai